Informatics Control Measurement
in Economy and Environment Protection

2/2019

Informatyka Automatyka Pomiary

w gospodarce i ochronie środowiska

www.e-IAPGOS.pl

ISSN 2083-0157

Kwartalnik Naukowo-Techniczny

70 lat prof. Waldemara Wójcika

2/2019

kwiecień – czerwiec

Wydanie pod redakcją naukową
prof. dr hab. inż. Waldemara Wójcika

INFORMATYKA AUTOMATYKA POMIARY
W GOSPODARCE i OCHRONIE ŚRODOWISKA
Informatics Control Measurement in Economy and Environment Protection

p-ISSN 2083-0157, e-ISSN 2391-6761, www.e-iapgos.pl

INTERNATIONAL PROGRAMME COMMITTEE – RADA PROGRAMOWO-NAUKOWA

EDITORIAL BOARD – KOMITET REDAKCYJNY

EDITOR STAFF – ZESPÓŁ REDAKCYJNY

EDITORIAL OFFICE – REDAKCJA

Redakcja czasopisma
Informatyka, Automatyka, Pomiary w Gospodarce i Ochronie Środowiska
Instytut Elektroniki i Technik Informacyjnych
Politechnika Lubelska
ul. Nadbystrzycka 38A
20-618 Lublin
tel. +48 81 53 84 309
fax: +48 81 53 84 312
www.e-iapgos.pl
iapgos@pollub.pl

PUBLISHER – WYDAWCA

Politechnika Lubelska
ul. Nadbystrzycka 38D
20-618 Lublin
tel. +48 81 53 84 100
www.pollub.pl

PRINTING HOUSE – DRUKARNIA

Agencja Reklamowa TOP
87-800 Włocławek
ul. Toruńska 148
tel. +48 54 423 20 40
nakład: 100 egzemplarzy

OTHER INFORMATION – INNE INFORMACJE

Czasopismo jest indeksowane w bazach:

BazTech:	baztech.icm.edu.pl
IC Journals Master List:	www.journals.indexcopernicus.com
Google Scholar	scholar.google.pl
POL-index	pbn.nauka.gov.pl

Czasopismo znajduje się w wykazie czasopism naukowych opublikowanym w Komunikacie Ministra Nauki i Szkolnictwa Wyższego z dnia 9 grudnia 2016 r. – część B, pozycja 685 – z liczbą punktów przyznawanych za publikację równą 7.

Zasady publikowania artykułów, przygotowania tekstów, zasady etyczne, procedura recenzowania, wykazy recenzentów oraz pełne teksty artykułów dostępne są na stronie internetowej czasopisma:

www.e-iapgos.pl

W celu zwiększenia oddziaływania czasopisma w środowisku naukowym redakcja zaleca:

- w artykułach publikowanych w IAPGOS cytować artykuły z renomowanych czasopism międzynarodowych (szczególnie indeksowanych w bazach Web of Science oraz Scopus) używając oficjalnych skrótów nazw czasopism,
- w artykułach publikowanych w innych czasopismach (zwłaszcza indeksowanych w bazach Web of Science oraz Scopus) cytować prace publikowane w IAPGOS – zwłaszcza posługując się numerami DOI, np.:
  Kluszczyński K. *Modelowanie – umiejętność czy sztuka?* Informatyka, Automatyka, Pomiary w Gospodarce i Ochronie Środowiska – IAPGOS, 1/2016, 4–15, DOI: 10.5604/20830157.1193833.

CONTENTS – SPIS TREŚCI

DOI: 10.5604/01.3001.0013.2538

OPPORTUNITIES FOR THE OUT OF THE 1550 nm WINDOW TRANSMISSION

Jarosław Piotr Turkiewicz[1,2]
[1]Warsaw University of Technology, Faculty of Electronics and Information Technology, Warsaw, Poland, [2]Orange Labs Poland, 7 Obrzeżna, Warsaw

Abstract. *In this paper, opportunities for transmission in the 850 nm and 1310 nm windows are reviewed. In particular, the mentioned windows can be utilized for the data centre related transmission.*

Keywords: optical communication, optical fibre, optical amplifier

MOŻLIWOŚCI WYKORZYSTANIA TRANSMISJI POZA PASMEM 1550 nm

Streszczenie. *W artykule dokonano analizy możliwości wykorzystania okien transmisyjnych 850 nm i 1310 nm. Rozważane okna można wykorzystać do realizacji transmisji dla potrzeb centrów danych.*

Słowa kluczowe: komunikacja optyczna, światłowód, wzmacniacz optyczny

Introduction

The ever growing number of information and communication network users like Internet, development of bandwidth hungry applications, e.g. high quality video streaming as well as increased quality requirements, e.g. low latency is driving development of the telecommunication networks. The optical fibre is the only one physical medium that can provide high transmission capacity, while maintaining very long transmission distances, up to trans continental ones. The importance of the optical fibre to the development of civilization, has been recognized by awarding Charles K. Kao in 2009 Nobel Prize in physics for "for ground breaking achievements concerning the transmission of light in fibres for optical communication" [4].

The potential of optical fibre transmission had been very quickly recognized and it has been widely adopted for the signal transmission. For the very long time, the key application area was high capacity (whatever did it mean at the given moment in time) over long distances, where the high cost of the transmission system was shared among many users. Recently, we observe rapid increase of data rates used in the computer inert and intra board communication as well as growth of the data storage and processing centres. In such application areas, copper cable transmission cannot handle high data rates transmission over the required distances. However, such demand can be fulfilled by the optical fibre transmission. One could say, that sarcastically the optical fibre transmission is covering shorter and shorter distances.

Due to the lowest attenuation of 0.2 dB/km and excellent amplification technology, namely erbium doped fibre amplifier (EDFA) the 1550 nm transmission window is a window of choice to realize optical fibre transmission. The other transmission windows like 850 nm or 1310 nm seemed to be until recently almost entirely forgotten. However, the rise of new application areas like inter- and intra-data centre transmission that put attention on the features like low cost and high energy efficiency, give prospect for efficient utilization of other transmission windows.

The high data rate ultrashort data links, called data interconnect, currently operate at the data rates 25 Gbit/s with the foreseen increase to 50 Gbit/s and even 100 Gbit/s over the distances up to a few hundred meters to cover the data centre area. The key requirements of the data interconnects are small footprint, limited energy consumption and overall low component cost. Such data interconnects can be realized in the 850 nm transmission window. The 1310 nm transmission window can be used to realize high data rate transmission over the distances up to few dozen kilometres, leveraging a key standard single mode fibre (SSMF) advantage at 1310 nm, namely low value of chromatic dispersion, which translates into the simplified system design (lack of dispersion compensation) as well as straightforward system installation, which is one of the most sought features of the data communication equipment. Table 1 shows comparison of the key transmission window characteristics.

Table 1. Optical fibre transmission window comparison

	1550 nm	1310 nm	850 nm
λ number	Over 100	Up to several	A few
Single data rate	400 Gbit/s	50 Gbit/s	25 Gbit/s
Range	>1000 km	< 50 km	< 1 km
Optical amplifier	EDFA	SOA	none
Total capacity	Tbit/s	100 Gbit/s	100 Gbit/s
Fibre	SSMF	SSMF	MM
Attenuation	0.2 dB/km	0.4 dB/km	4 dB/km

1. 850 nm data interconnects

The fibre of choice for the 850 nm window is a multi-mode fibre (MMF). Except the high attenuation at 850 nm around 4 dB/km, the multi-mode fibres transmission is affected by the modal and chromatic dispersion, which limits the available transmission bandwidth to about 4.7 GHz·km for the newest generation of MMF. However, for the ultra-short links, e.g. of 100 m, the fibre bandwidth increases to 47 GHz and even higher for meter range distances. Further, the core dimeter of MMF fibres is 50 μm. Such large core diameter allows easy coupling with the emitting lasers and receiving photo-detectors.

The vertical-cavity emitting lasers (VCSELs) at 850 nm are characterized by surface light emission, the modulation bandwidth up to 25 GHz, coupled output power of a few milliwatt and driving current of a few miliamper [5]. Figure 1 shows the spectrum and light-intensity-voltage characteristics of the 850 nm VCSEL. The high modulation bandwidth and low energy consumption, while maintaining desired optical power allows realization of the cost-effective transmission systems with a few dozen Gbit/s data rate over up to a few hundred meter distances based on MMF and VCSEL [19]. The system simplicity (direct modulation and detection) and limited power consumption translate into low transmission cost, which is a key feature required for the data interconnects, which number can exceed a few dozen thousand in a single data centre.

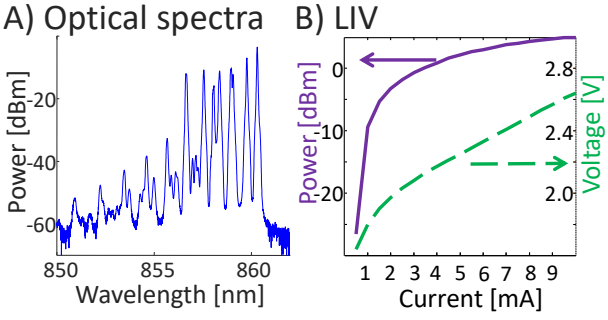

Fig. 1. 850 nm VCSEL spectral and LIV characteristics

Figure 2 shows the exemplary eye diagram of the 850 nm VCSEL operated at various data rates for the amplitude binary on-off keying (OOK) modulation. Up to the 35 Gbit/s the yes is almost not distorted, while distortions can be observed for higher data rates. The data rate related distortions are dueto the limited bandwidth of the utilized components like VCSEL and photo-receiver, which show bandwidth of about 22 GHz. Nevertheless, as we can see up to the data rate of 50 Gbit/s the eye diagram is widely open in the middle, indicating proper transmission and signal reception. The shown eye diagram, were captured in so called back-to-back (b2b) configuration, i.e. directly connecting transmitter to the receiver, as such the transmission distance was in the range of a few meters as the length of the pigtails attached to the components. It is important to note, that such a distance perfectly cover the distance required to connect components within a 19" standard rack of height up to 2 m.

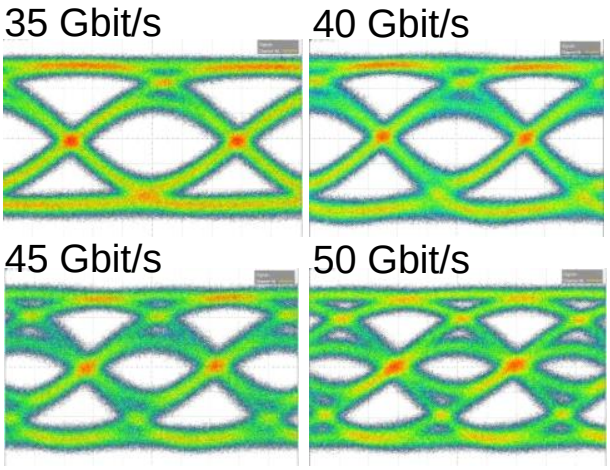

Fig. 2. 850 nm VCSEL eye diagrams at various data rates

Data interconnect transmission capabilities, in term of the achievable data rate will not only be affect by the limited bandwidth of the VCSEL and photo-detectors but more importantly as the distance grow by transmission properties of the MMF.

To overcome limitations related to the MMF chromatic dispersion, single mode (SM) VCSELs have been developed [7]. The single mode VCSELs are characterized by the limited optical spectrum width, since preferably only one wavelength mode occurs. In such a way, the influence of the chromatic dispersion is significantly limited. SM VCSEL offer potential to cover much higher distances that the multi mode (MM) VCSELs, which is critical to cover inter-rack/room/building distances in the data centre, without switching to another more complex and expensive transmission technology. Obviously, the SM VCSEL modulation bandwidth must stay in the range of a few dozen GHz

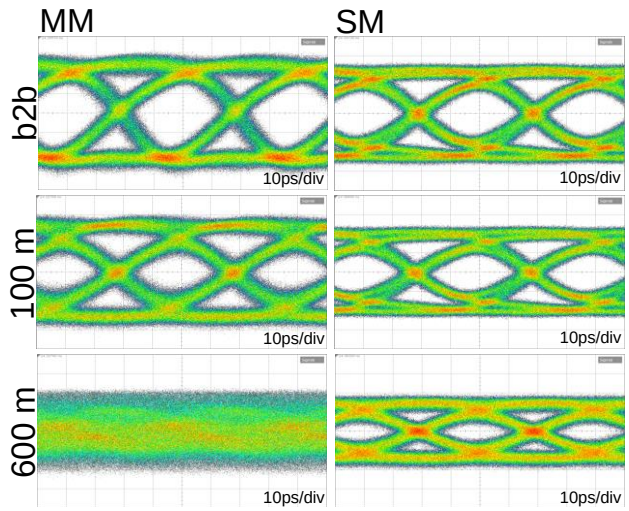

Fig. 3. 25 Gbit/s 850 nm MM and SM VCSEL eye diagrams at different distances

Figure 3 presents the eye diagrams at 25 Gbit/s captured at the various MMF lengths with MM and SM VCSELs. As we can see for b2b configuration (a few meter transmission) both SM and MM VCSEL signal are basically the same and show excellent system operation. With the increased transmission distance the signal distortion become visible. For the 100 m transmission, the MM VCSEL eye diagram is slightly closed compared to b2b, while at 600 it is completely distorted. For the SM VCSEL the eye diagram remains widely open up to 600 m, proofing that much longer transmission distances can be bridged with such type of VCSELs.

The realized transmission systems with MM VCSELs included transmission up to 54 Gbit/s with the OOK modulation over the distances up to 1 km [1] and 2.4 km [17]. Further, the MM and SM VCSEL can be utilized in transmission with advanced modulation formats. Advanced modulation formats, in opposition to the binary modulation, allow to transit more than one bit in one symbol, e.g. 2 bit/s for four level pulse-amplitude modulation (PAM-4) modulation. Therefor the spectrum utilization is significantly improved from 1 bit/s/Hz to 2 and more bit/s/Hz. That allows to overcome bandwidth limitations of the existing components and increase the achievable data rates. The drawback of the proposed solution is more complex structure of the transmitter and receiver. Further the required, signal-to-noise ratio is much higher than for binary modulation.

The performed work on the advanced modulation format transmission includes transmission with the PAM-4 modulation, again showing superior SM over MM VCSEL performance [16]. Even higher spectral efficiency was achieved with the carrier less amplitude-phase (CAP) modulation, which was utilized in many application with the very limited system bandwidth [25]. A variant of CAP modulation, namely multi-CAP was used in [14] to demonstrate the record at the time of publishing transmission of 107 Gbit/s. In multi-CAP transmission, the system bandwidth is divided into the sub-bands, in which one of the individual CAP signals are transmitted with the highest possible modulation order. In such a way, sub-bands with the excellent transmission properties transmit signals with high data rate, while the sub-bands with the limited transmission performance are utilized for the lower data rate signals. Further, the sub-band can be turned on-off adjusting to the varying traffic and therefore the variable data rate and energy efficient transmission can be realized [13].

To allow characterization and in general work with the newest VCSEL generations, a probe station had been designed and build. The probe station is based on the micrometric XYZ stages and allow connection of the electrical signals through the high bandwidth electrical probe as well as couple the optical signal into the fibre. The VCSEL chips can be observe though the side cameras. That simplifies the systems connections and adjustment. On Fig. 4., the photograph of the probe station is shown. The developed probe station can be used not only for the VCSEL testing but also for testing of other components like photo-detectors or even electronics circuits.

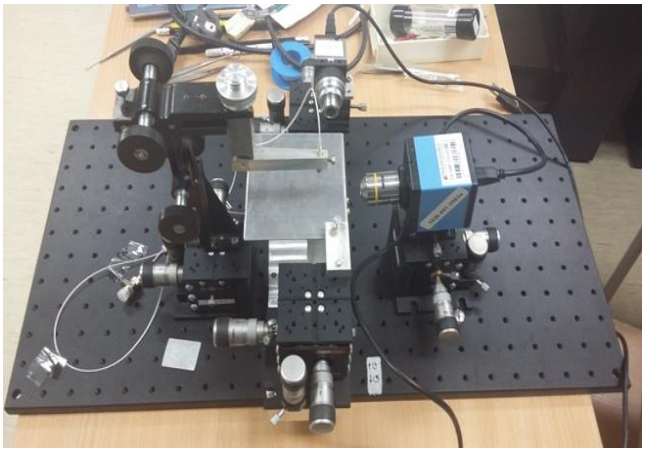

Fig. 4. Probe station used to test the bare (chip level) VCSELs

2. 1310 nm transmission

The 1310 nm transmission window (1260 nm – 1360 nm) was considered in the early years of optical fibre communication, namely mid 1970s as the key transmission band. That is reflected in the alternative 1310 nm window name O-band, where O stands for original. Fibre technology improvements resulted in conquering other bands like C-band (1550 nm), where C stand for conventional. For the very long time, the 1310 nm band has been utilized just for the upstream traffic in the passive optical networks (PON). In PON networks the downstream traffic to the user is realized in the 1550 nm band. Such wavelength band division comes from availability of the low cost and low loss 1310/1550 nm band splitters and combiners. The downstream PON data rates are up to 10 Gbit/s. In mid 2000s, work on the 100G and more Ethernet standard started, where one of the solutions is to transmit 100G and 400G Ethernet streams using multi-wavelength technology in the 1310 nm window. That is still bellow multi-terabit/s capacity of the 1550 nm band.

The key features of the 1310 nm transmission window are attenuation of about 0.3 dB/km – 0.4 dB/km, presence of the zero-dispersion wavelength and therefore limited chromatic dispersion as well as pronounced presence of the non-linear effects due to the low dispersion value. The higher than in the 1550 nm wavelength band losses (0.2 dB/km) must be compensated otherwise only very short unrepeated transmission can be realized. Three amplification technologies have been demonstrated for applications in the 1310 nm domain, namely semiconductor optical amplifier (SOA), praseodymium doped fibre amplifier (PDFA) and Raman amplifier. Recently, a bismuth doped fibre amplifier with the 25 dB gain, 3 dB saturation power of about 15 dBm and noise figure (NF) of about 5 dB has been demonstrated [18]. SOA and PDFA demonstrate moderate gain, high noise figure and moderate saturation power [2]. Progress in the high power quantum dot lasers allows realization of the 1310 nm Raman amplifier with the gain over 15–18 dB and very low noise figure [3, 12]. The 1310 nm Raman amplifier has been tested in the various transmission experiments, e.g. [10] outperforming SOA. Table 2 summarizes key transmission properties of the 1310 nm window amplifier technologies.

Table 2. 1310 nm optical amplifier comparison

	SOA	PDFA	Raman	BiDFA
Gain [dB]	25	25	18	25
Psat [dBm]	10	10	15	15
NF [dB]	>6	>6	4	5

Chromatic dispersion affects transmitted signals by limiting the available transmission range for the given data rate or limiting the data rate for the given transmission distance. The chromatic dispersion limits for SSMF are specified in ITU-T Recommendation G.652 [15]. The zero dispersion wavelength, a wavelength where no chromatic dispersion occurs must be between 1300 nm and 1324 nm. Figure 5 shows the chromatic dispersion limits for SSMF as specified in the ITU-T Recommendation G.652. The very low value of chromatic dispersion allows realization of the transmission systems without any form of the chromatic dispersion compensation. That just not only simplifies system design, but more importantly makes the installation straightforward, without necessity of dispersion measurements and compensation. These features are highly desirable in the data centre environment, where a large number of such systems must be installed. Further, the limited influence of the chromatic dispersion is a decisive advantage for the analog radio-over-fibre systems [6], where the signals are transmitted in the fibre in such a form than they can be directly emitted by the radio antenna just after the optical-to-electrical conversion. Such systems are of great importance for the development of the newest generation of mobile networks, namely 5G, in particular for the ultra-high carrier frequencies, which are needed to realize ultra-broadband and therefore high data rate radio transmission. The targeted here data rates are in the range of a few Gbit/s to the user.

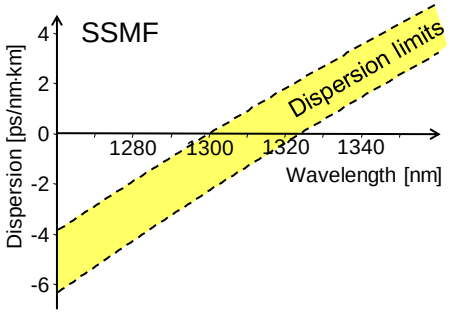

Fig. 5. SSMF chromatic dispersion limits at 1310 nm

However, looking at the Fig. 5. we can notice that at the edges of the O-band, namely 1260 nm and 1360 nm chromatic dispersion of a few ps/nm·km can be expected. Such high value of dispersion can influence high data rate transmission of 50 Gbit/s and more, even for distances of a few dozen kilometres. That dispersion value ca not be neglected and can be a source of severe performance limitations that can be omitted by the chromatic dispersion management in the fibre infrastructure [24].

Low value of chromatic dispersion can lead to pronounced nonlinear effect interactions like cross-phase modulation and in particular four-wave mixing (FWM). In FWM effect three co-propagating wave interacts with each other and a new wave is generated. A new FWM wave can appear at the data signal frequency, which will be a source of cross-talk. FWM can be effectively suppressed by lowering the signal power, transmission in the region with non-zero chromatic dispersion as well as large channel spacing. The conducted studies have shown that the channels spacing of about 250 GHz allows to effectively suppress FWM, while maintaining relatively high signal power in the range of 0 dBm for the 1310 nm band dense wavelength division multiplexed systems [8]. Obviously, spectral efficiency is not that high as in the 1550 nm band with the standard channels spacing of 50 GHz, nevertheless it is sufficient to realize transmission of a several and even few dozen channel with overall capacity in the order of Tbit/s.

Several research works have been devoted to that topic. In [20] n × 25 Gbit/s transmission in the 1310 nm band has been investigated, while [21] demonstrates up to 400 Gbit/s transmission with eight wavelength channels and data rates of 40 Gbit/s and 50 Gbit/s. Further, a single data channel transmission at 112 Gbit/s has been demonstrated in [9]. The polarization and wavelength multiplexing concept has been further expanded towards 1 Tbit/s transmission in [11].

One of the features of the 1310 nm band is feasibility of the parallel to the 1550 nm band utilization. The capacity of the optical fibre can be increased by the multi core or a few mode transmission. In such special fibre new spatial channels (multiple cores and/or multiple modes) are created. Obviously, the inter core and inter mode cross-talks must be compensated to achieve desired performance. Recognized alternative to that is utilization of the parallel to the 1550 nm wavelength bands like the 1310 nm or 1650 nm (U-band) [26]. That solution has advantage that the already existing fibre infrastructure can be used to carry additional data channels, postponing or even omitting necessity of the very expensive new fibre installation. Obviously, appropriate band multiplexers and demultiplexers must be inserted into the transmission line as well as suitable amplification technology must be used, with the most promising candidates of BiDFa and Raman amplifier. Due to the development of the all-optical signal processing techniques, the 1310 nm signals can be all-optically without any optical-electrical-optical conversion converted into the 1550 nm wavelength domain. Such an ultra-wide data wavelength conversion utilizing non-linear polarization rotation in the semiconductor optical amplifier has been demonstrated in [22]. In such a way, transparent all-bands optical networks can be realized. In other applications, the 1310 nm components were used for 1550 nm signal processing [20].

3. Conclusions

Optical fibre transmission technologies arc conquering new application areas. In particular, the growth of optical transmission is observed in the data center infrastructure. The deceive advantages of the optical fibre transmission are ultra-high data rates and energy efficiency, which cannot be fulfilled by the metal wire techniques. New transmission solution are tailored to the application needs. Here, the window of opportunity for the unutilized so far band has opened. The 850 nm window can be successfully applied to realize high data rate transmission at the ultra-short distances utilizing VCSELs and MMF. The 1310 nm window can be used to support intra data center transmission of high capacity over distances up to a few dozen kilometer.

Acknowledgements

The presented research has received funding from the European Union's Seventh Framework Programme (FP7/2007-2013) under grant agreement n°619197 – the ADDAPT project, Polish Ministry of Science and Higher Education science funds for years 2014-2017 granted for international project execution as well as the Polish National Science Centre NCN under the contract UMO-2011/03/D/ST7/02497. Further, I would like to thank VI Systems, Berlin, Germany (v-i-systems.com) for cooperation on the 850 nm VCSEL transmission.

References

[1] Chi K.-L., Shi Y.-X., Chen X.-N., Chen J., Yang Y.-J., Kropp J.-R., Ledentsov Jr. N., Agustin M., Ledentsov N.N., Stepniak G., Turkiewicz J.P., Shi J.-W: Single-Mode 850-nm VCSELs for 54-Gb/s ON–OFF Keying Transmission Over 1-km Multi-Mode Fiber. IEEE Photonics Technology Letters 12/2016, 1367–1370 [DOI: 10.1109/LPT.2016.2542099].

[2] Chorchos Ł., Turkiewicz J.P.: Experimental performance of semiconductor optical amplifiers and praseodymium-doped fiber amplifiers in 1310-nm dense wavelength division multiplexing system. Optical Engineering 56/2017, 046101 [DOI 10.1117/1.OE.56.4.046101].

[3] Czyżak P., Mazurek P., Turkiewicz J.P.: 1310 nm Raman amplifier utilizing high-power, quantum-dot pumping lasers. Optics & Laser Technology, 64/2014, 195–203 [DOI: 10.1016/j.optlastec.2014.05.013].

[4] https://www.nobelprize.org/prizes/physics/2009/kao/facts/ (available 30.05.2019).

[5] Kropp J.-R., Steinle G., Schäfer G., Shchukin V.A., Ledentsov N.N., Turkiewicz J.P., Zoldak M.: Accelerated aging of 28 Gb s−1 850 nm vertical-cavity surface-emitting laser with multiple thick oxide apertures. Semiconductor Science and Technology 30/2015 [DOI: 10.1088/0268-1242/30/4/045001].

[6] Larrode M.G., Koonen A.M.J., Vegas-Olmos J.J., Verdurmen E.J.M., Turkiewicz J.P.: Dispersion tolerant radio-over-fibre transmission of 16 and 64 QAM radio signals at 40 GHz. Electronics Letters 42/2006, 872–874 [DOI: 10.1049/el:20061311].

[7] Ledentsov N.N., Shchukin V.A., Kalosha V.P., Ledentsov N.N., Kropp J.-R., Agustin M., Chorchos Ł., Stępniak G., Turkiewicz J.P., Shi J.-W: Anti–waveguiding vertical–cavity surface–emitting laser at 850 nm: From concept to advances in high–speed data transmission. Optics Express 26/2018, 445–453 [DOI 10.1364/OE.26.000445].

[8] Markowski K., Chorchos Ł., Turkiewicz J.P.: Influence of the Four-Wave Mixing in short and medium range 1310 nm DWDM systems. Applied Optics 55/2016, 3051–3057 [DOI 10.1364/AO.55.003051].

[9] Mazurek P., Czyżak P., de Waard, H., Turkiewicz J.P.: Up to 112 Gbit/s single wavelength channel transmission in the 1310 nm wavelength domain. Microwave and Optical Technology Letters 2/2014, 263–265 [DOI: 10.1002/mop.28054].

[10] Mazurek P., Czyżak P., de Waardt H., Turkiewicz J.P.: SOA and Raman amplification for 1310 nm DWDM transmission. Optical Engineering 54/2015, 116104 [DOI: 10.1117/1.OE.54.11.116104].

[11] Mazurek P., de Waardt H., Turkiewicz J.P.: Towards 1 Tbit/s SOA based 1310 nm transmission for LAN/data center applications. IET Optoelectronics 9/2015, 1–9 [DOI: 10.1049/iet-opt.2014.0031].

[12] Nesset D., Wright P.: Raman extended GPON using 1240 nm semiconductor quantum-dot lasers. Optical Fiber Communication Conference (OFC) 2010, OThW6, April 2010.

[13] Puerta R., V. Olmos, J.J., Tafur Monroy I., Ledentsov N.N., Turkiewicz J.P.: Flexible MultiCAP Modulation and its Application to 850 nm VCSEL-MMF Links. IEEE Journal of Lightwave Technology 35/2017, 3168–3173 [DOI: 10.1109/JLT.2017.2701887].

[14] Puerta Ramirez R., Agustin M., Chorchos Ł., Tański J., Kropp J.R., Ledentsov Jr. N., Shchukin V.A.,. Ledentsov N.N, Henker R., Tafur Monroy I., Vegas Olmos J.J., Turkiewicz J.P.: Effective 100 Gb/s IM/DD 850 nm multi- and single-mode VCSEL transmission through OM4 MMF. IEEE Journal of Lightwave Technology 35/2017, 423–429 [DOI: 10.1109/JLT.2016.2625799].

[15] Recommendations ITU-T G.652 Characteristics of a Single-Mode Optical Fiber and Cable, (10/2009). Online. http://www.itu.int/rec/T-RECG.652-200911-I.

[16] Stępniak G., Chorchos Ł., Agustin M., Kropp J.-R., Ledentsov N.N., Shchukin V.A, Ledentsov Jr. N.N., Turkiewicz J.P.: Up to 108 Gb/s PAM 850 nm Multi and Single Mode VCSEL Transmission over 100 m of Multi Mode Fiber. ECOC 2016; 42nd European Conference on Optical Communication, Dusseldorf, Germany, 2016, 1–3.

[17] Stepniak G., Lewandowski A., Kropp J.R., Ledentsov N.N., Shchukin V.A., Ledentsov Jr. N., Schaefer G., Agustin M., Turkiewicz J.P.: 54 Gbps OOK transmission using single mode VCSEL up to 2.2 km MMF. IET Electronics Letters 52/2016, 633–635 [DOI: 10.1049/el.2015.4264].

[18] Thipparapu N.K., Umnikov A.A., Barua P., Sahu J.K.: Bi-doped fiber amplifier with a flat gain of 25 dB operating in the wavelength band 1320–1360 nm. Optics Letters 41/2016, 1518–1521 [DOI: 10.1364/OL.41.001518].

[19] Turkiewicz J.P., Kropp J.-R., Ledentsov N.N., Shchukin V.A., Schafer G.: High speed optical data transmission with compact 850nm TO-can assemblies. IEEE Journal of Quantum Electronics 50/2014, 281–286 [DOI 10.1109/JQE.2014.2304742].

[20] Turkiewicz J.P., Tangdiongga E., Rohde H., Schairer W., Lehmann G., Khoe G.D., de Waardt H.: Simultaneous high speed OTDM add-drop multiplexing using GT-UNI switch. Electronics Letters 10/2003, 795–796 [DOI: 10.1049/el:20030535].

[21] Turkiewicz J.P., de Waardt H.: Low Complexity up to 400-Gb/s Transmission in the 1310 nm Wavelength Domain. IEEE Photonics Technology Letters 11/2012, 942–944 [DOI: 10.1109/LPT.2012.2191278].

[22] Turkiewicz J.P., Khoe G.D., de Waardt H.: All-optical 1310 to 1550 nm wavelength conversion by utilising nonlinear polarisation rotation in semiconductor optical amplifier. Electronics Letters 1/2005, 29–30 [DOI: 10.1049/el:20057435].

[23] Turkiewicz J.P.: Cost-effective n × 25 Gbit/s DWDM transmission in the 1310 nm wavelength domain. Optical Fiber Technology 17/2011, 179–184 [DOI 10.1016/j.yofte.2011.01.010].

[24] Turkiewicz J.P: Analysis of the SSMF zero-dispersion wavelength location and its influence on high capacity 1310 nm transmission. 2013 Optical Fiber Communication Conference and Exposition and the National Fiber Optic Engineers Conference (OFC/NFOEC), Anaheim, CA, 2013, 1–3 [DOI: 10.1364/NFOEC.2013.JW2A.06].

[25] Wieckowski M., Jensen J.B., Tafur Monroy I., Siuzdak J., Turkiewicz J.P.: 300 Mbps transmission with 4.6 bit/s/Hz spectral efficiency over 50 m PMMA POF link using RC-LED and multilevel Carrierless Amplitude Phase modulation. 2011 Optical Fiber Communication Conference and Exposition and the National Fiber Optic Engineers Conference, Los Angeles, CA, 2011, 1–3.

[26] Winzer P. J.: Energy-efficient optical transport capacity scaling through spatial multiplexing. IEEE Photonics Technology Letters, 23/2011, 851-853 [DOI 10.1109/LPT.2011.2140103].

Ph.D. Jarosław Piotr Turkiewicz
e-mail: jturkiew@tele.pw.edu.pl

J.P. Turkiewicz received Ph.D. degree in optical communication from the Eindhoven University of Technology, The Netherlands in 2006 and D.Sc. in 2014 from the Warsaw University of Technology. Since 2007 he is with Institute of Telecommunication, Warsaw University of Technology. He published over 100 peer reviewed papers as well as contributed and led several national and international research projects. His scientific interests include high speed optical signal transmission and switching.

ORCID ID: 0000-0003-2345-4147

otrzymano/received: 15.05.2019 *przyjęto do druku/accepted: 15.06.2019*

DOI: 10.5604/01.3001.0013.2539

TOWARDS A DIFFERENT WORLD – ON THE POTENTIAL OF THE INTERNET OF EVERYTHING

Mirosław Płaza, Radosław Belka, Zbigniew Szcześniak
Kielce University of Technology, Faculty of Electrical Engineering, Automatic Control and Computer Science

Abstract. *Internet-based technologies are moving faster and faster into many spheres of our lives and at the same time are a key component of the ongoing technological revolution, which is why there are many ongoing scientific projects aimed at their development. The article presents a discussion on the development of Internet-based technologies known as the Internet of Everything (IoE). The paper presents the areas in which these technologies are most often used. A multi-layered reference model and a procedure for subsequent actions in designing innovative solutions in this area are presented.*

Keywords: Internet of Everything, Network, Telecommunication network, Cyberspace, Big Data analytics

W STRONĘ INNEGO ŚWIATA – CZYLI O POTENCJALE INTERENTU WSZECHRZECZY

Streszczenie. *Technologie internetowe wkraczają coraz szybciej w liczne sfery naszego życia i jednocześnie stanowią kluczowy komponent trwającej dziś rewolucji technologicznej, dlatego też prowadzonych jest obecnie wiele projektów naukowych ukierunkowanych na ich rozwój. Artykuł przedstawia dyskusję dotyczącą rozwoju technologii internetowych znanych pod nazwą Internetu wszechrzeczy (IoE). W pracy pokazano obszary, w których technologie te znajdują najczęściej zastosowania. Przytoczono wielowarstwowy model referencyjny oraz procedurę kolejnych działań przy projektowaniu nowatorskich rozwiązań w tym zakresie.*

Słowa kluczowe: Internet wszechrzeczy, sieć teleinformatyczna, cyberprzestrzeń, analityka Big Data

Introduction

The history of humanity has been repeatedly shaped by the achievements of science and progress in the development of new technologies. Civilisation would not be at its current level of advancement if it were not for a series of innovative solutions from different areas of science gradually adopted over subsequent centuries. The invention in the past of things we consider basic today, such as the wheel, writing, paper or print, was undoubtedly an important point in our history. The discovery of paper and printing has led to real revolutions in the area of communication and transfer of information between people. The discoveries of the 19th and 20th centuries were of great importance in the field of human communication. The invention of the telephone, car, radio or television revolutionised people's lives and, above all, made them easier. Today, these technologies are constantly evolving, introducing new solutions and services, which would not be possible without further inventions, such as computers and Internet technologies. The first computer in history is considered to be the ENIAC. As a curiosity it is worth mentioning that it occupied 167m^2 of area, consisted of 42 cabinets, reached over 2.6 meters in height and measured 24 meters in length. In turn, its total weight exceeded 27 tonnes [7, 8]. By comparison, the smallest computer today, developed by Michigan scientists, is only 0.3 millimetres long [24]. This example shows how fast and effective can the development of teleinformatic technologies be in present times. Nowadays, the complexity of the infrastructure and requirements for the specialised systems, force their designers to introduce interdisciplinary solutions from various fields of science combining issues from within computer science, telecommunication, electronics, electrical engineering or others areas [14, 15, 16].

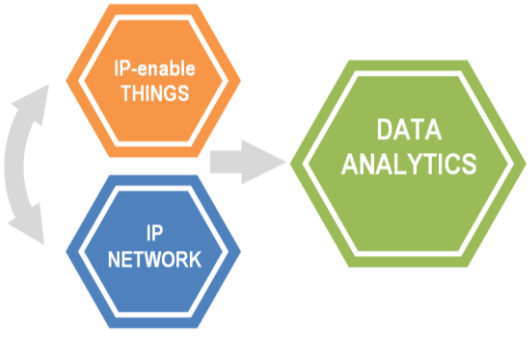

Fig. 1. A diagram presenting the idea of the IoT technology

The Internet of Things (IoT) concepts are currently one of the fastest growing ICT technologies, which have a significant impact on and benefit science and the economy. These solutions are based on the idea of linking everyday objects into a computer network, mainly for the exchange, processing and analysis of data. A simple diagram on figure 1 visualizing the idea of IoT technology.

The Internet of Things has been functioning in global solutions for many years, although not directly under the current name. So far, it has included the notions of telemetry, intelligent cities and buildings, sensory networks or other solutions based on technological applications of computer networks. The lack of detailed legal regulations and target standardisation in this area translates into the emergence of many separate terms for this concept used by scientific institutions, manufacturers of hardware or software. This means that due to its scale, innovation and constant dynamic development, a clear definition of the IoT issue is not a simple task. From the literature of the world we learn that the IEEE describes the concepts of IoT as: "A network of items – each embedded with sensors – which are connected to the Internet" [10]. In the ITU recommendation [18] the Internet of Things is defined as: "A global infrastructure for the information society, enabling advanced services by interconnecting (physical and virtual) things based on existing and evolving interoperable information and communication technologies". Another noteworthy definition of the IoT technology was proposed by the OASIS association: "System where the Internet is connected to the physical world via ubiquitous sensors" [4]. One step further in defining IoT was taken by the world leader in ICT – Cisco, dubbing the discussed solutions the Internet of Everything (IoE). According to [3], the Internet of Everything is "bringing together people, process, data and things to make networked connections more relevant and valuable than ever before, turning information into actions that create new capabilities, richer experiences and unprecedented economic opportunity for businesses, individuals and countries". The Internet of Everything is a natural successor to the concept of the Internet of Things, successfully entering today into many spheres of our lives, and at the same time being a key component of the technological revolution known as Industry 4.0 [23], incorporating into the web everything that has not yet been connected.

1. Connecting unconnected

The Internet of Everything is a network which is created with the use and adoption of existing solutions, among others, in the field of computer science, ICT, sensorics, automation, electronics or data analytics. Everything that has not yet been incorporated

into the global network infrastructure may soon become a part of it. This is largely due to the constant development of Internet protocols, which provide broad perspectives for the use of modules compatible with Ethernet, TCP/IP, Wi-Fi or LoRaWAN standards. The application potential of IoT/IoE solutions is practically unlimited. It includes for example: smart homes / buildings / cities, smart health solutions, smart businesses and industry, smart energy systems and grids, distributed metering systems or threat monitoring systems. A very important and at the same time popular issue is the application of the discussed technologies in environmental protection measures [17], which are related to e.g. monitoring of air, soil or water pollution. The positive impact on the environment is also reflected in the low energy consumption of equipment implemented in the IoT/IoE technologies, thus making the discussed solutions extremely important from the point of view of global problems. Other popular trends in the development of the described solutions are real-time object localization systems implemented in many branches of industry and business [1, 11, 12, 13]. Table 1 shows the areas where IoT/IoE projects have the widest applications [20]. The presented data show that the trend associated with the concepts of Smart City and Connected Industry is decidedly dominant. The use of these technologies in Connected Building, Connected Car and Smart Energy is at a slightly lower level. Other industries use modern Internet-based technologies to a lesser extent.

Table 1. Areas of application of IoT technologies [13]

IoT/IoE Segment	Number of IoT projects
Smart City	23%
Connected Industry	17%
Connected Building	12%
Connected Car	11%
Smart Energy	10%
Other	8%
Connected Health	6%
Smart Supply Chain	5%
Smart Agriculture	4%
Smart Retail	4%

A large set of Internet of Everything devices, which are combined in a single global network infrastructure, creates a powerful tool that can be adapted to different needs. However, this requires the integration of interdisciplinary solutions from the field of, among others, sensors, electronics, wireless communication, automation, information distribution networks, or data analytics or machine learning. The combination of all or some of these elements will ensure the learning of new, undiscovered knowledge.

2. Gathering the knowledge

One of the intentions of the implemented IoE solutions is to acquire large amounts of data, which after the initial acquisition and initial processing are sent through the web to the data centres for further processing and practical use. In the era of today's technological solutions, especially omnipresent video monitoring [9], these are usually very large data sets, in the analysis of which conventional statistical methods are not applicable. In addition, the literature indicates that the amount of data sent over the web will increase significantly in the coming years. According to the report Cisco Global Cloud Index: Forecast and Methodology [5], global Data Centers in 2021 will process 20 trillion of bytes of data per year, and this number will increase annually by an average of 20–25%. These data may come in unexpectedly and in various forms – they may be e.g. unstructured and/or non-relational, and additionally they do not always have to be reliable. Therefore, an important challenge for data analytics is to extract useful knowledge from the generated stream of diversified and difficult to interpret information sets. For this reason, the concepts of the Internet of Everything are usually based on innovative issues related to Big Data analytics. Big Data includes working with data that is compatible with the 4V model (Volume, Velocity, Veracity, Value) [19]. In the context of Big Data analytics methods, cloud computing (SaaS, PaaS), distributed file systems (Hadoop), parallel processing platforms (MapReduce), non-relational databases (noSQL), machine learning and artificial intelligence are also important. The way in which we obtain, send, store, secure and interpret information is the primary task of Big Data. In addition, Big Data methods have changed the approach to Analytic Lifecycle issues, which is presented on figure 2.

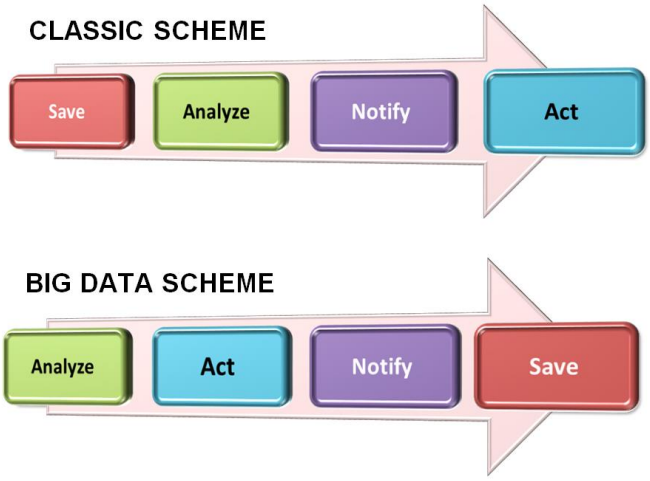

Fig. 2. Classic and Big Data schemes for Analytics Lifecycle

From the traditional Save – Analyse – Notify – Act scheme we move to the much more challenging scheme: Analyse – Act – Notify – Save [2]. The difference in the approach to Big Data issues in relation to conventional methods is apparent, among others, through the preliminary analysis of data already performed at the stage of their acquisition. Only data relevant to the examined problem are saved. All other data can be filtered out using network edge elements, e.g. single-board computers (SBC) as Raspberry Pi. It is the responsibility of the Edge Computing layer integrated into the multilayer reference model developed for Internet of Everything technologies, shown in figure 3.

Fig. 3. A multi-layer reference model for the IoE technology [21]

Physical Devices and Controllers layer is a collection of all "things" connected to the IoE infrastructure. These include, for example: precise real-time object location systems, video systems and various sensor networks. Thanks to the functionality of the second layer, these elements can communicate with each other, using dedicated network solutions, cooperating and generating large amounts of data pre-filtered at the level of the third layer. The filtered data are stored in the Data Accumulation layer and prepared for further applications and analysis in the Data Abstraction layer. Next, they are passed in a structured format to the Application layer, where they should be properly interpreted according to their specific applications. The top layer includes different areas of application of the received data in the implemented solutions [21].

3. Towards the another (better?) World

A Sustainability Summit was held in September 2015 in New York City, where the international community adopted a new world development plan until 2030 in the form of a Sustainable Development Agenda (Agenda 2030) [22]. The new Agenda contains 17 sustainable development objectives and 169 tasks to be achieved. Many of the agenda's guidelines pose new challenges to the Internet of Everything technology. Figure 4 presents a workflow showing subsequent sequences of activities aimed at using modern technologies from the IoE area in designing solutions for the needs of today's civilization.

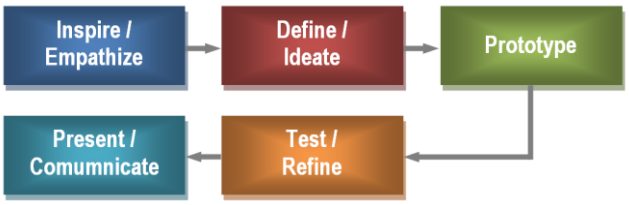

Fig. 4. IoE systems designing process [6]

Analysing Figure 4, we can notice that the whole process of action in designing innovative solutions begins with inspiration against the needs and stirring the empathy of the audience. This means that one of the most important elements is a suitably attractive, needs-oriented idea. Then, using the latest achievements in the field of modelling, prototyping, implementation and testing of ICT systems and Internet of Things technologies, we should strive to achieve the intended objectives. It is important to note that current technical solutions in the field of sensor electronics (nanoelectronics), localization and communication technologies (e.g.: RFID-2gen, IBeacon, Cisco Hyperlocation, UWB, NB-IoT, LoRaWAN), microcontrollers and single-board computers (e.g.: Arduino, SBC Raspberry Pi, ESP32, Rock Pi, Banana Pi and other), secure IPv6 network technologies (VPN, ASA, Cisco ISR, Meraki AP), as well as the availability of platforms and programming libraries used in the implementation of machine learning algorithms (e.g.: TensorFlow, PyTorch, Keras, scikit-learn-on Github-type public platforms) provide the possibility to create useful, competitive, flexible, scalable, secure and transparent IoE networks.

In reference to the concepts presented above and in order to meet human needs, visions of strictly pro-social projects are already proposed. One example is the PRO-HOMINIS System (PROgressive Health-Oriented Motivation System), proposed by us, based on the IoE Novel-Innovative Solution. This system is a concept of an intelligent tool activating its users to greater physical activity, which is also to contribute to the prevention of civilisation diseases of our times. As the proposed PRO-HOMINIS name suggests, the system would motivate people to be more active by monitoring their behaviour, in a way forcing them to visit specific places on a digital map of the area.

Another concept is the TARGET – "Tracking Adopted, Routing Guide application for Effective Transport" The task of the system would be to adapt the route strategy based on the technology of distributed sensory networks. This system would represent a product innovation for existing GPS-based transport monitoring systems. Thanks to IoE solutions and metaheuristic optimization algorithms, including the latest developments in Swarm Intelligence, it would be possible to create a product enabling reduction of direct and indirect costs of passenger and freight transport, as well as to reduce the energy consumption of the currently operating transport fleets.

The above-mentioned examples of projects utilising the Internet of Everything are clearly in line with the sustainable development objectives set out in the above-mentioned agenda [22]. The current literature also describes many other interesting examples which can be successfully implemented in the near future and which will be targeted at certain groups or even entire societies. It should be remembered that the broadly understood science and technology should serve primarily the common good, contribute to solving various social problems and achieve the intended objectives of specific social groups and individuals. At the same time, they should provide a wide range of ideas, concepts, solutions and innovations. Analysing the fate of humanity, one can easily point to many examples where science and technology were used in a way that threatened man. However, it is worth trusting that the Internet of Everything will bring spectacular benefits in solving both local and global socio-economic problems.

4. Conclusion

Generally speaking, the idea of implementing IoE systems involves the acquisition of sensory information (data) by means of distributed networks, which, transformed by successive layers of the reference model, constitute knowledge that brings significant benefits to the beneficiaries of these systems. It should also be noted that the Internet of Everything is first and foremost about the "Internet of Ideas", because the measure of these benefits depends on properly set goals and proper implementation of the IoE architecture. A great advantage of the devices used in the IoE is their low energy consumption, which in itself is a measurable benefit for both the beneficiary and our environment.

Currently in Poland the market of services related to IoT/IoE is developing very dynamically, annually increasing the number of its customers. This changes the quality of life in the society, but at the same time introduces new threats. In many cases there are problems with protecting the processed data. Therefore, in parallel with the development of IoT/IoE, a lot of cybersecurity research is being carried out.

Today, there are no ideal solutions that could fully exploit the potential of the Internet of Everything technologies yet. It is possible that such solutions will appear with the arrival of the 5G network, because the potential for IoE applications is immense. In December 1959, the renowned physicist Richard Feynmann said the famous words "There is plenty of room at the bottom", outlining the application potential of nanotechnology. Similarly, one could say "There is plenty of room on the Internet of Everything".

Acknowledgment

This paper was supported by the European Union's Smart Growth Operational Programme 2014-2020, under grant agreement no POIR.04.01.02-00-0041/17-00, „CyberMatryca – Integrated Visitors' Support Systems"

References

[1] Belka R., Deniziak S., Płaza M., Hejduk M., Pięta P., Płaza M., Czekaj P., Wołowiec P., Ludwinek K.: Integrated Visitor Support System for Ttourism Industry Based on IoT Technologies. Proceedings of SPIE, Photonics Applications in Astronomy, Communications, Industry, and High-Energy Physics Experiments, Wilga 2018, 108081J [DOI: 10.1117/12.2326403].
[2] Belka, R.: An Indoor Tracking Systems and Pattern Recognition Algorithms as Key Components of IoT-based Entertainment Industry. Proceedings of SPIE, Photonics Applications in Astronomy, Communications, Industry, and High-Energy Physics Experiments, Wilga 2019, 11176.
[3] Bradley J., Barbier J., Handler D.: Embracing the Internet of Everything to Capture Your Share of $14.4 Trillion. Cisco, 2013.
[4] Camarinha-Matos L. M., Tomic S., Graca P.: Technological Innovation for the Internet of Things. 4th IFIP WG 5.5/SOCOLNET Doctoral Conference on Computing, Electrical and Industrial Systems – DoCEIS, Costa de Caparica 2013, 3–12.
[5] Cisco Company.: Cisco Global Cloud Index: Forecast and Methodology 2016–2021. Cisco, November 19, 2018, 1–46.
[6] Cisco Company.: IoT – Connecting Things. Course Materials. Cisco Networking Academy, 2019.
[7] Cleveland D.: Seven Wonders of Communication. Twenty-First Century Books, Minneapolis 2010.
[8] Goldstine H. H., Goldstine A.: The Electronic Numerical Integrator and Computer (ENIAC). IEEE Annals of the History of Computing 18/1996, 10–16 [DOI: 10.1109/85.476557].
[9] Królikowski M., Płaza M., Szcześniak, Z.: Chosen Sources of Signal Interference in HD-TVI Technology. Proceedings of SPIE, Photonics Applications in Astronomy, Communications, Industry, and High-Energy Physics Experiments, Wilga 2017, 104455M [DOI: 10.1117/12.2280534].

[10] Minerva R., Biru A., Rotondi D.: Towards a Definition of the Internet of Things. IEEE Internet Initiative. Telecom Italia, Torino 2015.
[11] Pięta P., Deniziak S., Belka R., Płaza M., Płaza M.: Multi-domain Model for Simulating Smart IoT-based Theme Parks. Proceedings of SPIE, Photonics Applications in Astronomy, Communications, Industry, and High-Energy Physics Experiments, Wilga 2018, 108082T [DOI: 10.1117/12.2501659A].
[12] Płaza M., Belka R., Płaza M., Deniziak S., Pięta P., Doszczeczko S.: Analysis of Feasibility and Capabilities of RTLS Systems in Tourism Industry. Proceedings of SPIE, Photonics Applications in Astronomy, Communications, Industry, and High-Energy Physics Experiments, Wilga 2018, 108080C [DOI: 10.1117/12.2500558].
[13] Płaza M., Deniziak S., Płaza M., Belka R., Pięta P.: Analysis of Parallel Computational Models for Clustering. Proceedings of SPIE, Photonics Applications in Astronomy, Communications, Industry, and High-Energy Physics Experiments, Wilga 2018, 108081O [DOI: 10.1117/12.2500795].
[14] Płaza M., Szcześniak Z., Dudek J.: Generation of medium frequency electrotherapeutic signals. Proceedings of SPIE, Photonics Applications in Astronomy, Communications, Industry, and High-Energy Physics Experiments, Wilga 2017, 104452T [DOI: 10.1117/12.2274764].
[15] Płaza M., Szcześniak Z.: Signal processing system for electrotherapy applications. Proceedings of SPIE, Photonics Applications in Astronomy, Communications, Industry, and High-Energy Physics Experiments, Wilga 2017, 104452W [DOI: 10.1117/12.2280095].
[16] Płaza M.: Chosen models of VCVS having parameters set digitally. Proceedings of SPIE, Photonics Applications in Astronomy, Communications, Industry, and High-Energy Physics Experiments, Wilga 2008, 71240N [DOI: 10.1117/12.817952].
[17] Radu (Genete) L. D.: Internet of Things – A New Challenge for Environmental Protection. The 26th IBIMA Conference on Innovation Management and Sustainable Economic Competitive Advantage: From Regional Development to Global Growth, Madrid 1/2015.
[18] Recommendation ITU-T Y.2060.: Series Y: Global Information Infrastructure, Internet Protocol Aspects and Next-Generation Networks, Next Generation Networks – Frameworks and Functional Architecture Models. ITU-T , Geneva 2013.
[19] Sai Jyothi B., Jyothi S.: A Study on Big Data Modeling Techniques. International Journal of Computer Networking, Wireless and Mobile Communications, TJPRC Pvt. Ltd. 5/2015, 19–26.
[20] Scully P.: The Top 10 IoT Segments in 2018 – based on 1,600 real IoT projects. IOT Analytics, February 22, 2018. https://iot-analytics.com/top-10-iot-segments-2018-real-iot-projects/ (available: 25.05.2019).
[21] Shakib Y, Kirby S.: 2015 Predictions: The highest-impact IoE advancements in Retail. Digital Transformation, January 16, 2015. https://blogs.cisco.com/digital/2015- predictions-the-highest-impact-ioe-advancements-in-retail (available: 27.05.2019).
[22] United Nations.: Transforming Our World: The 2030 Agenda for Sustainable Development A/RES/70/1. New York 2015.
[23] Ustundag A., Cevikcan E.: Industry 4.0: Managing The Digital Transformation. Springer International Publishing, Switzerland 2018.
[24] Wu X. et al.: A 0.04MM316NW Wireless and Batteryless Sensor System with Integrated Cortex-M0+ Processor and Optical Communication for Cellular Temperature Measurement. IEEE Symposium on VLSI Circuits, Honolulu 2018, 191–192.

Ph.D. Mirosław Płaza
e-mail: m.plaza@tu.kielce.pl

Researcher at the Kielce University of Technology. Head of the ICT and IoT Laboratory. He is strongly involved in the development of modern ICT at the Faculty of Electrical Engineering, Automatic Control and Computer Science. Author of 2 award-winning patents and over 50 scientific publications. He holds instructor's qualifications i.a.: CCNA, CCNASecurity, IoT (Connecting Things, Big Data).

ORCID ID: 0000-0001-9728-3630

Ph.D. Radosław Belka
e-mail: r.belka@tu.kielce.pl

The assistant professor at the Kielce University of Technology and certified instructor of the Cisco Networking Academy program. Head of the R&D Grant no: POIR.04.01.02-00-0041/17 "Cybermatryca – an integrated tourist service system" dedicated to the use of IoE technology in the tourism industry. His work focuses on data analysis, electronic sensors and materials sciences.

ORCID ID: 0000-0002-6283-3724

Prof. Zbigniew Szcześniak
e-mail: z.szczesniak@tu.kielce.pl

Employee of the Kielce University of Technology. His scientific and professional interests focus mainly on automation and electronics devices, as well as measurement systems used in the automation of technological processes. He is the author of over 110 scientific and rsesearch papers, including 3 monographs and 13 patents, as well as the promoter and reviewer of over a hundred diploma papers.

ORCID ID: 0000-0002-7896-3291

otrzymano/received: 15.05.2019 *przyjęto do druku/accepted: 15.06.2019*

DOI: 10.5604/01.3001.0013.2540

USE OF THERMAL IMAGING IN CONSTRUCTION

Danuta Proszak-Miąsik
Rzeszow University of Technology, The Faculty of Civil and Environmental Engineering and Architecture/Department of Heat Engineering and Air Conditioning

Abstract. *Thermovision is a research method based on non-invasive and non-contact evaluation of temperature distribution on the surface of the examined body. These methods are based on observation and recording of the distribution of infrared radiation, sent by each body whose temperature is higher than absolute zero (-273℃) and visualization of the temperature field by thermal imaging equipment. In construction, thermovision is used to assess the quality of materials used in construction, structural solutions and the quality of construction work. With its help we can locate, for example, thermal bridges, which are the result of improperly made or damaged during the operation or installation of thermal insulation. Detection of thermal bridges helps to reduce the amount of fuel used and thus save on the costs of heat energy. Using thermal imaging it is also possible to assess the condition of heating pipelines (damage to insulation, corrosion, location of leaks), control heating devices such as: heat substations, radiators. The subject of the study is to show examples of how thermal imaging is used and useful in construction.*

Keywords: thermal imaging, infrared radiation, heat loss, thermal imaging camera

ZASTOSOWANIE TERMOWIZJI W BUDOWNICTWIE

Streszczenie. *Termowizja to metoda badawcza polegająca na bezinwazyjnej i bezdotykowej ocenie rozkładu temperatury na powierzchni badanego ciała. Metoda ta opiera się na obserwacji i zapisie rozkładu promieniowania podczerwonego, wysyłanego przez każde ciało, którego temperatura jest wyższa od zera bezwzględnego (-273℃). Wizualizacji pola temperaturowego wykonywana jest przez aparaturę termowizyjną. Zaletą pomiarów termowizyjnych jest ich mobilność, fakt że wyniki pomiarów otrzymujemy w tej samej chwili i możemy je rejestrować w formie zdjęć lub filmów w zależności od typu kamery. W budownictwie termowizja wykorzystywana jest do oceny jakości zastosowanych do budowy materiałów, rozwiązań konstrukcyjnych oraz jakości wykonania prac budowlanych. Przy użyciu termowizji można również dokonać oceny stanu rurociągów grzewczych (uszkodzenia izolacji, korozję, z lokalizować nieszczelności), dokonywać kontroli urządzeń grzewczych, takich jak: węzły cieplne, grzejniki. Przedmiotem opracowania jest pokazanie w jaki sposób termowizja jest wykorzystywana i przydatna w budownictwie. na przykładzie wykonanych badań i przy użyciu profesjonalnego oprogramowania do obróbki termogramów.*

Słowa kluczowe: termowizja, promieniowanie podczerwone, straty ciepła, kamera termowizyjna

Introduction

Thermovision is a research method based on non-invasive and non-contact evaluation of temperature distribution on the surface of the examined body. This method is based on the observation and recording of the distribution of infrared radiation, sent by each body whose temperature is higher than absolute zero (–273°C). The visualization of the temperature field is performed by thermal imaging equipment. The advantage of thermographic measurements is their mobility, the fact that the results of measurements are obtained at the same time and we can record them in the form of photos or films depending on the type of camera. In construction, thermal imaging is used to assess the quality of materials used in construction, structural solutions and the quality of construction work. With its help we can locate, for example, thermal bridges, which are the result of improperly made or damaged during the operation or installation of thermal insulation. Detection of thermal bridges can reduce the amount of fuel used and thus save on the cost of heat energy. Using thermal imaging it is also possible to assess the condition of heating pipelines (damage to insulation, corrosion, location of leaks), control heating equipment such as: heat exchangers, radiators and detect irregularities in the operation of equipment such as: pumps and electric motors, allowing early removal of damage and prevent the occurrence of more serious failures. The subject of the study is to show how thermal imaging is used and useful in the construction industry. On the example of research and using professional software to process thermograms [5].

1. Thermography and thermovision

Thermography is the conversion of an infrared image into a radiometric image, which allows to read temperatures. Because infrared radiation has more energy than visible radiation, it can be detected from a greater distance than visible radiation. This is done by means of an installed infrared radiation detector matrix and a cooperating image search system. The micro-bolometer detector used, which is designed to detect the temperature reaching the camera's thermal radiation, produces a type of electrical signal based on the reading from the pixel sensor matrix, which in the next stage is converted to a digital form, which is displayed on the camera's display. The obtained image is called a thermogram or thermal image. The temperature distribution in the studied objects is presented in the form of coloured isotherms, where one color corresponds to points of the same temperature.

It should be remembered, however, that the stream reaching the lens of the thermal camera is the sum of the streams: the proper one (sent by the examined object), scattered and reflected from the surface of the examined body. Each thermal radiation is also to some extent attenuated by the atmosphere between the camera and the examined body. The measurement results are also influenced by: sun rays absorbed and reflected by the observed surface, interfering factors coming from the environment (clouds, sky, high air humidity) and other objects of elevated temperature that are in the environment (furnaces, heaters, etc.).

Therefore, in order for the thermal imaging device to correctly determine the object temperature, the camera operator must enter the following data

- emission factor, which determines the amount of energy emitted by a given body to the energy that should be emitted by the so-called black body (which is the emission standard).
- the distance of the object-camera in order to determine the transmission of the atmosphere,
- the temperature of the atmosphere,
- humidity of the air,
- the temperature of the ambient radiation reflected from the object (in most cases it is assumed to be equal to the temperature of the atmosphere).

The main reason for measurement errors is incorrect camera setting and the introduction of false ambient and measurement parameters. [2, 3]

2. Use of thermal imaging in construction

The range of tests performed with thermal imaging cameras in the building industry is wide, but most often it is used for:

- to detect heat losses in the building by checking:
  - thermal insulation of buildings,
  - location of thermal bridges,
  - cracks in the structure of buildings,

- the work of ventilation, air conditioning and heating systems,
- the state of thermal insulation of boilers, pipelines,
- leaks in windows and doors,

- to search for leaks and leaks in pipes,
- for the detection of moisture in walls and structural elements (roof leaks),
- to monitor the drying of bulkheads,
- to locate the wires in the bulkheads,
- to evaluate the electrical installation [6].

3. Conditions under which photographs are taken

When detecting anomalies in the building industry, it is important to observe a few rules when taking pictures. They will depend on the location of the measurement. If the tests are carried out outside the building, they are carried out under certain atmospheric conditions, i.e. under certain conditions:

- if there is no sunlight, it is best to choose a cloudy day,
- at a wind speed not exceeding 1 m/s (windless day),
- with no precipitation (walls should be dry),
- the difference in temperature between the room temperature and the outside temperature should not be less than 15 K

in addition:

- the building should be stable and heated (select a period of stabilized outside temperature),
- we don't open windows,
- we avoid sharp angles of "looking at the object",
- we don't consider windows [7].

4. Examples of thermal imaging applications in construction

Below are some examples of the use of thermal imaging in construction. The results of the research were presented in the form of thermograms. Colour thermograms present quantitative distributions of temperatures in the form of colourful isotherms, each of which represents a certain range of temperatures. The temperature ranges together with the colour scale are given on the right side of each thermogram. For better orientation, linear profiles have been added to the thermograms, they represent the temperature variation along the determined profile. Most of the thermograms also include video photographs of the object being tested. The thermographs also show the maximum and minimum temperatures for the examined areas. The study was performed with IR 928+ camera. Detailed analysis of thermal images was performed with the use of Guide IR Analyser software [1, 4].

4.1. Checking the effect of thermal upgrading of the building

Measurements were made for the thermomodernized facility of the Rzeszów University of Technology. The measurements were carried out on 31 January after sunset (after midnight - the previous cloudy day) and a year later on 14 February, in similar weather conditions. The photos (Fig. 1–2) show a selected fragment of the building K, Rzeszów University of Technology at Powstańców Warszawy Street. The measurements were taken before and after the thermal modernization of the building. The obtained thermograms were corrected due to the emission of windows and the surface of external walls. The correct ambient temperature has also been taken into account. Thermograms were performed (depending on the terrain possibilities) from a distance of 10 m.

As can be seen in Fig. 3-4, the average temperature of the wall between windows at the temperature outside -6°C is 17.7°C, max. temp. 19°C and min. 15.8°C. After insulating the wall with 8 cm layer of polystyrene foam, the partition temperatures decreased in the same place during similar weather conditions (Fig. 5-6). The average temperature was 10.6°C, maximum 11.2°C and minimum 10.5°C. The heat losses through the walls decreased. The partition image became almost homogeneous. The assumed effect was obtained.

Fig. 1. A fragment of a wall of a thermal upgrading building (before thermal upgrading)

Fig. 2. A fragment of a wall of a thermal upgrading building (afterthermal upgrading)

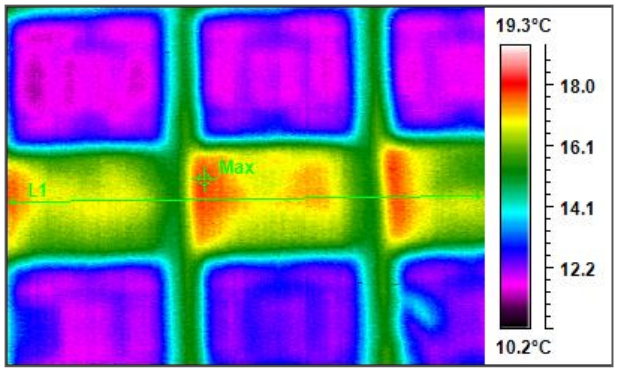

Fig. 3. Thermographic image of a selected fragment of the partition before thermal upgrading

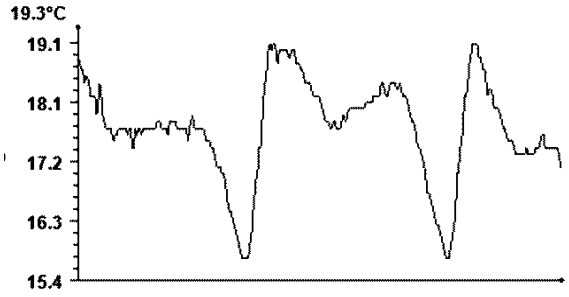

Fig. 4. Temperature linear profile

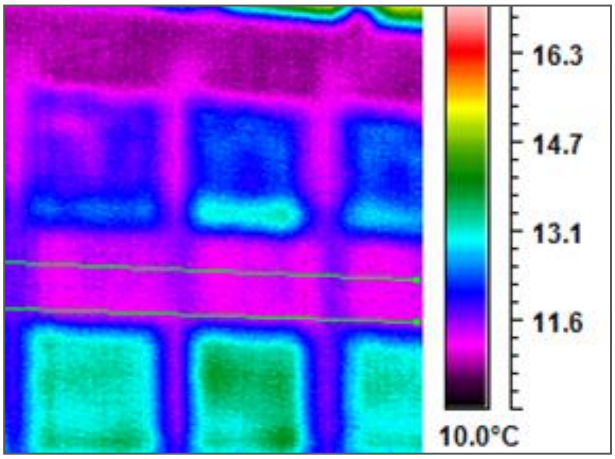

Fig. 5. Thermographic image of a selected fragment of the partition after thermal upgrading

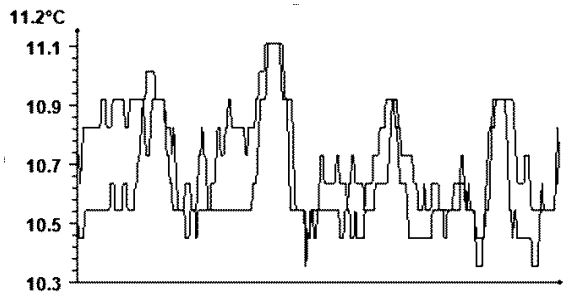

Fig. 6. Temperature linear profile

4.2. Temperature distribution on the building

The thermally inspected building is a single-family detached building that has been inhabited for a year. It is realized in the SUNDAY System technology. It is a steel skeleton made of thin-walled galvanized cold-formed sections. The heat transfer coefficient of walls is u = 0.28 W/m^{2}K, while the heat transfer coefficient of windows is u = 1.1 W/m^{2}K.

The temperature linear profile (Fig. 9) shows that there is an increase in temperature at the connection of the roof with the external wall, and at the connection of the external wall with the foundation (red line), at the corner (green line), losses at windows and balcony (blue line).

Fig. 10 shows intensive thermal bridges at window and door lintels and thermal bridges at the connection of the wall with the foundation and the roof. A higher temperature at the roof (about 2°C higher than the elevation temperature) is also a result of warm shade (surfaces shielded from the radiation influence of the cold sky). The setting of the balcony is not very effective in terms of thermal insulation.

Higher temperature of the upper part of window openings (at lintels) is also influenced by two phenomena: the phenomenon of warm shade and the accumulation of warmer air (which is why the upper edges of window openings are warmer, first of all). The windows themselves, on the basis of thermograms analysis, perform relatively well.

Fig. 7. View of the building under investigation

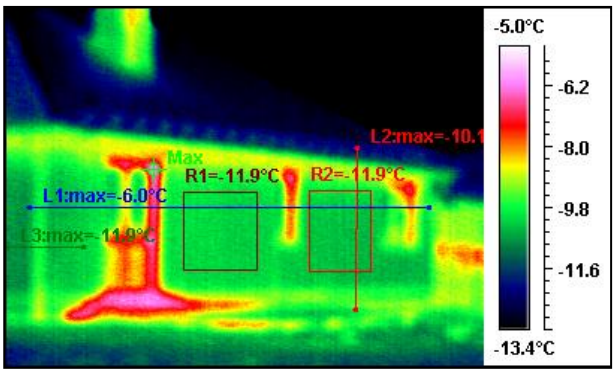

Fig. 8. Thermal imaging

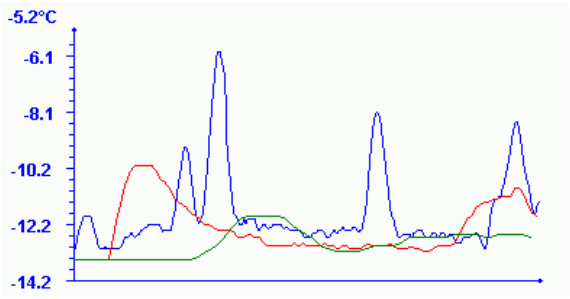

Fig. 9. Temperature linear profile

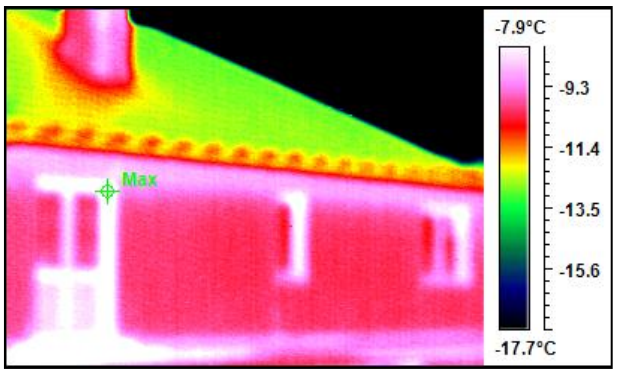

Fig. 10. Thermal imaging

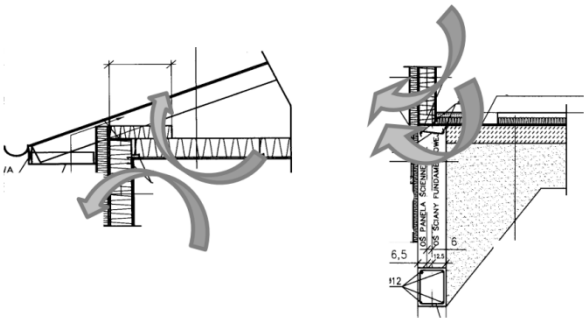

Fig. 11. Details of the connection: a) walls with a roof b) walls, foundations and floors

4.3. Control of the wall heating system implementation

Thanks to thermal imaging we can easily check and locate wires and pipes under the surface. On the photo (Fig. 12) there is a preview of the wall in which heat pipes are installed. Heat pipes are filled with low boiling liquid, which heats up from the heating medium flowing in the lower part of the pipes and changes its state of concentration to steam. The steam rises upwards and releases heat to the environment and cools and condenses, flowing down the tube and the cycle repeats itself. As you can see (Fig. 12), the middle tube was damaged during assembly, it is not filled with low boiling liquid, so it does not heat up. The linear section (Fig. 13, 14) confirms this.

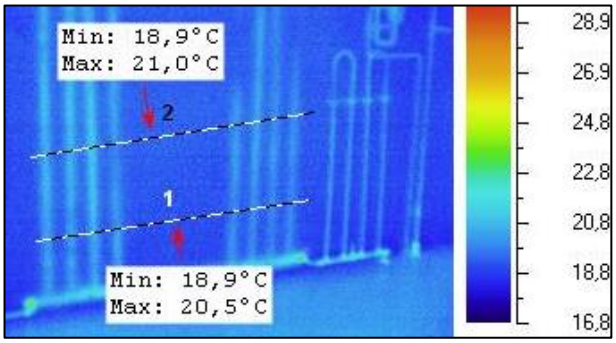

Fig. 12. Thermal imaging of heat pipes

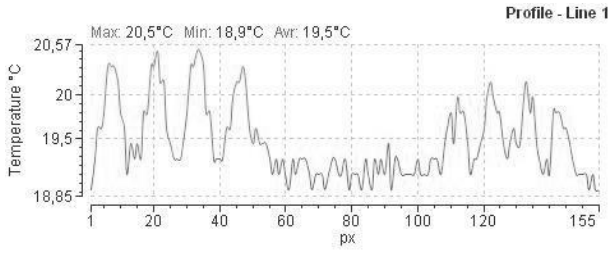

Fig. 13a. Temperature linear profile – profile-line 1

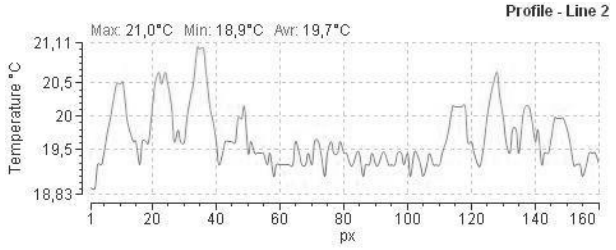

Fig. 13b. Temperature linear profile – profile-line 2

4.4. Detection of heat leakage

Another example shows how thermal imaging can be used to locate heat losses on a corroded heat pipe (Fig. 14, 15). As you can see in the visible picture, the heat pipe is strongly corroded. But only the thermovision photo indicated exactly where the largest heat losses are.

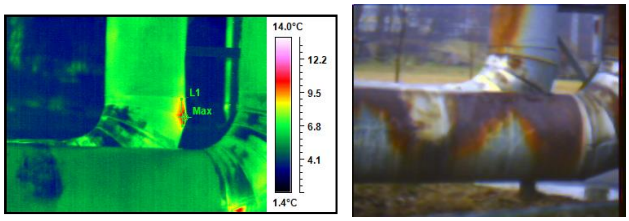

Fig. 14. Temperature distribution on the corroded heat pipe

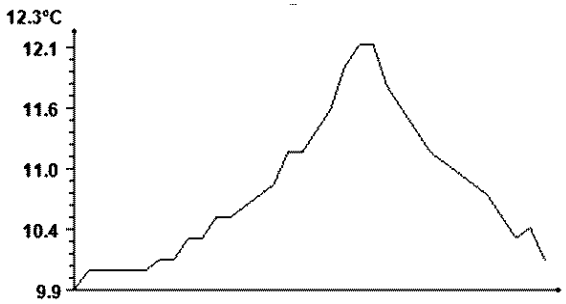

Fig. 15. Temperature linear profile

5. Conclusions

Thermography (thermal imaging) is a very useful tool for the qualitative assessment of thermal protection of buildings. It enables the detection of places with the greatest heat losses and possible defects or deviations from the design conditions, but in order to obtain high quality results it is necessary to meet a number of measurement requirements. It allows to check the effect of thermal modernization of buildings. Thermography can also be used to search for hidden installations in bulkheads as well as to locate leakages, as shown in the examples.

References

[1] Guide IR Analyser V 1.4.
[2] Jóźwicki R., Wawrzyniuk L.: Technika podczerwieni. Oficyna Wydawnicza PW, Warszawa 2014.
[3] Mandury H.: Pomiary termowizyjne w praktyce. Agenda wydawnicza PAKu, Warszawa 2004.
[4] Minkina W.: Pomiary termowizyjne – przyrządy i metody. Wydawnictwo Politechniki Częstochowskiej, Częstochowa 2004.
[5] PN-EN 13187 Właściwości cieplne budynków – Jakościowa detekcja wad cieplnych w obudowie budynku – metoda podczerwieni.
[6] Steidl T., Krause P.: Termowizja w ocenie jakości przegród budowlanych. Pomiary Automatyka Kontrola 55(11)/2009, 942–945.
[7] Więcek B., De Mey G.: Termowizja w podczerwieni. Podstawy i zastosowania. Wydawnictwo PAK, Warszawa 2011.

Ph.D. Eng. Danuta Proszak-Miąsik
e-mail: dproszak@prz.edu.pl

Danuta Proszak-Miąsik Ph.D. Eng., work at Rzeszow University of Technology in Department of Heating and Air-conditioning. Ph.D. dissertation deal on microelectronic humidity RC-sensors on the basis of composite material at Lublin University of Technology. Actually deal with renewable energy sources, using solar energy, production and processing of biomass. He also holds certificates authorizing him to conduct research on fuel properties She has completed a training course in thermal imaging. She performs thermal imaging expertise's in the building industry. She is the author and co-author of 1 patent, 64 scientific publications, three scripts. She is a promoter of 80 Master's and Engineer's theses.

ORCID ID: 0000-0003-3974-4835

otrzymano/received: 15.05.2019 *przyjęto do druku/accepted: 15.06.2019*

DOI: 10.5604/01.3001.0013.2541

THE CONSTRUCTION OF THE FEATURE VECTOR IN THE DIAGNOSIS OF SARCOIDOSIS BASED ON THE FRACTAL ANALYSIS OF CT CHEST IMAGES

Zbigniew Omiotek, Paweł Prokop
Lublin University of Technology, Faculty of Electrical Engineering and Computer Science/Institute of Electronics and Information Technology

Abstract. *CT images corresponding to the cross-sections of the patients' upper torso were analysed. The data set included the healthy class and 3 classes of cases affected by sarcoidosis. It was a state involving only the trachea – Sick(1), a state including trachea and lung parenchyma – Sick(2) and a state involving only lung parenchyma – Sick(3). Based on a fractal analysis and a feature selection by linear stepwise regression, 4 descriptors were obtained, which were later used in the classification process. These were 2 fractal dimensions calculated by the variation and box counting methods, lacunarity calculated also with the box counting method and the intercept parameter calculated using the power spectral density method. Two descriptors were obtained as a result of a gray image analysis, and 2 more were the effect of a binary image analysis. The effectiveness of the descriptors was verified using 8 popular classification methods. In the process of classifier testing, the overall classification accuracy was 90.97%, and the healthy cases were detected with the accuracy of 100%. In turn, the accuracy of recognition of the sick cases was: Sick(1) – 92.50%, Sick(2) – 87.50% and Sick(3) – 90.00%. In the classification process, the best results were obtained with the support vector machine and the naive Bayes classifier. The results of the research have shown the high efficiency of a fractal analysis as a tool for the feature vector extraction in the computer aided diagnosis of sarcoidosis.*

Keywords: fractals, sarcoidosis, computed tomography, image texture analysis

KONSTRUKCJA WEKTORA CECH W DIAGNOSTYCE SARKOIDOZY NA PODSTAWIE ANALIZY FRAKTALNEJ OBRAZÓW CT KLATKI PIERSIOWEJ

Streszczenie. *Przeprowadzono analizę obrazów CT górnej części tułowia pacjentów. Zbiór danych zawierał klasę pacjentów zdrowych i 3 klasy przypadków dotkniętych sarkoidozą. Był to stan obejmujący tylko tchawicę – Sick(1), stan obejmujący tchawicę i miąższ płucny – Sick(2) i stan obejmujący tylko miąższ płucny – Sick(3). Na podstawie analizy fraktalnej oraz selekcji cech metodą liniowej regresji krokowej otrzymano 4 deskryptory, które później wykorzystano w procesie klasyfikacji. Były to 2 wymiary fraktalne obliczone za pomocą metod variation i box counting, lakunarność obliczona również za pomocą metody box counting oraz parametr intercept obliczony za pomocą metody widmowej gęstości mocy. W wyniku analizy obrazu szarego otrzymano 2 deskryptory, a 2 kolejne były efektem analizy obrazu binarnego. Skuteczność deskryptorów zweryfikowano za pomocą 8 popularnych metod klasyfikacji. W procesie testowania klasyfikatorów, ogólna dokładność klasyfikacji wyniosła 90,97%, a przypadki zdrowe wykryto z dokładnością 100%. Z kolei, dokładność rozpoznania przypadków chorych była następująca: Sick(1) – 92,50%, Sick(2) – 87,50% i Sick(3) – 90,00%. W procesie klasyfikacji, najlepsze wyniki uzyskano za pomocą maszyny wektorów nośnych i naiwnego klasyfikatora Bayesa. Wyniki badań pokazały wysoką skuteczność analizy fraktalnej jako narzędzia do ekstrakcji wektora cech w komputerowej diagnostyce sarkoidozy.*

Słowa kluczowe: fraktale, sarkoidoza, tomografia komputerowa, analiza tekstury obrazu

Introduction

Sarcoidosis is a disease that attacks the body's immune system. A characteristic feature of sarcoidosis is a presence of inflammatory papules, called granulomas, which are on various organs and are not absorbed [1]. Sarcoidosis mainly affects the lungs and lymph nodes of the cavities, which are located in the mediastinum, i.e. in the part of the body which is located within the chest protected by the bony armor created by the ribs and the sternum [2, 9]. As a part of diagnostics of the disease, lung imaging is primarily performed. On this basis, there are 5 stages of sarcoidosis on which the treatment depends. However, to confirm the diagnosis, morphological examinations are performed, allowing the presence of characteristic granulomas to be visible under the microscope [7, 27]. Neglect of treatment of sarcoidosis can lead to respiratory failure and irreversible changes in the lungs, which is why it is very important to detect the disease at an early stage. The use of the computer aided diagnosis system, which based on CT images would provide the physician with a second diagnostic opinion, could be of great benefit here. In the construction of such a system, a fractal analysis could be used. The results we present in the article, confirm the high effectiveness of this method in identifying of healthy cases and different categories of sick cases. It should be noted here, that we are not aware of the works of other authors, where CT images would be used in the computer aided diagnosis system for detecting of sarcoidosis.

1. Material and methods

1.1. Material

CT images corresponding to the cross-sections of the patients' upper torso have been used. The data set included the class of healthy cases and 3 classes of cases diagnosed with sarcoidosis. These 3 kind of sick cases included only a trachea, a trachea and a pulmonary parenchyma, and only a lung parenchyma. The ground truth of whether a given CT image belongs to the healthy or sick person was determined by a pulmonologist (an expert in the field) based on clinical tests. Each category contained images belonging to 15 patients. In most cases, 4 areas of interest (ROIs) were identified for each patient (2 for each lung). ROIs were selected manually and their size of 80x150 piksels was determined in such a way that they would present the lesion area as accurately as possible (Fig. 1).

1.2. Fractal analysis

A computer representation of a medical image (e.g. radiological, ultrasound or computer tomography) is an image matrix where greyscale (intensity) levels corresponding to elements x, y form a more or less complex surface (Fig. 2). There are many algorithms for estimating the fractal dimension of such surfaces. In this paper, methods based on the power spectral density [10, 28], triangular prism surface area [8, 15] and variation [13, 30] were applied, as well as the box counting method [17, 24], which utilised a binary image in the analysis process. The aforementioned methods gave good results in other studies performed by the authors in which the subject of analysis was a flame area [26] and thyroid ultrasound images [19].

1.3. Image segmentation

The grey images to be analyzed using the box counting method were segmented. As a result of this process, binary images were obtained that were used to calculate the fractal dimension and lacunarity. The results of several segmentation methods were compared, including: local and global Otsu thresholding [23], local Bradley thresholding [3], level set method, adaptive thresholding and active contour method. The basic criterion for the

segmentation quality was a faithful reproduction of disease areas, visible in the CT images in the form of bright spots (Fig. 1). The best results were achieved using the global Otsu thresholding method. Therefore, in further studies, this method was selected for segmentation of grey images. In order to improve the quality of images after segmentation, binary images were subjected to operations of closing (dilation + erosion) and noise removal (removal of objects smaller than 10 pixels). Exemplary segmentation results are shown in Fig. 3.

1.4. Feature selection

Feature selection is a very important process because a properly chosen set of discriminating features allows one to build a high accuracy classifier [20–22]. In this study, a linear stepwise regression method was used for feature selection. This method involves the systematic addition and elimination of features to the set of input attributes given to the input of the linear classifier model depending on their statistical impact on the result of the system operation.

The influence of a feature on the operation of the system is measured by the factor with which it enters the linear model. The method starts from the start-up model, comparing its performance when increasing or decreasing the number of input attributes selected from the full set of potential diagnostic features. At every step (after adding or subtracting a specific attribute), the *F-Snedecor* statistics are determined for the training set. On the basis of a comparison of the *p*-value of this statistic with the assumed *p_enter* tolerance, a decision is made whether a specified feature should be entered into the set of features or not. In turn, as a result of comparing the *p*-value of the *F* statistic with the assumed *p_remove* tolerance, a decision is made to remove (or not) a specified feature from the current set of features. If the specified feature is not in the current set of input attributes, the null hypothesis is tested that its effect on the model's operation is zero. If the hypothesis is not confirmed as a result of the calculation, the attribute is added to the current set of attributes. Conversely, if a particular feature is in the model's input attribute set, the hypothesis is tested that its effect is zero. If this hypothesis is not confirmed, the feature remains in the attribute collection, but if confirmed, it is deleted.

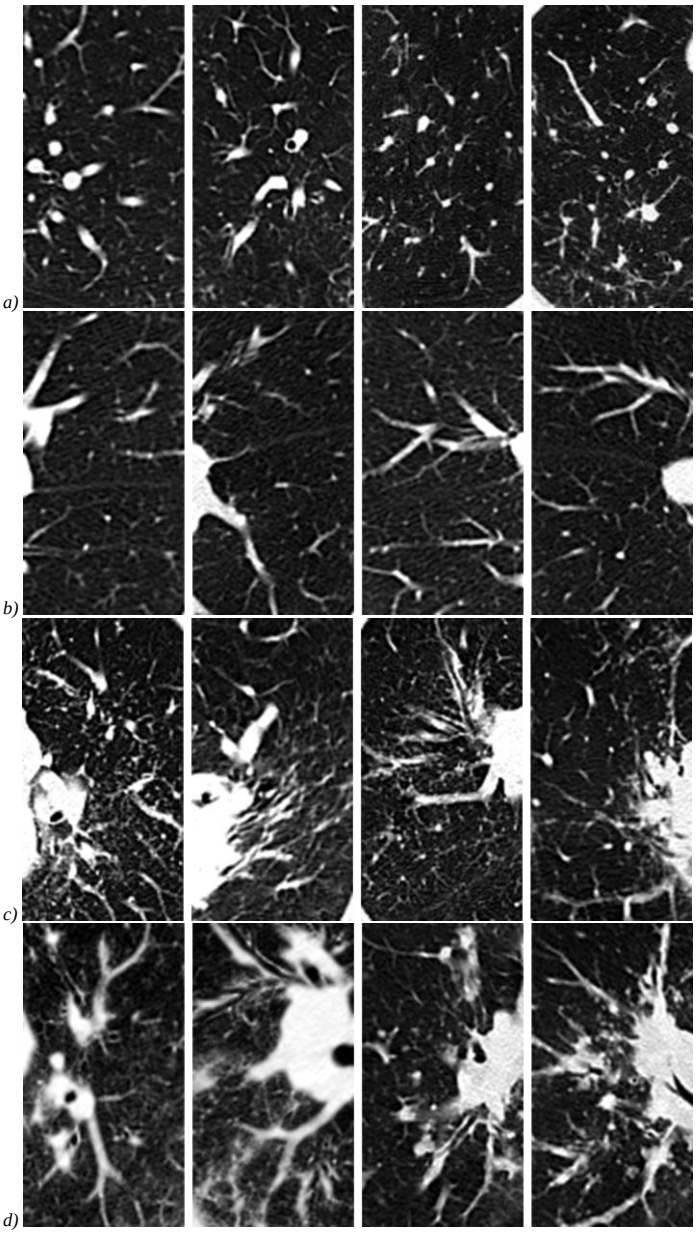

Fig. 1. ROIs characteristic for the 4 analyzed categories: a) healthy cases – Healthy; b) disease includes only a trachea – Sick(1); c) disease includes a trachea and a pulmonary parenchyma – Sick(2); d) disease includes only a pulmonary parenchyma – Sick(3)

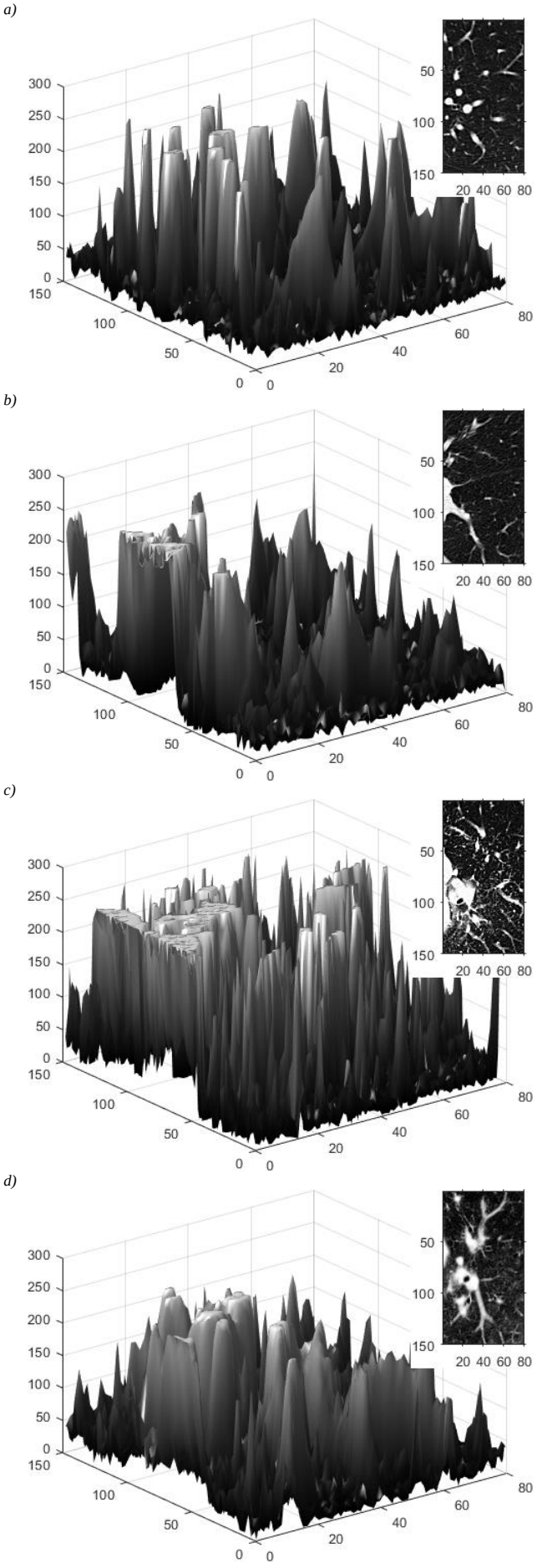

Fig. 2. Sample ROIs and their representation in three-dimensional space: a) Healthy; b) Sick(1); c) Sick(2); d) Sick(3)

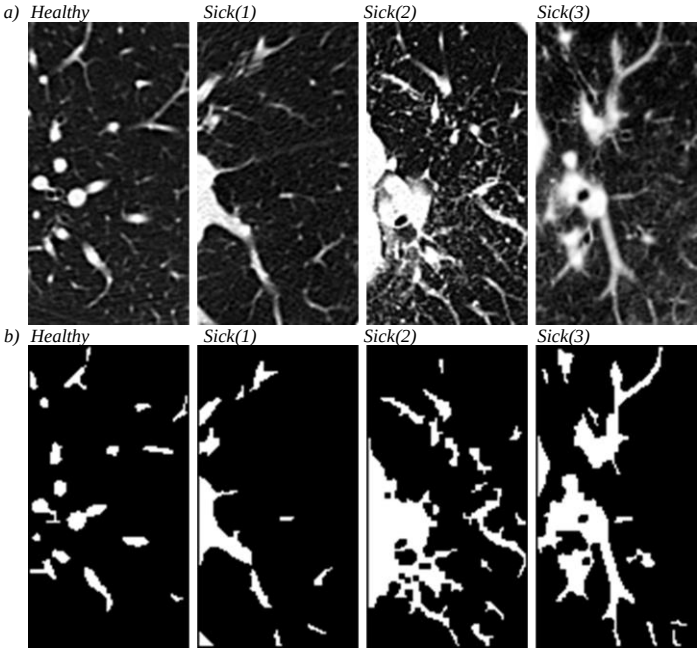

Fig. 3. Sample results of image segmentation for individual categories by the global Otsu thresholding method: a) grey images; b) binary images

2. Results

Images belonging to 4 categories of patients were subjected to fractal analysis to obtain feature descriptors. The following methods were used: power spectral density, triangular prism surface area, variation (filter 1, transect – first differences, transect – second differences) and box counting. On the basis of the power spectral density method, the fractal dimension and intercept of grey images were obtained. The box counting method allowed to estimate the fractal dimension and lacunarity of binary images. The effect of the triangular prism surface area and variation methods was the fractal dimension of grey images.

The results obtained were analyzed for the occurrence of outliers and extreme values. This kind of observations have been removed from the data set. The final number of cases belonging to particular categories was as follows: Healthy – 50, Sick(1) – 50, Sick(2) – 58, Sick(3) – 60. Table 1 presents a summary of average values of individual descriptors and their standard deviation after removal outliers and extreme values. For a binary image, the fractal dimension is in the range of 1-2, and for the grey image in the range of 2-3 (except the power spectral density method for the class Healthy). These values are in line with the theoretical values for this type of images. This situation confirms that the analyzed images have fractal features and justifies the use of fractal analysis as a method for estimating the feature descriptors.

Figure 4 presents box charts prepared on the basis of data from table 1. Observing the dispersion of values of variables defined in Table 1, it can be seen that relatively good separation of observations takes place only between cases belonging to the class Healthy and all the other cases of the sick category (Sick(1), Sick(2), Sick(3)). The best in this respect seem to be the *PSD* and *Int* variables estimated using the power spectral density method. Unfortunately, for observations of the sick category, no variable separates all classes of this category in an unambiguous way. One can only indicate a moderately good separation of one class of cases in relation to other classes of this category. One can give 2 examples in this regard. The first one is the *BC* variable, which can be used to distinguish the class Sick(1) from the classes Sick(2) and Sick(3). The second example are variables *Int* and *Var_FD*, which can be used to distinguish the class Sick(3) from the classes Sick(1) and Sick(2). Box charts in figure 4 don't suggest any variables that could be used to distinguish the class Sick(2) from the classes Sick(1) and Sick(3).

Table 1. Mean value and standard deviation of fractal descriptors

Image	Method	Descriptor	Variable name	Class	Mean	Std dev
Grey	Power spectral density	Fractal dimension	*PSD*	Healthy	3.15	0.08
				Sick(1)	2.83	0.18
				Sick(2)	2.91	0.11
				Sick(3)	2.72	0.09
Grey	Power spectral density	Intercept	*Int*	Healthy	21.76	0.47
				Sick(1)	23.29	0.98
				Sick(2)	23.64	0.40
				Sick(3)	24.43	0.36
Grey	Triangular prism surface area	Fractal dimension	*TPSA*	Healthy	2.39	0.05
				Sick(1)	2.32	0.06
				Sick(2)	2.37	0.04
				Sick(3)	2.31	0.05
Grey	Variation (Filter 1)	Fractal dimension	*Filter*	Healthy	2.68	0.04
				Sick(1)	2.57	0.07
				Sick(2)	2.60	0.05
				Sick(3)	2.49	0.06
Grey	Variation (Transect – first differences)	Fractal dimension	*Var_FD*	Healthy	2.66	0.07
				Sick(1)	2.54	0.06
				Sick(2)	2.56	0.05
				Sick(3)	2.45	0.04
Grey	Variation (Transect – second differences)	Fractal dimension	*Var_SD*	Healthy	2.51	0.10
				Sick(1)	2.36	0.05
				Sick(2)	2.40	0.09
				Sick(3)	2.28	0.05
Binary	Box counting	Fractal dimension	*BC*	Healthy	1.01	0.10
				Sick(1)	1.10	0.08
				Sick(2)	1.42	0.15
				Sick(3)	1.46	0.11
Binary	Box counting	Lacunarity	*Lac*	Healthy	0.68	0.08
				Sick(1)	1.09	0.22
				Sick(2)	0.91	0.27
				Sick(3)	0.83	0.22

The results of the fractal analysis presented in Table 1 and figure 4 do not allow to indicate a set of descriptors that could be used in a system for automatic classification of the 4 analysed categories of observations. Therefore, the data were subjected to statistical analysis aimed at selecting features that would enable to build the classifier. A linear stepwise regression method was applied for this purpose. The *stepwisefit* function of the Matlab program was used, in which the aforementioned method was implemented. The built-in values of the *F* statistics tolerance thresholds were as follows: *p_enter* = 0.05 and *p_remove* = 0.1.

Table 2 presents the results obtained. The meaning of individual columns is as follows:

- B – coefficients with which particular features affect the accuracy of model mapping. The greater the value (as to the module), the greater the influence of a given feature.
- SE – standard deviation of the values of B coefficients for individual features.
- PV – a *p-value* variable containing *p* statistic values for individual features. The smaller the value, the more difficult it is to reject the hypothesis about the low importance of a given feature.
- Status – value 1 means that the given feature is included as the input attribute of the model, 0 – means its elimination.

Table 2. Results of feature selection by linear stepwise regression

Feature	B	SE	PV	Status
PSD	-0.4538	0.7979	0.5702	0
Int	**0.2719**	**0.0568**	**0.0000**	**1**
TPSA	1.2231	0.7954	0.1256	0
Filter	**-2.3626**	**0.5089**	**0.0000**	**1**
Var_FD	-0.7321	0.7476	0.3286	0
Var_SD	-0.5577	0.4419	0.2084	0
BC	**2.7786**	**0.2521**	**0.0000**	**1**
Lac	**0.4693**	**0.1663**	**0.0052**	**1**

The results obtained show that the features *Int*, *Filter*, *BC* and *Lac* (the smallest *p-value* values) have the greatest influence on the model. They are marked in bold in Table 2. Also, the values of *p* statistics for individual features show a large difference in their impact on the result.

A matrix scatter plot was made for variables selected using the linear stepwise regression method (Fig. 5). On the basis of this plot you can see that observations of the healthy category form a compact group, quite well separated from the observation of the sick category. Apparently this can be seen for the variable pairs *Int-Lac* and *BC-Lac*. Observations of the sick category have a larger dispersion of variable values compared to observations of the healthy category. Therefore, in the scatter plots you can not indicate clear groups of cases that would allow you to unequivocallly distinguish between different classes of the sick category. Nevertheless, in the scatter plots one can observe some areas in which observations of individual classes tend to cluster.

It seems that this is best seen for the variables *Filter-BC*. The spatial chart gives better possibilities for observing cases clustering. Figure 6 shows such a graph for variables *Filter-BC-Lac*. Admittedly, there are no separate groups of observations there, but there is a clear tendency to clustering of cases belonging to particular classes. This situation gives a base for the construction of classifiers.

For this purpose, 4 features highlighted in bold in table 2 were used: *Int*, *Filter*, *BC* and *Lac*. Eight popular supervised learning methods were used [4–6, 11, 12, 14, 16, 18, 25, 29]: artificial neural network with multilayer perceptron (MLP), decision tree (DT), *K*-nearest neighbors (*K*-NN), naive Bayes classifier (NBC), quadratic and linear discriminant analysis (QDA, LDA), random forests (RF), support vector machine (SVM). The full data set was randomly divided into a training, validation and test part. The size of each of these subsets was 1/3 of the full set. A combined training and validation sets were used for the final classifiers training. Testing was carried out using an independent test set. Training, validation and classifiers testing have been repeated 10 times. An average value from all tests was taken as the final result of the testing process. The overall classification accuracy (ACC), classification sensitivity and classification specificity was used to assess the accuracy of classifiers. The overall classification accuracy is defined as the ratio of the number of samples correctly classified to the number of all analyzed samples. There were 4 classes of cases in the study, therefore the other 2 measures were generalized to a classifier operating on the principle of "one specific class against all", i.e. assigning results to only one class or beyond it. Therefore, the classifier sensitivity means the probability of correct classification of the sample belonging to the selected class. In turn, the specificity is defined as the probability that samples belonging to other classes will not be assigned to the selected class.

Figure 7 shows the average value of the overall classification accuracy obtained for the test set. The largest value, equal to 90.97%, was achieved for the SVM classifier. Comparable accuracy was also obtained by the MLP classifier, for which ACC was equal to 90.83%. The difference from the SVM classifier was only 0.14%. It should be noted that ACC exceeded 82% for all classification methods.

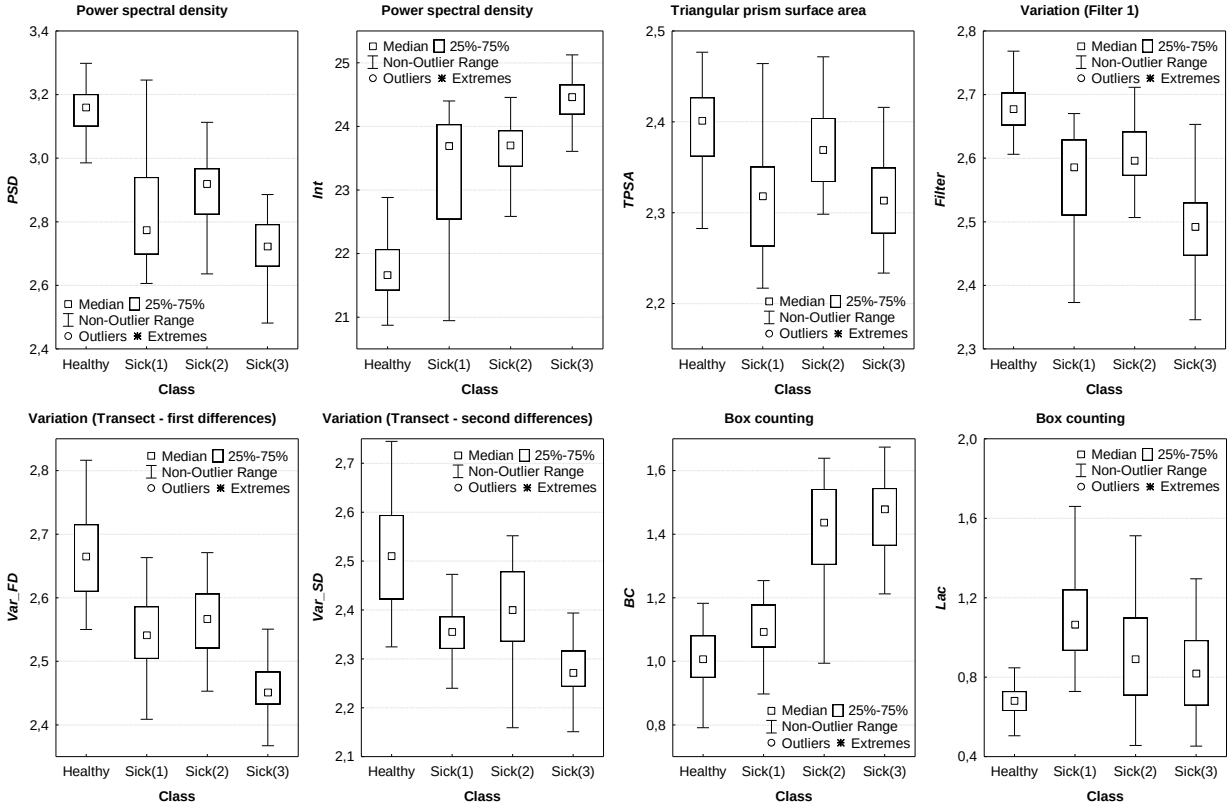

Fig. 4. Dispersion of a mean value of individual variables. A title of each chart shows a name of a method used. A meaning of variables is explained in Table 1

The results regarding the estimation of the classification sensitivity (separately for each class) are shown in Table 3. For the class Healthy, the highest sensitivity of 100% was achieved for 4 classifiers, i.e. SVM, NBC, LDA and 7-NN. For classes belonging to the sick category, the results obtained were as follows (the best classifier was given in brackets): Sick(1) – 92.50% (SVM); Sick(2) – 87.50% (MLP); Sick(3) – 90.00% (NBC).

Table 3. Classification sensitivity

Classifier	Healthy	Sick(1)	Sick(2)	Sick(3)
SVM	**100**	**92.50**	86.50	87.00
MLP	99.38	91.88	**87.50**	86.50
QDA	98.75	82.50	85.00	85.00
NBC	**100**	80.63	80.00	**90.00**
RF	95.63	90.63	80.00	84.50
LDA	**100**	75.00	84.00	83.50
7-NN	**100**	81.25	79.00	80.50
DT	93.13	80.63	74.00	83.00

Table 4 presents the classification specificity for each of the 4 observation classes. For the class Healthy, the best result (100%) was obtained for SVM and NBC classifiers. A similar specificity value (99.82%) was also provided by the MLP classifier. In turn, for the other classes the results were as follows: Sick(1) – 97.86% (SVM); Sick(2) – 95.19% (MLP and LDA); Sick(3) – 96.15% (NBC).

Table 4. Classification specificity

Classifier	Healthy	Sick(1)	Sick(2)	Sick(3)
SVM	**100**	**97.86**	94.81	95.00
MLP	99.82	97.68	**95.19**	94.81
QDA	98.39	97.32	92.88	94.42
NBC	**100**	94.46	92.31	**96.15**
RF	98.57	95.54	94.42	94.04
LDA	94.82	95.89	**95.19**	94.62
7-NN	97.14	95.54	92.31	94.23
DT	98.93	94.82	89.62	92.50

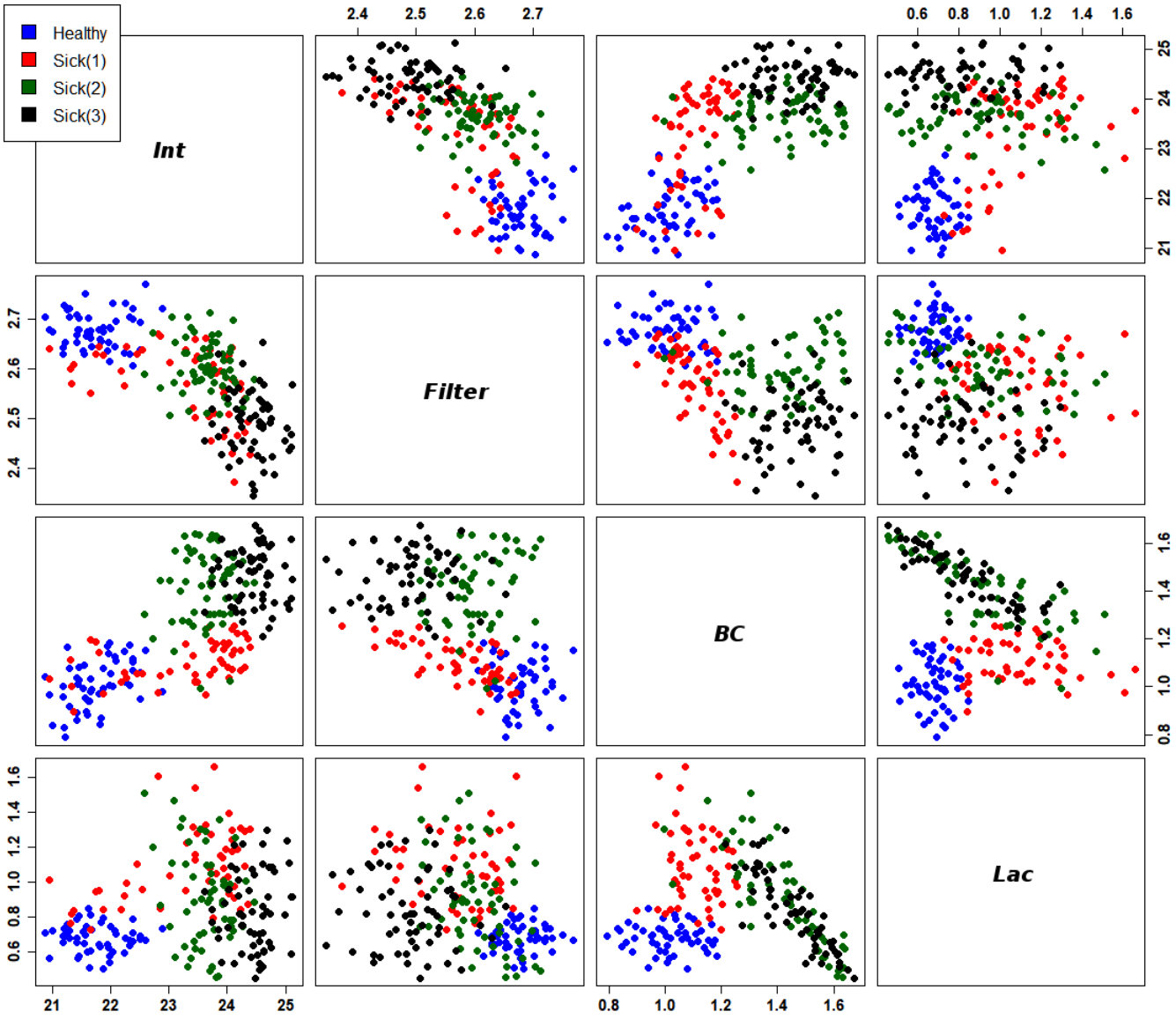

Fig. 5. Scatter plots for the variables selected by the linear stepwise regression method. Variables of the specified symbols are described in Table 1

3. Discussion

The study used 8 fractal descriptors estimated by various methods. Their values confirm the fractal nature of the studied CT images (Table 1) and justify the use of fractal analysis as a research tool. Using the linear stepwise regression method, 4 descriptors were selected from this set for constructing classifiers. These were: intercept – calculated using the power spectral density method; 2 fractal dimensions – calculated by the variation and box counting methods; lacunarity – also calculated using the box counting method. The first 2 descriptors (*Int*, *Filter*) were calculated based on a grey image analysis, while the next 2 (*BC*, *Lac*) based on a binary image.

Table 5 gives a summary of the best results obtained while classifiers testing. The highest overall classification accuracy was obtained for the SVM classifier (ACC=90.97%). In the case of classification sensitivity and specificity, the test results depend on the class of observation. The best results have been

achieved here for the class Healthy. Both sensitivity and specificity are at the level of 100%. Healthy cases are the easiest to distinguish from the other classes, because they not contain large, bright areas corresponding to the disease state (Fig. 1a). Taking into account the Sick cases, the best accuracy was achieved for the class Sick(1), where the disease state includes the trachea (Fig. 1b). The sensitivity was 92.50% here and the specificity was 97.86%.

Table 5. A summary of the best classification results

Index	Class	Value (%)	Classifier
ACC	All classes	90.97	SVM
Classification sensitivity	Healthy	100	SVM, NBC, LDA, 7-NN
	Sick(1)	92.50	SVM
	Sick(2)	87.50	MLP
	Sick(3)	90.00	NBC
Classification specificity	Healthy	100	SVM, NBC
	Sick(1)	97.86	SVM
	Sick(2)	95.19	MLP, LDA
	Sick(3)	96.15	NBC

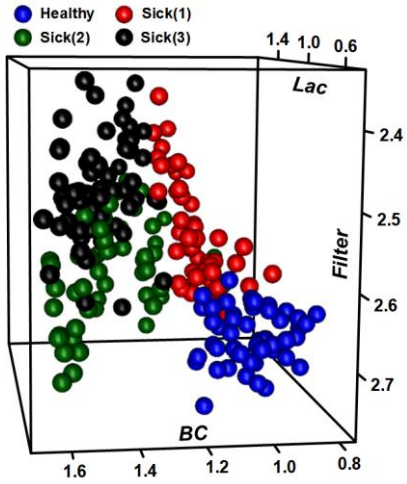

Fig. 6. Spatial scatter plot for the variables Filter-BC-Lac

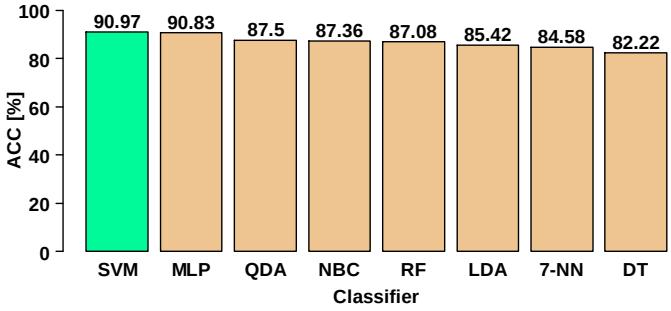

Fig. 7. Overall classification accuracy. The meaning of the classifier symbols is as follows: SVM – support vector machine; MLP – artificial neural network with multilayer perceptron; QDA – quadratic discriminant analysis; NBC – naive Bayes classifier; RF – random forests; LDA – linear discriminant analysis; 7-NN – K-nearest neighbours for K=7; DT – decision tree

The second place in terms of classification accuracy is occupied by the class Sick(3), for which the disease state includes pulmonary parenchyma (fig. 1d). For this class of observations, the sensitivity was at the level of 90.00%, and the specificity was 96.15%. The worst results were obtained for the class Sick(2), where the disease state includes both trachea and pulmonary parenchyma (fig. 1c). In this case, the sensitivity was 87.50%, and the specificity was 95.19%. The class Sick(2) has proved to be the most difficult to classify because it includes symptoms occuring both in Sick(1) and Sick(3) class. The effectiveness of the SVM and NBC classifiers is also worth noting. Out of 9 classification accuracy indicators, the SVM classifier turned out to be the best in 5 cases, and the NBC classifier in 4 ones (table 5). Such results provide the basis for the use of these classifiers in a computer system for the automatic diagnosing of sarcoidosis.

The results obtained also show that in the case of observations of the sick category, for each of the classes, the classification sensitivity is a few percent worse than the specificity. These differences for the classes Sick(1), Sick 2) and Sick(3) are respectively 5.36%, 7.69% and 6.16%. This means that the probability of a correct classification of observations belonging to a given class is lower than the probability that observations belonging to other classes will not be assigned to a given class. Unfortunately, this relation between the values of both classification quality parameters is not beneficial for the patient from a medical point of view. Therefore, further research is required to increase the classification sensitivity at least to the level of specificity. It seems that good results would be obtained by combine the effects of fractal analysis with the results of other methods for calculating the feature descriptors of image textures, e.g. autoregression model, wavelet transform and statistical methods (greyscale histogram, co-occurrence matrix, higher-order statistics, run-length matrix, matrix gradient) [14].

The results obtained are difficult to compare with the results of other authors, because (as noted in the introduction) there are no known publications regarding the automatic detection of sarcoidosis based on CT images. The advantages of the presented method include the fact that it is non-invasive and offers relatively high accuracy in recognizing cases belonging to particular classes. Let us remind that the worst of the results (87.50%), concerning the classification sensitivity of the class Sick(2), was at a relatively high level. Another advantage is the fact that the method is based on only a few features selected solely on the basis of the fractal analysis. This situation should simplify the construction of the future computer system. On the other hand, a certain drawback of the applied method of analysis is the fact that there is a lack of standardization of methods for estimating the fractal dimension. Consequently, the values of this parameter for the same image, estimated by different methods, are similar but not identical. In addition, the estimation range of the regression line slope can be

determined in various ways, which influences the value of the estimated parameter. Finally, the presented method must be tested on data sets of a larger size so as to obtain statistical significance of the results. Let us recall that the number of observations for particular classes was: Healthy – 50, Sick(1) – 50, Sick(2) – 58, Sick(3) – 60. The tests carried out showed that in order to obtain statistical significance, the number of individual subsets should exceed 100 observations. Future studies should also consider the impact of changes in volume, turnover and ROI position on classification results. Despite the problems indicated, the fractal analysis seems to be an interesting tool in the study of CT image textures. The relatively high classification accuracy achieved thanks to fractal descriptors gives the basis for their use in a computer system for the automatic diagnosis of sarcoidosis.

4. Conclusions

The research has shown the high effectiveness of the fractal analysis as a tool for the feature vector extraction in diagnosis of sarcoidosis. The following results were obtained: overall classification accuracy – 90.97%; classification sensitivity – 100% (Healthy), 92.50% (Sick(1)), 87.50% (Sick(2)), 90.00% (Sick(3)); classification specificity – 100% (Healthy), 97.86% (Sick(1)), 95.19% (Sick(2)), 96.15% (Sick(3)). Achieving high classification accuracy was possible due to the simultaneous use of fractal descriptors of grey and binary images. These were: intercept – calculated using the power spectral density method; 2 fractal dimensions – calculated by the variation and box counting methods; lacunarity – also calculated using the box counting method. Fractal analysis can be an alternative approach in studies of CT image textures aimed at automatic diagnosis of sarcoidosis. Its results, combined with such classification methods as support vector machine or naive Bayes classifier, give interesting possibilities in the construction of an automated computer system that could help the physician in the preliminary diagnosis of difficult cases based on CT images. Thanks to this, the doctor would have a quick and objective additional opinion that would be very valuable at the initial diagnosis stage. In the case of sarcoidosis, this is particularly important because the detection of the disease at an early stage increases the patient's chances for effective therapy.

References

[1] Arkema E. V., Cozier Y. C.: Epidemiology of sarcoidosis: current findings and future directions. Ther Adv Chronic Dis 9(11)/2018, 227–240.
[2] Baughman R. P., Culver D. A., Judson, M. A.: A Concise Review of Pulmonary Sarcoidosis. Am J Respir Crit Care Med 183/2011, 573–581.
[3] Bradley D., Roth G.: Adaptive Thresholding Using the Integral Image. http://www.scs.carleton.ca/~roth/iit-publications-iti/docs/gerh-50002.pdf (available: 19.05.2019).
[4] Breiman L.: Bagging Predictors. Mach Learn 24/1996, 123–140.
[5] Breiman L.: Random Forests. Mach Learn 45/2001, 5–32.
[6] Breiman L., Friedman J., Olshen R., et al.: Classification and Regression Trees. CRC Press, London 1984.
[7] Bonifazi M., Gasparini S., Alfieri V., Renzoni E. A.: Pulmonary Sarcoidosis. Semin Respir Crit Care Med 38/2017, 437–449.
[8] Clarke K. C.: Computation of the fractal dimension of topographic surfaces using the triangular prism surface area method. Comp Geosci 12/1986, 713–722.
[9] Criado E., Sánchez M., Ramírez J., Arguis P., de Caralt T. M., Perea R. J., et al.: Pulmonary Sarcoidosis: Typical and Atypical Manifestations at High-Resolution CT with Pathologic Correlation. RadioGraphics 30/2010, 1567–1586 [DOI: 10.1148/rg.306105512].
[10] Dennis T. J., Dessipris N. G.: Fractal modelling in image texture analysis. IEEE Proc.-F. 136/1989, 227–235.
[11] Enas G. G., Chai S. C.: Choice of the smoothing parameter and efficiency of the k-nearest neighbor classification. Comput Math Appl 12/1986, 235–244.
[12] Freund Y., Schapire R. E.: A decision-theoretic generalization of on-line learning and an application to boosting. J Comput Syst Sci Int 55/1996, 119–139.
[13] Gneiting T., Sevcikova H., Percival D.: Estimators of Fractal Dimension: Assessing the Roughness of Time Series and Spatial Data. Statistical Science 27(2)/2012, 247–277.
[14] Hothorn T., Lausen B.: Bundling classifiers by bagging trees. Comput Stat Data An 49(4)/2005, 1068–1078.
[15] Iftekharuddin K. M., Jia W., Marsh R.: Fractal analysis of tumor in brain MR images. Mach Vision Appl 13(5-6)/2003, 352–362.
[16] Liao S. H., Chu P. H., Hsiao P. Y.: Data mining techniques and applications – A decade review from 2000 to 2011. Expert Syst Appl 39/2012, 11303–11311.
[17] Mandelbrot, B., [The fractal geometry of nature], W. H. Freeman and Company, New York, (1983).
[18] Omiotek Z.: Improvement of the classification quality in detection of Hashimoto's disease with a combined classifier approach. P I Mech Eng H 231(8)/2017, 774–782.
[19] Omiotek Z.: Fractal analysis of the grey and binary images in diagnosis of Hashimoto's thyroiditis. Biocybern Biomed Eng 37(4)/2017, 655–665.
[20] Omiotek Z., Wójcik W.: Zastosowanie metody Hellwiga do redukcji wymiaru przestrzeni cech obrazów USG tarczycy. Informatyka, Automatyka, Pomiary w Gospodarce i Ochronie Środowiska – IAPGOS 3/2014, 14–17 [DOI: 10.5604/20830157.1121333].
[21] Omiotek Z., Wójcik W.: An efficient method for analyzing measurement results on the example of thyroid ultrasound images. Przeglad Elektrotechniczny 11/2016, 15–18.
[22] Omiotek Z., Stepanchenko O., Wójcik W., Legieć W., Szatkowska M.: The use of the Hellwig's method for feature selection in the detection of myeloma bone destruction based on radiographic images. Biocybern Biomed Eng 39(2)/2019, 328–338.
[23] Otsu N.: A Threshold Selection Method from Gray-Level Histograms. IEEE Transactions on Systems, Man, and Cybernetics 9(1)/1979, 62–66.
[24] Plotnick R. E., Gardner R. H., O'Neil R. V.: Lacunarity indices as measures of landscape texture. Landsc Ecol 8(3)/1993, 201–211.
[25] Quinlan J. R.: Induction of decision trees. Mach Learn 1/1986, 81–106.
[26] Sawicki D., Omiotek Z.: Evaluation of the possibility of using fractal analysis to study the flame in the co-firing process. Proc. SPIE 10808/2018.
[27] Soto-Gomez N., Peters J. I., Nambiar A. M.: Diagnosis and Management of Sarcoidosis. American Family Physician 93(10)/2016, 840–848.
[28] Super B. J., Bovik A. C.: Localized measurement of image fractal dimension using Gabor filters. J Visual Commun Image Represent 2(2)/1991, 114–128.
[29] Venables W. N., Ripley B. D.: Modern Applied Statistics with S-PLUS. Springer, Berlin 1998.
[30] Zhu Z., Stein M.: Parameter estimation for fractional Brownian surfaces. Statistica Sinica 12/2002, 863–883.

Ph.D. Eng. Zbigniew Omiotek
e-mail: z.omiotek@pollub.pl

A graduate of the Faculty of Electronics at the Military University of Technology in Warsaw. In the years 1995-2013 – research and teaching assistant. Since 2015 – assistant professor at the Lublin University of Technology. His scientific interests are focused around methods for digital image processing, machine learning and computer aided diagnosis.

ORCID ID: 0000-0002-6614-7799

M.Sc. Eng. Paweł Prokop
e-mail: pawel.prokop@pollub.edu.pl

In 2012 he graduated with a degree in Computer Science of the Faculty of Electrical Engineering and Computer Science at the Lublin University of Technology. Currently a Ph.D. student at the Faculty of Electrical Engineering and Computer Science. His scientific interests are focused around computer science and biomedical engineering.

ORCID ID: 0000-0002-3078-8287

otrzymano/received: 20.05.2019 *przyjęto do druku/accepted: 15.06.2019*

DOI: 10.5604/01.3001.0013.2542

CROSS PLATFORM TOOLS FOR MODELING AND RECOGNITION OF THE FINGERSPELLING ALPHABET OF GESTURE LANGUAGE

Serhii S. Kondratiuk[1], Iurii V. Krak[1,2], Waldemar Wójcik[3]
[1]Taras Shevchenko National University of Kyiv, [2]Glushkov Institute of Cybernetics of NAS of Ukraine, [3]Lublin University of Technology

Abstract. *A solution for the problems of the finger spelling alphabet of gesture language modelling and recognition based on cross-platform technologies is proposed. Modelling and recognition performance can be flexible and adjusted, based on the hardware it operates or based on the availability of an internet connection. The proposed approach tunes the complexity of the 3D hand model based on the CPU type, amount of available memory and internet connection speed. Sign recognition is also performed using cross-platform technologies and the tradeoff in model size and performance can be adjusted. the methods of convolutional neural networks are used as tools for gestures of alphabet recognition. For the gesture recognition experiment, a dataset of 50,000 images was collected, with 50 different hands recorded, with almost 1,000 images per each person. The experimental researches demonstrated the effectiveness of proposed approaches.*

Keywords: cross platform, sign language, fingerspelling alphabet, 3D modeling, Convolutional Neural Networks

CROSS-PLATFORMOWE NARZĘDZIA DO MODELOWANIA I ROZPOZNAWANIA ALFABETU PALCOWEGO JĘZYKA GESTÓW

Streszczenie. *Zaproponowano rozwiązanie problemów z alfabetem daktylograficznym w modelowaniu języka gestów i rozpoznawaniu znaków w oparciu o technologie wieloplatformowe. Wydajność modelowania i rozpoznawania może być elastyczna i dostosowana, w zależności od wykorzystywanego sprzętu lub dostępności łącza internetowego. Proponowane podejście dostosowuje złożoność modelu 3D dłoni w zależności od typu procesora, ilości dostępnej pamięci i szybkości połączenia internetowego. Rozpoznawanie znaków odbywa się również z wykorzystaniem technologii międzyplatformowych, a kompromis w zakresie wielkości modelu i wydajności może być dostosowany. Jako narzędzia do rozpoznawania gestów alfabetu wykorzystywane są metody konwolucyjnych sieci neuronowych. Na potrzeby eksperymentu rozpoznawania gestów zebrano zbiór danych obejmujący 50 000 obrazów, przy czym zarejestrowano 50 różnych rąk, a na każdą osobę przypadało prawie 1000 obrazów. Badania eksperymentalne wykazały skuteczność proponowanego podejścia.*

Słowa kluczowe: cross platform, język migowy, alfabet palcowy, modelowanie 3D, konwolucyjne sieci neuronowe

Introduction

Gesture based communication is one of real methods for data transition, close by with content and discourse. Signs can be utilized to define explicit letters, words, states and can be handled, encoded and put away in a different ways. Building up a technology for storing, modeling and demonstrating signs and communications via gestures is a challenging issue because of contrasts in accessible platforms. Different platforms have different working operating systems, (for example, mobile – iOS, Android, desktop – MacOS, Linux, Windows, and web – ChromeOS, and so forth), which infers diverse execution level and requires porting the codebase on every stage; some platforms require web connection, (for example, distributed computing technologies [10]) and others don't, and so forth. Displaying such a technology for sign language is a real issue for individuals with hearing disabilities and their relatives, yet in addition is significant in a more extensive usage, due to universality of sign language.

Cross-platform development [17] give an approach to beat this issue. Cross-platform development can be utilized instead of virtual-machines [15] or a lot of mono-platforms development. Utilizing these advances permits to build up a single codebase for various sort of platforms, types of CPU, operating systems of equipment execution and to send it on all platforms consistently.

In this article an answer for the issue of sign language demonstrating is proposed dependent on cross-platform development. The technology of communication through signs can be adaptable and balanced, depending on the equipment it works on or dependent on accessibility of internet connection. The proposed methodology tunes the 3D hand model (parameters, for example, the quantity of polygons for rendering the hand and the step of signs progress) in view of the CPU type, measure of accessible memory and web connection speed. The sign recognition is additionally performed utilizing cross-platform developments and can be alter ed for the tradeoff in model size and execution speed. The sign (gesture) modeling and recognition is a part of a single gesture communication technology and this paper is a further development of author's previous works [5, 7].

1. Existing approaches for modeling and recognition of sign language and their implementation on different platforms

A technology for both sign language displaying and recognition can be considered as a pair of modules for gesture demonstrating and gesture recognition. Some of frameworks give just a single module, regularly just for a particular platform. American Sign Language Online Dictionary [2] is one of the systems which were collected for signal displaying, it depends on a lot of recorded recordings, stored in a database, and this methodology was used in a lot of organizations [1]. In any case, because of its strategy for storing motions and no conceivable capacity to adjust them, this framework isn't adaptable and constrained distinctly to a lot of pre-recorded records. Likewise, no gesture recognition method is pro-vided.

Three-dimensional hand model is a significant piece of gesture language displaying. Two gatherings of hand demonstrating approaches are investigated in the work [4]. In the paper, spatial approach considers situating of the hand sign and their parametrical set. The methodology depends on the rules of advances of a sign.

In the paper [11] builds up an approach for demonstrating motion for an input content. The technology comprise of a factual model for given input handling and a generative calculations for ap-propriate hand motion displaying, utilizing indicated kinematics. As a result of the work, authors provide ANVIL tools for an-notation, DANCE library for sign transition and sign generator NOVA [14]. However, the technology is specified to work only on Windows operating system and x86 CPU. Comparative technology for displaying signs is proposed in [9], but additionally just for a single platform.

2. Problem statement

The proposed technology should comprise of two sections, which are communication through signs [8, 9] displaying and recognition module. The two modules ought to have the option to

keep running without codebase alteration on various platforms and ought to be created utilizing cross-platform developments.

Sign recognition module should comprise of a model which can recognize and distinguish the gesture, determined by the client, from a camera input. Set of gestures is constrained by the Ukrainian dactyl language, however can be broadened further. A fitting dataset of Ukrainian dactyl language ought to be gathered for testing the model execution. The sign language displaying module ought to have the option to recreate a gesture specified by a lot of parameters, stored in a database, and ought to be restricted by a lot of Ukrainian dactyl language signs, yet can be expanded further with different languages. The gesture displaying module ought to likewise have the option to show gesture motions, which means it can demonstrate flawlessly words and sentences, comprising of Ukrainian dactyl language signs.

3. Proposed approach

To built up a technology for fingerspelling letters in order to demonstrate and recognize gestures, which can keep running on numerous platforms, without changing the codebase, a methodology based on cross-platform instruments is proposed. Gesture displaying module should comprise of a virtual three dimensional hand model and a user interface (UI), which ought to furnish the client with ability to input a sequence of letters, which at that point will be changed into a sequence of gestures. To implement both hand model and UI, a cross-platform framework Unity3D [18] was utilized. Contrasting with other 3D engine, it provides a unified development process for all available platforms (mo-bile, desktop and web) and provides a seamless way to deploy the application on all of them without changing the codebase. To build up a sign recognition module, a cross-platform tool Tensorflow [16] is proposed. This methodology based on cross-platform tools for AI permits to created and train a sign recognition model once, and after that convey it on different platforms (portable, desktop and web) with no changes to the model or the code for training. As a model engineering, the MobileNet design is considered, upgraded with 3D convolutions, to take into account data from a grouping of frames from the camera. Overall, the proposed approach novelty is that it assembles together cross-platforms technology for Ukrainian dactyl language displaying and recognition, with improved MobileNet design for improved recognition of the Ukrainian dactyl letters.

4. Infologic model

The framework design chart (Fig. 1) shows the communication of fundamental parts of the proposed technology.

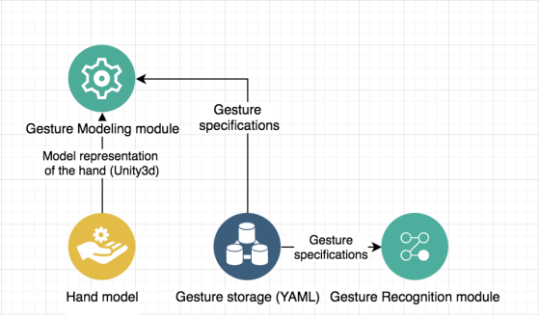

Fig. 1. Infologic model of cross platform gesture communication technology

The signs for gesture demonstrating are stored in a predefined format (YAML [16]) in a database, and are used by the gesture displaying engine for setting an arrangement of a spatial three-dimensional hand model utilizing indicated parameters for the motion from a database section. The sign modeling module works over the gesture database and is a piece of the application, which comprises of gesture displaying and UI parts, them two being created with Unity3D system, utilizing C# programming language. The virtual hand model is determined by a skeleton and a lot of parameters and their restrictions for every skeleton joint. The sign recognition module is executed with Tensorflow system, using Python programming language. The sign recognition module run autonomously of gesture demonstrating module and database. Primary segments of the gesture recognition module is the model which performs gesture recognition and the wrapper which changes over camera input to appropriate data for the model.

5. Gesture modeling

The three-dimensional hand model skeleton was implemented in view of human hand structures. Skeleton model comprises of: 8 bones in wrist, 3 bones in the thumb and 1 metacarpus and 3 phalanges in every one of different fingers. Each joint of each pair of bones has it's own sort of association and it's own parameters for setting this joint, it's very own level of freedom and it's restrictions. Generally speaking, the hand model is represented with a skeleton which comprises of 27 bones and has 25 degrees of portability. The thumb has 5 degrees of freedom, middle and pointers have four degrees of freedom, four degrees of freedom are situated in the metacarpal-carpal joint to the little finger and thumb to empower development of the palm.

Unity3D framework was utilized for developing the three dimensional hand model, since building up your very own cross-platform rendering engine is a non-trivial assignment. Unity3D was chosen because of friendly UI, capacity to actualize through it's methods both the scene and UI. Over the hand skeleton, a sensible hand model was created, rendered with in excess of 70,000 polygons (Fig. 2), Unity3D system can deal with such model with satisfying execution.

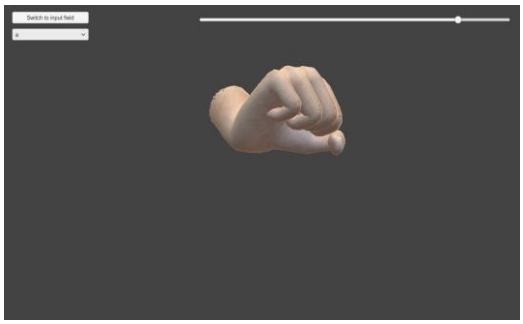

Fig. 2. Gesture modeling under iOS platform

6. Gesture recognition

Gesture learning and gesture recognition modules, developed with cross platform tools (frameworks based on Python, C++) can be embedded into information and gesture communication cross platform technology. Multiple approaches were considered as an approach for gesture recognition. Automatic sign language recognition can be approached similarly to speech recognition, with signs being processed similar to phones or words. Conventionally, sign language recognition consists of taking an input of video sequences, extracting motion features that reflect sign language linguistic terms, and then using pattern mining techniques or machine learning approaches on the training data.

Convolutional Neural Networks (CNNs) [12] have shown robust results in image classification and recognition problems, and have been successfully implemented for gesture recognition in recent years. In particular, deep CNNs have been used in researches done in the field of sign language recognition, with input-recognition that utilizes not only pixels of the images. With the use of depth sense cameras, the process is made much easier via developing characteristic depth and motion profiles for each sign language gesture. Multiple existing researches done over various sign languages show that CNNs achieve state-of-the-art accuracy for gesture recognition [6, 12].

Convolutional neural networks have such advantages: no need in hand crafted features of gestures on images; predictive model is able to generalize on users and surrounding not occurring during training; robustness to different scales, lightning conditions and occlusions. Although, selected approach has couple of disadvantages, which may be overcome with a relatively big dataset (1,000 images for each gesture, among more than 10 people of different age, sex, nationality and images taken under different environment conditions and scales): need to collect a rather big and labeled gesture images dataset; black-box approach which is harder to interpret. Usage of cross platform neural network framework such as Tensorflow allows to implement gesture recognition as a cross platform module of proposed technology and serve trained recognition model on server or transfer it to the device [3].

For experiment there was collected (Fig. 3) a dataset with Ukrainian dactyl language letters. Each gesture consists of 1500 sample images, and 50 different people hands were showing gestures, with distribution of 70% male and 30% female hands. Different light conditions were used (with distribution of 20% images in bad light conditions, 30% in mediocre light conditions and 50% in good light conditions). About 10% of images were distorted with noise and blur.

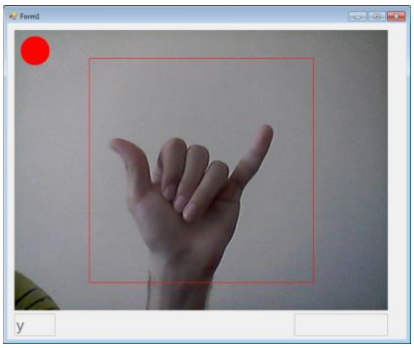

Fig. 3. UI tool for collection gesture database

MobileNet [6] architecture was used as a basis for CNN architecture. It has multiple advantages, such as good trade-off on accuracy and performance, especially on mobile devices, which are aimed to use, as the technology is cross-platform. The MobileNet model is based on depth wise separable convolutions which is a form of factorized convolutions which factorize a standard convolution into a depth wise convolution and a 1×1 convolution called a point wise convolution. For MobileNets the depth wise convolution applies a single filter to each input channel. The point wise convolution then applies a 1×1 convolution to combine the outputs the depth wise convolution. A standard convolution both filters and combines inputs into a new set of outputs in one step. The depth wise separable convolution splits this into two layers, a separate layer for filtering and a separate layer for combining. This factorization has the effect of drastically reducing computation and model size.

Process of training MobileNet network for gesture detection takes ~ 200.000 iterations, which is approximately 10 epochs. Figure 4 shows example UI of how the proposed technology detects specific gesture from Ukrainian dactyl and draws a bounding box over a detected gesture.

7. Gesture recognition experiment

For the training process of MobileNet architecture based Convolutional Neural Network for the task of gesture recognition of Ukrainian dactyl alphabet gestures an appropriate dataset should have been collected, due to no available datasets for Ukrainian sign language in free access. A specific software was developed for recording a short video sequences of Ukrainian dactyl alphabet gestures shown by different people. Since the recording software isn't direct part of the proposed technology, but rather a helper tool, it was developed only under Windows family of operating systems, using C# programing language and .NET framework. The pipeline of recording a single entry looks like this:

The person sits in front of the webcam, connected to the recording software;

The person needs to put one's hand into the region of interest of the recording software;

The person shows specific gesture from the Ukrainian dactyl alphabet;

The recording operator starts the recording;

The person showing the gesture starts to smoothly move the hand across different axis's;

After video of appropriate length was recorded, the operator stops the recording;

The process goes on with the next gesture.

Fig. 4. Example of recognition UI

8. Dataset and model architecture

Since training of the Convolution Neural Network hardly depends on a big and diverse dataset, to achieve a high enough accuracy metrics level, dataset of Ukrainian dactyl language letters with diverse characteristics was collected. More than 50,000 original images were collected as a training dataset. After applying additional dataset augmentation techniques (such as rotation, random crop, mirroring etc.) the final dataset became about 150,000 images. For testing purposes a fraction of 10% of the dataset was selected, making final training dataset of 135,000 images and final testing dataset of 15,000 images.

Table 1. Different architectures trained

Architecture 1	Architecture 2	Architecture 3	Architecture 4	Architecture 5
Conv / s2	Conv / s2	Conv / s2	Conv / s2	Conv / s2
Conv dw / s1	Conv dw / s1	Conv dw / s1	Conv dw / s1	Conv dw / s1
Conv / s1	Conv / s1	Conv / s1	Conv / s1	Conv / s1
Conv dw / s2	Conv dw / s2	Conv dw / s2	Conv dw / s2	Conv dw / s2
Conv / s1	Conv / s1	Conv / s1	Conv / s1	Conv / s1
Conv dw / s1	Conv dw / s1	Conv dw / s1	Conv dw / s1	Conv dw / s1
Conv / s1	Conv / s1	Conv / s1	Conv / s1	Conv / s1
Conv dw / s2	Conv dw / s2	Conv dw / s2	Conv dw / s2	Conv dw / s2
Conv / s1	Conv / s1	Conv / s1	Conv / s1	Conv / s1
Conv dw / s1	Conv dw / s1	Conv dw / s1	Conv dw / s1	Conv dw / s1
Conv / s1	Conv / s1	Conv / s1	Conv / s1	Conv / s1
Conv dw / s1	2 x Conv dw / s1	3 x Conv dw / s1	Conv dw / s2	Conv dw / s2
Conv / s1	2 x Conv / s1	3 x Conv / s1	Conv / s1	Conv / s1
Conv dw / s2	Conv dw / s2	Conv dw / s2	4 x Conv dw / s1	5 x Conv dw / s1
Conv / s1	Conv / s1	Conv / s1	4 x Conv / s1	5 x Conv / s1
Avg Pool / s1	Avg Pool / s1	Avg Pool / s1	Conv dw / s2	Conv dw / s2
FC / s1	FC / s1	FC / s1	Conv / s1	Conv / s1
Softmax / s1	Softmax / s1	Softmax / s1	Avg Pool / s1	Conv dw / s2
			FC / s1	Conv / s1
			Softmax / s1	Avg Pool / s1
				FC / s1
				Softmax / s1

Standard techniques of fighting overfitting of the neural network were applied on each training. Different architectures (Table 1) and their metrics and confusion matrixes are shown. Architecture 5 stopped showing growth in f1 score although having more complex performance. Architecture 4 (Fig. 5) was selected as the final option for the proposed technology as the best tradeoff of architecture size to performance.

During the training process of MobileNet architecture based Convolutional Neural Network multiple architecture modifications were set up in order to find the best trade-off in number of layers to accuracy. At some point the accuracy of the trained model stopped increasing, which is show in Fig. 5 so the architecture No 4 as decided as optimal in terms of the smallest architecture with best accuracy (macro average f1-score).

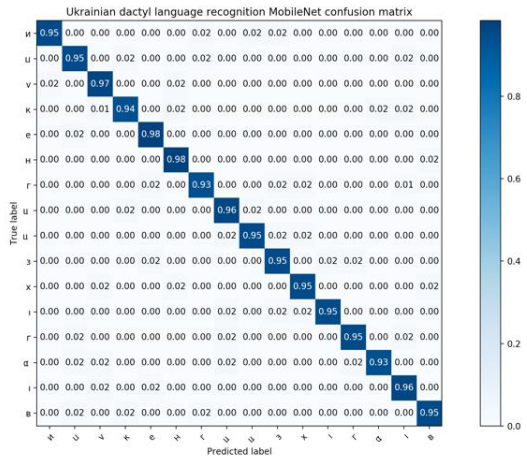

Fig. 5. Confusion matrix of the best trained architecture No 4

9. Conclusions

The proposed technology consists of two main modules: gesture modeling and gesture recognition modules, which use the database with gestures specifications stored in YAML format in a PostgreSQL database.

The proposed technology implements gesture modeling and gesture recognition for Ukrainian dactyl alphabet gestures with cross-platform development tools. Gesture modeling was implemented using Unity3D framework, which is cross-platform and shows satisfying performance on different platforms (mobile, web and desktop) while rendering a realistic three-dimensional hand model. Number of polygons and animation step of gesture transitions can be adjusted for the sake of performance.

A dataset of more than 50.000 images was collected using diverse conditions and different persons hands. The dataset was augmented using specific techniques and final dataset consists of 150.000 images. Gesture recognition module was implemented using Tensorflow framework, which provides ability to deploy its model on different platforms without any codebase modifications. As a model for gesture recognition, MobileNet architecture was chosen, as a model with best trade-off of size and accuracy, especially on low performance platforms (such as mobile and web). The model was trained on the collected Ukrainian dactyl language dataset. Due to augmentations, the model showed state-of-the-art level of performance. Based on experiments, optimal model architecture was chosen in order to keep the best performance level with the least model size possible. According experiments results were shown. The performance of CNN model was compared to other approaches and showed similar or superior values.

The proposed gesture communication technology can be further augmented with other gestures and languages and with other cross-platform modules.

References

[1] Apple Touchless Gesture System for iDevices http://www.patentlyapple.com/patently-apple/2014/12/apple-invents-a-highly-advanced-air-gesturing-system-for-future-idevices-and-beyond.html (available 15.05.2019).
[2] ASL Sign language dictionary http://www.signasl.org/sign/model (available 15.05.2019).
[3] Howard A.G., Wang W.: MobileNets: Efficient Convolutional Neural Networks for Mobile Vision Applications https://arxiv.org/pdf/1704.04861.pdf (available 15.05.2019).
[4] Khan R.Z., Ibraheem N.A., Meghanathan N., et al.: Comparative study of hand gesture recognition system. SIPM, FCST, ITCA, WSE, ACSIT, CS & IT 06/2012, 203–213.
[5] Krak I., Kondratiuk S.: Cross-platform software for the development of sign communication system: Dactyl language modelling, Proceedings of the 12th International Scientific and Technical Conference on Computer Sciences and Information Technologies, CSIT 1/2017, 167–170 [DOI: 10.1109/STC-CSIT.2017.8098760].
[6] Krizhevsky I. Sutskever, Hinton G.E.: Imagenet classification with deep convolutional neural networks. Advances in neural information processing systems 2012, 1097–1105.
[7] Kryvonos I.G., Krak I.V., Barchukova Y., Trotsenko B.A.: Human hand motion parametrization for dactylemes modeling. Journal of Automation and Information Sciences 43(12)/2011, 1–11.
[8] Kryvonos I.G., Krak I.V., Barmak O.V., Shkilniuk D.V.: Construction and identification of elements of sign communication. Cybernetics and Systems Analysis 49(2)/2013, 163–172.
[9] Kryvonos I.G., Krak I.V.: Modeling human hand movements, facial expressions, and articulation to synthesize and visualize gesture information. Cybernetics and Systems Analysis 47(4)/2011, 501–505.
[10] Mell P., Grance T.: The NIST Definition of Cloud Computing (Technical report). National Institute of Standards and Technology: U.S. Department of Commerce, 2011 [DOI:10.6028/NIST.SP.800-145].
[11] Neff M., Kipp M., Albrecht I., Seidel H.P.: Gesture Modeling and Animation by Imitation. MPI–I 4/2006.
[12] Ong E.I., et al. : Sign language recognition using sequential pattern trees. Computer Vision and Pattern Recognition (CVPR), 2012 IEEE Conference on. IEEE, 2012, 2200–2207.
[13] Raheja J.: Android based portable hand sign recognition system. 2015 [DOI: 10.15579/gcsr.vol3.ch1].
[14] Shapiro A., Chu D., Allen B., Faloutsos P.: Dynamic Controller Toolkit, 2005 http://www.arishapiro.com/Sandbox07_DynamicToolkit.pdf (available 15.05.2019).
[15] Smith J., Navi R.: The Architecture of Virtual Machines. Computer. IEEE Computer Society 38(5)/2005, 32–38.
[16] Tensorflow framework documentation https://www.tensorflow.org/api/ (available 15.05.2019).
[17] The Linux Information Project, Cross-platform Definition.
[18] Unity3D framework https://unity3d.com/ (available 15.05.2019).
[19] YAML – The Official YAML Web Site http://yaml.org/ (available 15.05.2019).

M.Sc. Serhii Kondratiuk
e-mail: kondratiuk@univ.net.ua

In 2013 graduated from the faculty of cybernetics KNU of Taras Shevchenko. In 2015-2019 studied as a Ph.D. student at faculty of computer science and cybernetics. Since 2017 works as an assistant of cathedral of Theoretical Cybernetics.

ORCID ID: 0000-0002-5048-2576

Prof. Iurii Krak
e-mail: krak@univ.kiev.ua

In 1980 graduated from the Faculty of Cybernetics Taras Shevchenko National University of Kyiv (KNU), in 1984 – Post Doctorate, in 1999 - Doctorate of KNU, 1998 - Internship at the Yale University (USA). 1989 – Assistant Professor, 1992 - Associate Professor, 1999 – Full Professor, 2014 - Head of Theoretical Cybernetics Department of KNU, 2018 – Corresponding Member of NAS of Ukraine.

ORCID ID: 0000-0002-8043-0785

Prof. Waldemar Wójcik
e-mail: waldemar.wojcik@pollub.pl

Director of Institute of Electronic and Information Technologies, Faculty Electrical Engineering and Computer Science, Lublin University of Technology. His research interests include electronics, automatics, advanced control techniques, the optimization of the industrial processes, and fiber optic sensors including fiber Bragg gratings.

ORCID ID: 000-0002-0843-8053

otrzymano/received: 15.05.2019 *przyjęto do druku/accepted: 15.06.2019*

DOI: 10.5604/01.3001.0013.2543

RESEARCH OF PARAMETERS OF FIBER-OPTICAL MEASURING SYSTEMS

Waldemar Wójcik[1], Aliya Kalizhanova[2,3], Gulzhan Kashaganova[2,4], Ainur Kozbakova[2,3], Zhalau Aitkulov[2,3], Zhassulan Orazbekov[2,5]

[1]Lublin University of Technology, [2]Institute of Information and Computational Technologies, SR MES RK, [3]Al-Farabi Kazakh National University, [4]Kazakh-American University, [5]Abai Kazakh National Pedagogical University

Abstract. *At present there exist a lot of technical devices, the failure of which can be connected not only with huge financial losses, but with the treat to the environment as well. Therefore, an important problem is the effective devices conditions diagnostics, including electronic components and check of their operation. Timely faults detecting allows introducing the prevention measures and avoiding serious consequences. Fiber-optic sensors have several advantages, more important of which include the immunity to electromagnetic disturbances, little weight and possibility to be included into the structure being measured. The most perspective are the sensors based on the Bragg fiber gratings. Bragg fiber gratings have several advantages, for instance, they allow creating the distributed measuring massifs, which contain several sensors. As well, they are insensitive to the optic power source vibrations. Variety of using the fiber sensors based on the Bragg fiber gratings has led to producing the Bragg fiber gratings with different spectral characteristics. Homogeneous Bragg fiber gratings have the spectra with solid side lobes, which can influence at the temperature sensor processing characteristics. To level the side lobes there is applied the apodization method, which is one of the means to affect the spectral form. The article herein considers the issues of the Bragg fiber gratings mathematical and computer modeling using the transfer matrix method. Transfer matrix method allows defining the optical components spectral characteristics based on the bound modes theory and description of electromagnetic wave, passing through an optic fiber. In the article there have been analyzed the Bragg fiber gratings in compliance with spectral features, such as transmission and reflectance spectra. As well, there has been carried out the experiment with influence of various parameters at the Bragg fiber gratings spectral characteristics. There have been studied the Bragg fiber gratings spectral features and selected the grating optimal parameters for designing the fiber-optic sensors based on the Bragg fiber gratings.*

Keywords: Bragg gratings, optical sensors, temperature, mathematical model

BADANIE PARAMETRÓW ŚWIATŁOWODOWYCH SYSTEMÓW POMIAROWYCH

Streszczenie. *Obecnie istnieje wiele urządzeń technicznych, których awarię można powiązać nie tylko z ogromnymi stratami finansowymi, ale także z troską o środowisko. Dlatego ważnym problemem jest skuteczna diagnostyka warunków pracy urządzeń, w tym elementów elektronicznych i kontrola ich działania. Wykrywanie błędów w odpowiednim czasie umożliwia wprowadzenie środków zapobiegawczych i uniknięcie poważnych konsekwencji. Czujniki światłowodowe mają kilka zalet, z których ważniejsze to odporność na zakłócenia elektromagnetyczne, niewielka waga i możliwość włączenia do mierzonej struktury. Najbardziej perspektywiczne są czujniki oparte na siatkach Bragga (FBG). Optyczne siatki Bragga mają kilka zalet, na przykład umożliwiają tworzenie rozproszonych układów pomiarowych, które zawierają kilka czujników. Są również niewrażliwe na wibracje źródła zasilania optycznego. Różnorodność wykorzystania czujników światłowodowych opartych na siatkach Bragga doprowadziła do wytworzenia siatek Bragga o różnych charakterystykach spektralnych. Jednorodne, optyczne siatki Bragga mają widma z pełnymi płatkami bocznymi, które mogą wpływać na charakterystykę przetwarzania czujnika temperatury. Aby wyrównać płatki boczne, stosuje się metodę apodyzacji, która jest jednym ze sposobów wpływania na formę widmową. W niniejszym artykule omówiono zagadnienia światłowodowych siatek Bragga, modelowania matematycznego i komputerowego z wykorzystaniem metody macierzy transferu. Metoda macierzy transferu pozwala na określenie charakterystyki widmowej składników optycznych w oparciu o teorię modów wiązanych i opis fali elektromagnetycznej, przechodzącej przez światłowód. W artykule przeanalizowano siatki Bragga zgodnie z cechami widmowymi, takimi jak widma transmisji i odbicia. Przeprowadzono również eksperyment z wpływem różnych parametrów na charakterystyki widmowe siatek Bragga. Zbadano cechy widmowe siatek Bragga i wybrano optymalne parametry siatki do projektowania czujników światłowodowych opartych na siatkach Bragga.*

Słowa kluczowe: siatki Bragga, czujniki optyczne, temperatura, model matematyczny

Introduction

Nowadays there are great many of technical devices, the failure of which can be connected not only with huge financial losses, but with the treat to the environment as well. Therefore, an important problem is the effective devices conditions diagnostics, including electronic components and check of their operation. Timely faults detecting allows introducing the prevention measures and avoiding serious consequences.

Measuring systems based on optic-electronic systems find application in the machines and processes diagnostics [12]. Separate place occupies the optic-fiber sensors, characterized by a number of advantages, amongst which the most important are the resistance to electric-magnetic disturbances and possibility of their building into the structure being measured [15]. In case of the sensor systems based on the Bragg fiber gratings' advantages are measurement accuracy self-sufficiency form, the light source fluctuation, the possibility of creating more complicated measuring systems, positioning several sensors on one optic fiber. Bragg fiber gratings in the sensitive applications are much sought after by the scientists all over the world during many years. Their basic feature is an ability to reflect the light radiation with well-defined wave length, with simultaneous transparency for the light with various waves lengths [7, 8].

Being based on defining the wave's relative central length offset, the fluctuations of the light source optic power does not affect its accuracy. There are a lot of methods for specifying the Bragg wave length, as well, allowing its defining, based on the spectra with big noise [2, 14]. Linear processing of the value having been measured upon transmitting the wave's standard length setoff, called the Bragg wave's central length, makes them natural transformers of physical values, such as power [3, 5, 10], temperature or deformation [11, 13].

The parameter, making the certain influence at the Bragg grating spectrum is apodization. In the simplest case we differentiate homogeneous gratings, in which the modulation depth of interference fringes fracturing factor is the same along the structure's whole length. Multitude of the fiber-optic homogeneous structures definite applications made introducing the apodised function into their production methods, which led to modulation variable depth of grating fringes refraction index.

One of the most frequently used interrogation methods of temperature sensor based on the Bragg fiber gratings is the filtration by means of the second grating with the same wave length, having been created in the identical primary conditions [6]. In such system an important parameter, conditioning the given cyclical structure's practicality is the minimization of the so called side lobes [1]. One of the means to reach the effect thereof is the apodization through changing the modulation depth of refraction factor alterations in the core of the optical fiber along its axis. Cyclical structures production with any apodization functions often linked with the necessity to redesign the system and therefore the possibility to use mathematical models for simulating grating spectrum with a denoted apodization is justified.

1. Mathematical model of approximated Bragg gratings

One of modeling techniques is the transfer matrix method (TMM) [4], which allows specifying the optic elements spectral characteristics based on the bounded modes theory and matrix describing the electro-magnetic wave, passing through the optic fiber following periods [9].

In such approach we suppose, that the grating overall length L is broken down into exactly determined sections N, so that each section, having been created in such a manner with a length $\Delta z = L/N$, can be considered as homogeneous. Transmission matrix, describing the i- section will be defined as follows [17]:

$$T_i = \begin{bmatrix} \cosh(\gamma \otimes z) - \frac{\sigma}{\gamma}\sinh(\gamma \otimes z) & -i\frac{k}{\gamma}\sin(\gamma \otimes z) \\ i\frac{k}{\gamma}\sin(\gamma \otimes z) & \cosh(\gamma \otimes z) - \frac{\sigma}{\gamma}\sinh(\gamma \otimes z) \end{bmatrix} \quad (1)$$

For the definition above, it is also assumed, that κ- variable, coupling factor constituent for refraction coefficient contrast ratio $v = 1$, being analyzed wave's length λ and envisaged apodization function g will be $g(z)$:

$$k = \frac{\Pi}{\lambda} \cdot v \cdot \hat{\sigma}_{eff}(z) \quad (2)$$

$$\bar{\delta}_{eff}(z) = \delta_{eff} \cdot g(z) \quad (3)$$

During Bragg grating simulation the variable coupling ratio component value κ depends on the selecting the refraction factor envelope function (2). General coupling coefficient is defined with the equation (4). It is as well known, that λ_B – Bragg wave length, and n_{eff} – effective refraction factor.

$$\hat{\sigma} = \delta + \sigma - \frac{1}{2}\frac{d\varphi}{dz} \quad (4)$$

$$\delta = 2\Pi n_{eff}\left(\frac{1}{\lambda} \cdot \frac{1}{\lambda_B}\right) \quad (5)$$

$$\sigma = \frac{2k}{v} \quad (6)$$

Parameter γ for transmission matrix is specified as follows:

$$\gamma = \sqrt{k^2 + \hat{\sigma}^2} \quad (7)$$

Overall grating features can be described as

$$\begin{bmatrix} R_0 \\ S_0 \end{bmatrix} = T \begin{bmatrix} R_N \\ S_N \end{bmatrix} \quad (8)$$

$$T = [T_N] \cdot [T_{N-1}] \cdots [T_3] \cdot [T_2] \cdot [T_1] \quad (9)$$

Values of matrix parameters T might be used for defining characteristics of both reflected (10), and transmitted (11) waves. Further the indexed components T_{ij} indicate the elements values under the i-column and j-line of transmission matrix.

$$R = \frac{T_{21}}{T_{11}} \quad (10)$$

$$S = \frac{1}{T_{11}} \quad (11)$$

2. Modelling spectral characteristics using simulation original application

Comprehension of the Bragg fiber gratings features and basic parameters is possible without their production. However, for that purpose the modeling instruments are necessary. Their usage can minimize the abnormal grating creation, also adjust it to a target-oriented application early enough. Apodization function proper selection allows optimize additionally the grating features with account of its target-oriented application site, for instance, as an optic filter or measuring sensor [16].

Own-grown simulation instrument based on TMM mathematical model has been used for modeling the transmission spectrum change for Bragg different length gratings.

In view of that there was used the Bragg grating with a wave length of 1550 mm and with an effective refraction factor 1.447. Simulation outcomes are presented on the Fig. 1.

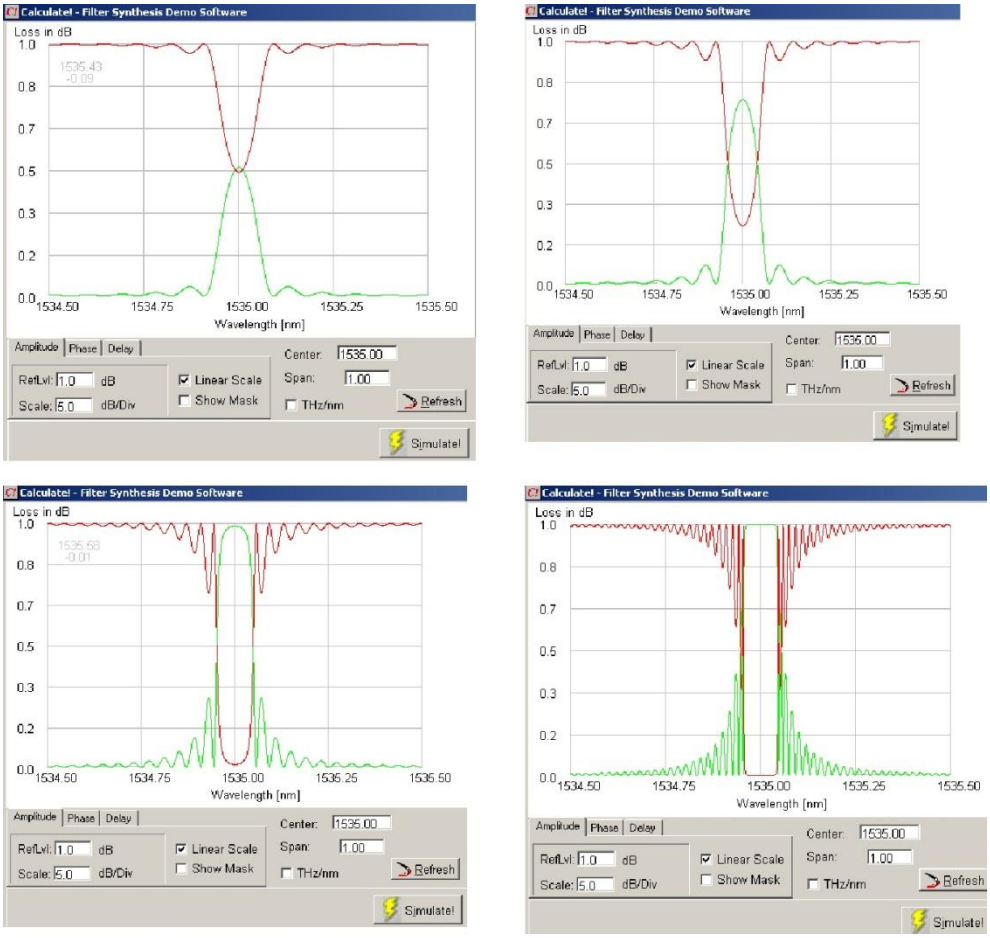

Fig. 1. Characteristics of transmission spectrum for Bragg various waves lengths

Legality of the used instrument has been proved with additional simulations for Bragg various waves' lengths (1546 nm, 1550 nm). Observations outcomes have been placed on sequential graphs, Fig. 2.

Presented opportunities are only a part of modeling accessible parameters. It is possible to define the apodization function, being used upon Bragg gratings recording. But the topic will be discussed in detail in one of the following subsections of the article herein.

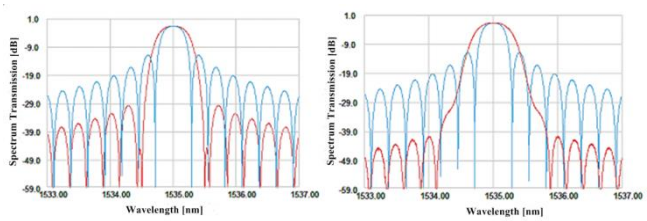

Fig. 2. Transmission spectrum for Bragg various wavelengths (1546 nm, 1550 nm)

3. Optical system mathematical and physical models

Optical systems simulation using computer instruments, based on mathematical models, can turn out to be very useful, but it is worth to get a sense, that a computer language is not able to reproduce completely the physical optical system and all prevailing physical phenomena. The article section herein compares the features being simulated to the real reflection spectrum. It has been specified, to what extent the object being simulated can differ from the actual system.

Within the experiment frame the Bragg grating has been built up in the system, similar to the one, that is shown on the Figure 3. There has been applied a phase mask with constant period along its overall length. Laser with a profile bundle, introducing apodization with the function, being defined with the formula (12), has been used for combustion of the sequential structure in the optic fiber core. Figure 3 shows, that a reflected spectrum has been measured using a spectrum analyser with a reduction 0.02 nm.

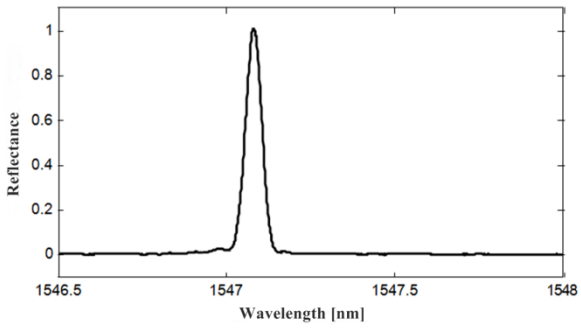

Fig. 3. Real optic system reflectivity spectrum

```
clear;
clc;

lambda= linspace(1.4,1.6,500)*1e-6;

ok=5.0e-7;
nbar = 1.500; % mean value of n
Dn = 0.0004; % variation in n

hold on;
plot(BornApprox(lambda,ok,nbar,Dn))
```

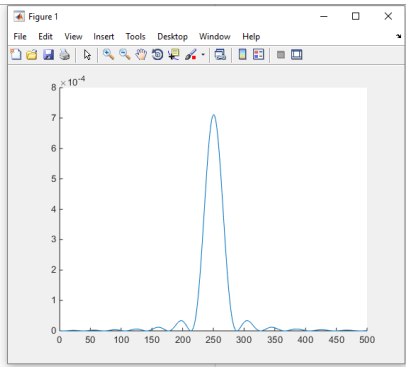

Fig. 4. Apodization grating simulated reflectivity spectrum in compliance with laser beam profile

In case of mathematical model, as input data for modeling instrument, there have been introduced analog grating parameters (there has been accounted the previously set apodization function). Outcomes of the modeling herein are presented on the Figure 4.

Comparing the spectrum, shown on the Figure 3, and simulation characteristics, demonstrated on the Figure 4, clearly prove compatibility of the Bragg grating nature with the model being used in the application. Both characteristics go with the fact, that applying the apodization with a profile, compatible with Gaussian curve with accordingly selected parameters, brings to disappearance of the side lobes, typical for homogeneous Bragg fiber gratings.

4. Temperature sensor processing characteristics

Measurements for the sensor temperature sensitivity definition are based on the Bragg wavelengths, considering the spectral characteristics, having been measured within different temperatures range. The most frequently used method of the central wavelength definition is the extemum search (minimum for transmission spectrum or maximum for reflectivity one). Figure 5 shows the measuring system scheme, in which the climatic chamber has been used for the temperature setting. During measurements the relative humidity has been maintained constant at the level of 30%.

The graph on the figure 5 shows the tested temperature sensor processing characteristics together with the linear regression line, obtained based on the measurement points.

Linear correlation factor, having been obtained for characteristics points in the measured temperature range, equals to r = 0.9997 and standard deviation s = 0.473. Those parameters show, that the temperature changes along the Bragg wavelength, and it is linear. System's sensitivity, realized as the central wavelength shifting to *1* degree Celcium, can be expressed as the difference ratio in the Bragg wavelengths, at measured temperatures to the temperatures differentials:

$$\frac{\Delta\lambda_B}{\Delta T} = \frac{\lambda_{T1} - \lambda_{T2}}{T_1 - T_2} \tag{12}$$

Sensitivity S of the sensor being tested is defined as follows

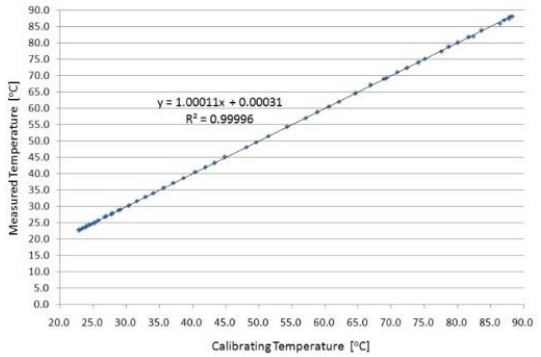

Fig. 5. Characteristics of temperature sensor processing

5. Conclusion

Physical multitudes fiber-optic sensors occupy an important place in the sensors area thanks to a few of advantages, which differentiate them from electronic analogs. A special type is a sensor on the basis of the Bragg fiber-optic gratings, which apart from the standard function, characterizing the opto-fiber sensors, also allows multiplexing, which creates a wide network, consisting of dozens sensors, placed in one optic fiber.

A great many applications for the Bragg fiber gratings brought to the necessity to influence at the grating optic spectrum nature. Upon temperature measuring the selection criterion consists in the most effective reduction of the so-called side lobes, presence of which might severely affect the sensors' characteristics, particularly while using interrogation filtration system. One of the

means to eliminate the spectrum unfavorable features is apodization, commonly including the refraction index change depth modulation along the structure. Applying the mathematical model, taking into consideration the apodization function and own simulation application function, allows forecasting the influence of apodization parameters change at the outlet spectrum. Examples show the effect of selected inlet modeling parameters at the form of the outlet characteristic.

The quality of the model, used in simulations, has been checked through comparing the characteristics, having been measured for actual Bragg grating with apodization, transmitted by laser beam profile to a resulting modeling outcome for introduced apodization function, corresponding to laser beam power distribution. Both characteristics show clear suppression of the side lobes, adding the Gaussian character of the basic peak spectrum.

The Bragg fiber grating, used as a temperature sensor, secures the being measured linear characteristic for shifting the grating wavelength. The experiment, fulfilled for the formulated grating, allowed defining its temperature sensitivity, which constitutes 10.37 h/°C. There has been confirmed the temperature processing linear character for shifting the Bragg wavelength, which is proved with the statistical parameters denoted characteristics.

Experimental studies have been conducted in the optoelectronic laboratories of the Lublin University of Technology, Faculty of Electrical Engineering and Computer Science in the frame of the state financing project No AP05132778 “Research and development of interrogation signals system with optic-fiber refractometer using the telecommunication networks” IICT SR MES RK.

References

[1] Abdulina S. R., Vlasov A. A.: Suppression of side lobes in the Bragg fiber grating reflection spectrum. Optoelectronics, Instrumentation and Data Processing 50(1)/2014, 75–86.
[2] Chen Y., Chen L., Liu H., Wang K.: Research of FBG sensor signal wavelength demodulation based on improved wavelet transform. Optic 124/2013, 4802–4804.
[3] Cięszczyk S., Kisała P.: Inverse problem of determining periodic surface profile oscillation defects of steel materials with a Bragg fiber grating sensor. Appl. Opt. 55/2016, 1412–1420.
[4] Demirdag O., Yildirim B.: Comparing transmission matrix method and AN- FIS in free vibration analysis of Timoshenko columns with applications. Res. Eng. Struct. Mat. 2/2016, 1–18.
[5] Harasim D., Gulbakhar Y.: Improvement of FBG peak wavelength demodulation using digital signal processing algorithms. Proc. SPIE 9662, 2015, 966212.
[6] Harasim D., Kisała P.: Układy przesłuchujące multipleksowane światłowodowe czujniki Bragga. Informatyka, Automatyka, Pomiary w Gospodarce i Ochronie Środowiska – IAPGOS 5(4)/2015, 77–84.
[7] Kashyap R.: Fiber Bragg Gratings. Academic Press San Diego 2009.
[8] Kenneth O., Meltz G.: Bragg Fiber Grating Technology Fundamentals and Overview. Journal of Lightwave Technology 15(8)/1997, 1263–1276.
[9] Khalid K. S., Zafrullah M., Bilal S. M., Mirza M. A.: Simulation and analysis of Gaussian apodized Bragg fiber grating strain sensor. Journal of Optical Technology 7(10)/2012, 667–673.
[10] Kisała P., Cięszczyk S.: Method of simultaneous measurement of two direction force and temperature using FBG sensor head. Applied Optics 54(10)/2015, 2677–2687.
[11] Kisała P.: Method of simultaneous measurement of bending forces and temperature using Bragg gratings. Proc. SPIE 9506, 2015.
[12] Kotyra A.: Optoelektroniczne systemy w zastosowaniach diagnostycznych i pomiarowych. Informatyka, Automatyka, Pomiary w Gospodarce i Ochronie Środowiska – IAPGOS 4(2)/2014, 9–10.
[13] Majumder M., Gangopadhyay T. K., Chakraborty A. K., Dasgupta K., Bhattacharya D. K.: Bragg fiber gratings in structural health monitoring – present status and applications. Sensors and Actuators 147/2008, 150–164.
[14] Negri L., Nied A., Kalinowski H., Paterno A.: Benchmark for Peak Detection Algorithms in Bragg Fiber Grating Interrogation and a New Neural Network for its Performance Improvement. Sensors 11/2011, 3466–3482.
[15] Pereira G., McGugan M., Mikkelsen L.P.: Method for independent strain and temperature measurement in polymeric tensile test specimen using embedded FBG sensors. Polymer Testing 50/2016, 125–134.
[16] Wójcik W., Kisała P.: The application of inverse analysis in strain distribution recovery using the Bragg fiber grating sensors. Metrology and Measurement Systems 16(4)/2009, 649–660.
[17] Wójcik W., Kisała P.: Metoda wyznaczania funkcji apodyzacji światłowodowych siatek Bragga na podstawie ich charakterystyk widmowych. Przegląd Elektrotechniczny 86(10)/2010, 127–130.

Prof. Waldemar Wójcik
e-mail: waldemar.wojcik@pollub.pl

Director of Institute of Electronic and Information Technologies, Faculty Electrical Engineering and Computer Science, Lublin University of Technology. His research interests include electronics, automatics, advanced control techniques, the optimization of the industrial processes, and fiber optic sensors including fiber Bragg gratings.

ORCID ID: 000-0002-0843-8053

Ph.D. Aliya Kalizhanova
e-mail: kalizhanova_aliya@mail.ru

Candidate of physical and mathematical sciences, associate professor, the deputy general director of the Institute of Information and Computational Technologies of the Ministry of Education and Science CS of the Republic of Kazakhstan. Scientific interests of the leader: mathematical modeling of systems, models of transport systems network analysis, optimization methods, technologies for developing sensor systems for signals receive-transmit, mathematical modeling of Bragg fiber gratings.
ORCID ID: 000-0002-0843-8053

Ph.D. Gulzhan Kashaganova
e-mail: guljan_k70@mail.ru

Ph.D. on a specialty "Radio engineering, electronics and telecommunications" the senior scientific employee of Institute of Information and Computational Technologies of the Ministry of Education and Science CS of the Republic of Kazakhstan. Scientific interests: protection of information in telecommunication networks, optical fiber in telecommunication systems and networks, technologies for development of sensor systems for receiving and transmitting signals, mathematical modeling of Bragg fiber gratings.

ORCID ID: 0000-0001-8150-1621

Ph.D. Ainur Kozbakova
e-mail: ainur79@mail.ru

Ph.D. on a specialty "Information Systems", a senior fellow at the Institute of Institute of Information and Computational Technologies of the Ministry of Education and Science CS of the Republic of Kazakhstan. Research interests: mathematical modeling of discrete systems, evacuation tasks, operations research, technology design of complex systems.

ORCID ID: 0000-0002-5213-4882

M.Sc. Zhalau Aitkulov

Doktorant Ph.D. on a specialty "Information Systems", a programmer at the Institute of Institute of Information and Computational Technologies of the Ministry of Education and Science CS of the Republic of Kazakhstan. Research interests: mathematical modeling of discrete systems, evacuation tasks, operations research, technology design of complex systems.

ORCID ID:0000-0002-5928-3258

Ph.D. Zhassulan Orazbekov
e-mail: o.jas@mail.ru

Ph.D. on a specialty "Information Systems", a senior fellow at the Institute of Institute of Information and Computational Technologies of the Ministry of Education and Science CS of the Republic of Kazakhstan. Research interests: mathematical modeling of discrete systems, operations research, technology design of complex systems.

ORCID ID: 0000-0003-4332-1966

otrzymano/received: 15.05.2019 *przyjęto do druku/accepted: 15.06.2019*

DOI: 10.5604/01.3001.0013.2544

DETERMINATION OF THE PROBABILITY FACTOR OF PARTICLES MOVEMENT IN A GAS-DISPERSED TURBULENT FLOW

Saltanat Adikanova[1], Waldemar Wójcik[2], Natalya Denissova[3], Yerzhan Malgazhdarov[3], Ainagul Kadyrova[1]

[1]S. Amanzholov East Kazakhstan State University, Ust-Kamenogorsk, Kazakhstan, [2]Lublin University of Technology, Lublin, Poland, [3]D. Serikbayev East Kazakhstan State Technical University, Ust-Kamenogorsk, Kazakhstan

Abstract. *The goal of the work is to define the probability factor of particles movement in a gas-dispersed turbulent flow. The object of the research is the description of harmful impurities transfer process in the atmosphere with the help of mathematical modelling of variability of gas and aerosol composition of atmosphere. Another object is assessment atmospheric impurities on the environment. The novelty of the research is that probability-statistical approach is used in modelling the transfer of harmful impurities from anthropogenic sources into the atmosphere.*

Keywords: probability factor of particles movement, transfer of harmful impurities, environment, anthropogenic sources, pollutions, information system.

WYZNACZENIE WSPÓŁCZYNNIKA PRAWDOPODOBIEŃSTWA RUCHU CZĄSTEK STAŁYCH W TURBULENTNYM PRZEPŁYWIE DYSPERSYJNYM W FAZIE GAZOWEJ

Streszczenie. *Celem pracy jest określenie współczynnika prawdopodobieństwa ruchu cząstek w przepływie turbulentnym dyspersyjnym w gazie. Celem pracy jest opisanie procesu przenoszenia szkodliwych zanieczyszczeń do atmosfery za pomocą matematycznego modelowania zmienności składu gazów i aerozoli atmosferycznych oraz ocena wpływu zanieczyszczeń atmosferycznych na środowisko. Nowością tych badań jest zastosowanie probabilistycznego i statystycznego podejścia do modelowania transferu szkodliwych zanieczyszczeń ze źródeł antropogenicznych do atmosfery.*

Słowa kluczowe: współczynnik prawdopodobieństwa ruchu cząstek, transfer szkodliwych zanieczyszczeń, środowisko, źródła antropogeniczne, zanieczyszczenia, system informacyjny

Introduction

Anthropogenic sources of pollution influence the environment and affects the state of air basin. The problems of air basin protection are included in a wide research area on the junction of several sciences. Pollution of atmosphere surface layer is the most relevant problem nowadays.

The pattern of flow and dissemination of harmful substances and their compounds that locally contaminate air surface layer considerably differs from these phenomena in fee atmosphere. The solution of scientific and applied problems of environment protection requires detailed description of processes of harmful substances dissemination in air basin of industrial regions. Recently, these problems have become urgent especially in large industrial cities due to the activities of big industrial enterprises.

Experimental researches in this sphere are connected with significant investments and hampered due to large spatial scale of the process. Besides, the experiment enables to build up situation forecast in case of atmospheric conditions change (speed and direction of wind, atmospheric pressure) Mathematical modeling in this direction enables to track and forecast impurities dissemination in atmosphere surface layer taking into account real conditions of a region and change of meteorological parameters that will help to make due administrative decisions.

Long term experience in studying air pollution have been accumulated, natural experiments on control of impurities dissemination have been carried out, and basic regularities of transfer have been obtained [1]. Accuracy of models intended for calculation of impurities dissemination in atmosphere is the main thing for environment protection activities. Calculation methods for impurities dissemination in atmosphere is basically suitable for the conditions of thermally uniform and smooth relief [7, 8].

The relevance of this work is determined by the necessity to model pollution of air basin of industrial centres for complex study of pollutants dynamics in air basin of certain region, by providing the opportunity to carry out computational experiments taking into account the current information, and by studying different situations within the frameworks of the chosen scenario.

1. Determination of the probability factor of particles movement

The given article considers determination of the probability factor of particles movement in a gas-dispersed turbulent flow of atmospheric boundary layer for probable – statistical model described in the work [8].

The work [8] considered impurity particles movement as a sequence of step movements that are h long in small periods of time Δt in one of four possible directions on the vertical plane.

Movement directions were defined every time by corresponding probabilities p_i: p_{+x}, p_{-x}, p_{+y}, p_{-y}, and naturally in accordance with normalization requirement that is at any moment of time

Błąd! Nie można tworzyć obiektów przez edycję kodów pól.(1)

Applying approximants for recurrent Poissonian flow of events and law of large numbers, passing to the limit when $\Delta t \to 0$ and adding the function describing sources of harmful impurities emissions we have got the following equation in the plane (x, z):

$$\begin{aligned}\frac{\partial \phi}{\partial t} &= \mu_{+x,i,j}\left(\phi^n_{i-1,j}-\phi^n_{i,j}\right)+\\ &+\mu_{-x,i,j}\left(\phi^n_{i+1,j}-\phi^n_{i,j}\right)+\\ &+\mu_{+z,i,j}\left(\phi^n_{i,j-1}-\phi^n_{i,j}\right)+\\ &+\mu_{-z,i,j}\left(\phi^n_{i,j+1}-\phi^n_{i,j}\right)+f\end{aligned} \tag{2}$$

The equation (2) is identical to difference analogue of transfer equations. Difference analogue of transfer equations in continuous medium can be in the following form taking into account diffusion process and using the scheme accounting the sign:

$$\begin{aligned}\frac{\varphi^{n+1}_{i,j}-\varphi^n_{i,j}}{\tau} &= \left[\frac{\mu_x}{h_1^2}+\frac{u+|u|}{2h_1}\right]\left(\varphi^n_{i-1,j}-\varphi^n_{i,j}\right)+\\ &+\left[\frac{\mu_x}{h_1^2}+\frac{u-|u|}{2h_1}\right]\left(\varphi^n_{i+1,j}-\varphi^n_{i,j}\right)+\\ &+\left[\frac{\mu_z}{h_2^2}+\frac{w+|w|}{2h_2}\right]\left(\varphi^n_{i,j-1}-\varphi^n_{i,j}\right)+\\ &+\left[\frac{\mu_z}{h_2^2}+\frac{w-|w|}{2h_2}\right]\left(\varphi^n_{i,j+1}-\varphi^n_{i,j}\right)+f_{i,j}\end{aligned}$$

It is seen to be that transitions intensity **Błąd! Nie można tworzyć obiektów przez edycję kodów pól.** and **Błąd! Nie można tworzyć obiektów przez edycję kodów pól.** are defined as follows

Błąd! Nie można tworzyć obiektów przez edycję kodów pól.(3)

Instantaneous speed of atmosphere at any point of the flow in every direction can be presented as the sum of average speed and pulsation speed:

Błąd! Nie można tworzyć obiektów przez edycję kodów pól., **Błąd! Nie można tworzyć obiektów przez edycję kodów pól.** (4)

where **Błąd! Nie można tworzyć obiektów przez edycję kodów pól.** are components of wind speed, **Błąd! Nie można tworzyć obiektów przez edycję kodów pól.**– stochastic process. When there is no wind in atmosphere, intensity of turbulent pulsations can be considered equal in all directions, i.e. **Błąd! Nie można tworzyć obiektów przez edycję kodów pól.**, so probabilities of movement can also be considered equal, i.e. **Błąd! Nie można tworzyć obiektów przez edycję kodów pól.**.

When equations (2) were calculated, transitions intensity **Błąd! Nie można tworzyć obiektów przez edycję kodów pól.** and **Błąd! Nie można tworzyć obiektów przez edycję kodów pól.** were defined according to (3) taking into account normalization requirements (1). Such approach provides implementing the terms of mass conservation and enables to define the amount of emitted pollutants into the atmosphere for certain period of time.

During numerical simulations two boundary conditions were taken into account:
first – free boundary

$$\left.\frac{\partial\phi}{\partial t}\right|_{x=X} = \mu_{+x,m,j}\left(\phi^n_{m-1,j}-\phi^n_{m,j}\right)+ \\ +\mu_{-x,m,j}\left(-\phi^n_{m,j}\right)+ \\ +\mu_{+z,m,j}\left(\phi^n_{m,j-1}-\phi^n_{m,j}\right)+ \\ +\mu_{-z,m,j}\left(\phi^n_{m,j+1}-\phi^n_{m,j}\right)+f \quad (5)$$

it means that impurity flows out easily but doesn't flow in. Thus, if it is required, we can define amount of impurities that were brought out from computational region for self-purification with wind regimes and second – solid boundary.

$$\left.\frac{\partial\phi}{\partial t}\right|_{z=0} = \mu_{+x,i,1}\left(\phi^n_{i-1,1}-\phi^n_{i,1}\right)+ \\ +\mu_{-x,i,1}\left(\phi^n_{i+1,1}-\phi^n_{i,1}\right)+ \\ +\mu_{+z,i,j}\left(-\phi^n_{i,1}\right)+ \\ +\mu_{-z,i,1}\left(\phi^n_{i,2}\right)+f \quad (6)$$

in this case the impurity neither flows in nor flows out. In the same way it is possible to get boundary conditions for other boundaries of the considered area.

2. Results

The model that was described above with the help of probability-stochastic approaches was used for defining transition intensity. This helped to carry out methodological calculations of point and linear sources.

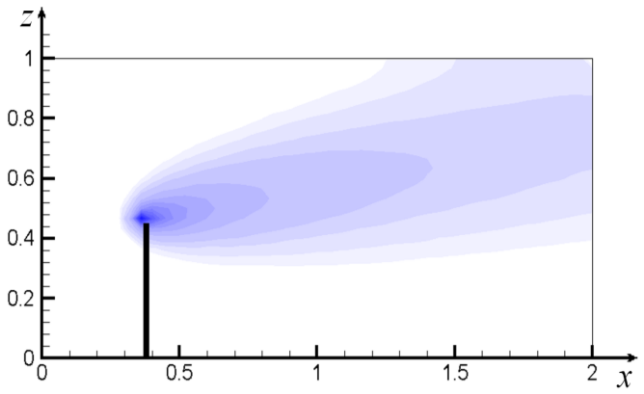

Fig. 1. Wind speed 1 m/s, point source

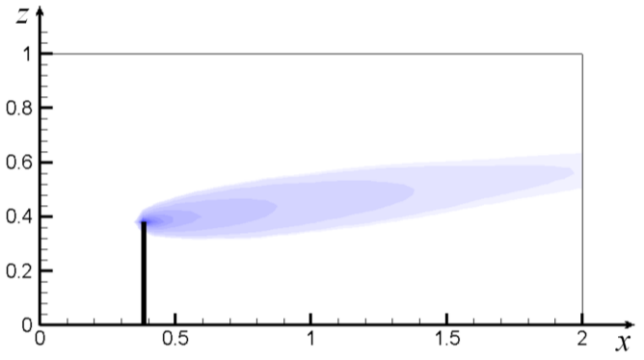

Fig. 2. Wind speed 3 m/s, point source

When model for dissemination of harmful impurities from stationary sources (Figures 1 and 2) is used, the influence of wind speed regime can be seen well. When wind speed is 1 m/s the transfer process goes on more slowly and influence of diffusion processes (Figure 1) is evident. When wind speed is 3 m/s impurity is carried away faster, avoiding diffusion processes influence (Figure 2).

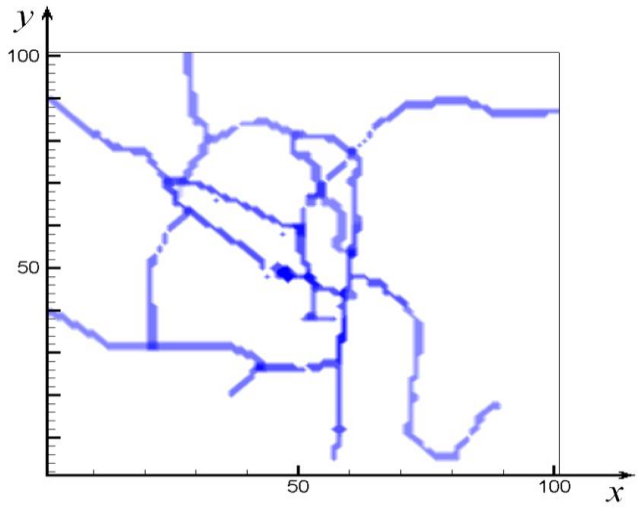

Fig. 3. Input data of linear source

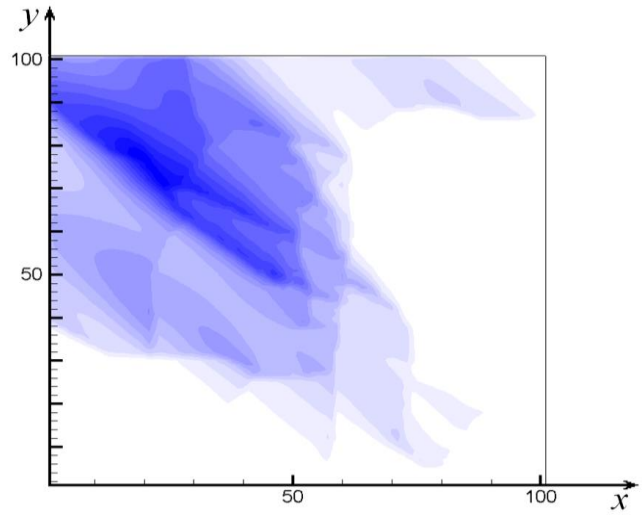

Fig. 4. Expansions from linear source, wind speed is 5 m/s

Figures 3 and 4 represent the results of calculations of harmful contaminants transfer from linear sources on horizontal section. Initial values from linear sources represented in figure 3 (road network of cities) were taken from works [6–8], and Figure 4 provides the results of numerical calculation of the task (2), (5), (6), coincide with the result of the work [7, 8].

In order to simulate the process of harmful impurities dissemination from vehicles in atmospheric air, Web-oriented information system was developed on the basis of probability-statistical model. The system evaluates the level of pollution from vehicles in surface layer of city atmosphere. The results of emissions dissemination are shown in Figure 5.

Fig. 5. Dissemination of emissions from vehicles

3. Conclusion

There are different methods of mathematical modelling of information systems for ecological monitoring of air basin: empiric-statistical method, method of forecasting increased pollution level, method of Gaussian plume model, dynamical-stochastic method.

The basic method chosen in the work is probability-statistical method. It is used for development of the algorithm of numerical modeling of harmful substances transfer process in atmosphere.

Thus, due to turbulent gas flow, it is characteristic that pulsations of speed in all directions are random and chaotic in all points of atmospheric air flow that makes processes be stochastic [8].

The use of probability-statistical modeling for harmful contaminants transfer in atmosphere enables to build up effective numerical algorithms of calculations and considerably reduces amount of calculations, computing time without loss of accuracy.

Information system is based on the model. The developed computer technology enables to display graphically the level of pollution in surface layer of atmosphere on the map of city territory. It also enables to simulate emissions under different traffic conditions and in different regimes of industrial enterprises operation, and to assess the degree of ecological conflict for every condition. Monitoring results can be used for development of routes, traffic schedules of public transport, and operation modes at industrial enterprises where sanitary standards of pollution are observed.

References

[1] Antonia R.A., Luxton R.E.: The Response of a Turbulent Boundary Layer to a Step Change in Surface Roughness, Pt. 1. Smooth to Rough. J. Fluid Mech. 48/1971, 721–762.
[2] Betchov R.: Transition, Handbook of Turbulence, Vol. 1. eds. W. Frost & T. H. Moulden. Plenum Press, New York 1977.
[3] Cao Y., You J., Shi Y., Hu W.: Evaluation of automobile manufacturing enterprise competitiveness from social responsibility perspective. Problemy Ekorozwoju/Problems of Sustainable Development 11(2)/2016, 89–98.
[4] Castillo L.: Similarity analysis of turbulent boundary layers. Ph. D. Thesis, The Graduate School of the State University of New York, Buffalo.
[5] Cel W., Czechowska-Kosacka A., Zhang T.: Mitigation of greenhouse gases emissions. Problemy Ekorozwoju/Problems of Sustainable Development 11(1)/2016, 173–176.
[6] Danaev N.T., Temirbekov A.N., Malgazhdarov E.A.: Modelling of Pollutants in the Atmosphere Based on Photochemical Reactions. Eurasian Chemico-Technological Journal 16(1)/2014, 61–71.
[7] Temirbekov N., Abdoldina F., Madiyarov M., Malgazhdarov E.: Journal of Computational Technologies, Special Issue 11/2006, 41–45.
[8] Wojcik W., Adikanova S., Malgazhdarov Y.A., Madiyarov M.N., Myrzagaliyeva A.B., Temirbekov N.M., Junisbekov M.: Probabilistic and Statistical Modelling of the Harmful Transport Impurities in the Atmosphere from Motor Vehicles. Rocznik Ochrona Środowiska 19/2017, 795–808.

Ph.D. Saltanat Adikanova
e-mail: ersal_7882@mail.ru

Saltanat Adikanova is a senior lecturer of sub-department "Computer modeling and information technologies" of S.Amanzholov East Kazakhstan state university.
She defended Doctor's thesis "Development of information system for modeling air pollution by vehicles" in 2018.
Research interests are modeling of complicated processes, development of monitoring information systems.
ORCID ID: 0000-0003-0085-8384

Prof. Waldemar Wójcik
e-mail: waldemar.wojcik@pollub.pl

Director of Institute of Electronic and Information Technologies, Faculty Electrical Engineering and Computer Science, Lublin University of Technology. His research interests include electronics, automatics, advanced control techniques, the optimization of the industrial processes, and fiber optic sensors including fiber Bragg gratings.

ORCID ID: 000-0002-0843-8053

Ph.D. Natalya Denissova
e-mail: nata69_07@mail.ru

Natalya Denissova, takes position of vice-rector on informatization, and director of Information Technology Department at D.Serikbaev East Kazakhstan state technical university.
She graduated I.Polzunov Altai state technical university and defended Candidate's dissertation „Computer modeling of thermo-activated structural change in biocrystal Ni-Al" in 2006.
Scientific interests: modeling information processes and systems, new communication technologies.
ORCID ID: 0000-0005-0525-730X

Ph.D. Yerzhan Malgazhdarov
e-mail: malgazhdarov_e@mail.ru

Ye. Malgazhdarov is Head of sub-department „Instrument engineering and automation of technological processes" at D.Serikbaev East Kazakhstan state technical university.
Ye. Malgazhdarov defended successfully his Candidate's dissertation on January 29, 2010 on specialty 05.13.18 – „Mathematical modeling, numerical methods, and software systems".
Scientific interests: modeling of complicated processes, new communication technologies.
ORCID ID: 0000-0003-4218-3469

Ph.D. Ainagul Kadyrova
e-mail: k_ainagul07@mail.ru

Ainagul Kadyrova works at sub department „Computer modeling and information technologies" of S.Amanzholov East Kazakhstan state university..
She defended Candidate's thesis successfully in 2010.
Research interests are high school pedagogics, teaching mathematical modeling, artificial intelligence, natural language processing.

ORCID ID: 0000-0001-6897-9380

otrzymano/received: 15.05.2019 *przyjęto do druku/accepted: 15.06.2019*

DOI: 10.5604/01.3001.0013.2545

DEVELOPMENT OF WIND ENERGY COMPLEX AUTOMATION SYSTEM

Kuanysh Mussilimov[1], Akhmet Ibraev[1], Waldemar Wójcik[2]
[1]Satbayev University, [2]Lublin University of Technology

Abstract. *Wind power is one of the three main renewable energy sources, along with solar and hydropower, which are widely used to produce electricity worldwide. As an energy resource, wind is widespread and can provide electricity to much of the world, but it is both intermittent and unpredictable, making it difficult to rely on wind power alone. However, when used in combination with other types of production or in combination with energy storage, wind can make a valuable contribution to the global energy balance. Over the past few decades, wind power has emerged in a number of countries as a separate energy sector that has successfully competed with conventional energy. Attention is paid to wind power plants (WT) as part of distribution and transmission networks. In this regard, an urgent scientific and technical task is the efficient use of wind potential, which is not only to improve aerodynamic characteristics WT, but also to increase productivity WT as a whole. This article presents the type of wind turbines, among the possible applications and very promising is the wind turbine Bolotov (WRTB), which by its technical characteristics surpasses the traditional propeller and other installations using wind energy in the production of electrical energy. The increase (WEUF - wind energy utilization factor*) in all modes of operation *WT by improving various methods of automatic control is relevant, and the proposed work is devoted to this issue.*

Keywords: wind energy, automation of wind turbines, wind farm monitoring

OPRACOWANIE ZŁOŻONEGO SYTEMU AUTOMATYZACJI ENERGETYKI WIATROWEJ

Streszczenie. *Energia wiatrowa jest jednym z trzech głównych źródeł energii odnawialnej, obok energii słonecznej i wodnej, które są szeroko wykorzystywane do produkcji energii elektrycznej na całym świecie. Jako źródło energii, wiatr jest szeroko rozpowszechniony i może dostarczać energię elektryczną do wielu części świata, ale jest on zarówno nieciągły, jak i nieprzewidywalny, co sprawia, że trudno jest polegać wyłącznie na energii wiatrowej. Jednakże w połączeniu z innymi rodzajami produkcji lub w połączeniu z magazynowaniem energii wiatr może wnieść cenny wkład w światowy bilans energetyczny. W ciągu ostatnich kilkudziesięciu lat energia wiatrowa pojawiła się w wielu krajach jako odrębny sektor energetyczny, który z powodzeniem konkurował z energią konwencjonalną. Szczególną uwagę zwraca się na elektrownie wiatrowe (EW) w ramach sieci dystrybucyjnych i przesyłowych. W związku z tym pilnym zadaniem naukowym i technicznym jest efektywne wykorzystanie potencjału wiatru, co ma na celu nie tylko poprawę właściwości aerodynamicznych turbin wiatrowych, ale również ogólne zwiększenie wydajności turbin wiatrowych. W artykule przedstawiono typ turbin wiatrowych, wśród możliwych zastosowań i bardzo obiecujący jest turbina wiatrowa Bolotov (WRTB), która swoją charakterystyką techniczną przewyższa tradycyjne śmigło i inne instalacje wykorzystujące energię wiatrową w produkcji energii elektrycznej. Istotne jest zwiększenie (WEUF - wind energy utilization factor) we wszystkich trybach pracy turbin wiatrowych poprzez udoskonalenie różnych metod automatycznej kontroli, a proponowane prace poświęcone są tej kwestii.*

Słowa kluczowe: energia wiatrowa, automatyzacja turbiny wiatrowej, monitoring farm wiatrowych

Introduction

Wind is a renewable, clean and endless source of energy, that meet demands of the growing energy in many countries. Thus, wind power is growing rapidly worldwide, especially over the past two decades, and the total installed capacity of wind power in the world has changed from 1.29 GW in 1995 to 370 GW by the end of 2015 [11]. Due to environmental considerations and the constant quest for energy security, this level will increase in nearest future, along with an increase in the size and installed capacity of wind turbines (WT).

Wind turbines have evolved from simple designs to complex multifunctional installations installed together in large arrays called "wind farms". The complexity of modern wind turbines necessitates a control system, which becomes a key component of a wind turbine to ensure safe and efficient operation of these complex wind energy conversion systems [5].

This is because, unlike other sources of energy, the wind cannot be regulated. Wind flow is largely a random process, variable both in time and space. This variability leads to difficulties in the transformation of energy, as WT is exposed to non-uniform and non-stationary resources, variable mechanical loads and nonlinear dynamics. Therefore, automatic monitoring and control systems are very important for WT. They allow to cope with wind variability and produce energy in a reliable and economical way. The main objectives of the control systems built into the WT are to maximize power generation, reduce dynamic and static mechanical loads and ensure uninterrupted power supply to the grid in accordance with the requirements of the power system. In order to achieve these goals WT should have operating control systems designed to regulate the parameters of turbines up to the desired target values [10]. Pitch angle of blades and torque of the generator are the main parameters subject to control in WT. Pitch adjustment allows to control the wind input torque to ensure uninterrupted power generation and reduce mechanical loads. On the other hand, generator torque control allows you to change the rotor speed of the BT in accordance with the maximum power point tracking (MPPT) strategy to extract as much energy as possible from the wind flow.

In addition, WT should also have network integration control to control the power supply to the network to ensure uninterrupted power supply. This is necessary because the integration of WT networks becomes a challenge because of the random nature of the wind, which can cause problems with network frequency stability [15].

Each of the above mentioned control systems (pitch control, generator torque control and grid integration control) has its own technology and methods that should be implemented depending on the operation modes of WT and their respective control purposes.

1. WRTB automation

Industrial generation of electricity is one of the most important priorities in the development of the Republic of Kazakhstan. The existing deficit in the generated capacity of power plants can be covered by the use of renewable energy sources (RES), the share of which in the country's energy sector is currently less than one percent. Potential wind energy reserves of Kazakhstan are incommensurable and theoretically exceed the total capacity of all currently operating power plants of Kazakhstan more than 300 times. All this makes the task of increasing the share of RES in the energy balance of the country very urgent [1, 3].

Among the possible types of wind turbines, the Bolotov Rotary Turbine (WRTB) is distinguished by its technical characteristics superior to traditional propeller and other installations using wind energy in the production of electrical energy. Advantages WRTB are the use of wind energy independent of direction (360 degrees), an extended range of wind speed from 2 to 45 m/s and increased efficiency [8].

This paper deals with the creation of an automation system for the wind energy complex (WEC) using WRTB and, in addition, solar panels.

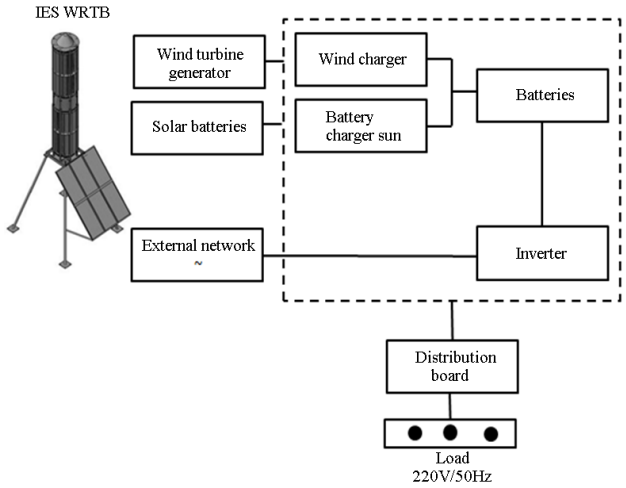

Fig. 1. Structural scheme of autonomous power supply system

The automation system under development is designed for automatic control and management of the wind energy complex (WEC). Automation objects covered by the automation system include both separate WRTB units and the whole complex. Automated types of activity are control of mechanical and electric variable units of WRTB, condition and position of equipment units, alarm system of deviation of variables and change of condition, centralized storage and presentation of information to personnel automatically and upon request, automatic and dispatch control.

The purpose of creating an automation system is to increase the efficiency of functioning WEC, which is provided by automatic control and operational monitoring of the state of equipment to reduce (or eliminate) undesirable and emergency modes of operation, to ensure the generation of electricity in specified parameters and quantities.

WRTB is a complex cylindrical structure with vertical arrangement of guides. An energy unit designed to generate electricity using wind energy to rotate the turbine rotor, which is mechanically connected to the generator rotor and consists of three parts: the turbine stator, the turbine rotor and the generator to generate electricity.

Anemometers are used to obtain information about wind speed and voltmeters and ammeters are used for electrical variables. The values of all measured variables are transmitted to the PLC. The automation scheme provides control of hydraulic pushers and magnetic starters.

In order to provide the consumer with qualitative and stable power, automatic switching on (off) of separate generators is provided.

The technical support of the automated process control system (APCS) WEC includes:

- measuring transducers, meters, etc.;
- actuators, including starters, limit switches, etc;
- programmable logic controllers;
- programmers;
- communication cables [12].

Intelligent monitoring and analysis of turbine condition

Wind turbines are generating units without the need for constant presence of personnel. They are often located in remote locations where the wind energy potential can be fully exploited. Given the size and complexity of today's wind farms, remote monitoring and modern diagnostic tools are a must.

Round-the-clock monitoring of the turbine

Wind turbines are equipped with a unique SCADA-system Genesis64. This system provides remote control, as well as the issuance of many variants of reports on the state of the turbine, viewed in a regular Internet browser. The status view displays information about the electrical and mechanical parameters of the turbine, its operation, failures, meteorological data, as well as the parameters of the electric substation. SCADA-system is connected to wind turbines and weather towers via the internal data transmission network. Depending on the needs, additional external equipment can be connected to the system. It regulates the output active power of wind turbines and acts as a "brain center" of the wind farm.

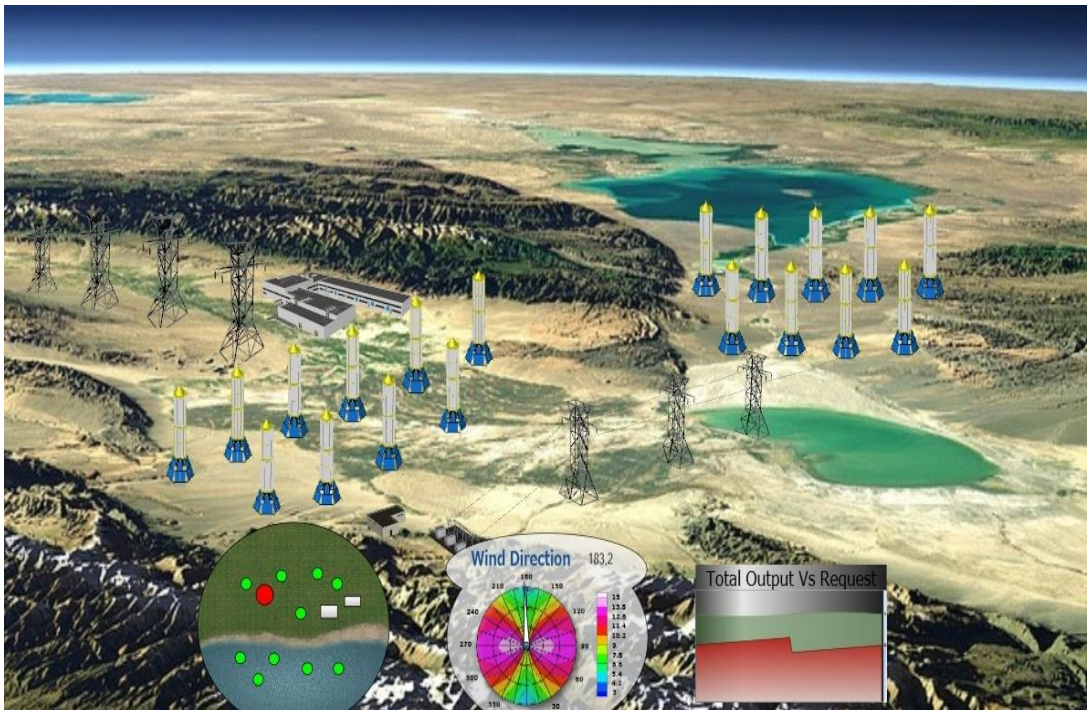

Fig. 2. SCADA-system for visualization of wind energy complex

2. Development of the wind power plant model

The efficiency of the development process and design of control systems for complex objects depends on the use of simulation modeling, which will be shown on the example of development of a universal controller. The control system model should support programming in a high-level language to ensure that the control program is portable to the target system. MATLAB/Simulink package of programs for mathematical calculations from Mathworks Inc. has been chosen as a development and research environment, which is widely spread both in the scientific environment and in various design organizations [7].

The purpose of imitation modeling of computational experiment over computer models is to study the efficiency of WT when using different strategies and control algorithms.

The main characteristic influencing the efficiency of a wind power plant is the wind energy utilization factor (WEUF, further in the formulas and drawings designated as C_P) - the ratio of the mechanical power of the wind wheel to the total power of the wind energy passing through the ometable area of the wind wheel WT [2].

The computer model of the wind power plant was developed with a predetermined (WEUF) wind turbine and a universal controller to provide the possibility of changing the control algorithm, the functional scheme of the model is shown in Figure 3.

The peculiarity of the proposed model is the module of the controller of the wind power plant, working according to the user-defined algorithm [12]. Thus it is possible to allocate following ways of management applied in various types of wind turbines which are supported by computer model:

- wind turbine operating at a constant wind turbine speed;
- wind turbine operating at several fixed wind turbine speeds by switching generator windings;
- wind turbine operating at several fixed wind turbine speeds by switching the multiplier gear ratio;
- a wind turbine that operates at variable speeds and uses an electrical converter with a power regulator.

Calculation of the turbine output power is carried out according to the formula:

$$P_m = C_p(\lambda, \beta)\rho A^2 \upsilon^3 \quad (1)$$

where P_m is the output power of the turbine (W), C_p is the wind energy utilization factor (WEUF), λ is the speed, β is the angle of the rotor guides, ρ is the density of air (kg/m^3), A^2 is the omnipresent area of the turbine (m^2), υ^3 is the wind speed (m/s).

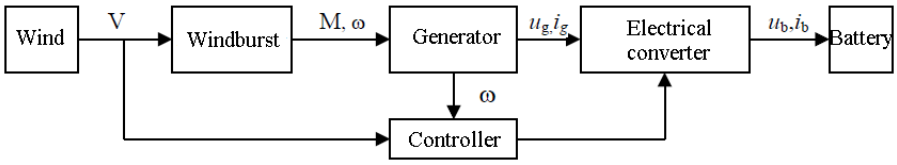

Fig. 3. Functional diagram of the simulation model of the wind power plant

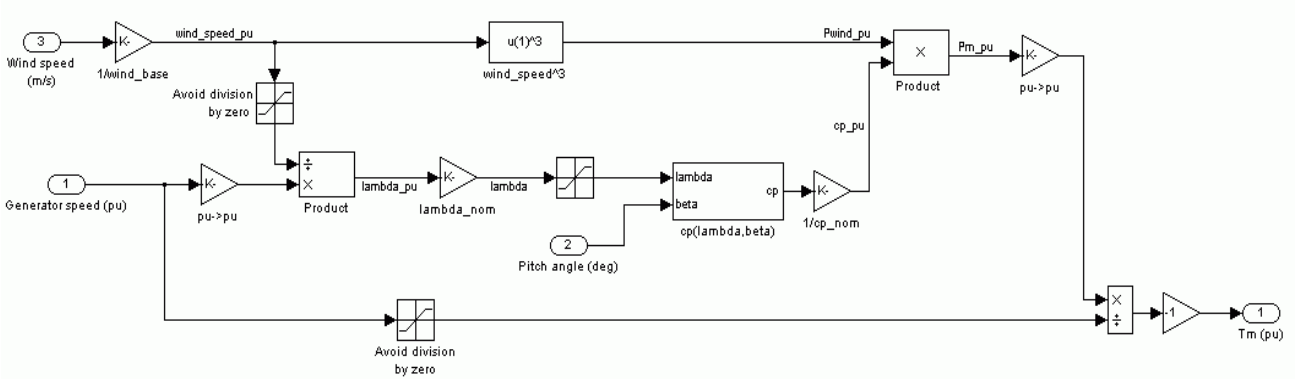

Fig. 4. A model of a WRTB turbine

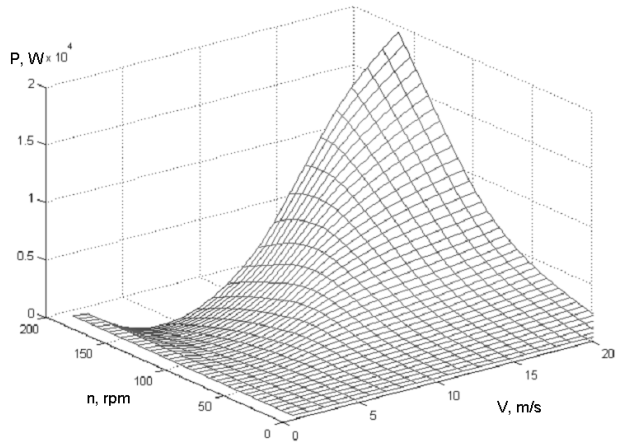

Fig. 5. Graph of rotor power distribution depending on wind speed and speed

3. Description of the electric generator model of the wind power plant

Electric generators are used in wind turbines to convert the mechanical energy of the wind turbine shaft rotation into electrical energy [9]. Electric generators used in wind turbines are subject to special requirements that take into account the peculiarities of their operation. One of the most important features is that the generator is driven into the rotation of the wind wheel, the speed of which depends on the wind speed and is not constant [13].

When changing the rotor speed of the generator and the alternating load, it is necessary to stabilize the voltage at the generator output, which creates the need for the use of voltage control device. This regulation is usually done by changing the current in the special excitation winding set by the voltage regulator. The use of the field winding leads to the need to increase the overall dimensions, as an additional space in the design of the generator to accommodate the windings. Also, the current in the field winding leads to additional electrical losses in

the generator, sometimes reaching a value of 10...20% of the useful power.

Analysis of different types of electrical machines suitable for use in wind power plants shows that the choice of type and design of the generator is not unambiguous.

The development of a generator working together with the wind power plant control system has its own peculiarities [14]. The process of development of an electric machine for a wind power plant is significantly accelerated by modern computer facilities and appropriate software. At the stage of calculation of electromagnetic parameters and thermal calculations it is possible to use both engineering techniques for accelerated calculation and software packages based on the finite element method, such as Ansys EMAG or Maxwell [9]. At the design stage, solid-state modeling in computer-aided design systems like SolidWorks facilitates the developer's work.

Modeling of the generator of the wind power plant is carried out on the basis of studying of some features of the electric machine. The applied generator is a synchronous electric machine with excitation from permanent magnets and with axial direction of magnetic flow and ironless anchor containing stator windings [4]. The peculiarity of designing a generator with an axial gap is the absence of losses on the magnetization due to the lack of steel magnetic wire and low inductance of windings, the influence of which in the simulation of wind turbine can be neglected.

The following model of electric generator is proposed for simulation modeling of the algorithms of wind power control turbines in order to optimize the requirements to computational resources within the framework of the task. Based on the substitution scheme, the voltage of the generator phase winding is equal to

$$u = e - r \cdot i - L\frac{di}{dt} \tag{2}$$

where e electromotive force (EMF), r active resistance of phase winding, i current in phase winding, L inductance of phase winding.

In order to reduce the influence of electric machine parameters resulted by the study of windings control algorithms it was assumed that r and L are equal to zero, and the electric current in the generator windings is set by the following equations:

$$\begin{cases} e_A = k \cdot \omega \cdot \sin(2p \cdot \omega \cdot t), \\ e_B = k \cdot \omega \cdot \sin(2p \cdot \omega \cdot t + \frac{2\pi}{3}), \\ e_C = k \cdot \omega \cdot \sin(2p \cdot \omega \cdot t - \frac{2\pi}{3}) \end{cases} \tag{3}$$

where e_A, e_B, e_C EMF of the corresponding generator windings, k generator design factor, $2p$ number of pairs of poles, ω generator rotor angle speed, t time.

Figure 6 shows a block diagram of the generator model in the MATLAB/Simulink package.

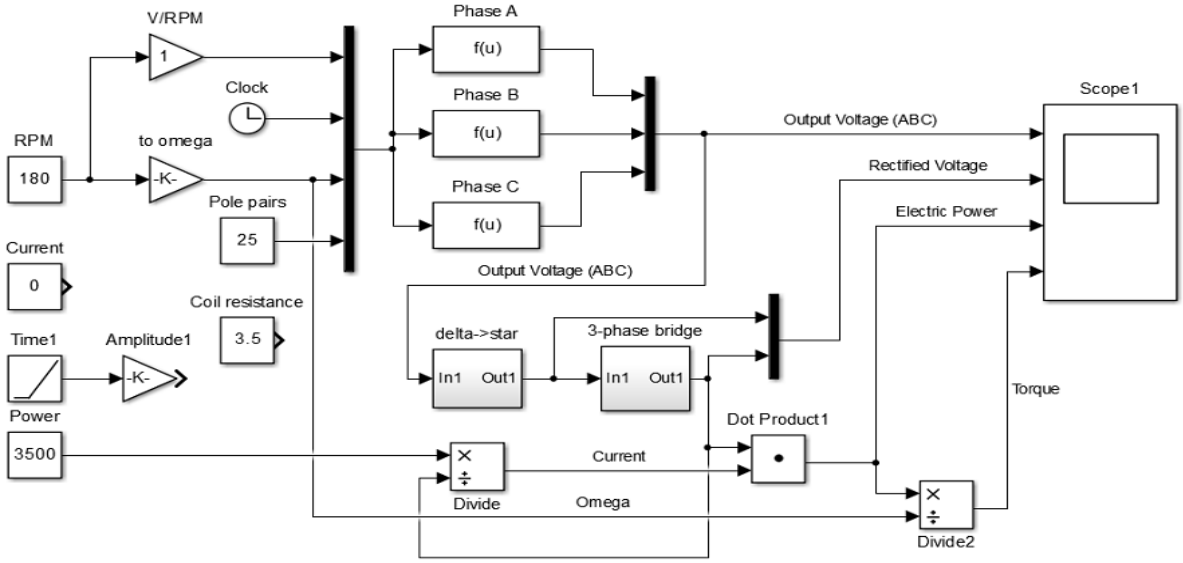

Fig. 6. Block diagram of the generator model

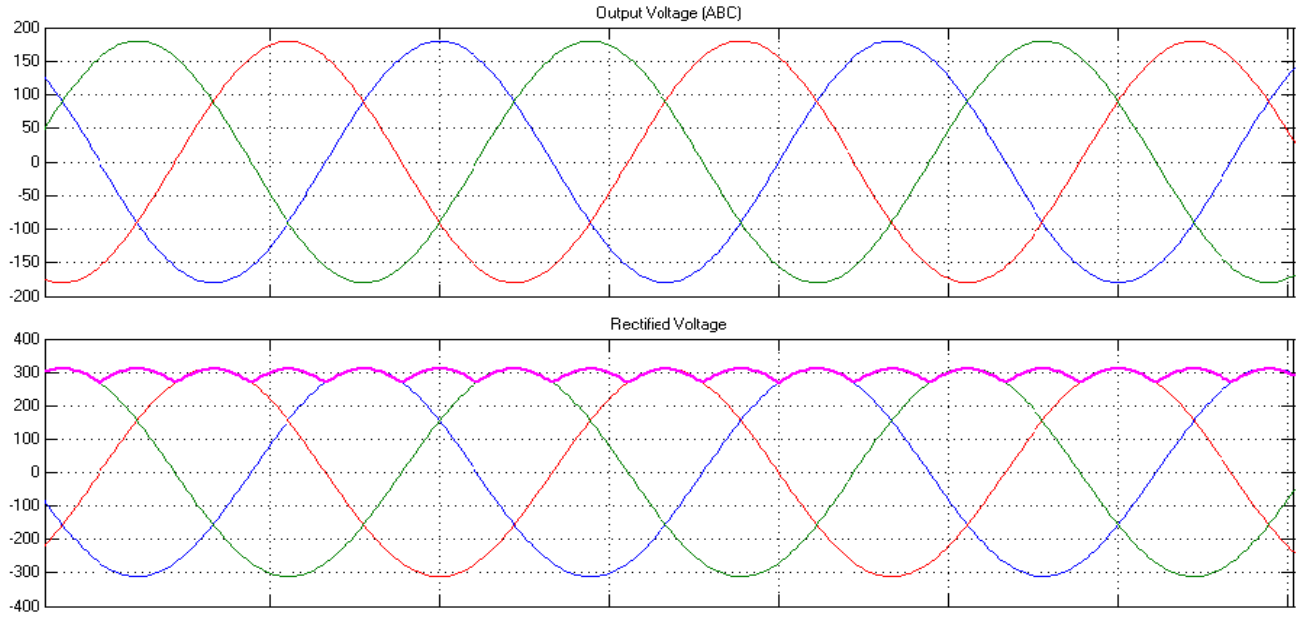

Fig. 7. Voltages on phase winding and rectifier output

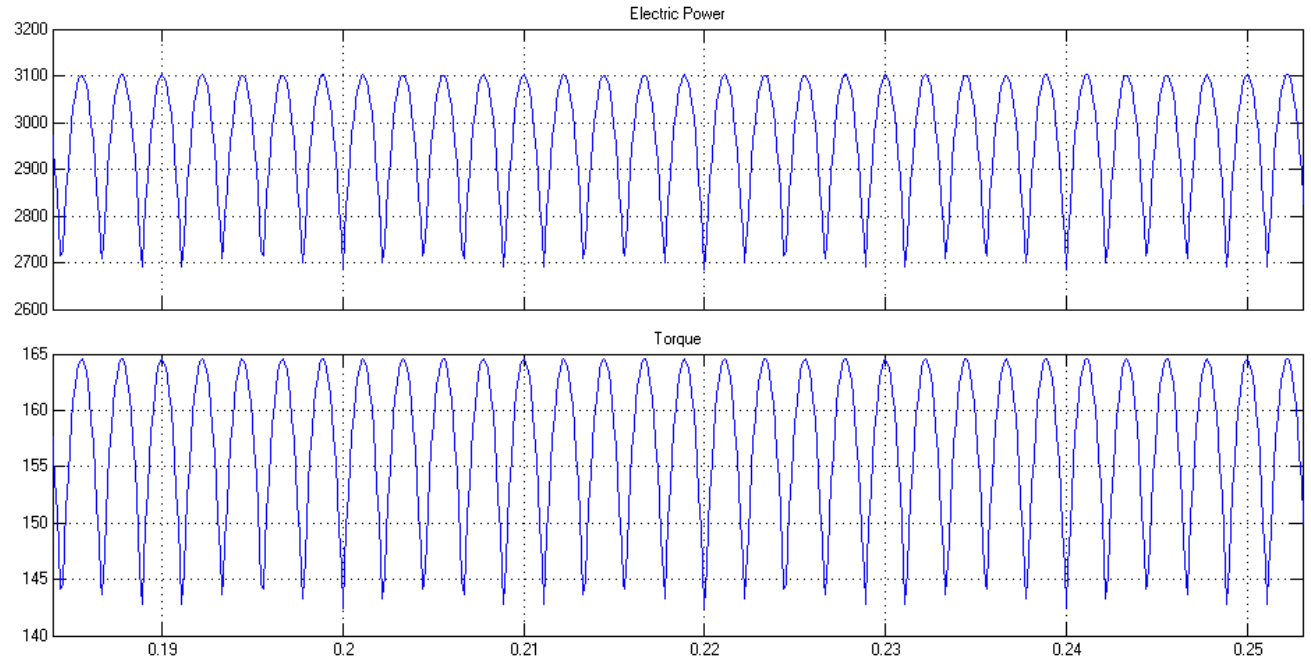

Fig. 8. The result of simulation of generator operation with a three-phase rectifier bridge on the load

Figure 7 shows the result of simulating the alternator at 180 rpm at idling speed. The upper graph shows the EMF in the generator phase windings and the lower graph shows the voltages at the rectifier input and output.

Figure 8 shows a simulation of the alternator at 180 rpm and 10A load. The upper graph shows the electrical power of the generator, and the lower graph shows the electromagnetic pulsations.

The result of the numerical experiment showed that the use of a three-phase uncontrolled rectifier bridge leads to significant fluctuations in the electromagnetic moment of the generator because of the non-sinusoidal nature of the current of the phase windings of the generator. In order to eliminate the specified rectifier deficiency, the use of an active voltage rectifier as a load of the wind turbine generator is proposed, which allows to consider that the generator phase windings are loaded with active resistances. Then the current in the generator winding is sinusoidal and correspondingly in phase voltage in the appropriate winding, and the electromagnetic moment of the generator $M_{\text{el}} = 3 \cdot k \cdot I_{\Phi}$, where I_{Φ} the amplitude of the generator phase current.

References

[1] Bolotov A. V., Bakenov K. A.: Netraditsionnyye i vozobnovlyayemyye istochniki energii. Konspekt lektsiy dlya studentov vsekh form obucheniya spetsial'nosti 050718 – Elektroenergetika. AIES, Almaty 2007.
[2] Bolotov A. V.: Energosberezheniye: strategiya, taktika i tekhnologii. Vestnik Natsional'noy Inzhenernoy Akademii Respubliki Kazakhstan 1,2, 2014, 2015.
[3] Bolotov A. V.: Netraditsionnyye i vozobnovlyayemyye istochniki elektroenergii: Uchebnoye posobiye. AUES, Almaty 2011.
[4] Gandzha S. A., Martyanov A. S.: Metodika inzhenernogo rascheta ventil'nykh elektricheskikh mashin s aksial'nym magnitnym potokom. Vestnik YUUrGU. Seriya „Energetika" 13/2013, 85–87.
[5] Global wind report 2015. Gwec. Wind energy Technol. 75, 2016.
[6] Kopylov I. P., Klokov B. K. (red.): Spravochnik po elektricheskim mashinam. T. l. Energoatomizdatm, Moscow 1989.
[7] Kozlitin L. S., Katsurin A. A.: Razrabotka sistemy upravleniya vetroenergeticheskoy ustanovkoy. Elektrotekhnika. Sb. tezisov dokladov nauchno-tekhnicheskoy konferentsii: Vologdinskiye chteniya, 1998, 14–15.
[8] Kukhartsev V. V.: Sovershenstvovaniye parametricheskikh kharakteristik energoeffektivnykh i ekologicheski bezopasnykh sistem kompleksnogo teploenergosnabzheniya avtonomnykh potrebiteley na baze vetroustanovok. Moscow 2005.
[9] Lubosny Z., Lubosny Z., Bialek J. W., Bialek J. W.: Supervisory control of a wind farm. IEEE Trans. Power Syst. 22/2007, 985–994.
[10] Manwell J. F., McGowan J. G., Rogers A. L.: Wind Energy Explained: Theory, Design and Application. Wiley 2010.
[11] Martynov N.N., Ivanov A.P. MATLAB 5.x: Vychisleniya, vizualizatsiya, programmirovaniye. KUDITS-OBRAZ, Moscow 2000.
[12] Matveyenko O. V.: Kompleksnaya programmno-matematicheskaya model' vetroenergeticheskoy ustanovki. Al'ternativnaya energetika i ekologiya 5(85), 2010, 64–70.
[13] Nikitenko G. V., Konoplev Ye. V., Konoplev P. V.: Stabilizatsiya chastoty vrashcheniya generatora vetroustanovki. Mekhanizatsiya i elektrifikatsiya sel'skogo khozyaystva 5/2012, 24–25.
[14] Sergeyev V. D., Kuleshov Ye. V.: Sinkhronnyy generator s postoyannymi magnitami dlya vetroelektricheskoy ustanovki. Materialy rossiyskoy konferentsii Avtonomnaya i netraditsionnaya energetika – Vladivostok 1998, 26–27.
[15] Yingcheng X., Nengling T.: System frequency regulation in doubly fed induction generators. Int. J. Electr. Power Energy Syst. 43/2012, 977–983, [DOI: 10.1016/j.ijepes.2012.05.039].

M.Sc. Kuanysh Mussilimov
e-mail: k-u-a@mail.ru

Kuanysh B. Mussilimov, born in 1994, PhD student at the Institute of Information and Telecommunication Technologies of the Kazakh National Research Technical University named by K.I. Satbayev, Almaty. Authored 4 publications. The area of his scientific interests is the Automation of the wind energy complex based on the Bolotov rotary turbine (WRTB).

ORCID ID: 0000-0002-8401-7541

Prof. Akhmet Ibrayev
e-mail: Ibr_1946@mail.ru

Akhmet Kh. Ibraev, born in 1946, defended his thesis on technical sciences (Ph.D.) in 1971, became an associate professor in 1975, an associate professor in 2016. Associate Professor, Department of Automation and Control, Kanysh Satbayev Kazakh National Research University, Republic of Kazakhstan. The author of more than 150 publications, 5 copyright certificates (patents), 3 textbooks. His research interests include the creation of automatic control systems, modeling and optimization of technological processes.

ORCID ID: 0000-0002-8474-0385

Prof. Waldemar Wójcik
e-mail: waldemar.wojcik@pollub.pl

Director of Institute of Electronic and Information Technologies, Faculty Electrical Engineering and Computer Science, Lublin University of Technology. His research interests include electronics, automatics, advanced control techniques, the optimization of the industrial processes, and fiber optic sensors including fiber Bragg gratings.

ORCID ID: 000-0002-0843-8053

otrzymano/received: 15.05.2019 *przyjęto do druku/accepted: 15.06.2019*

DOI: 10.5604/01.3001.0013.2546

PULVERIZED COAL COMBUSTION ADVANCED CONTROL TECHNIQUES

Konrad Gromaszek
Lublin University of Technology, Faculty of Electrical Engineering and Computer Science

Abstract. *The paper describes the selected methods of adaptive control of the pulverized coal combustion process overview with various types of prognostic models. It was proposed to use a class of control methods that are relatively well established in industrial practice. The presented approach distinguishes the use of an additional source of information in the form of signals from an optical diagnostic system and models based on selected deep structures of recurrent networks. The research aim is to increase the efficiency of the combustion process in the power boiler, taking into account the EU emission standards, leading in consequence to sustainable energy and sustainable environmental engineering*.

Keywords: combustion control, adaptive algorithms, artificial neural networks

ZAAWANSOWANE METODY STEROWANIA PROCESEM SPALANIA PYŁU WĘGLOWEGO

Streszczenie. *W artykule opisano wybrane metody adaptacyjnego sterowania przeglądem procesu spalania pyłu węglowego z wykorzystaniem określonych modeli prognostycznych. Zaproponowano użycie metod, które są stosunkowo dobrze znane w praktyce przemysłowej. Przedstawione podejście wyróżnia wykorzystanie dodatkowego źródła informacji w postaci sygnałów z optycznego systemu diagnostycznego i modeli opartych na strukturach sieci głębokich. Badania mają na celu zwiększenia efektywności procesu spalania w kotle energetycznym, z uwzględnieniem norm emisji UE, prowadząc w konsekwencji do zrównoważonej energii i zrównoważonej inżynierii środowiska.*

Słowa kluczowe: sterowanie procesem algorytmy adaptacyjne, sztuczne sieci neuronowe

Introduction

The combustion process, as already mentioned, in particular, carried out in industrial conditions, is characterized by very high complexity. This is due to the nature of the phenomena accompanying the process as well as the difficult measurement conditions, including the unavailability of specific quantities and the impact of high temperature, vibration, and dustiness on measuring and recording devices. The issues discussed in this monograph, regardless of trends in the pulverized coal combustion in the power industry, raise a number of intensive issues, developed many research works. It attempts to control one of the most challenging processes using analytical, heuristic and hybrid methods. The conducted research is in line with the directions of searching for algorithms for non-linear processes that will be numerically reliable, robust and, above all, will allow meeting technological limitations in the conditions of the uncertainty of model parameters

1. Combustion process modelling

In commercial power plants, many subsystems can be distinguished, which include: supply of fuel, water, fuel combustion (combustion chamber), steam generating system, turbine and generator system, and boiler safety system. Hence, developing a holistic (comprehensive) model of such a complicated process is a tough challenge. For this reason, in general, decomposition takes place, i.e., a division into smaller parts, describing specific subsystems or modules, due to the implemented functions or specific tasks. An unquestionable advantage of modularity is the simplification of the analysis and validation of the proposed solutions. The starting point for the classical mathematical model's development is the description of the physical and physicochemical phenomena of a given system using the principle of energy conservation, thermal balance and mass balance [7]. Based on the mathematical description of the phenomena occurring in the boilers [8], a mathematical model of the combustion chamber was developed and used to compare various constructional solutions. Unfortunately, in most cases, there was a lack of consistency between the measurement data for specific measurement conditions and the variables necessary for the model use. This required further research in the field of parametric identification of the process based on the collected data.

In the practical diagnostics and control algorithms, the detailed and simultaneously noncompliant models are desirable, due to the strong non-linearity, complexity and high dynamics of the combustion process. The heuristic methods presented in the monograph allow for effective finding approximate solutions, from which the final result is calculated later. The limitation of these solutions is the lack of direct knowledge about the state of the model and the lack of knowledge about the response of the neural model to the non-standard range of input signals. Lack of direct knowledge about the model's condition and lack of knowledge about the neural model's response to the non-standard range of input signals is a limitation of this type of solution.

This mainly applies to methods of deep learning. In addition to class selection, structure and learning methods, there are also opportunities to influence the learning process through regularization techniques and more effective activation functions. Recursive neural networks (RNNs) are modelled on the behaviour of many occurring in nature many cells with content-addressable memory, capable of capturing the whole sequence of information, given as fragments. While forward networks trigger their neurons in one direction, RNNs use strong feedback. RNNs model non-linear dynamic systems whose phase space dynamics is determined by a significant number of locally stable nodes [4].

During long-term context storage, RNN gradients can become difficult to remove because they use their feedback to memorize the structure of the last inputs. Similarly, backwardly propagating error signals over time can have large values (causing oscillations of weights) or recede (making it difficult to determine slow-change weights). These changes during the backward propagation errors depend exponentially on the value of the weights [1, 2].

2. Modern approaches

The classic structure of a multi-layer perceptron and the long short-term memory (LSTM) was used for neural combustion process modelling in the monograph The advantage of LSTM is that it truncates gradients in the network, wherever it is harmless, and at the same time enforces continuous error flows in individual multiplicative units (MUs). The continuous error flow is regulated by nonlinear MUs that learn to open or close gates in a cell. The diagram of such a structure is shown in Figure 1.
They are structures whose forgetting gates allow for precise learning in time.

The analysis of the combustion process in coal-fired boilers reveals three main factors that adversely affect the boiler efficiency. These include the level of slagging and contamination of heating surfaces and measuring instruments, heat losses due to exhaust gases as well as a large share of unburnt coal. The possibility of assessing combustion quality is significant for proper operation of the power boiler [6]. Considering the combustion process in pulverized coal boilers, it should be noted that: chemical reactions, heat transfer efficiency, flame stability as well as the intensity of NOx and CO formation have the significant influence on it. The burners and the fuel delivery method have a crucial influence on

the combustion aerodynamics. Low-emission coal burners use the reduction properties of a rich pulverized coal flame by organizing sub-stoichiometric combustion zones using air staging or fuel staging. This, in turn, may worsen the combustion stability and increase the loss of the flame.

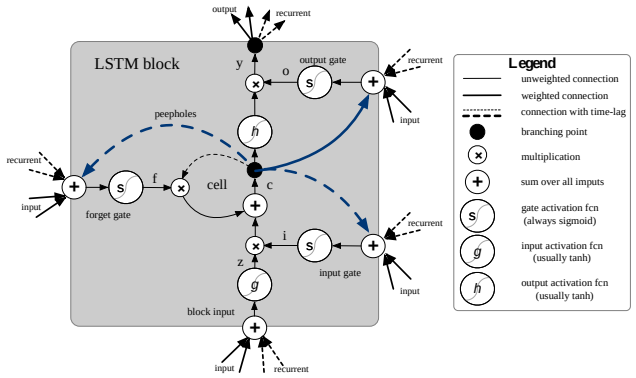

Fig. 1. The Long Short-Term Memory (LSTM) single cell model

Taking into account these factors and significant ecological aspects, there is a need to develop a combustion process control system that will optimize boiler operation based on information obtained from conventional equipment and will take into account innovative techniques to assess the quality of the process. From the technological side, an important parameter is to ensure flame stability and detection of emergency states. Therefore, the control system should be enriched with flame diagnostic information using vision technologies or fiber optic probes. Quantitative information on the concentration of nitrogen oxides, carbon oxides, and sulphur dioxide is equally essential in order to meet normative limitations.

Continuous measurement of the dust flow in dust-conductors will undoubtedly bring valuable information about the input parameters of the process, but it is difficult to measure. Similarly considering the process output, it would be crucial to obtain information online about the content of flammable parts in ash and slag (especially the organic carbon content). To obtain this information, it is necessary to carry out measurements on the real object using expensive measuring equipment.

The use of this information in the solutions proposed in the monograph was possible thanks to the research carried out at the Institute of Power Engineering in Warsaw, on the experimental stand for testing the combustion process with a heat output of 0.5 MW using a coal burner. The layout of the station, in the configuration for the co-firing process testing, is shown in Figure 2.

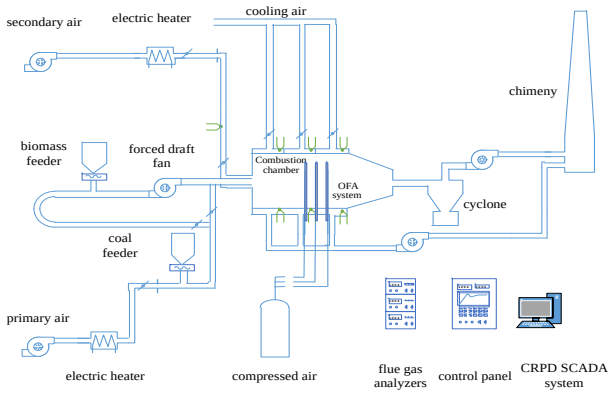

Fig. 2. Diagram illustrating the experimental stand for testing combustion processes

The central element of the station is a cylindrical combustion chamber, the inner part of which is covered with insulating material, and the external one is cooled with air. The front wall of the combustion chamber is cooled by water. A dust burner is installed in the front wall axis. The auxiliary oil burner is used to heat the station before the ignition of pulverized fuel. The primary air is supplied to the coal burner in the amount of 250 m^3N/h and secondary air - up to 500 m^3N/h.

The identification of combustion process model parameters for a single low-emission burner was an essential element of the control system synthesis, including both diagnostic information and those from the optical flame monitoring system. In order to develop a mathematical model of the process, carried out with the use of a single low-emission burner, the measurements were carried out on the IEN test stand. The experiments included the stabilization of the working point of the laboratory stand at different powers, different types of fuel (including coal and biomass) and exchangeable three types of low-emission burners. Measurements of process variables were made at 1Hz. The registered values include multi-point measurements of exhaust gas concentrations (NOx, O_2, CO, CO_2), measurements of temperatures, pressures, and flows as well as levels of air fans. Optical measurements on the flame were made at 1kHz.

The initial stage of work included the analysis of selected, registered input and output quantities. For the synthesis of multidimensional models (MIMO), the vectors of input signals describing the secondary air flow, fuel output and output signal vectors including NOx concentration, CO and chamber temperature respectively were determined. The data were divided into training and testing sets, using a 70% and 30% distribution respectively. Using the System Identification Toolbox, parameters were identified for parametric models in the state space. The tested object was treated as a serial structure. Thus, the outputs of the models on the first level were the inputs for the second-level models and described the relationships between the NOx and CO concentrations, the temperature in the chamber and the corresponding values at the appropriate measurement point. Using the Matlab / Simulink platform tools, the MPC controller was designed, in order to test the credibility of the models obtained. Such an approach allows imposing boundaries on outputs and control signals, that interfered signals and prediction and control horizons. Thus, it allows checking the models in the context of normative restrictions (e.g. regarding NOx emissions).

The Simulink diagram of pulverized coal combustion process control system is presented in Figure 3. It allows modifications of the used models and the design of MPC controllers.

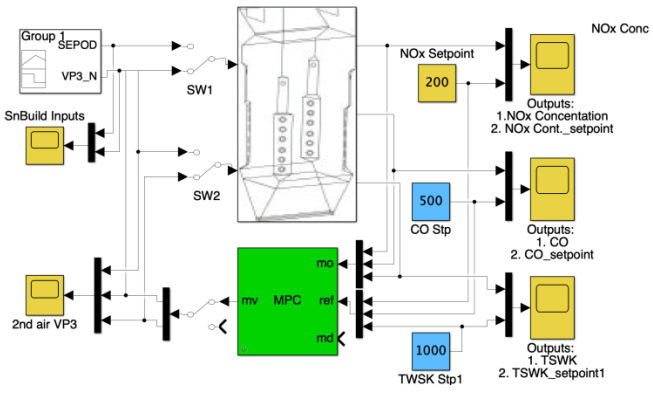

Fig. 3. Simulink diagram of the tested control system

As part of the conducted tests, taking into account the NOx emission standards restrictions (300 ppm), the best results in the sense of NRMSE were obtained for the low emission coal burner first (D1M1_4s6) and third (D3M1_4s3) model. Figure 4 gives an example of the analysis of the obtained results, for models P1 for with test data from the combustion process.

In the case of selected models (P2), compliance with emission limits was achieved with the occurring oscillations (D2M1_4s5), and in the case of (D2M1_4s6) - they were unsuccessful. The serial configuration yielded the best results in combination with model structures (D2M2_4s4 and D2M2_4s10).

3. Pulverized coal combustion and co-combustion with biomass process using optical signals from the flame

Combustion tests were carried out on the Institute of Power Engineering test bench. A low-emission NOx burner mounted horizontally on the front wall of the chamber with a diameter of 0.1 m. Previously prepared pulverized coal was stored in the bunker and delivered by a feeder. In case of biomass fuel, the coal dust was mixed with biomass (mainly with straw) in appropriate proportions.

There are inspection holes on both sides of the combustion chamber, allowing observation of the combustion process and providing data acquisition capability. As part of the research, a fast camera with a CMOS sensor was placed near the nozzle of the burner. The camera enabled image recording with a resolution of 1280 × 1024 pixels at a rate of 500 frames per second. The 0.7 m length borescope with camera set was used to record flame images. The optical system was cooled with a water jacket. In order to avoid contamination of the probe's lens, purified air purge was used. This operation was important due to the image registration but introduced minor disturbances in the area near the burner.

The course of the experiment required proper preparation, therefore the research was divided into several stages. Initially, the combustion chamber was heated with heating oil. After reaching the appropriate temperature level, pulverized coal was introduced into the burner with the primary air. The next phase was switching off the oil burner and introducing a mixture of coal and biomass. The coefficient of excess air was determined by the secondary air flow [3].

During the tests, nine variants were assumed, in which the thermal power (Pth) and the excess air coefficient (λ) were set independently for the known biomass content. It should be noted that λ is defined as the quotient of the combustion air weight 1 kg of fuel to the stoichiometric air mass.

The measurements were carried out for three heat power values (250 kW, 300 kW, and 400 kW) at the object output and the specified values of the excess air factor λ, equal to 0.65, 0.75 and 0.85, respectively. Besides, the tests included two fuel mixtures containing 10% and 20% straw-based biomass. The studies assumed fixed parameters of biomass physical properties (like particle size, natural humidity, etc.) as well as all image acquisition parameters (such as frame rate and time of exposure).

For the measurements carried out, an attempt was made to determine the optical parameters of the flame that can be used during diagnostics and control of the combustion process.

It was assumed that due to the need to develop an online control algorithm, the images from the camera were transformed by conversion to an 8-bit grayscale. The area of the flame in each frame of the obtained sequence was determined based on the amplitude of the pixels to distinguish the flame from other recorded objects in the field of view of the borescope. Thus, the sum of all bright pixels in the analysed flame determined its area. The coordinates (x, y) of the flame field center were calculated as the mean value of the coordinates of the lines or columns of all the pixels in the flame region, respectively. Flame contour length is defined as the sum of all envelope pixels, assuming that the distance between two adjacent contour points parallel to the coordinate axis has the value 1.

In the proposed solution, the classic approach is supplemented with information about the flame based on selected image parameters registered with a fast camera.

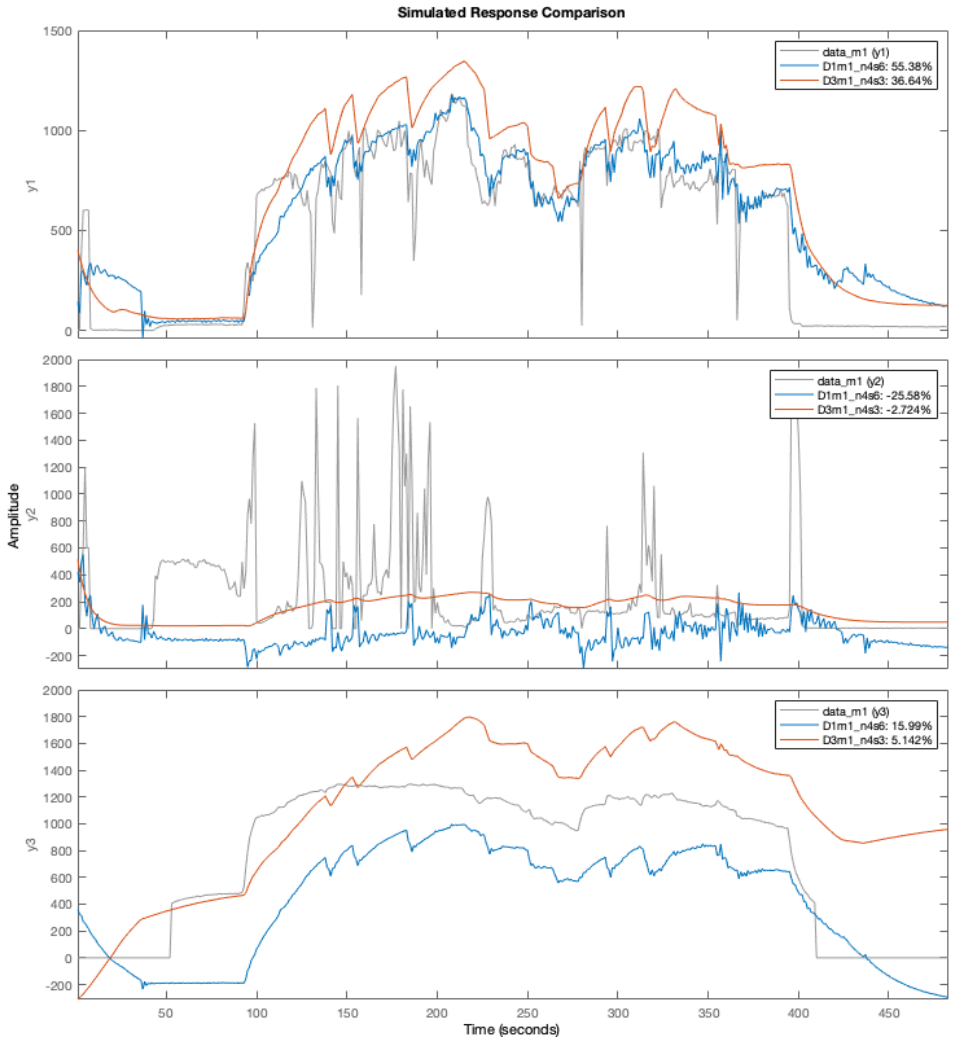

Fig. 4. Comparison of P1 model responses for test data from the combustion process

As a result of the analysis, there was the relationship between the parameters describing changes in the flame image and the temperature of the flue gases and the amount of secondary air. Primary air is mainly used to supply coal dust to the nozzle of the burner, while secondary air is used to change the conditions of the combustion process (deviation from stoichiometry). The input parameters, such as the amount of fuel in the form of a coal-biomass mixture and air flows, were changed several times during tests to create different states of the combustion process.

An adaptive control seems to be a reasonable approach in case of incomplete knowledge about the controlled object or its rapid changes in operation.

The nonlinear autoregressive network with exogenous inputs (NARX) is a dynamic network with reverse connections including several layers. The NARX model is based on a linear ARX model, which is widely used in modeling time series. In the NARX model equation, each subsequent value of the dependent output signal is determined relative to the previous values of the output signal vector and the previous values of the independent (exogenous) input signal. The NARX model can be implemented using a forward-facing neural network to approximate a specific function. This implementation also allows for a vector ARX model in which input and output data can be multidimensional.

The outputs of the NARX network can be considered as an estimation of the results of the modeled non-linear dynamic system that are transmitted to the neural network input using feedback within the standard NARX architecture. Since the result is available during network training, it is possible to create a serial-parallel architecture (see [5]), in which the actual output is used instead of the estimated result. The custom architecture used for further analysis is the adaptive control algorithm (MRAC). This control architecture has two subnets. One subnet is a controlled process model, and the other subnet is a controller.

The trained NARX model can be used both to create the entire MRAC system and incorporate it inside the controller structure. In order for the closed loop MRAC system to respond in the same way as the reference model (used to generate data), the weights from the trained network should be placed in the MRAC system. The training of the MRAC system took much longer than training the NARX model because dynamic backward propagation was used in the network. After training procedures, the MRAC network was verified using test data. Two MRAC systems have been designed and compared. The first of them used a standard set of input vectors based on measurements, quantitatively describes the secondary air flow, the amount of fuel and vectors describing the air temperature in the chamber, recorded in the first measuring point, respectively. The second scheme used the secondary air flow control signal and the selected flame area descriptors. These optical information-based descriptors were determined using the Otsu method and the contour length. Figure 5 shows the system response to the input setpoint of the system in both cases: with standard measurements (a) and after using optical measurements in the form of a contour length vector for the flame descriptor (b). The simulation results shown in Figure 6 show that the output of the developed model follows the reference input with the correct, suppressed response, even if the input sequence was not the same as the input sequence in the training data. The steady state reaction may have an oscillating course at each stage, but this can be improved by using a larger training set and perhaps more neurons in the hidden layer. From the obtained results of the proposed adaptive control algorithm, it can be concluded that the constraints imposed on the values of control signals ensure stabilization of the process.

Nevertheless, the boundaries imposed on the signals will be a limitation also for the control system, because sudden changes in the process parameters may require the rapid reaction.

As mentioned above, imposing boundaries on signals can be a way to guarantee stability. The analyzed control system was subjected to a rapid step change of load, that illustrated the critical situation that may occur in case of an unexpected change in system parameters.

The algorithm took into account all the imposed boundaries, both on the controls and the outputs. The obtained results confirm its robustness, and thus the possibility of implementation in real systems. Boiler combustion efficiency and NOx emission are usually chosen as the main parameters of the target function in control with the SSN model. The neural model enables the mapping of dependencies between control parameters and outputs for different operating conditions. As a result, the control algorithm can be used as an advisory system for the operator or directly to control the combustion process in the boiler.

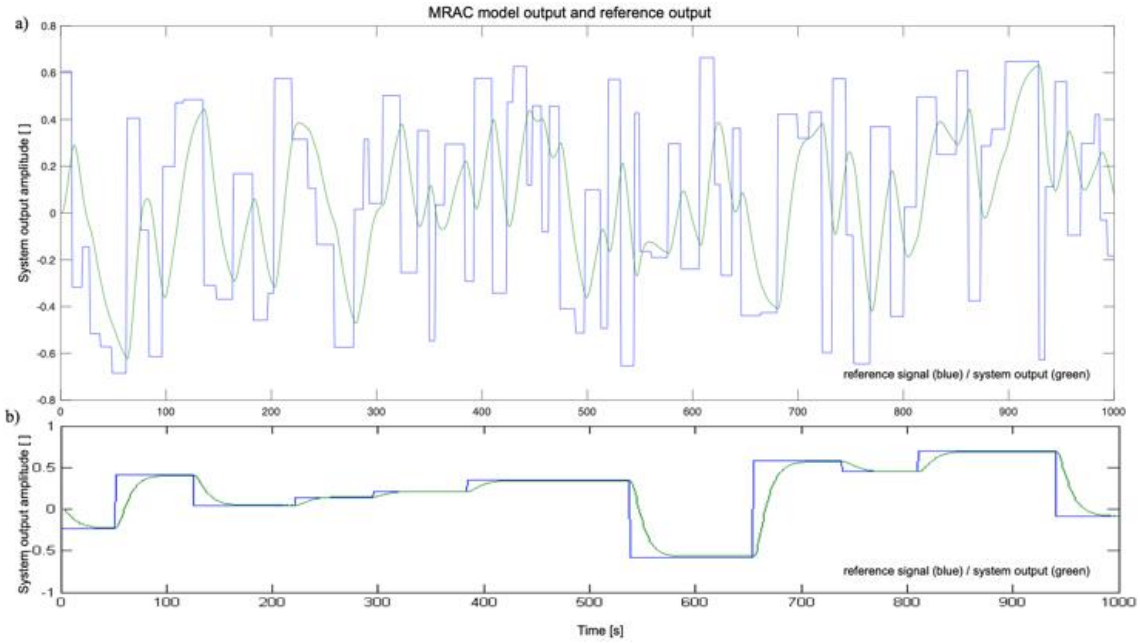

Fig. 5. The response of the modeled boiler control system using (a) the input data vector (b) the input data extended with optical information

4. Hybrid methods

The attempt to solve the problem of identification and control of the strongly non-linear phenomenon related to the pulverized coal and biomass co-combustion was undertaken in the book "Advanced control techniques of pulverized coal combustion control".
The dynamics of this process is too complex to be modeled with a limited number of differential equations. Therefore, three selected structures of deep neural networks were considered for research: MLP, simple recursive network, and Long Short-Term Memory cells. Due to the unusually high variability of signals, the use of individual AI models is usually associated with getting stuck in local minima, and this leads to suboptimal solutions. It excludes obtaining satisfactory performance of the model in diagnostics and control tasks. However, in order to eliminate these limitations, hybrid algorithms are becoming more popular [10,11]. There are two main trends in the construction of hybrid models. One of them is a combination of several predictors, where their prediction results constitute a composite for final prediction.

5. Conclusion

Denote The results of tests and analyses presented in the monograph do not solve all of the problems associated with combustion process control. The issues of combustion dynamics with more detailed parametric stability analysis as well as conditions of turbulence require improvement. The control system may include other optical signals, including flame color and extension of hybrid methods with the use of fuzzy algorithms. According to the author, advanced control algorithms will be further developed and used in a wide range not only in industrial installations. One can risk the statement that these methods will shift towards the hybridization of artificial intelligence methods with other approaches.

References

[1] Bengio Y., Simard P., Frasconi P.: Learning Long-Term Dependencies with Gradient Descent is Difficult. IEEE Trans. Neural Networks 5/1994, 157–166.
[2] Computation N.: Long Short-term Memory. Neural Comput. 9/2016, 1735–1780.
[3] Gromaszek K., Kotyra A., et al.: Signal Process. - Algorithms, Archit. Arrange. Appl. Conf. Proceedings SPA 3/2015, 133–136.
[4] Hopfield J.J.: Neural networks and physical systems with emergent collective computational abilities. Proc. Natl. Acad. Sci. 79/1982, 2554–2558.
[5] Kauranen P., Andersson-Engels S., Svanberg S.: Spatial mapping of flame radical emission using a spectroscopic multi-colour imaging system. Appl. Phys. B Photophysics Laser Chem. 53/1991, 260–264.
[6] Kordylewski W., Bulewicz E., Dyjakon A., Hardy T., et al.: Spalanie i Paliwa. Oficyna Wydawnicza Politechniki Wrocławskiej, Wrocław 2008.
[7] Lhner R.: Applied Computational Fluid Dynamics Techniques: An Introduction Based on Finite Element Methods. J. Fluid Mech. 1/2001, 375–376.
[8] Ordys A.W., Pike A.W., Johnson M.A., Katebi R.M., Grimble M.J.: Modelling and Simulation of Power Generation Plants, Springer–Verlag, 1994.
[9] Sepp H., Schmidhuber J.: Long short-term memory. Neural Comput. 9/1997, 1735–1780.
[10] Tascikaraoglu A., Uzunoglu M.: A review of combined approaches for prediction of short-term wind speed and power. Renew. Sustain. Energy Rev. 34/2014, 243–254.
[11] Zhou H., Cen K., Fan J.: Multi-objective optimization of the coal combustion performance with artificial neural networks and genetic algorithms. Int. J. Energy Res. 29/2005, 499–510.

Ph.D. Eng. Konrad Gromaszek
e-mail: k.gromaszek@pollub.pl

Senior lecturer in Institute of Electronics and Information Technologies at Lublin University of Technology. Research field covers diagnosis and control algorithms as well as applications of artificial intelligence methods in industrial complex systems. Computer networks, PLC and mechatronics enthusiast.

ORCID ID: 0000-0002-3265-3714

otrzymano/received: 15.05.2019 *przyjęto do druku/accepted: 15.06.2019*

DOI: 10.5604/01.3001.0013.2547

THE PROSPECTS FOR THE USE OF INTELLIGENT SYSTEMS IN THE PROCESSES OF GRAVITATIONAL ENRICHMENT

Batyrbek Suleimenov, Yelena Kulakova
Kazakh National Technical Research University after K.I. Satpayev, Department of Automotion and Control

Abstract. *Intelligent control systems are actively developing and can significantly reduce financial costs and improve the environmental performance of ore-dressing processes. Usage of intelligent control systems for gravitational enrichment allows to minimize costs and negative influence of ore tails on the environment, exclude losses of concentrate and energy resources in the ore-dressing process. The paper discusses the problems and prospects for the application of intelligent control systems of gravity concentration equipment. A structure of the control system and an intelligent model for determining the frequency of pulsation jigging machine based on fuzzy logic are proposed. The model is based on data obtained from experts, it is researched. The obtained results allow to judge about the prospects for the implementation of intelligent systems in the management of ore enrichment.*

Keywords: gravitational enrichment, intelligent system, jigging machine, centrifugal concentrator, fuzzy model

PERSPEKTYWY WYKORZYSTANIA SYSTEMÓW INTELIGENTNYCH W ZARZĄDZANIU PROCESAMI WZBOGACANIA METODĄ GRAWITACYJNĄ

Streszczenie. *Zastosowanie inteligentnych systemów zarządzania wzbogacaniem grawitacyjnym zminimalizuje koszty i negatywny wpływ odpadów przeróbczych na środowisko, wyeliminuje straty koncentratu i zasobów energetycznych w procesie zagęszczania rudy. W artykule omówiono problemy i perspektywy zastosowania inteligentnych systemów sterowania urządzeń do wzbogacania metodą grawitacyjną. Zaproponowano strukturę systemu sterowania i model inteligentny do określania częstotliwości maszyny sedymentacyjnej na bazie logiki rozmytej. Model opiera się na danych otrzymanych od ekspertów. Uzyskane wyniki pozwalają nam ocenić perspektywy wdrożenia inteligentnych systemów w procesach kontroli przerobu rudy.*

Słowa kluczowe: wzbogacanie grawitacyjne, system inteligentny, maszyna osadowa, koncentrator odśrodkowy, model rozmyty

Introduction

Modern reality requires the development of not only economical but also environmentally friendly technologies for the production of mineral raw material.

Consequently, there is a need for a thorough processing of ore, especially small and fine classes, which previously fell into the waste of production.

Gravity enrichment methods are known from ancient times and to the end of the XIX century, they were the only methods of mineral processing, because of other methods were practically not used. The concept of gravitational methods is the separation of mineral particles under the action of gravity and resistance forces. Consequently the variety of particles with their individual properties makes it difficult to reliably quantitatively describe gravitational processes. Therefore, the development of this method of enrichment, despite the centuries-old history and wide application, is mainly through experimentation [8].

In the field of gravitational enrichment, in particular, the jigging process, to date, sufficiently effective technologies have been created that allow controlling the process, reducing energy costs for production, and facilitating the work of the operator. However, existing control systems have several disadvantages, which do not allow to achieve maximum enrichment indicators.

1. The equipment of gravity enrichment

The main technological units of gravity enrichment are screens, various separators (screw, magnetic, etc.), concentrators, and also jigging machines. Consider two units for the enrichment of ores of fine and small classes. They are jigging machine and centrifugal concentrator.

Jigging machine – mining machine, equipped with special equipment (sieve, chamber). The jigging process is based on the Rittenger equation:

$$v_r = k_r \sqrt{d * (\delta - 1)} \quad (1)$$

where: v_r is speed of free fall of particles in water, k_r is Rittenger coefficient, d is diameter of particle in mm, δ is density of particle in g/mm^3.

Jigging machine is used for gravitational enrichment of ores in the aquatic environment, through the separation of minerals mainly by density. Since the only consumable material is water, the operation of jigging machines is economical and environmentally friendly. These machines work reliably around the world because of their reliability and high performance.

The principle of operation of the centrifugal concentrator consists in the forced separation of the material being processed into two fractions: “heavy” and “light” in the centrifugal field. The separation of material into fractions occurs as a result of the interaction of the flow of wash water, centrifugal forces and the gravitational field acting on the particle in a horizontally or obliquely rotating rotor.

At present, jigging machines and concentrators are widely represented by manufacturers and all, without exception, are equipped with automatic control systems based on modern automation tools [2]. But it is important to note that these systems are automation systems that certainly facilitate the work of a technologist, give average, but not maximum technological indicators of enrichment.

The vulnerability of classical management methods is connected with the multidimensionality of the processes of gravitational enrichment.

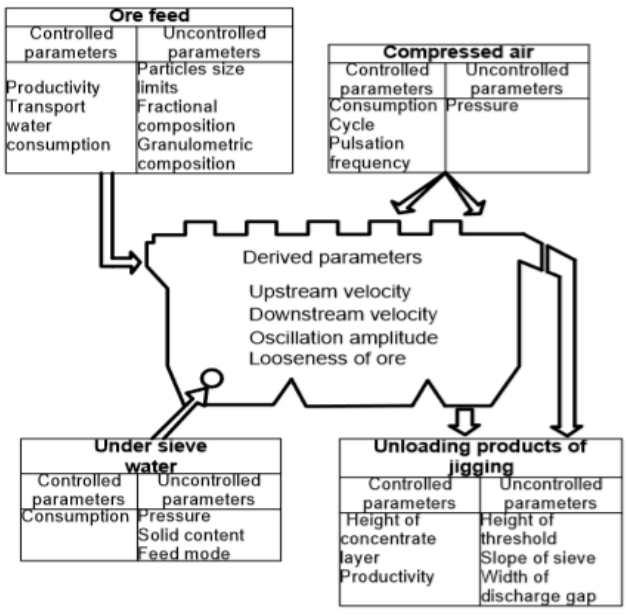

Fig. 1. The parameters of jigging machine

For example, the technological indicators of the enrichment of jigging machines are simultaneously affected by about 20 factors determined by the characteristics and feed mode of the jigging machines, technological and hydrodynamic parameters of the process (Fig. 1). Many of them are in complex interaction with each other and manifest themselves in different conditions ambiguously.

Consequently, the disadvantage of the existing control systems is that the key variables of gravitational enrichment units are not constantly regulated depending on disturbing factors, they have a fixed value and are changed by the technologist only 2–3 times per shift. A technologist decides on the optimal value of these variables, based on their competence, that is, the human factor is of great importance.

Thus, the analysis of literary sources [1, 4, 7] and long-term communication with expert technologists, working directly on the equipment of gravity enrichment, suggests that the use of intelligent algorithms in the control systems of the processes of gravitational enrichment will eliminate the shortcomings of the existing automation systems.

2. Concept of control system for gravitational enrichment processes

To improve the technological indicators of the enrichment of small classes ore in gravity enrichment equipment to proposed developing a three-level control system (Fig. 2). The proposed system consists of:

- intelligent system generates the optimal value of key variables. To do this the system uses data obtained from field automation units (the composition of the original ore Q, and others) and base of knowledge from the experience of a competent expert technologist;
- controller that maintains the optimal value of the key variables obtained by the intelligent subsystem.
- field automation units (sensor, ore analyzer, actuators, VS converters) directly measure the process variables and produce a physical effect according to the control law adopted by the intelligent system.

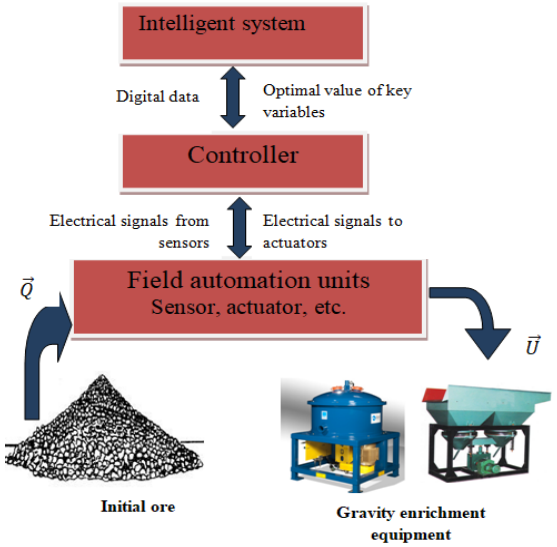

Fig. 2. Concept of control system for gravitational enrichment processes

A distinctive feature of the system being developed is that the value of the key variables of the enrichment process is set not by the operator-technologist, but by the intellectual system. This system is built on the experience of qualified technologists. The adjustment process includes a large number of input variables and, accordingly, all existing control systems leave the right to make decisions for a operator. In this regard, factors such as qualifications, fatigue, inattention of staff, etc., do not allow to achieve the maximum possible technological indicators of enrichment.

Not every technologist has sufficient experience to adjust the parameters of the equipment, and a number of factors depend on the individual characteristics of the worker. That is, the intelligent system allows you to use the experience of the most competent specialist constantly, regardless of the shift and the presence or absence of the person in the workplace. This approach will eliminate the influence of the human factor and improve enrichment rates.

3. Intelligent model for determining the frequency of pulsation of jigging machine

The development and research of intelligent models make it possible to assess the effectiveness of the use of intelligent systems for control of the processes of gravitational enrichment. In this regard, the intelligent model for the determining of the key variable of the jigging technology — the pulsation frequency of the jigging part of jigging machine was developed and researched. The modeling was performed in the Matlab environment using the Fuzzy Logic interface.

The developed model allows to determine the optimal values of the pulsation frequency (Y), depending on the initial ore concentration (X1) and chromium concentration in the reject material (X2). The stages of modeling are:

- expert survey, getting the PFE matrix;
- data normalization;
- designation of linguistic variables ;
- definition of the membership function
- selecting a base term-set of a linguistic variable or a set of its values (terms);
- forming the rules of fuzzy products;
- obtaining 2 fuzzy models: one using triangular terms; the second with trapezoid terms;
- testing resulting models.

At the first stage of the synthesis of intelligent models, a planning matrix of a full factorial experiment (PFE) is compiled. Using this matrix, a control model of an object or process is created. In PFE, all possible combinations of levels of factors are implemented. When the number of levels is equal to four for each factor, the PFE matrix consists of m = 4n rows, where n is the number of factors (controlled variables), and m is the number of experiments [5].

As a result of the questioning of experienced operators, which have been working with jigging machine for a long time the PFE matrix was obtained (table 1).

Table 1. The PFE matrix

Factors		Optimal value
Concentration of initial ore	Chromium concentration in reject material	Frequency of pulsation
X1	X2	Y
28	2	55
32	2	60
36	2	69
40	2	75
28	8	60
32	8	69
36	8	70
40	8	75
28	14	63
32	14	63
36	14	66
40	14	72
28	20	60
32	20	65
36	20	70
40	20	75

Next, the normalization of input and output variables is carried out in the range from 0 to 1 according to the equation:

$$\bar{x} = \frac{x - x_{min}}{x_{max} - x_{min}} \quad (2)$$

where: $\bar{x}$ is the normalized value of the input or output variable, x is the current value of the variable, x_{min}, x_{max} is the minimum and maximum value of the variable.

As a result of data normalization is table 2.

Table 2. Normalized data

Factors		Optimal value
Concentration of initial ore	Chromium concentration in reject material	Frequency of pulsation
X1	X2	Y
0.00	0.00	0
0.33	0.00	0.25
0.67	0.00	0.7
1.00	0.00	1
0.00	0.33	0.25
0.33	0.33	0.7
0.67	0.33	0.75
1.00	0.33	1
0.00	0.67	0.4
0.33	0.67	0.4
0.67	0.67	0.55
1.00	0.67	0.85
0.00	1.00	0.25
0.33	1.00	0.5
0.67	1.00	0.75
1.00	1.00	1

In table 2, all variables are given to normalized form in the range from 0.0 to 1.0. The concentration of chromium in the original (initial) ore 28% corresponds to 0.0 and 40% – 1; chromium concentration in reject material material (tailings) 2% corresponds to 0.0 and 20% – 1, the minimum frequency of pulsation 55% – 0, maximum 75% – 1.

At the next stage notation for the linguistic variables is introduced: input: the initial concentration of ore (X1) and the concentration of chromium in reject material (tails)(X2); output: pulsation frequency of jigging part of machine (Y).

When solving practical problems of fuzzy modeling, the simplest fuzzy numbers and intervals – triangular and trapezoidal – have found the greatest use. At the same time, the expediency of using trapezoid fuzzy intervals and triangular fuzzy numbers is due not only to the simplicity of performing operations on them, but also to their graphic interpretation [3].

After determining the membership functions for each llinguistic variable, the rules of fuzzy production are formed, that is, each experiment from table 2 corresponds to its own production rule. The rules written in the Matlab Rule Editor program are shown in Figure 3.

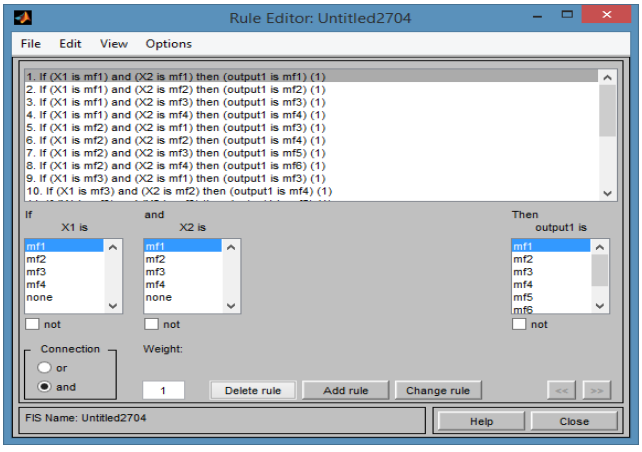

Fig. 3. Matlab Rule Editor

The rules were prescribed for the models using trapezoidal and triangular terms. As a result, two fuzzy models of optimal control of the chromium enrichment process were obtained. The interface presented in figure 4 is an optimal control model with which you can simulate various modes of operation of a jigging machine with various combinations of input variables.

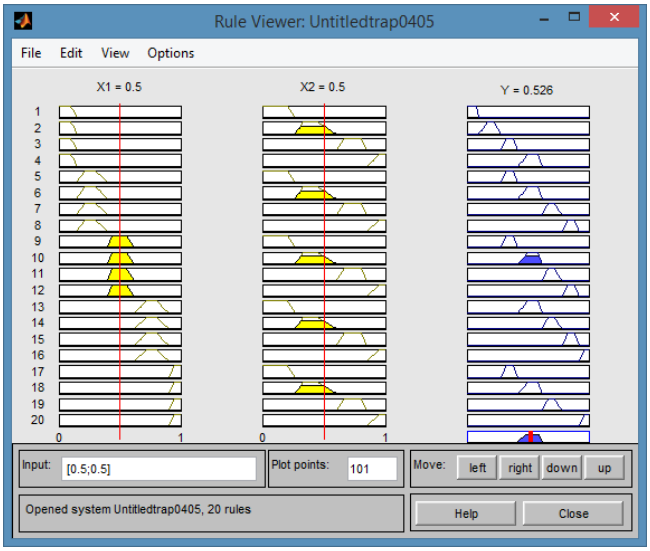

Fig. 4. Fuzzy control model with trapezoidal terms

To test the resulting models and evaluate the its adequacy a expert survey was carried out again and 20 modes of operation of the jigging machine (20 combinations of input variables) were obtained and the experts indicated the optimal output variables for these combinations. The data were tested on the obtained fuzzy models using two types of terms. The results are summarized in table 3.

Table 3. Comparative analysis of experimental and data obtained by using fuzzy models

Factors		Optimal value			Error, %	
Concentration of initial ore	Chromium concentration in reject material	Frequency of pulsation				
X1	X2	Y^E	Y^{trian}	Y^{trapez}	trian. term	trapez term.
0.00	0.00	0.00	0.03	0,04	3,00	4,00
0.00	0.33	0.25	0.232	0,240	2,53	2,33
0.00	0.67	0.4	0.452	0,463	1,87	2,97
0.00	1.00	0.25	0. 26	0,257	2,90	1,70
0.22	0.00	0.33	0.363	0,352	2,97	1,87
0.22	0.33	0.50	0.517	0,529	1,70	2,90
0.22	0.67	0.67	0.673	0,698	0,63	3,13
0.22	1.00	0.83	0.827	0,852	0,63	1,87
0.44	0.00	0.33	0.363	0,352	2,97	1,87
0.44	0.33	0.50	0.517	0,529	1,70	2,90
0.44	0.67	0.67	0.673	0,698	0,63	3,13
0.44	1.00	0.83	0.827	0,852	0,63	1,87
0.72	0.00	0.50	0.517	0,529	1,70	2,90
0.72	0.33	0.67	0.673	0,698	0,63	3,13
0.72	0.67	0.83	0.827	0,852	0,63	1,87
0.72	1.00	1.00	0.970	0,973	3,00	2,70
1.00	0.00	1	0.963	0,952	2,97	1,87
1.00	0.33	1	0.917	0,929	1,70	2,90
1.00	0.67	0.85	0.873	0,898	0,63	3,13
1.00	1.00	1.00	0.970	0,973	3,00	2,70
		Average error. %			1.82	2.59

In this table, Y^E is the output value of the pulsation frequency indicated by the experts, Y^{trian} is the value of the pulsation frequency obtained from the fuzzy model using triangular terms, Y^{trap} is the value of the pulsation frequency obtained from the fuzzy model using trapezoidal terms.

As a result of analyzing the data presented in table 3, can conclude that the absolute error in the variable "Pulsation frequency" was 1.82% for the model with triangular terms and

2.59% for the model with trapezoid terms. Since these values do not exceed 5%, both models obtained using fuzzy logic are adequate. Obviously, the best is a fuzzy model with triangular terms.

The graph presented in figure 5 shows the ratio of the pulsation frequency values obtained from the models and indicated by experienced experts.

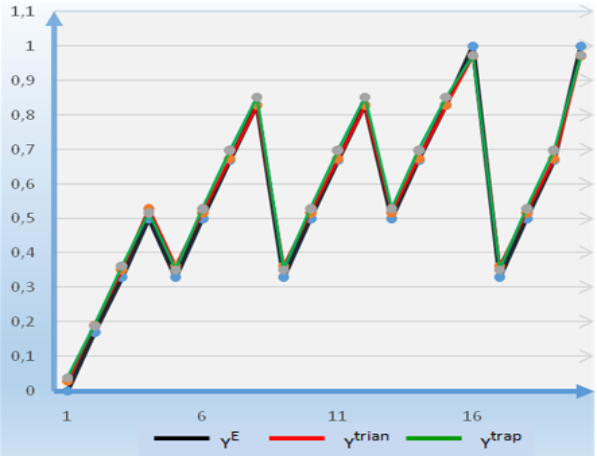

Fig. 5. The ratio of expert values, the values of the fuzzy model

4. Conclusion

Due to the complexity of the theoretical description and the multifactorial nature of the processes of gravitational enrichment, the application of intelligent algorithms in control them has great prospects. The use of intelligent systems to determine the key variables of the enrichment process will allow to reduce the influence of the human factor on the ore-dressing control process, which will ensure high technological performance.

Of the research made it can be concluded that the intelligence system built on the basis of fuzzy logic is able to determine the values of process variables at the level of an experienced expert technologist.

The introduction of automated controls system with intelligent subsystems of ore-dressing process, on the one hand, is associated with the costs of their acquisition. On the other hand, it allows to exclude losses of commodity concentrate and its getting into production waste. This certainly has an ecological and economic effect.

References

[1] Kozin V.Z., Tikhonov V.N.: Testing, control and automation of beneficiation processes. Nedra, Moscow 2010.
[2] Morozov V.V., Topchaev V.P, Ulitenko K.Ya., Ganbaatar Z., Delgerbat L.: Development and use of automated control systems for mineral processing. Ore and Metals, Moscow 2017.
[3] Nedjah N.M., Macedo L.: Fuzzy Systems Engineering. Theory and Practice. Springer Verlag, Berlin 2005.
[4] Shohin V.M.: Gravitational Enrichment Methods. Nedra, Moscow 1993.
[5] Suleimenov B.A, Sugurova L.A., Suleimenov A.B.: Intelligent systems of optimal control and operational diagnostics (methods of synthesis and application). Shikula: Almaty 2016.
[6] Swingler K.: Applying Neural Networks, a Practical Guide. Academic Press, London 1993.
[7] Tikhonov O.N.: Regularities of the effective separation of minerals in the processes of beneficiation. Nedra, Moscow 2015.
[8] Verhoturov M.: Gravitational Enrichment Methods. MAX PRESS, Moscow 2006.

Prof. Batyrbek Aitbaevich Suleimenov
e-mail: batr_sul@mail.ru

He is head of the Department of Automotion and Control, KazNRTU after K.I. Satpayev; Doctor of Technical Sciences, Professor. Since 1975, engaged in the development and implementation of systems of optimal process control in non-ferrous metallurgy in Kazakhstan, Russia and Ukraine. Since 1990 he has been working on the problems of the use of artificial intelligence in process control. He has more than 200 publications, including 4 books in the field of research of artificial intelligence in process control.

ORCID ID: 0000-0002-9177-9237

M.Sc. Yelena Kulakova
e-mail elena_winters@mail.ru

Doctoral student of the Department of Automotion and Control, KazNRTU after K.I. Satpayev; Master of technical sciences. She specializes in the field of development of automation systems, has practical experience at Donskoy Ore Mining and Processing Plant. Scientific interest: control systems of ore enrichment processes.
Publications: 6 publications – including 1 Scopus base, 1 proceedings of conference.

ORCID ID: 0000-0001-5307-4730

otrzymano/received: 15.05.2019 *przyjęto do druku/accepted: 15.06.2019*

DOI: 10.5604/01.3001.0013.2548

MODELING OF PROCESSES IN CRUDE OIL TREATED WITH LOW-FREQUENCY SOUNDS

Yelena Blinayeva, Saule Smailova
D. Serikbayev East Kazakhstan state technical university, Faculty/Department Information Technology

Abstract. *These days new methods of purification of crude oil from paraffin are being sought to improve the quality of oil, reduce its cost and optimize the processes of technological preparation of oil. The paper describes the method of conducting an experiment to study the impact of low-frequency sounds on oil samples of the Zhanazhol field, and presents the results of experiments, the input parameters of the experiment (exposure time and frequency of infrasound), at which the maximum reduction of the kinematic viscosity of oil is achieved. Further study of processes in crude oil under the influence of low-frequency sounds is planned to be investigated in COMSOL Multiphysics®.*

Keywords: crude oil, low frequency sounds, kinematic viscosity

MODELOWANIE PROCESÓW OCZYSZCZANIA SUROWEJ ROPY NAFTOWEJ WYKORZYSTUJĄCYCH DŹWIĘKI O NISKICH CZĘSTOTLIWOŚCIACH

Streszczenie. *Obecnie poszukiwane są nowe metody oczyszczania surowej ropy naftowej z parafiny, prowadzące do obniżenia kosztów i optymalizacji procesów przetwarzania ropy naftowej. W artykule opisano sposób prowadzenia eksperyment polegającego na badającego wpływ dźwięków o niskiej częstotliwości na parametry próbek ropy naftowej pochodzące z pola Zhanazhola. Przedstawiono wyniki doświadczeń, parametry wejściowe eksperymentu (czas ekspozycji i częstotliwość infradźwięków), przy których osiągane jest maksymalne obniżenie lepkości kinematycznej ropy naftowej. Dalsze badania procesów zachodzących w ropie naftowej pod wpływem dźwięków o niskiej częstotliwości planowane są w środowisku COMSOL Multiphysics.*

Słowa kluczowe: surowa ropa naftowa, dźwięki o niskiej częstotliwości, lepkość kinematyczna

Introduction

Due to the development of light oil reserves, oil fields with a high content of paraffin hydrocarbons and tar-asphaltene components are increasingly put into operation. Such oil is characterized by high values of viscosity, pour point and density. In the process of production, transportation and storage of high-paraffin and paraffin oils, asphalt-resin-paraffin deposits are often formed on the surface of oil equipment, to combat which additional investments are necessary [3].

In recent years, there has been a significant increase in interest in the possibility of using physical processing methods, in particular ultrasonic technologies, which are proposed to be used to intensify the processes of oil production and transportation, and cleaning oil equipment from paraffin deposits [2]. In this paper, we consider the use of low-frequency acoustic waves on crude oil samples to identify the degree of impact of infrasound on the paraffin content in the samples under study.

Mullakayev M. [7] describes the results of ultrasonic treatment of the samples of crude oil with a high content of resins and asphaltenes. As a result of the studies, a decrease in viscosity and pour point was recorded. The efficiency of ultrasonic treatment increased with the increase in exposure time.

The paper [10] gives an account of the effect of ultrasound on the flow of fluid moving through the channel, the size of which is much smaller than the length of the sound wave. As a result of the studies, the change in the viscosity of the liquid and the change in its rheological properties were recorded.

Various approaches to the organization of studies on ultrasonic effects on crude oil are described in papers [1,4,5,8,16]. The analysis of these works allowed us to make an unambiguous conclusion about the effectiveness of acoustic stimulation of crude waxy oil to decrease the concentration of wax and improve its fluidity.

1. Materials and methods

Oil dispersed systems are typical non-Newtonian fluids. Rheological properties, as well as the shape, size and structure of particles of the disperse phase of the oil disperse system significantly depend on their composition and on the presence and structure of the main structural components, which include paraffins, resins and asphaltenes. As numerous studies have shown, oils with high content of asphaltenes, resins and paraffins have structural and mechanical properties.

It has been shown in [6] that for oil disperse systems the transition from Newtonian to non-Newtonian properties is typical at decreasing temperature. According to modern notions at the increased temperature (above the melting point) wax molecules contained in the oil dispersed system are in the dissolved state and oil is a free disperse or liquid. At decrease in temperature of oil the spatial position of molecules of n-alkanes changes, energy of their thermal movement decreases and dissolving ability of light fraction of oil system decreases. Later on, due to saturation and oversaturation of the paraffin solution, primary crystallization centers are formed and grow. At the temperature close to the oil paraffin crystallization temperature, the size and number of crystalline structures increase, which leads to the formation of a three-dimensional spatial grid over the entire volume of the oil dispersed system, strongly branched alkanes form an amorphous phase. Structural mesh formation is characterized by the appearance of a coherent disperse system with viscoplastic properties.

The nature and peculiarities of structural formation and rheological behavior of high-viscosity waxy oils and natural bitumens were studied in detail in the works of A. Ratov [11-14]. The authors believe that the main reason for the structural formation in high-viscosity oils and natural bitumens, which causes their high viscosity and manifestation of structural-mechanical strength, are the intermolecular interactions of high-molecular fragments of resin-asphaltene components, which are associated with a strong paramagnetism of their polyaromatic structures. It was noted that sharp changes in rheological properties were observed against the background of a smooth change in the chemical composition of oil dispersed systems, which is expressed in a gradual increase in the concentration of resinous and asphaltene components, which is due to the unified physical and chemical nature of structural formation in high-viscosity oils and natural bitumens and corresponds to their genetic commonality. It is known that highly paraffinic oils are thixotropic dispersed systems. The phenomenon of thixotropy is expressed in the hysteresis of the rheological curves of the current "stress – shear rate", obtained by increasing and decreasing the shear rate (γ), as well as in reducing the effective viscosity (μ) with increasing γ. The dependence of μ on the value of γ is associated with the process of destruction of the structure at the increase of the velocity and its restoration at the decrease of γ.

The authors [15] have studied the ways of reducing the viscosity of the highly paraffinic oil of the Loidminster field. It has been established that mixing of heavy oil with lighter oil leads

to improvement of rheological parameters and is the most appropriate method of viscosity reduction (by 96%). Studies were carried out with the addition of ethyl alcohol, which at the same temperature reduced the viscosity by 90% of the original value. When using a mixture of water and ethyl alcohol, a 35% decrease in viscosity is observed.

As the influences controlling the structure of the substance, different variants of electric, electromagnetic, magnetic, ultrasonic, pulsating, vibrating fields or their different combinations are usually used. At the same time, the processes leading to both increase and decrease of the degree of orderliness of the structure of oil disperse systems proceed quite easily.

Until the 60s, most researchers believed that sonochemical reactions occur only in water systems. The first successful works on the sound chemistry of non-aqueous systems were carried out in 1963. It was shown that the non-aqueous systems are also characterized by a significant increase in speed and selectivity of sound-chemical reactions. Currently, the possibility of using ultrasound for the needs of the oil industry is widely studied: ultrasonic treatment of wells and formations; increase of oil recovery factor; cleaning of tanks, tanks and parts of oil equipment from deposits. Ultrasonic impact is aimed at changing both physical and chemical properties of oils, which allows for deeper processing and increased recovery of light fractions.

In general, the following ways to reduce the viscosity of oil and oil systems can be distinguished:

1) thermal methods;
2) mixing oil with solvents;
3) adding reagents-depressors and detergents in oil;
4) Removal of structure-forming components - resins, ashatenes, paraffins;
5) processing by physical fields.

The first four methods are well known and comparatively widely used. The use of physical fields, although it has a long history, is still relatively little present in the oil industry. For the most part, for operations related to the physical impact on oil, the extraction of paraffins, resins or asphaltenes from it is not contemplated, but the directed action on the colloidal or intermolecular interaction of the structure-forming components is considered. Here there is an infinite amount of research and patented developments considering ways of applications of this or that radiation or a complex of radiations.

Among a great number of ways to influence viscous liquids by different physical fields, special attention is paid to acoustic fields.

Ultrasonic influence leads to the destruction of polymer molecules, has a dispersing and colloidal chemical action, accelerates chemical processes.

Acoustic vibrations (f>20 kHz) are called ultrasonic. Under the influence of ultrasonic vibrations of a varied frequency range there is a change in the state of the processed medium and energy transfer, yet without the transfer of matter. Physical and chemical phenomena taking place in the propagation of acoustic waves are caused by nonlinear effects, including cavitation. An important feature of cavitation is the local concentration of the energy of the ultrasonic field in small amounts, due to which high densities of energy arise [9].

Cavitation means the rupture of the liquid medium in the event of negative pressures in it. Both liquids and solids are subject to stretching, and when a certain pressure is created, their structure breaks, and cavities are formed. Vapors and gases dissolved in the liquid penetrate into the cavities. Liquids are characterized by high strength under tensile stresses.

The presence in liquids of various micro-inhomogeneities, which violate the continuous structure of the medium, significantly reduce its tensile strength. Cavitation also results from the presence of solid particles in real liquids that contain adsorbed gases on their surface. The formation of cavitation bubbles takes place even in the presence of only one micro-embryo in the test fluid. The tensile strength, or cavitation strength, of a liquid depends on the nature of the substances it contains, the volume and concentration of the gas. The liquid, subjected to significant static pressures, is more homogeneous due to the dissolution of a larger proportion of micro bubbles in it.

The bubbles – cavitation embryos, oscillating under the action of the sound field, gradually increase in size. This occurs as a result of the predominant diffusion gas flow into the bubble as a result of the "one-way" gas diffusion and due to the micro-flows around the bubble, intensifying this process. In addition, under the influence of constant forces arising in the sound field, gas bubbles fusion takes place.

Increased in size bubbles reduce the cavitation strength of the liquid, so a significant impact on the characteristics of its cavitation strength is made by the time of exposure to the acoustic field.

Ultrasonic cleaning, dispersion and a number of other processes in most cases are carried out in liquids with low viscosity, but some chemical processes occur in environments with high viscosity. If the coefficient of viscosity is close to the viscosity of water ($\mu \approx 10^{-3}$ Pa*s), the influence of viscosity on the implosion of cavitation bubbles is negligible. Yet, when the coefficient of viscosity is 10^{-2} - 10^{-1} Pa*s, the action of viscous forces is already beginning to impact the behaviour of cavitation bubbles. By increasing the viscosity to 1 Pa*s, which corresponds to the viscosity of glycerine at room temperature, the bubbles are no longer closed and become pulsating.

Another specific feature of a viscous liquid is its high gas content ($\delta \approx 0{,}05$), which is explained by the low rate of ascent and removal of gas bubbles from the liquid. The constant presence of relatively large gas bubbles in viscous liquids greatly reduces their cavitation strength.

As part of the study, a hypothesis was put forward about the effect of infrasound on the change in the concentration of paraffin in the crude oil of the Kazakhstan Zaisan field. The reduction of paraffin concentration can be achieved at the account of the low-frequency cavitation in the studied oil, followed by intensification of chemical reactions.

2. Conducting an experimental study and its results

The authors of the study conducted an experiment on the effects of low-frequency sounds on crude oil samples. The experimental studies were based on the theory of experiment.

Experimental studies on the impact of low-frequency sounds on the oil of Kazakhstan fields were carried out with the samples obtained from the Zaisan field of the East Kazakhstan region.

After the experiments were over, the processed crude oil samples were examined in the laboratory of the center for certification tests of automotive fuels and technical oils to determine the viscosity and the pour point of oil.

The sample volume was 0.0005 m^3; the frequency of infrasound was 10 Hz, 20 Hz, 26 Hz; the duration of infrasound exposure was 15 min, 30 min, and 60 min.

The control sample of 0.5 l volume was not exposed to low-frequency influence.

As a result of laboratory studies of oil treated with low-frequency sounds, some changes in the pour point of oil were established. The results are presented in Table 1

The control sample of 0.5 l volume was not exposed to low-frequency influence, the control sample pour point made – 6°C.

Table 1. The values of the pour point of crude oil

No	Frequency, Hz	Exposure, min.	The pour point, °C
1	10	15	-6,3
2	10	30	-6,5
3	10	60	-7,6
4	20	15	-8,3
5	20	30	-7,9
6	20	60	-7,5
7	26	15	-8,3
8	26	30	-7,6
9	26	60	-7,2

The received results of the experiment allow concluding the following:

1) As a result of the impact of low-frequency sounds in the range from 10 to 26 Hz on crude oil, a decrease in pour point and some improvement in fluidity at low temperatures were achieved. The greatest decrease in the pour point of oil was recorded at the frequency of 20 Hz: – 31.7%, the lowest – at the frequency of 10 Hz: – 13.3%.
2) The greatest decrease in the pour point of oil was recorded at the exposure time of 15 min: – 37.2%, the lowest – at the exposure time of 30 min: – 22.2%.

As a result of laboratory studies of oil treated with low-frequency sounds, changes in the kinematic viscosity indices were established (Table 2).

Table 2. The values of kinematic viscosity at 100°C, 20°C

No	Frequency, Hz	Exposure, min.	Kinematic viscosity at100°C, m^2/s	Kinematic viscosity at 20°C, m^2/s
1	10	15	2.2272×10^{-6}	14.8829×10^{-6}
2	10	30	2.1059×10^{-6}	14.9117×10^{-6}
3	10	60	2.1156×10^{-6}	15.1556×10^{-6}
4	20	15	2.1737×10^{-6}	15.0988×10^{-6}
5	20	30	2.1430×10^{-6}	14.8531×10^{-6}
6	20	60	2.1420×10^{-6}	14.1374×10^{-6}
7	26	15	2.1227×10^{-6}	14.5859×10^{-6}
8	26	30	2.1538×10^{-6}	14.1723×10^{-6}
9	26	60	2.1616×10^{-6}	14.3682×10^{-6}

The control sample of 0.5 l volume was not exposed to low-frequency influence, the control sample kinematic viscosity at100°C made 2.1616×10^{-6} m^2/s; at 20°C it amounted to 14.9356 $x10^{-6}$ m^2/s.

Figures 1 and 2 show the dependence of the kinematic viscosity of oil on the frequency of infrasound and the time of exposure.

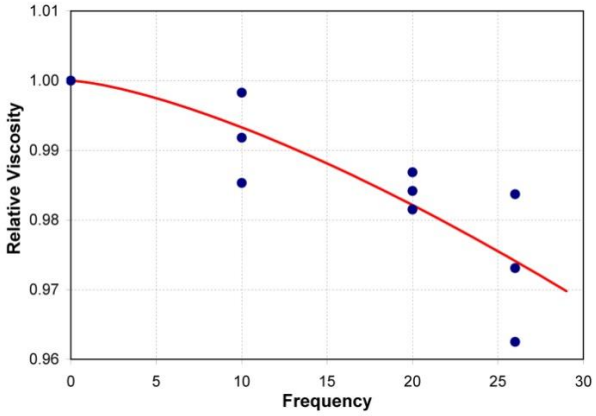

Fig. 1. The dependence of the kinematic viscosity of oil on the frequency of infrasound.

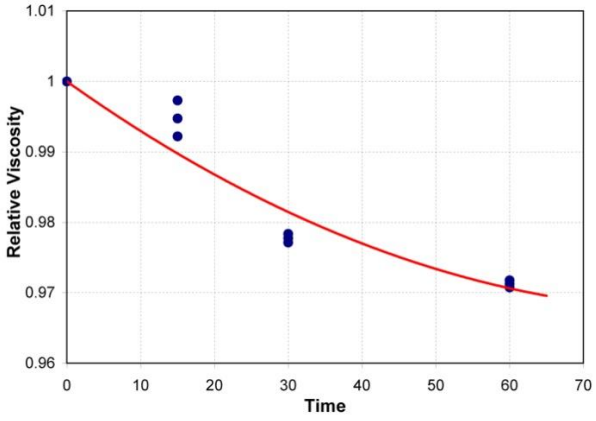

Fig. 2. The dependence of the kinematic viscosity of oil on infrasound exposure time

The results of the experiment allow us to draw a conclusion about the dependence of the kinematic viscosity of crude oil on the frequency and time of exposure to infrasound and the improvement of the fluidity of crude oil at low temperatures.

3. Further computer simulation

On the basis of the experimental data it is planned to conduct computer simulation of infrasonic impact on crude oil in COMSOL Multiphysics®, the environment of numerical simulation, using the "Acoustics" module. The Acoustics module provides a set of tools for modeling acoustic waves and vibrations in loudspeakers, mobile devices, microphones, sound absorbers, sensors, sonars and flow meters. For more detailed studies, acoustics can be considered together with other physical effects, including structural mechanics, piezoelectric phenomena and hydrodynamics. The COMSOL® software package contains multiphysical connections that allow calculating the performance characteristics of devices and structures as close to real conditions as possible.

A number of interfaces from the "scalar acoustics" group will be used to model classical acoustic phenomena such as scattering, diffraction, radiation, and sound wave propagation. For problems in the frequency domain the Helmholtz equation is used, for research in the time domain – the classical scalar wave equation.

The Helmholtz equation is a differential equation $\Delta u+\lambda u=0$, where D is the Laplace operator, λ is a constant; at $\lambda=0$ the boundary condition passes into the Laplace equation. The boundary condition can be obtained from the wave equation, if the time dependence is described by the $\exp(i\omega t)$ function, in this case $\lambda=\omega^2c^{-2}$ (c is the wave propagation velocity).

For boundary conditions in a bounded domain, ordinary boundary value problems (Dirichlet, Neumann, etc.) are considered. The values of λ for which there is a nonzero solution of a homogeneous boundary condition are called eigenvalues of the Laplace operator. For such values of λ the solution of the boundary value problem is not unique. Using the Green's function, the boundary value problem can be reduced to an integral equation. In the case of an unbounded domain, the solution of the boundary condition decreasing at infinity is not unique at $\lambda>0$. In this case for discrimination of the only decision additional conditions are set.

Sound waves are the solution of hydrodynamic equations. For an ideal (without absorption) fluid in which the dynamic processes take place at a constant entropy S, these equations are: Euler equation (motion)

$$\frac{dv}{dt}=\frac{\partial v}{\partial t}+(v\nabla)v=-\frac{\nabla P}{\rho}+f \tag{1}$$

the law of conservation of mass (continuity equation):

$$\frac{\partial\rho}{\partial t}=-\nabla(\rho v) \tag{2}$$

and the equation of state:

$$\frac{dP}{dt}=c^2\frac{d\rho}{dt},\quad c^2=\left(\frac{\partial P}{\partial\rho}\right)_S \tag{3}$$

where v is velocity of liquid particles, P is pressure, ρ – density, c – adiabatic speed of sound propagation, f – density (per unit mass) of external forces. Here, $d/dt = \partial/\partial t + (v\nabla)$ denotes the total time derivative, which characterizes the change of the corresponding value on the moving particle of the liquid, as opposed to the partial derivative $\partial/\partial t$, which characterizes the change at a fixed point in space.

The equation of state (3) is actually a form of the law of all-round compression in the theory of elasticity, it is easy to see if instead of density ρ we enter the specific volume (per unit mass) $\vartheta = 1/\rho$, $\Delta\vartheta = -\Delta\rho/\rho^2 = -\vartheta\Delta\rho/\rho$, $\Delta\rho = -\rho\Delta\vartheta/\vartheta$ and write equation (3) as: $\Delta p = -\rho c^2(\Delta\vartheta/\vartheta)$, where the bulk modulus of elasticity is $K=1/\rho c^2$, ρc^2 – the compressibility of the medium. This very mechanism is responsible for acoustic waves. All other dynamic processes are virtually unaffected by compressibility, so an incompressible fluid approximation is usually used to describe

them $d\rho/dt=0$ ($c^2 \to \infty$). In their turn, the sound waves are weakly affected by gravity and Coriolis force included in f and responsible for surface, internal, inertial waves and Rossby waves. Therefore, when considering sound waves, these forces are also usually neglected.

Sound waves slightly disturb the equilibrium parameters of the medium p_0, ρ_0 and $v_0=0$. As a result, substituting into equation (1) – (3) $P= p_0 + p$, $\rho= \rho_0 + \rho'$ and leaving under the conditions: $p << p_0$, $\rho' << \rho_0$, $|v| = v << c$ only linear in p, ρ' and v members, we get the linear acoustic equations:

$$\frac{\partial v}{\partial t}=-\frac{\nabla p}{\rho_0}, \quad \frac{\partial p}{\partial t}=-\rho_0 c^2 \nabla v \tag{4}$$

which, considering the equilibrium density of the medium constant (ρ_0=const), are easily reduced to the wave equation:

$$\Delta p-\frac{1}{c^2}\frac{\partial^2 p}{\partial t^2}=0 \tag{5}$$

where Δ – Laplace operator, $\Delta=\partial^2/\partial x^2 + \partial^2/\partial y^2 + \partial^2/\partial z^2$ in Cartesian coordinates. For harmonic waves, when the time dependence in p and v is given by the factor $\exp(-i\omega t)$, the expression (5) transfers into the Helmholtz equation:

$$\Delta p-k^2 p=0 \tag{6}$$

where $k=\omega/c$, ω – wave frequency. Vector $I=pv$ it is a vector of acoustic power flux density (energy per unit of time). This is easy to understand for physical reasons: $pndS$ – the sound pressure force acting on the platform dS with the normal n, $pvndS$ – the power of this force, therefore, the vector of the power flow density will be the value $I=pv$.

4. Conclusions

In the conducted research the analysis of methods of acoustic influence on crude oil allowing to reduce concentration of paraffin in it has been carried out. The experimental studies of the effect of low-frequency sounds on crude oil in order to reduce the paraffin content in the oil have been described. The prospects of further research based on the results of experiments by conducting computer simulation based on the finite element method in the COMSOL Multiphysics® environment have been presented.

Acknowledgements

This work supported within a grant of the Ministry of Education and Science № 35-293-18 “Analysis and modeling of the effect of low-frequency sounds on the change in the sulfur content and the viscosity of crude oil from Kazakhstan’s fields”.

References

[1] Abramov V., et al.: Sonochemical Approaches to Enhanced Oil Recovery. Ultrasonics Sonochemistry 25/2015, 76–81.
[2] Anufriev R.: Influence of Ultrasonic Treatment on Structural and Mechanical Properties and Composition of Oil Disperse Systems. Thesis for the degree of candidate of chemical Sciences. Russia, Tomsk 2017.
[3] Baydeldina O., Daribaeva N., Nuranbaeva B.: Features of the Structure and Properties of Crude Oils of Kazakhstan Influencing the Effectiveness of Interventions in the Fight against Paraffin Deposition. Modern High Technologies 4/2015, 100–106.
[4] Ershov M., et al.: Mathematical Processing of Results of Experiments on Ultrasonic Effects on the Viscosity of the Oil. Vestnik of SSTU 1/2012, 250–253.
[5] Guoxiang Y., et al.: Application of Ultrasound on Crude Oil Pretreatment. Chemical Engineering and Processing 47/2008, 2346–2350.
[6] Iktisanov V., et. al.: Rheological studies of paraffin oil at different temperatures. Colloidal journal 61(6)/1999, 776–779.
[7] Mullakaev M., Volkova G., Gradov O.: Effect of Ultrasound on the Viscosity–Temperature Properties of Crude Oils of Various Compositions. Theoretical Foundations of Chemical Engineering 49(4)/2015, 287–296.
[8] Mullakaev M., et al.: Development of Ultrasonic Equipment and technology for Well Stimulation and Enhanced Oil Recovery. Journal of Petroleum Science and Engineering 125/2015, 201–208.
[9] Nemchin A., et al.: Influence of Cavitation Influence on Hydrocarbon Fuel. Prom. Thermotechnics 24(6)/2002, 60–63.
[10] Prachkin V., Mullakaev M., Asylbaev D.: Improving the Productivity of Wells by Means of Acoustic Impact on High-Viscosity Oil in the Channels of the Face Zone of a Well. Chemical and Petroleum Engineering 50/2015.
[11] Ratov A., et. al.: Features of structure formation in high-viscosity paraffinic oils. Chemistry and technology of fuels and oils 1/1995, 22–24.
[12] Ratov A.: Mechanisms of structure formation and anomalies of rheological properties of high-viscosity oils and bitumen. Russian chemical. journal 39(5)/1995, 106–113.
[13] Ratov A.: Physical and chemical nature of structure formation in high-viscosity oils and natural bitumen and their rheological differences. Petrochemistry 36(3)/1996, 195–208.
[14] Ratov A., et. al.: Structure formation in high-viscosity oils and natural bitumen. Chemistry and technology of fuels and oils 3/1997, 36–38.
[15] Shadi W.: Heavy crude oil viscosity reduction and rheology for pipeline transportation. Fuel 89/2010, 1095–1100.
[16] Shedid A.: An Ultrasonic Irradiation Technique for Treatment of Asphaltenes Deposition. Journal of Petroleum Science and Engineering 42/2004, 57–70.

Ph.D. Yelena Blinayeva
e-mail: blinaeva-helen@mail.ru

The area of scientific interest is the use of low-frequency acoustic fields to influence various media (gas, crude oil) in order to identify the degree of influence of infrasound on the processes occurring in the medium under study.
Head of research in the framework of grant financing of the Ministry of Education and Science of the Republic of Kazakhstan. She has more than 30 publications of scientific articles in magazines in Kazakhstan, Russia, Ukraine. Author of articles in journals indexed in Scopus.
She participated in international conferences and seminars (Turkey, Bulgaria), with a speech at breakout sessions.
ORCID ID: 0000-0001-7251-3292

Ph.D. Saule Smailova
e-mail: Saule_Smailova@mail.ru

S. Smailova is currently a lecturer at the Department of Information Technology. She is a co-author over 60 papers in journals, book chapters, and conference proceedings. Member of Expert Group in the Computer Science specialization of IQAA. Her professional interests are teaching, artificial intelligence, software engineering, data processing.

ORCID ID: 0000-0002-8411-3584

otrzymano/received: 15.05.2019 *przyjęto do druku/accepted: 15.06.2019*

DOI: 10.5604/01.3001.0013.2549

INFORMATION TECHNOLOGIES FOR THE ANALYSIS OF THE STRUCTURAL CHANGES IN THE PROCESS OF IDIOPATHIC MACULAR RUPTURE DIAGNOSTICS

Sergii Pavlov[1], Yosyp Saldan[2], Dina Vovkotrub-Lyahovska[2], Yuliia Saldan[2], Valentina Vassilenko[3], Yuliia Yakusheva[2]

[1]Vinnitsa National Technical University, [2]Vinnitsa Pirogov National Medical University, [3]Universidade Nova de Lisboa, Faculdade de Ciências e Tecnologia

Abstract. *Process of eye tomogram obtaining by means of optical coherent tomography is studied.Stages of idiopathic macula holes formation in the process of eye grounds diagnostics are considered. Main stages of retina pathology progression are determined: Fuzzy logic units for obtaining reliable conclusions regarding the result of diagnosis are developed. By the results of theoretical and practical research system and technique of retinal macular region of the eye state analysis*

Keywords: tomogram, optical coherent tomography, macular area, fuzzy logic, membership function, idiopathic macular break.

TECHNOLOGIE INFORMACYJNE W CELU ANALIZY ZMIAN STRUKTURALNYCH W PROCESIE DIAGNOSTYKI IDIOPATYCZNYCH OTWORÓW PLAMKI

Streszczenie. W artykule omówiono proces uzyskiwania tomogramu oka za pomocą optycznej tomografii koherentnej. Rozważane są etapy powstawania idiopatycznych plamek żółtych w procesie diagnostyki podstawy oka. Określono główne etapy progresji patologii siatkówki: opracowanie modeli logiki rozmytej, w celu uzyskania wiarygodnych wniosków dotyczących wyniku diagnozy. Na podstawie wyników badań teoretycznych i rezultatów uzyskanych z układu badawczego i techniki regionu plamki żółtej przeprowadzono analizy stanu oka.

Słowa kluczowe: tomogram, optyczna tomografia koherentna, obszar plamki, logika rozmyta, funkcja przynależności, idiopatyczna przerwa plamkowa

Introduction

Nowadays the enlargement of knowledge concerning the development of the pathologic changes in human organism occurs, that is why, there appears the necessity to create modern information devices and methods of the processing of biomedical information, in particular, images. It is known that while making a diagnosis and carrying out treatment doctors often use biomedical images, obtained by means of various hardware – software complexes. In particular, in the field of the ophthalmology these complexes include optic coherent tomography, Heidelberg Retinal Tomography, Laser-based Retinal Polarimetry, Rectal Thickness Scanner analyzer, etc.

The most widely used are 1D, 2D and 3D images of the eye, including the fundus of eye; interpretation of these images takes a lot of efforts and much time. The diagnostician has to adjust his manner of thinking to obtain the aggregate picture, avoid the mistakes and make a correct diagnosis. That is why, very often there appears the need in using the algorithms of the analysis and processing of biomedical images which will help the staff to cope with large volume of data, providing the reliable support in diagnostics and treatment.

1. Aim and tasks of the research

The aim of the research is the enhancement of the reliability of the biomedical data analysis, developing the method of the processing the tomograms of the eye retina, the method is used in the system of the diagnostics of idiopathic macular ruptures (IMR).

2. Methods of the fundus of the eye visualization and processing of results obtainer

The authors made the assessment of the characteristics of various types of the equipment, in particular, their technical data, characteristic features, advantages and disadvantages. Such diagnostic devices were considered:

1) HPT – Heidelberg Retina Tomography, Heidelberg Engineering, Heidelberg, Germany;
2) GDx x VCC – Glaucoma Diagnostics Variable Cornea Compensation, till 2004 it was manufactured by the company Laser Diagnostics Technologies, San Diego, USA, after 2004 by the company Carl Zeiss Meditec, Dublin, USA;
3) OCT – Optical Coherence Tomograph, Carl Zeiss Meditec, Dublin, USA;
4) RTA – Retinal Thickness Analyzer, Talia Technology, Neve – Ilan, Israel.

Image obtaining is performed applying non-invasive method, quickly, at a low level of lighting that enables to use the technology in every-day clinical practice. The accuracy of CSLO is based on the optic law of the confocality, when the beam, reflected from the preset plane, by-passes the diaphragm, located in front of the detector and is taken into account by the device and the beam, reflected from the plane, located outside the investigated zone – is absorbed by the diaphragm.

For obtaining the images of HRT the diode laser is used (wave length – 670 nm). In HPT the system of automatic control of measurements quality is built-in, the system reveals and reshapes the scanned images of a poor quality, which are connected with possible winking or the change of gaze fixation of the patient. This enables to obtain for the analysis three series of scans. In order to create the necessary topographic image the program automatically centers and averages the scanned images for each series of the scanning.

At the same time the given method has some limitations: the necessity to plot the contour line by the operator; dependence of the greater part of the studied parameters on the basis plane; dependence of the image quality on the level of the ocular pressure; complexity of the research in case of artifacts and astigmatism of high degree; very high variability of the normative base of the healthy men creates problems in the diagnostic search during the first investigation.

Laser polarimetry, which is the base of GDx devices, was suggested for the determination of the thickness of the retinal nerve fibers layer [8, 9, 22]. Its principle is that in the middle of the eye, across the pupil, the laser beam with the polarized light is directed. The beam meets on its way the structural hindrance, for instance, the layer of axons, and is divided into two beams, located perpendicular to each other. Velocity of the beams across the axons is not the same due to the braking effect, which, in its turn, depends on the thickness of the axons layer.

By means of the software the device measures the thickness of the given structure, separating power of which is rather high [6]. The accuracy of polarimetric studies suffered for a long time due to the impossibility to compensate birefringence [3, 4, 7]. More wide spreading the technique obtained after the developers managed to neutralize the action of such optical structures of the eye, as the eye cornea and crystal, which have the ability to birefringence, that in its turn, gave the error in the process of measurements [5, 23]. Fig. 1 shows the results of GDx device scanning with the compensator of the birefringence and without it.

Optic Coherence Tomography (OCT) – is the method of diagnostics, which enables to obtain in vivo 2D transverse images of the retina, optic disk and the structures of the front part of the eye. The method was introduced into the clinical practice in 1991 and is based on the principles of Michelson interferometry.

Low-coherent light beam passing through the retina tissue is reflected by the structures, located in its layers and the degree of the reflection depends on the density and thickness of the layers as well as on the preset distance, at which the studied structure is located from the source of light. Another, reflecting beam, allows with high separation power to record and diagnose the smallest structural changes [1, 11, 12].

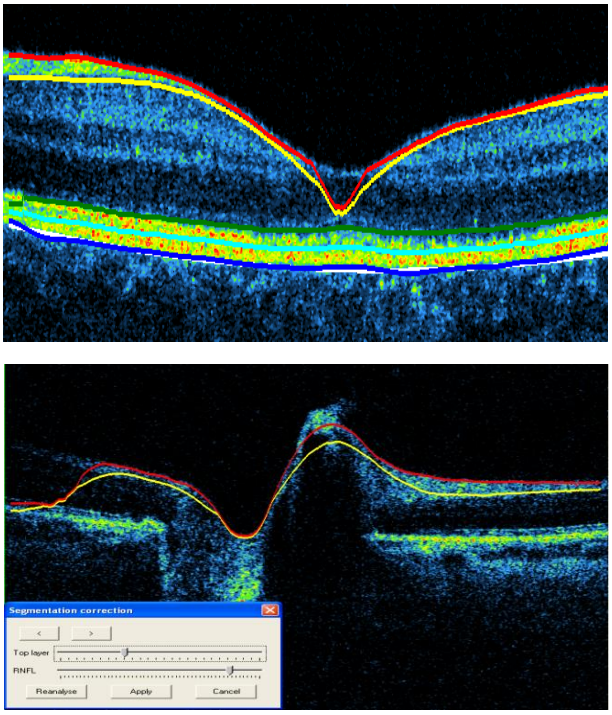

Fig. 1. Tomograms of the macular eye region with the allocated contours by the standard procedure: a) normal retina tomogram of the macular region, b) tomogram of the optic nerve

Studies, performed at Retinal Thickness Analyzes (RTA), are based on scanning of the retina surface and formation of its topographic map by means of HeNe laser with the wavelength of 543 nm. The laser beam layer-wise passes through the retina, deliminating and fixing peaks between vitreoretinal and chorioretinal surfaces, determining the output thickness of the retina. Total scanning depth of the device – up to 3 mm (16 optic partitions, one partition – 0.1875 mm). Taking into account high measurement error in the process of using the given method (up to 20%) it did not find wide application both in Ukraine and abroad [16].

The limitations of the method are the following: the need of the basis plane for certain topographic parameters; need of the mydriasis for the macular scanning; lack of quality autocontrol; very high variability of the normative base of the healthy men creates problems during the first investigation; high error of the reproducibility (up to 20%); changed crystal (cataract) absorbs the green colour of the laser and worsens the quality of the research in 50% of cases; the need of additional mydriasis.

3. Realization of the method of the eye retina macular region tomograms processing

OCT is used for the treatment of all the diseases of the central region of the retina and has some advantages: possibility of the application in any age; determination of the exact layer-wise structure of the retina; accurate visualization of the retina changes in case of various pathologies; determines the smallest structural changes at any stage of the process; the method is irreplaceable for the intermediate (dynamic) observation and assessment of the retina diseases treatment efficiency [7]

Tomograms are presented in the real-time by means of the color scale that shows the amount of light, dissipated by the tissues at different depth. Fig. 2 shows the image of the normal tomogram of the retina.

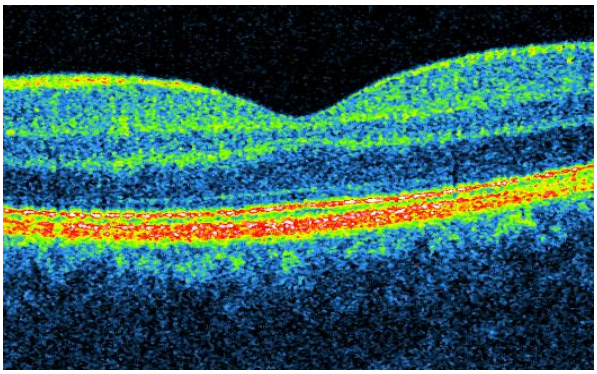

Fig. 2. Initial image of the retina of the macular region without processing

For the determination of the retina thickness, nerve fiber layer, various parameters of the macular the standard procedure is used , it includes the allocation of the zones in the tomogram, as a result, the needed calculations can be performed. Standard procedure, carried out after obtaining the eye tomogram, allocates tones only with 70 % validity.

As it is seen from Fig. 1a, there arises the problem of the distinct allocation of the boundaries on the tomogram, that would give the possibility to improve not only the determination of the retina layers of the macular region, but as a result perform more reliable eye diagnostics. To realize the unit of the preliminary processing of the tomograms, allocate the contour, in particular, fovea macular zone, a number of the transformations of the given image was performed.

Preliminary results of the analysis of the cell structures in the process of the histological examinations allows to make a conclusion that the greater part of the images in the process of their formation (photographing, scanning, etc.) fall under the impact of a number of negative factors, this leads to the appearance of the low-contrast and noisy sections [9].

For the beginning the author selected the retina tomogram of the macular region of the healthy patient. (Fig. 2a).

That is why it is expedient to apply the process of image cleaning from noise during the preprocessing of the image [6, 22]

To carry out this procedure the smoothing 2D median filter was chosen, the result of its application is shown in Fig. 3.

The window of the median filter gradually slides on the image and at each step turns one of the elements, which fell into the aperture of the filter. The given filtration realizes the change of counting's values in the centre of the aperture. The output signal y_m of the median filter of $2n+1$ of width for the current counting of m is formed from 12 input time series ..., x_{m-1}, x_m, x_{m+1}, ...:

$$y_m = med(x_{m-n}, x_{m-n+1}, ..., x_{m-1}, x_m, x_{m+1}, ..., x_{m+n-1}, x_{m+n}), \quad (1)$$

where $med(x_1, ..., x_k, ..., x_{2n+1}) = x_{n+1}$, x_k – elements of the variational series, x_k:

$$x_1 = min\,(x_1, x_2, ..., x_{2n+1}) \le x_{(2)} \le x_{(3)} \le ... \le x_{2n+1} = max\,(x_1, x_2, ..., x_{2n+1}). \quad (2)$$

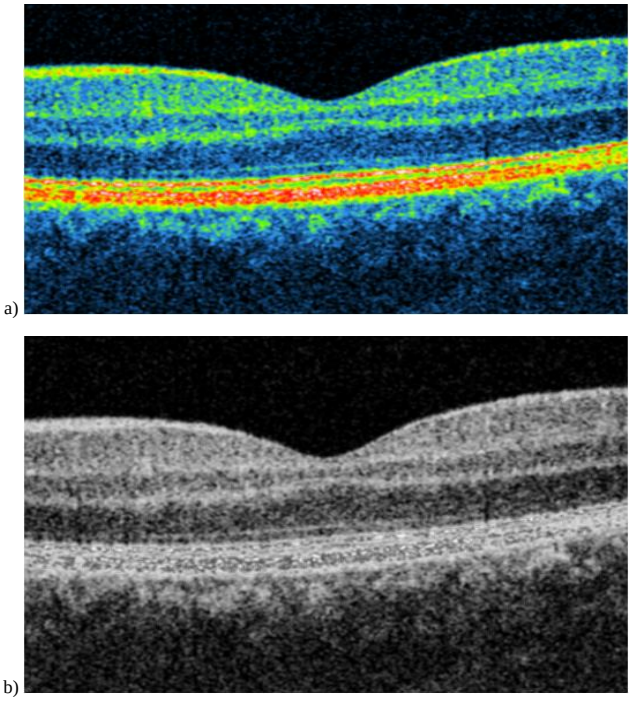

Fig. 3. a) Image after the application of the smoothing 2D median filter, b) image of the retina of the macular zone after the transformation in black and white format

Since the image is information oversaturated to perform the next steps, namely, colors inversion, it is better to turn the image into black and white one (Fig. 3b).

Conversion of the color image into grayscale is carried out by means of the multiplication of three colors of each pixel on the image and obtaining the number of the grayscale by the formula 2.

$$F(x,y) = 0.2989 \cdot f(x,y).R + 0.587 \cdot f(x,y).G + 0.114 \cdot f(x,y).B \quad (3)$$

$f(x,y).R$ – value of the color number of the red scale;

$f(x,y).G$ – value of the color number of the green scale;

$f(x,y).B$ – value of the color number of the blue scale.

Each obtained number of the gray shade is written into a new matrix at the same place of the matrix coordinates that in the matrix of the color image. [6].

Thus, a new image in gray scale was obtained from the color image of the tomogram of the retina of the macular zone (Fig. 3b).

For obtaining well defined contours of the macular region, the given tomogram is necessary to invert, this will give us the possibility to deliminate the boundaries better (Fig. 4). The process of colors inversion is the search through of each pixel and assigning it the reversed color and, as we have black and white image, then this process is simplified in order to assign the black color to the white with the corresponding coefficient, and black to the white with the corresponding coefficient.

Binarization of the images was carried out for the conversion of the images in gray gradations into monochromatic, i.e. the image where only two types of pixels are available (dark and light). Image binarization is performed applying Bernsen method, also known as the threshold binarization.

This contrast threshold is a constant for the white image but for each input image it is selected on the base of the histogram analysis.

The following steps are made in the process of image binarization: the input image with the allocated contour is obtained; histogram is made and analyzed and the value of the threshold is obtained; each pixel of the image is verified, if in the given coordinate the value is less than the threshold value, «1» is written, otherwise «0» is written; binary image is obtained (Fig. 4b).

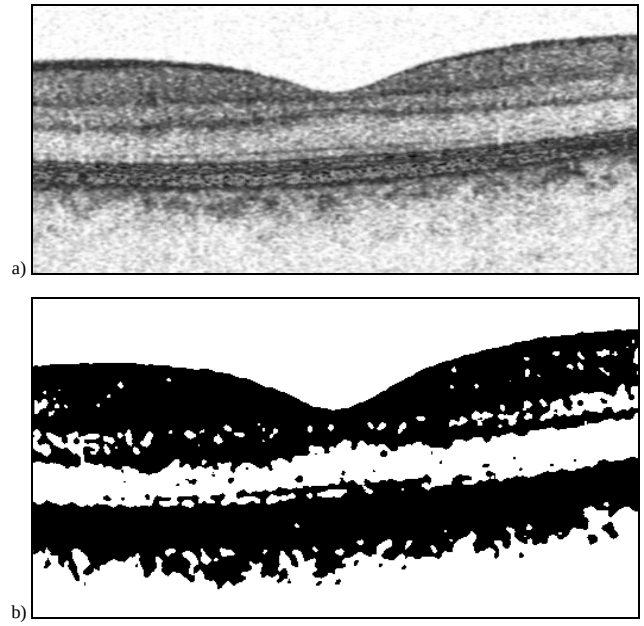

Fig. 4. Image of the retina of macular zone a) Image of the retina of macular zone after the inversion is performed; b) Image of the retina of macular zone after the binarization

Also the optimal value of the threshold can be obtained after the determination of the maximum value of the amplitude of the gray g_{max} and minimum value g_{min}, after that average number of pixels which entered the range from the minimal value to the average is calculated:

$$T_{opt} = (g_{\max} - g_{\min}) \sum_{g=g_{\min}}^{gmid} p(g) \quad (4)$$

where T_{opt} – optimal threshold; g_{max}, g_{min}, g_{mid} – maximum, minimum and average value of the amplitude of the gray; $p(g)$ – set of the gray.

As it is seen from Fig. 5 visually it is possible to recognize the boundaries but for more accurate results it is necessary to use Sobel filter (Fig. 5a). As the contour is the contrast region of the image, that contains sharp difference of the brightness between two neibouring pixels, then such drops of the brightness as a rule, are the boundaries of the object, where background and brightness of the object itself differ greatly. Algorithm of boundaries determination establishes both horizontal and vertical boundaries (Fig. 5a).

For Sobel filter the window is used:

$$M_{Sobel} = \begin{vmatrix} f_{i-1,j-1} & f_{i-1,j} & f_{i-1,j+1} \\ f_{i,j-1} & f_{i,j} & g_{i,j+1} \\ f_{i+1,j-1} & f_{i+1,j} & g_{i+1,j+1} \end{vmatrix} \quad (5)$$

where $(i,j)^{th}$ – pixel is attributed the value of the brighness instead of $f(i,j)$

$$g_{i,j} = \left(X^2 + Y^2\right)^{\frac{1}{2}}, \quad (6)$$

or

$$g_{i,j} = |X| + |Y|, \quad (7)$$

$$X = \left(f_{(i-1),(j-1)} + 2 f_{(i-1)j} + f_{(i-1),(j+1)}\right) - \left(f_{(i+1),(j-1)} + 2 f_{(i+1)j} + f_{(i+1),(j+1)}\right), \quad (8)$$

$$Y = \left(f_{(i-1),(j-1)} + 2 f_{i,(j-1)} + f_{(i+1),(j-1)}\right) - \left(f_{(i-1),(j+1)} + 2 f_{i,(j+1)} + f_{(i+1),(j+1)}\right). \quad (9)$$

Unlike the smoothing filters and filters that increase the contrast rate, which do not change average intensity of the image,

as a results of using difference operators the images with the average value of the pixel close to zero are obtained. Pixels with large by modulus values on the finite image correspond to the vertical boundaries of the output image.

That is why difference filters are also called filters that find the boundaries. As it is seen from Fig. 5a Sobel filter allocated the contours, we invert the colors for obtaining distinct lines (Fig. 5b) that can be plotted as a mask on the initial biomedical image.

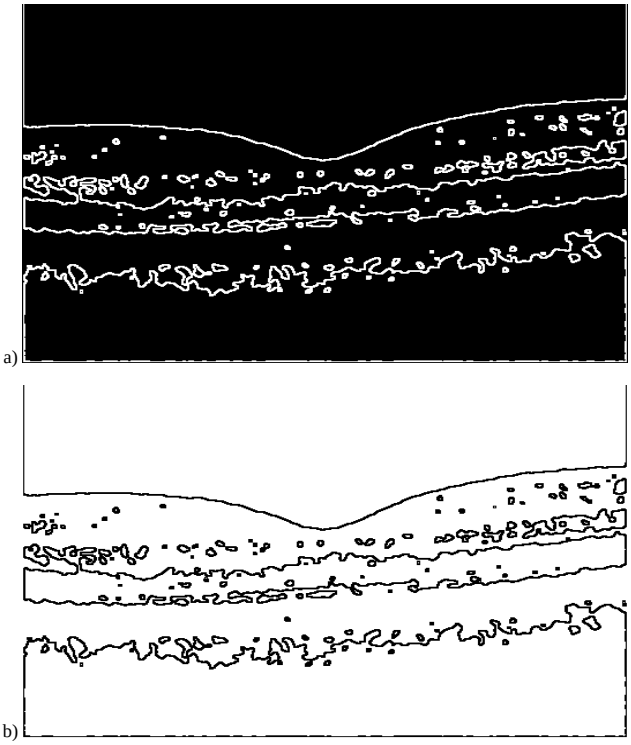

Fig . 5. a) Image of the retina of the macular zone after using Sobel filter, b) image of the retina of the macular zone after the inversion is performed

4. Practical realization

Fig. 6 shows what form has the obtained image with the plotted mask, the red color shows the upper boundary. The condition for carrying out the research was the development of the technology for the processing of the tomogram of the macular region retina, that would give the possibility to improve the accuracy of the macular region contour determination to the value of 98%.

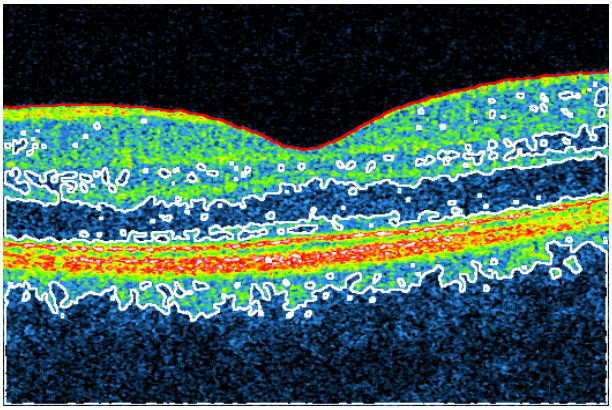

Fig. 6. Initial image of the retina of the macular zone with the applied mask

The author developed the technology of such images processing which allocates the macular region with high accuracy. Visually this can be demonstrated comparing the images, which were processed by the standard procedure and by our technology (Fig. 7, 8) [3, 4, 7].

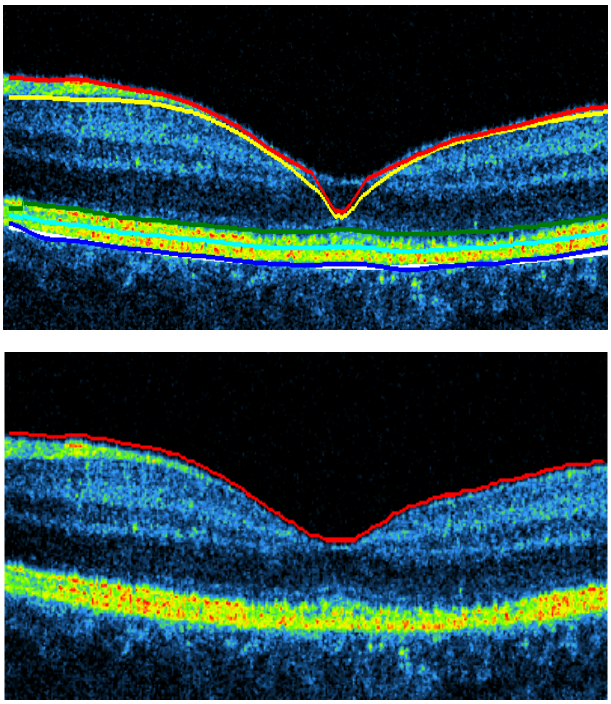

Fig. 7. a) Normal tomogram of the macular zone retina; a) standard technology, b) suggested technology

Procceding from the above-mentioned we can state that having applied the developed method of processing for the tomograms of the macular zone retina, better efficiency of the contrours allocation is achieved. In its turn, this improves the accuracy of the macular region parameters determination.

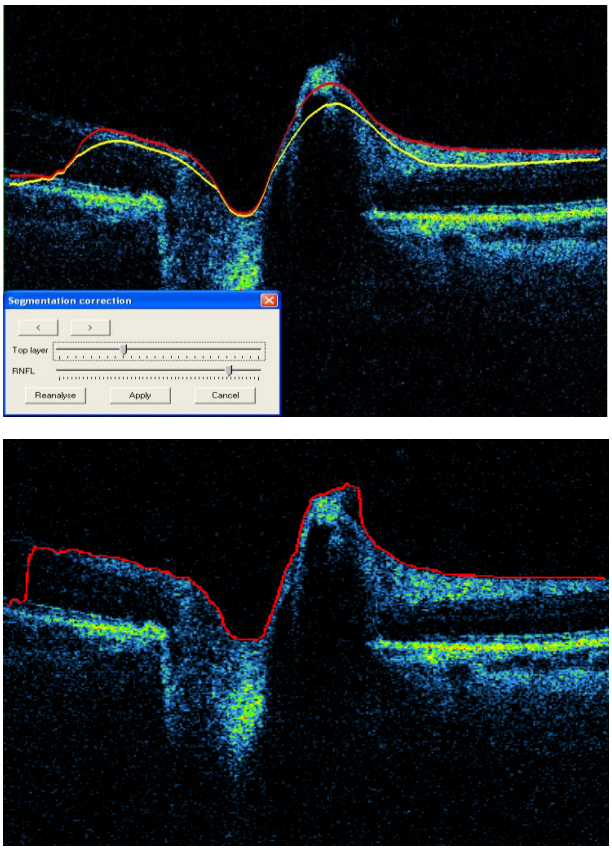

Fig. 8. Tomogram of the optic nerve disk using a) standard technology, b) suggested technology

Realization of the information input and processing unit of the biomedical expert system is presented in Fig. 9, where 1 – open the file; 2 – close the file; 3 – save the file; 4 – initial image; 5 – chromatity (represent the values of R, G, B); 6 – contour allocation; 7 – graphs plotting; 8 – improvement of the image parameters; 9 – full screen mode; 10 – help; 11 – image analysis; 12 – button; 13 – histograms by R, G, B; 14 – language.

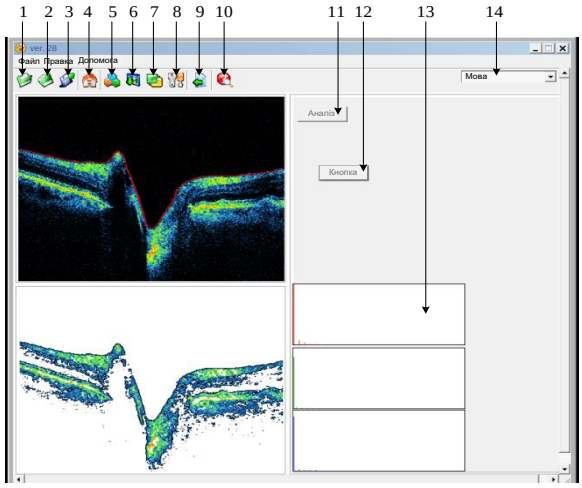

Fig. 9. Program for the processing of the tomogram of retina of the macular region of the eye

It was established practically that image processing by means of masks in the space range is more efficient that the realization of the similar actions in the frequency range because less time is needed for carrying out the processing.

The rate of the frequency filtration does not depend on the size of the mask, performing of convolution of the image with the mask of the super large dimensions (approximately 120×120 elements and more) is expedient to carry in the frequency range.

5. Conclusions

The given research further develops the mathematical models for the analysis of the biomedical images of the macular area of the retina using the methods of fuzzy sets on the base of the experimental knowledge bases that allowed to carry out complex qualitative diagnostics and improve its reliability by 22% as well as the developed method of processing the fundus of eye, which, unlike the existing one, has the possibility to create the sliceable mask, that enables to determine more exactly the contours of the macular region of the eye retina.

The expediency of application the methods of image brightness correction, in case of its general blurring and the technique of the sliceable masking for the improvement of the image definition was proved practically. Better quality of the periodic noise elimination by the median filtration as compared with adaptive Wiener filtering is established. Minor advantage in speed of realization the adaptive Wiener filtering over the median filtration in MATLAB package is practically determined, that is why the given peculiarity must be taken into account when creating new methods of the space processing of the images, which will use the above mentioned filters.

References

[1] Alamouti B., Funk J.: Retinal thickness decreases with age: an OCT study. Br. J. Ophthalmol. 87/2003, 899.
[2] Alamouti B., Funk J.: Retinal thickness decreases with age: an OCT study. Br. J. Ophthalmol. 87/2003, 899.
[3] Bagga H., Greenfield D.S., Knighton R.W.: Scanning laser polarimetry with variable corneal compensation: identification and correction for corneal birefringence in eyes with macular disease. Invest. Ophthalmol. Vis. Sci. 44/2003, 1969–1976.
[4] Bagga H., Greenfield D.S., Feuer W., Knighton R.W.: Scanning laser polarimetry with variable corneal compensation and optical coherence tomography in normal and glaucomatous eyes. Am. J. Ophthalmol. 135/2003, 521–529.
[5] Bowd C., Zangwill L.M., Weinreb R.N.: Association between scanning laser polarimetry measurements using variable corneal polarization compensation and visual field sensitivity in glaucomatous eyes. Arch. Ophthalmol. 121/2003, 961–966.
[6] Bowd C., Zangwill L.M., Medeiros F.A., et al.: Confocal scanning laser ophthalmoscopy classiliers and stereophotograph evaluation for prediction of visual field abnormalities in glaucoma-suspect eyes. Invest. Ophthalmol. Vis. Sci. 45/2004, 2255–2262.
[7] Greenfield D.S., Knighton R.W., Feuer W.J., Schiffman J.C.: Normative retardation data corrected lor the corneal polarization axis with scanning laser polarimetry. Ophthalmic. Surg. Lasers. Imaging. 34/2003, 165–171.
[8] Gurses-Ozden R., Hon H., Ishikawa S.TLiebmann., J.M.: Increasing sampling density improves reproducibility of optical coherence tomography measurements. J. Glaucoma 8/1999, 238–241.
[9] Jones A.L., Sheen N.J., North R.V., et al.: The Humphrey optical coherence tomography scanner: quantitative analysis and reproducibility study ol the normal human retinal nerve fibre layer. Br. J. Ophthalmol. 85/2001, 673.
[10] Pavlov S.V., et al.: Methods of processing biomedical image of retinal macular region of the eye, Proc. SPIE 9961, Reflection, Scattering, and Diffraction from Surfaces V, 99610X (September 26, 2016); [DOI:10.1117/12.2237154].
[11] Pavlov S.V., et al.: Tele-detection system for the automatic sensing of the state of the cardiovascular functions in situ. Information Technology in Medical Diagnostics II. CRC Press Balkema book, London 2019, 289–296.
[12] Pavlov S.V., Martianova T.A., Saldan Y.R., et al.: Methods and computer tools for identifying diabetes-induced fundus pathology. Information Technology in Medical Diagnostics II. CRC Press, Balkema book, London 2019, 87–99.
[13] Romanyuk O.N., et al.: Method of anti-aliasing with the use of the new pixel model, Proc. SPIE 9816, Optical Fibers and Their Applications 2015, 981617 (December 18, 2015), [DOI:10.1117/12.2229013].
[14] Romanyuk S.O.: New method to control color intensity for antialiasing. Control and Communications (SIBCON), 2015 International Siberian Conference. 21-23 May 2015. [DOI**:** 10.1109/SIBCON.2015.7147194].
[15] Saldan Y.R., et al.: Efficiency of optical-electronic systems: methods application for the analysis of structural changes in the process of eye grounds diagnosis. Proc. SPIE 10445, Photonics Applications in Astronomy, Communications, Industry, and High Energy Physics Experiments 2017, 104450S, [DOI: 10.1117/12.2280977].
[16] Sergey I., et al.: Offsetting and blending with perturbation functions. Proc. SPIE 11045, Optical Fibers and Their Applications 2018, 110450W, 2019 [DOI: 10.1117/12.2522353].
[17] Timchenko L.I., et al.: Bio-inspired approach to multistage image processing. Proc. SPIE 10445, Photonics Applications in Astronomy, Communications, Industry, and High Energy Physics Experiments 2017, 104453M, [DOI: 10.1117/12.2280976].
[18] Timchenko L.I., et al.: Precision measurement of coordinates of power center of extended laser path images. Proc. SPIE 10808, Photonics Applications in Astronomy, Communications, Industry, and High-Energy Physics Experiments 2018, 1080810 [DOI: 10.1117/12.2501628].
[19] Vyatkin S.I., et al.: Offsetting and blending with perturbation functions. Proc. SPIE 10808, Photonics Applications in Astronomy, Communications, Industry, and High-Energy Physics Experiments 2018, 108082Y, [DOI: 10.1117/12.2501694].
[20] Vyatkin S.I., et al.: A GPU-based multi-volume rendering for medicine. Proc. SPIE 11045, Optical Fibers and Their Applications 2018, 1104513, 2019 [DOI 10.1117/12.2522408].
[21] Vyatkin S.I., et al.: Using lights in a volume-oriented rendering. Proc. SPIE 10445, Photonics Applications in Astronomy, Communications, Industry, and High Energy Physics Experiments 2017, 104450U, [DOI: 10.1117/12.2280982].
[22] Weinreb R.N., Bowd C., Greenfield D.S., Zangwill L.M.: Measurement of the magnitude and axis of corneal polarization with scanning laser polarimetry. Arch. Ophthalmol. 120/2002, 901–906.
[23] Zhou Q., Weinreb R.N.: Individualized compensation of anterior segment birefringence during scanning laser polarimetry. Invest. Ophthalmol. Vis. Sci. 43/2002, 2221–2228.

Prof. Sergii Pavlov
e-mail: psv@vntu.edu.ua

Doctor of Technical Sciences, Professor, Academician of the International Academy of Applied Radioelectronic. Vice-rector of for Scientific Work of Vinnytsia National Technical University, professor of biomedical Engineering
Scientific direction – biomedical information optoelectronic and laser technologies for diagnostics and physiotherapy influence. Deals with issues of improving the distribution of optical radiation theory in biological objects, particularly through the use of electro-optical systems, and the development of intelligent biomedical optoelectronic diagnostic systems and standardized methods for reliably determining the main hemodynamic cardiovascular system of comprehensive into account scattering effects.

ORCID ID: 0000-0002-0051-5560

Prof. Yosyp Saldan
e-mail: ysaldan@ukr.net

Doctor of Medical Sciences, Professor of Eye Diseases and Eye Microsurgery Department, Pirogov National Medical University of Vinnytsia
Scientific direction - information technologies for the analysis of the structural changes in the process of idiopathic macular rupture diagnostics, development of biomedical technologies through the use of new technologies in the field of research of image processing, development of information-measuring systems diagnostic monitoring.

ORCID ID: 0000-0002-3925-9197

Ph.D. Dina Vovkotrub-Lyahovska
e-mail: vovkotrub@vntu.edu.ua

Senior lector of Vinnytsia National Technical University, researcher of Company "Sperko" , Vinnytsia
The scientific direction of work is the creation of systems for the diagnosis of fundus abnormal pathologies, the technology of standardization of methods for biomedical information analysis, and the processing of biomedical images.

ORCID ID: 0000-0001-6793-5407

Ph.D. Yuliia Saldan
e-mail: ysaldan@ukr.net

Docent of Eye Diseases and Eye Microsurgery Department, Pirogov National Medical University of Vinnytsia.
Scientific direction – information technologies for the analysis of the structural changes in the process of idiopathic macular rupture diagnostics, development of biomedical technologies through the use of new technologies in the field of research of image processing, development of information-measuring systems diagnostic monitoring.

ORCID: 0000-0001-7420-598X

Prof. Valentina B. Vassilenko
e-mail: vv@fct.unl.pt

D.Sc., prof. Universidade Nova de Lisboa, Faculdade de Ciências e Tecnologia, 2829-516 Caparica, Portugal.
Development of biomedical technologies through the use of new technologies in the field of research of image processing, machine learning, deep learning, artificial intelligence, development of optoelectronic, microelectronic and nanotechnology in the creation of opto-electronic means, biomedical optics; development of information-measuring systems diagnostic monitoring.

ORCID: 0000-0002-7913-7047

Ph.D. Yuliia Yakusheva
e-mail: yakusheva@vnmu.edu.ua

Candidate of Biological Sciences, Senior Lecturer. Department of Physical Education and Therapeutic Physical training of National Pirogov Memorial Medical University
Scientific direction – features of the indicators of central hemodynamics, depending on the parameters of the body structure of athletes

ORCID ID: 0000-0002-4811-8089

otrzymano/received: 15.05.2019 *przyjęto do druku/accepted: 15.06.2019*

DOI: 10.5604/01.3001.0013.2550

GENERATORS OF ONE-TIME TWO-FACTOR AUTHENTICATION PASSWORDS

Olga Ussatova[1], Saule Nyssanbayeva[2]
[1]Al-Farabi Kazakh National University, Almaty, Kazakhstan, [2]Institute of Information and Computational Technologies, Almaty, Kazakhstan

Abstract. *The paper presents algorithms for generating a one-time two-factor authentication passwords where application of trigonometric functions have been considered. To protect the opening of a one-time password, a secret string is read that consists of a sequence of randomly generated characters. The second factor is due to the fact that that the code has a certain validity period. The presented password generators allow the formation of secret words and trigonometric functions that the proposed two-factor authentication method consists of. The algorithm presented was implemented in Java Script. The algorithm includes blocks for checking randomly generated words and functions.*

Keywords: password generator, two-factor authentication, data protection

GENERATORY JEDNORAZOWYCH DWUCZYNNIKOWYCH HASEŁ AUTORYZACJI

Streszczenie. *W pracy przedstawiono algorytmy generowania jednorazowych, dwuczynnikowych haseł uwierzytelniających, w których uwzględniono zastosowanie funkcji trygonometrycznych. Aby chronić otwarcie jednorazowego hasła, odczytywany jest tajny ciąg składający się z sekwencji losowo generowanych znaków. Drugi składnik wynika z faktu, że kod ma określony okres ważności. Przedstawione generatory haseł umożliwiają tworzenie tajnych słów i funkcji trygonometrycznych, z których składa się proponowana metoda dwuczynnikowego uwierzytelniania. Przedstawiony algorytm został zaimplementowany w Java Script. Algorytm zawiera bloki do sprawdzania losowo generowanych słów i funkcji.*

Słowa kluczowe: generator hasła, uwierzytelnianie dwuskładnikowe, ochrona danych

Introduction

Ensuring the safety of confidential information must begin with identifying a system of threats, that is, negative processes that contribute to information leakage. In the modern world, the storage of electronic information, its value and significance has increased many times over. The need to ensure the safety of data storage, regular change and verification of passwords and control of the probability of information leakage have become an integral part of the information system. One of the most common methods of protecting information is password access to data. However, along with the undoubted advantages, this method of data protection has certain disadvantages: you can forget the password, it can be "hacked". A two-factor authentication data protection system based on one-time password generation is proposed.

This article describes the results obtained when developing a generator of trigonometric functions and secret words for generating a one-time two-factor authentication password based on an application using a smartphone.

1. Material and methods

The proposed system of information protection based on two-factor authentication using a combination of two factors: permanent and one-time passwords [7]. The user chooses a permanent password (the first factor) himself and uses it when registering an account. Before authorization must be registered in the application. After that, the application starts to enter user data (login and password), which must correspond to the registered data.

Then you need to enter the application on your smartphone and enter the initial data to generate a temporary password. A one-time or temporary password (the second factor) is generated on the server by the proposed algorithm [7] and is valid for a specific period of time for one authentication session. The time in the application is 20 seconds. The advantage of a one-time password is that the password is not reused. Thus, an attacker who intercepted data from a successful authentication session cannot use the copied password to gain access to the protected system. One-time password generation is possible online. The software sends a request to the authorization server to generate a temporary password. It is generated on the server and displayed to the user in additional software on the smartphone. The password has a short duration – 20 seconds. The one-time password is generated based on the result of the selected trigonometric function, which has a number of variables generated based on the result of the SHA256 hash function [4, 5]. The input string for the hash function is a combination of user credentials, the current Greenwich Mean Time, and an additional secret string. The result of the hash function is divided into individual numbers, which will be the indices for selecting the function and its initial data. The secret string is a required field that will be randomly selected from the array. The secret line is changed at each input, due to which it will be much more difficult to open the initial input line, which allows to further strengthen the protection. The data for the input string has the values: login, password, current date, time and secret string. The next step to generate a password will be the result of the SHA256 hash function, which underlies the choice of the trigonometric function.

2. Secret word generating

For the formation of a secret string, a generator has been developed that allows one to randomly form words. Word dictionaries were not used, as words are easier to crack [3, 6]. The generator is based on the use of the Latin alphabet of capital and uppercase characters in a total of 52. The length of the generated word is 5 characters.

In the final code, the algorithm described above is implemented in the Java Script language and has the following form:

```
letfuncVariblesList = []
letfuncComponents = []
let expressions = ['+', '-', '/', '*']

module.exports.getWord = function() { // word generator
let chars = 'ABCDEFGHIJKLMNOPQRSTUVWXYZa-
bcdefghijklmnopqrstuvwxyz'
letwordLength = getRandomInt(5, 10)
let word = ''
for (let i = 0; i <= wordLength; i++) {
letcharIndex = getRandomInt(0, chars.length - 1)
word += chars[charIndex]
  }
return word
}
```

For the analysis of the generator used the method of complete enumeration [1, 2]. According to this method, the length of the string is taken into account (the length of the string is 5 characters in the appendix) and, for example, the search speed of 100,000 words per second is used. The number of options is calculated by the formula:

$$S = A^n \quad (1)$$

where A is the number of characters and n the length of the string.

An example of the analysis of the generator is presented in table 1.

Table 1. Analysis of the generator

Number of characters	Number of options	Persistence	Search Time
1	52	5 byte	Less than a second
5	380204032	26 byte	63 minutes

$S= 52^5=380204032$

Due to the fact that, according to the developed two-factor authentication algorithm, the generation of a one-time password occurs every 20 seconds, the probability of hacking the generated secret word is almost impossible. This confirms the efficiency of the proposed generator.

3. Trigonometric Function Generator

As stated above, the generation of a one-time password is based on the result of the selected trigonometric function, which has a number of variable parameters. The choice is made in accordance with the result of the obtained hash function of the SHA256 standards, where the first characters are used, which will be indices in a table of 256x256 dimension. By this index, the function will be selected and its parameters will be determined. According to the results of the calculation, digits after the comma are taken as a one-time temporary password, starting from the 5th position and 6 digits long.

The resulting number will be a temporary password that must be entered into the application. To implement this method, a generator of trigonometric functions has been developed, the use of which will greatly facilitate the formation of these functions. The algorithm of the generator of the trigonometric function is shown in Figure 1–3.

To generate a trigonometric function, the number of variables is taken as the basis. There are 7 of them in this generator: a, b, c, x, y, p1, p2. Initially, a list of variables is formed, resulting in a random number of variables Count from 1 to the number of variables minus 1. Then, the array is searched through the array with certain variables N- times based on a random number from 0 to the length of the array minus 1.

Read variable from the array, which is added in the new array and removed from the old.

After the cycle is completed, a list of variables for the function is formed.

Based on this list, the constituent parts (Math.sin (a), 1 / Math.tan (p2)) of the format – "['Math.sin ()', 'Math.cos ()', 'Math.tan ( ) ',' (1 / Math.tan ()) ',' () '] ".The ComponentsCount function (the number of elements minus 1) starts the loop through the array with the generated variables. In the loop at each step, a random number componentIndex from 0 to componentsCount is formed. The element with the corresponding value of the componentIndex index is converted by replacing the symbol "with a variable from the list and added to the new array.

As a result, a list of component parts with variables is formed. Next, rows are formed based on a random number from 1 to 3. In the cycle, the components, separated by signs of mathematical expressions, merge randomly.

After receiving the strings, they are joined separated by mathematical expressions.

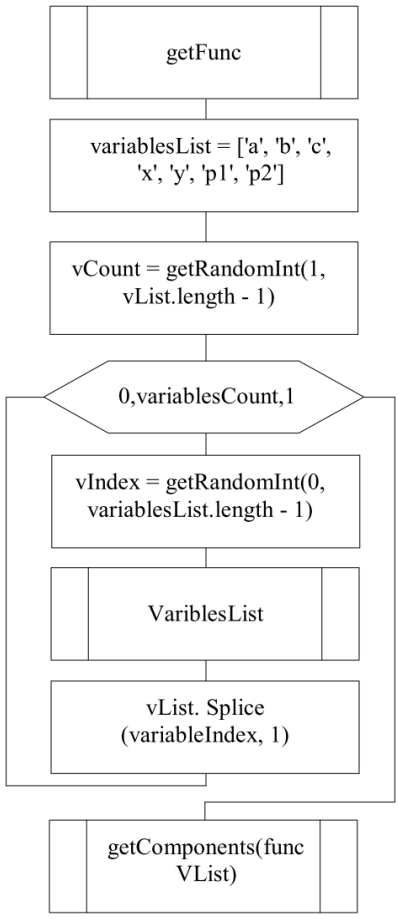

Fig. 1. Function getFunc

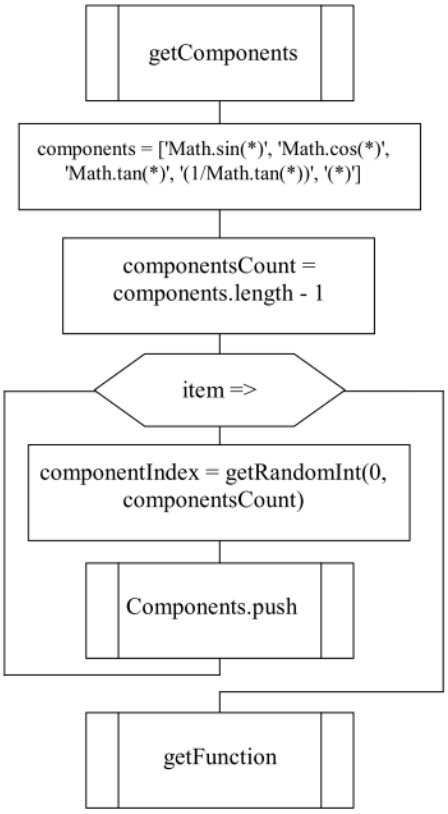

Fig. 2. Function getComponents

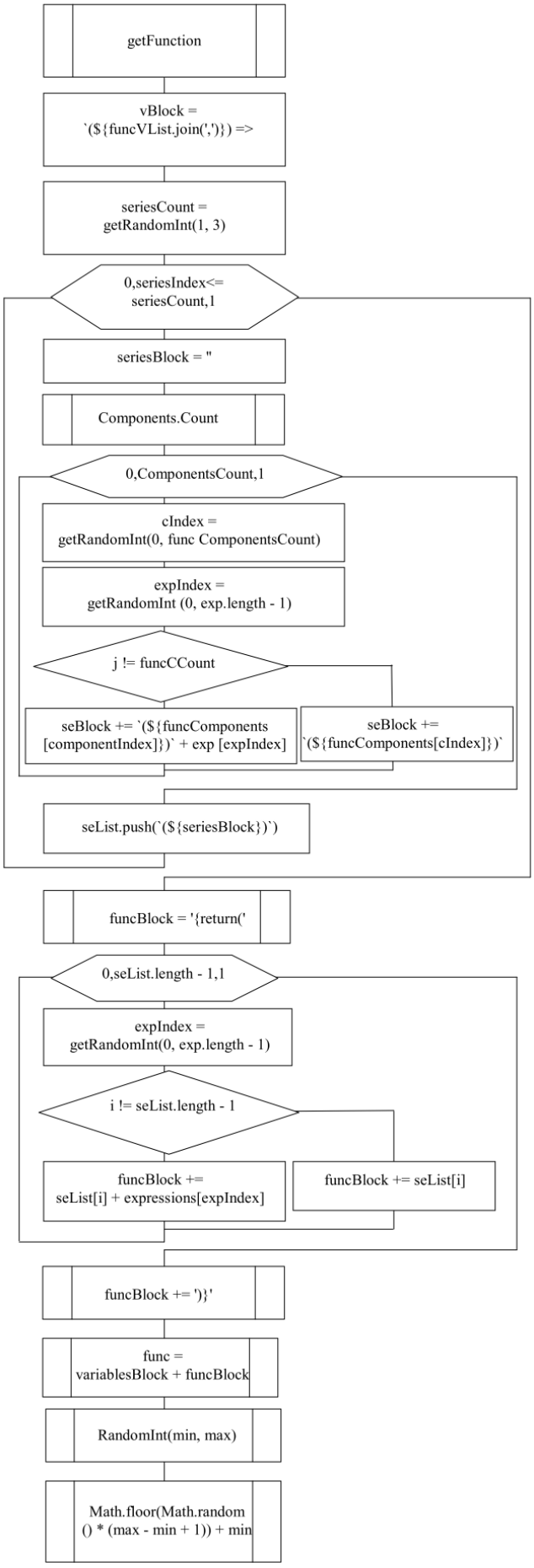

Fig. 3. Function getFunction

Software implementation of the generator has the following form:

```
module.exports.getFunc = function()
{ // function generator
funcVariblesList = []
  let variablesList = ['a', 'b', 'c', 'x', 'y', 'p1', 'p2']
letvariablesCount = getRandomInt(1, variablesList.length - 1)
for (let i = 0; i <= variablesCount; i++)
{
letvariableIndex = getRandomInt(0, variablesList.length - 1)
funcVariblesList.push(variablesList[variableIndex])
variablesList.splice(variableIndex, 1)
  }
returngetComponents(funcVariblesList)
}
functiongetComponents(variablesList)
{
funcComponents = []
let components = ['Math.sin(*)', 'Math.cos(*)', 'Math.tan(*)',
'(1/Math.tan(*))', '(*)']
letcomponentsCount = components.length - 1
variablesList.forEach(item =>
{
letcomponentIndex = getRandomInt(0, componentsCount)
funcComponents.push(components[componentIndex].replace('*',
item))
  })
returngetFunction()
}
functiongetFunction()
{
// forming a block of variables
letvariablesBlock = `(${funcVariblesList.join(',')}) => `
// forming a body function
letseriesCount = getRandomInt(1, 3)
letseriesList = []
for (let seriesIndex = 0; seriesIndex<= seriesCount; seriesIn-
dex++) { // there will be 2 rows
letseriesBlock = ''
letfuncComponentsCount = funcComponents.length - 1
for (let j = 0; j <= funcComponentsCount; j++)
{
letcomponentIndex = getRandomInt(0, funcComponentsCount)
letexpressionIndex = getRandomInt(0, expressions.length - 1)
if (j != funcComponentsCount)
{
seriesBlock += `(${funcComponents[componentIndex]})` + ex-
pressions[expressionIndex]
     } else
{
seriesBlock += `(${funcComponents[componentIndex]})`
     }
   }
seriesList.push(`(${seriesBlock})`)
  }
letfuncBlock = '{return('
for (let i = 0; i<= seriesList.length - 1; i++)
{
letexpressionIndex = getRandomInt(0, expressions.length - 1)
if (i != seriesList.length - 1)
{
funcBlock += seriesList[i] + expressions[expressionIndex]
   } else {
funcBlock += seriesList[i]
   }
  }
funcBlock += ')}'
  // string of results
returnfunc = variablesBlock + funcBlock
}
```

```
FunctiongetRandomInt(min, max) { // function to get a random number for a given range
returnMath.floor(Math.random() * (max - min + 1)) + min;
}
```

As a result, we obtain a generated string function, which we use to calculate a one-time two-factor authentication password.

4. Conclusion

The use of generators to work in the formation of a one-time password, allows you to enhance the level of protection of the described system. Entropy is traditionally a measure of the strength of passwords - a measure of uncertainty, usually measured in bits. One bit entropy corresponds to the uncertainty of the choice of two passwords, two bits of 4 passwords, etc. The strength of a password should be considered only in the context of a specific password authentication system. This is due to the fact that different systems in varying degrees implement (or do not implement at all) the mechanisms for counteracting attacks aimed at breaking passwords, and also because some systems contain errors or use unreliable algorithms.

References

[1] Alata E., Nicomette V., Kaaniche M., Dacier M., Herrb M.: Lessons learned from the deployment of a high-interaction honeypot. Proc. Dependable Computing Conference (EDCC06), Coimbra, Portugal, October 18-20, 2006, 39–46.

[2] Ayankoya F., Ohwo B.: Brute-Force Attack Prevention in Cloud Computing Using One-Time Password and Cryptographic Hash Function. International Journal of Computer Science and Information Security (IJCSIS) 17(2)/2019, 7–19.

[3] Bahaa Q.M.: Preventing brute force attack through the analyzing log. Iraqi Journal of Science 55(3)/2013, 663–667.

[4] https://www.nist.gov (available 02.09.2018).

[5] https://www.seagate.com/files/www-content/solutions-content/security-and-encryption/id/docs/faq-fips-sed-lr-mb-605-2-1302-ru.pdf (available 12.10.2018).

[6] Lamar A.: Types of threats to database security (http://www.brighthub.com/computing/smbsecurity/articles/61402.aspx), 2012, (available 18.03.2019).

[7] Nyssanbayeva S., Ussatova O.: Two-factor authentication in the automated control system. International scientific conference Information Science and Applied Mathematics. Almaty, 2018, Vol. II, 239–242.

M.Sc. Olga Ussatova
e-mail: uoa_olga@mail.ru

Al-Farabi Kazakh National University, Institute of Information and Computational Technologies Ph.D. student in the specialty: «Information Security Systems». In 2003 graduated of the KazNTU – specialty 3704 – "Software computer technology and automated systems". In 2014 graduated of the Turan University – master's degree of "Computing system and Software". Research interests research theme - database protection using two-factor authentication.

ORCID ID: 0000-0002-5276-6118

Prof. Saule Nyssanbayeva
e-mail: sultasha1@mail.ru

Institute of Information and Computational Technologies, Information Security Laboratory. A specialist in the field of information security. The goals and objectives of the research are development and analysis of methods, algorithms and means of cryptographic protection of information based on modular arithmetic during its transmission and storage in info communication systems and networks.

ORCID ID: 0000-0002-5835-4958

otrzymano/received: 15.05.2019 *przyjęto do druku/accepted: 15.06.2019*

DOI: 10.5604/01.3001.0013.2551

MATHEMATICAL MODELING OF THE PROCESS OF DRAWING AN OPTICAL FIBER USING THE LANGEVIN EQUATION

Aliya Tergeussizova
Al-Farabi Kazakh National University, Faculty of Information technology/Department Artificial intelligence and Big Date

Abstract*. In order to design stochastic pulse frequency systems for automatic control of objects with delay, this article shows how we obtained their models in the form of stochastic differential equations. The method of dynamic compensation of objects with delay is considered. A stochastic differential system in the Langevin form is obtained.*

Keywords: transport delay, object with delay, dynamic compensation method, Langevin differential equations

MODELOWANIE MATEMATYCZNE PROCESU WYCIĄGANIA ŚWIATŁOWODU WYKORZYSTUJĄCE RÓWNANIE LANGEVINA

Streszczenie*. W celu zaprojektowania stochastycznych systemów impulsowych przeznaczonych do automatycznego sterowania obiektami z opóźnieniem pokazano, jak uzyskano te modele w postaci stochastycznych równań różniczkowych. Rozważano metodę dynamicznej kompensacji obiektów z opóźnieniem. Uzyskano stochastyczny układ różnicowy w postaci Langevina.*

Słowa kluczowe: opóźnienie transportu, opóźnienie obiektu, metoda kompensacji dynamicznej, równania różniczkowe Langevina

Introduction

As it is known, the optical fiber (OF) as a physical medium for the information transfer has a number of significant advantages in comparison with others, namely: a wide bandwidth and low signal attenuation provides the transmission of large amounts of information over long distances without the need for signal regeneration. The optical fiber is insensitive to electromagnetic fields, which prevents the occurrence of induced interference in the information transmission, fiber-optic communication lines have a much smaller volume and mass per unit of transmitted information than any thers.

The technological process of manufacturing the gradient optical fibers consists of two technological stages - the preform (parison) preparation of the parabolic profile from the core's refractive index and the subsequent drawing of the fiber from the preform.

The node in which the optical properties of the fiber are formed is a high-temperature furnace into which a billet is introduced, at the lower end of which a melt drop is formed-the pulling zone (bulb).

The specified optical properties of the fiber, including the attenuation coefficient, are achieved by a particular hood regime. According to the results of measuring the parameters of a specific preform, the individual values of the extract's main regime parameters are determined for the pulling speed - v_T and the pulling tension - F_0, the combination of which provides the optimal shape of the constriction zone at the end of the preform, which determines the given optical characteristics of the finished fiber. The hood tension is the tension force of the fiber F_0, between the constriction zone and with a primary lacquer coating. In the production of optical fibers and in the relevant production documentation, the hood tension is taken to be measured and normalized in grammaxiles (gf), and not in SI units.

The purpose of the projected automation system control is the temperature control of the high temperature furnace (HTF) – T_{HTF}, which determines the hood tension at a known speed, and the drives control of the preform and traction wheel feeding device, which determines the preform feed rate - v_n and the hood speed - v_T. In this case, the control algorithm of the drawing process must provide a given combination of tension and hood speed with the existing disturbing influences [10–16].

1. Research model

The construction of an automatic control system for the tension hood and fiber diameter, in its turn, requires the construction of adequate models of the controlled object. As a control object, a nozzle zone is considered in the work, in which the tension and fiber diameter are formed. Namely, the control action (the temperature of the high temperature furnace – T_{HTF}) enters the input of a nonlinear static inertia-free substructure, the output effect of which is transformed by a linear inertial substructure. Physically, the nonlinear characteristic can be explained by the nonlinear dependence of the surface tension of the nozzle zone on its temperature. A linear non-rationality can be explained by the fact that when changing to a different temperature of the furnace, the volume of the hood zone changes smoothly.

Figure 1 shows the block diagram for controlling the fiber hood system, which contains a loop for automatically controlling the fiber diameter and hood tension [9].

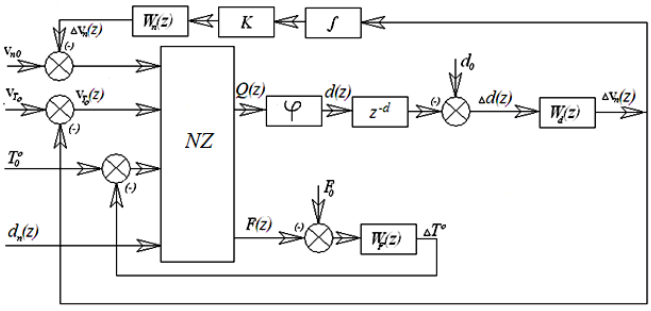

Fig. 1. The block diagram of the fiber process control system

In Figure 1: NZ - nozzle zone; d – the delay is equal to the time of motion from the hooded fiber diameter for the bulb to the sensor; $W_n(z)$ - is the digital regulator of the preform feed rate; $W_F(z)$ - The digital tension control for the hood; $W_d(z)$ - is a digital fiber diameter regulator; K - is the coefficient of proportionality between the fiber sections and the preform; φ - is the static coefficient reflecting the relationship between the fiber diameter and the melt flow coming from the bulb.

Another important task is to increase the dynamic accuracy of regulation. The low dynamic accuracy of regulation is due to the inertia of the regulated object and the so-called "transport delay". The latter is determined by the time of passage of the extracted glassware from the formation zone to the sensor determining the dimensions of the cross section. As a result, self-oscillations may appear.

To solve the problem of temperature control, the most promising activity will be the use of dynamic frequency-pulse systems for automatic control of objects with delay. Control systems of this class are characterized by the presence of nonlinear transformations of signals, as well as parametric feedbacks [4].

In the present work, a frequency-pulse stabilization system (FPSS) is considered for the temperature of a high-temperature extraction furnace for an optical fiber.

FPSS temperature of high-temperature hood furnace for the optical fiber is a closed system consisting of Σ-FPS and the reduced continuous part (RCP), its block diagram is shown in figure 2 [5].

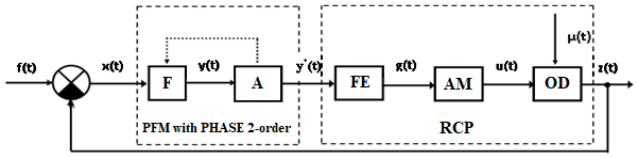

Fig. 2. Structural diagram of Σ- FPSS

At the input of the system, there is a stationary random process f(t). The reduced continuous part - RCP consists of a series connection of the controlled object with delay - OD, an actuating mechanism (AM), and a forming element (FE), which defines the desired shape of the control pulses. In the general case, RCP is characterized as a nonlinear dynamical system with random parameters and is represented by some functional equation of the following form:

$$z(t) = H[\lambda, \tau_0, z(\tau), g(\tau)/t_0 \le \tau \le t] \quad (1)$$

where H is a continuous non-linear functional; the parameter characterizes the randomness of the functional parameters H; g(t) - is a sequence of control random pulses of a given shape; τ_0 - is the delay time of the controlled object.

The motion equation of the Σ - frequency-pulse modulator consists of the motion equation of the filter *F* and the equations determining the moments of appearance and the sign of the pulses, and the operations of resetting.

Σ-FPM of the second order is a serial connection of a filter realized as a 2-order aperiodic link and an impulse device of the ID.

A filter realized as an aperiodic link of the first order is described by the following transfer function:

$$D(p) = \frac{k_\phi}{p+\alpha_\phi} \quad (2)$$

where k_ϕ is the gain coefficient of the aperiodic link of 1-order, and α_ϕ-is the time of inertia.

In this paper, as a control object, the waist zone is considered, in which both tension and fiber diameter are formed. Experimental studies of the extraction process in various modes allow us to determine that the object has a second-order degree, the static transfer coefficient has nonlinearity, and the object also has a transport time delay due to the distance from the waist area to the diameter sensor. The continuous transfer function of the waist zone depends on the temperature of the waist zone and the temperature in the high-temperature furnace. These findings allow us to describe mathematically the dependence of fiber diameter on temperature in a high-temperature furnace in the form of a continuous transfer function of the form [11]:

$$W_L(p) = \frac{T_L(p)}{T_{HTF}(p)} = \frac{e^{-p\tau_L}}{(1+T_1 p)(1+T_2 p)} \quad (3)$$

where, T_1 – is the time constant determined by the hydrodynamic properties of the waist zone; T_2 – is the time constant, which determines the heating time of the waist area; τ_L – lag time, determined by the length of the waist area, T_L – the temperature of the waist area.

$$W_L(p) = \frac{T_L(p)}{T_{HTF}(p)} = \frac{e^{-p\tau_L}}{(1+T_1 p)(1+T_2 p)} = \frac{e^{-p\tau_L}}{T_1 T_2 p^2+(T_1+T_2)p+1} = \frac{e^{-p\tau_L}}{T_1 T_2 (p^2 + \frac{T_1+T_2}{T_1 T_2} p + \frac{1}{T_1 T_2})}$$

$$K_1 = \frac{1}{T_1 T_2}, L_1 = \frac{1}{T_1 T_2}, L_2 = \frac{T_1+T_2}{T_1 T_2}$$

The main channels for controlling the parameters of the temperature mode of an optical fiber drawing process, taking into account the transfer functions of the actuator - AM and the form-building element - FE with an acceptable accuracy, the transfer function (1) is represented by a transfer function of the form [1]:

$$W_L(p) = \frac{K_1 e^{-p\tau_L}}{p^2+L_2 p+L_1}$$

$$W_L(p) = \frac{x_2}{u} = \frac{K_1 e^{-p\tau_L}}{p^2+L_2 p+L_1} \quad (4)$$

As a control algorithm in this system, the Σ-FPM algorithm is used, the filter in this algorithm is the main control element defining the control pulse.

2. Construction of the mathematical model

In order to design stochastic pulse frequency systems for automatic control of objects with delay, one should first of all get their models in the form of stochastic differential equations. Equivalent and majorization systems can be used for this purpose. Describing them directly, one can obtain stochastic differential equations in the form of Langevin. Then they should be converted to Ito form. Consider the construction of mathematical models of the subsystem of direct digital control (DDC) control parameters of the temperature process of drawing optical fiber. According to Figure 3, this system is described by the following equations [6]:

$$x(t) = x_2(t) - z(t) \quad (5)$$

$$x_2^{(2)} + L_2 x_2^{(1)} + L_1 x_2 = u K_1 e^{-p\tau_L} \quad (6)$$

$$z(t)=\vec{q}_0^T \vec{z}(t-\tau_L) \quad (7)$$

$$y_v(t) + [\alpha_\phi + s(t)] y_v(t) = k_\phi x(t-\tau_m) \quad (8)$$

$$u(t)=\varphi[\frac{y_v(t)}{\Delta}] \quad (9)$$

where, k_ϕ – is the filter gain factor ∑-FPM, Δ – is the threshold value of the pulse device of the PD; τm – is the modulator modification parameter.

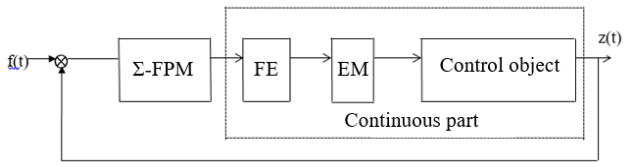

Fig. 3. Block diagram of the control circuit control parameters of the temperature regime of the process of drawing optical fiber

The continuous part of the system containing the control object with delay is described by differential – difference equations of the form [8]:

$$\dot{\vec{z}}(t) = \overrightarrow{A_0}\vec{z}(t) + \overrightarrow{C_0}u(t) \quad (10)$$

$$z(t) = \overrightarrow{B_0^T}\vec{z}(t-\tau_0) \quad (11)$$

where, $0 < \tau_0 < \infty$ the lag time of the control object, $\overrightarrow{A_0}, \overrightarrow{B_0^T}$ *and* $\overrightarrow{C_0}$ are respectively real constants of n×n, n×1, m×n matrices.

$$\begin{bmatrix}\dot{x}_1\\ \dot{x}_2\end{bmatrix} = [A]\begin{bmatrix}\dot{x}_1\\ \dot{x}_2\end{bmatrix} + [B]u, \begin{cases} x = Ax + Bu \\ y = Cx \end{cases}$$

To reduce the differential order, we make the assumption that:

$$\dot{x}_1 = x_2 \rightarrow \ddot{x}_1 = \dot{x}_2$$

$$\begin{bmatrix}\ddot{x}_1\\ \dot{x}_2\end{bmatrix} = \begin{bmatrix}0 & 1\\ -L_1 & -L_2\end{bmatrix}, \begin{bmatrix}\dot{x}_1\\ \dot{x}_2\end{bmatrix} + \begin{bmatrix}0\\ K_1\end{bmatrix} u$$

We get:

$$\overrightarrow{A_0} = \begin{bmatrix}0 & 1\\ -L_1 & -L_2\end{bmatrix}, \overrightarrow{B_0}\begin{bmatrix}0\\ K_1\end{bmatrix}, \overrightarrow{C_0} = [1 \quad 0]$$

respectively, matrices of dimensions (2 × 2), (2 × 1) and (1 × 2).

2.1. Dynamic compensation method of delays in an object

The drawing tower of an optical fiber, or rather, the waist area, is an object having a time delay in the measurement channels, which functions according to (10) and (11). The principle of one of the approaches to the design of regulators for such objects is to apply the method of dynamic compensation of delays in the object [7].

Since in our object only the signals in the measurement channels are late, i.e. T=0, then the equation of the dynamics of the object will take the form:

$$H: \dot{x}(t) = Ax(t) + B_0u(t) + f(t) \quad (12)$$

$$y(t) \sum_{L=0}^{i} C_L x(t-\tau_L) + \eta(t) \quad (13)$$

Along with our object, we consider a device whose input is given by a signal u(t), which is the input control for object H, and which functions according to the equations:

$$K: \dot{\mu}(t) = A\mu(t) + B_0u(t) \quad (14)$$

$$\delta y(t) = R\mu(t) - \sum_{L=0}^{i} C_L x(t-\tau_L) \quad (15)$$

where $t \epsilon R$, $\mu \epsilon R^n$ – is the phase vector of the device, $\delta y(t) \epsilon R^m$ – is its output. The constant real matrix R is determined by the equality:

$$R = \sum_{L=0}^{i} C_L \exp(-A\tau_L)$$

Next, we consider the composite system H*K with the control input u(t) and the output $y_k(t)$ formed according to the parallel connection of the device K to the object H.

$$y_k(t) = y(t) + \delta y(t) \quad (16)$$

The following argue that the correction device K allows you to compensate for the delay in the object H.

The behavior of the composite system H*K, functioning according to equations (11) and (15), obeys the equations:

$$H_k: \dot{x}(t) = Ax(t) + B_0u(t) + f(t) \quad (17)$$

$$y_k(t) = Rx(t) + \eta_k(t) \quad (18)$$

where, $t \epsilon R$, and $\eta_k(t) \epsilon R^m$ depends only on disturbing influences:

$$\eta_k(t) = \eta(t) - \sum_{L=0}^{i} C_L \int_0^L \exp\big(A(\theta - \tau_L)\big) f(t-\theta) d\theta \quad (19)$$

Proof: Subtracting (13) from (16), you can get:

$$d(x(t) - \frac{\mu(t)}{dt} = A\big(x(t) - \mu(t)\big) + f(t)$$

From here, according to the Cauchy formula, we get:

$$x(t) - \mu(t) =$$

$$\exp(A\tau_L)\left(x(t-\tau_L) - \mu(t-\tau_L)\right) + \int_0^L \exp(A\theta) f(t-\theta) d\theta$$

Multiply this equality on the left by $C_L \exp(-A\tau_L)$, setting L = 0,1,…,i and performing summation over this index, we get:

$$\sum_{L=0}^{i} C_L \exp(-A\tau_L)\, x(t) - \sum_{L=0}^{i} C_L \exp(-A\tau_L)\, \mu(t) =$$

$$\sum_{L=0}^{i} C_L x(t-\tau_L) - \sum_{L=0}^{i} C_L \mu(t-\tau_L) +$$

$$\sum_{L=0}^{i} C_L \int_0^L \exp\big(A(\theta - \tau_L)\big) f(t-\theta) d\theta$$

From this equality, taking into account (19) and relations (15), (16) and (13), it is easy to obtain (18).

Thus, the corrective device K is a dynamic compensator for delays in the object N, figure 4.

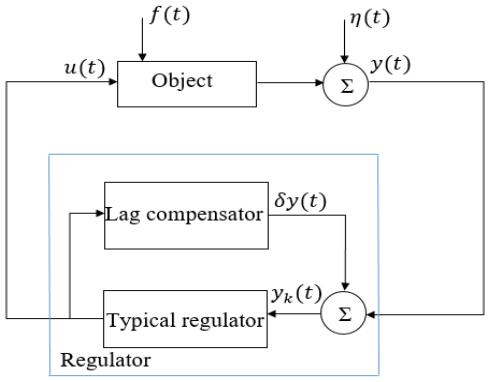

Fig. 4. Block diagram of the regulation system realizes the principle of dynamic compensation for delays

The system H_k, functioning according to equations (17) and (18), which, in essence, is a completely manageable and identifiable part of the component system H*K, will be called a compensated object. Since the compensated object is a finite-dimensional dynamic system, its state can be regulated by means of a typical regulator.

So, if we first compensate for delays in the object, and then adjust the state of our compensated object with a typical regulator, the latter will ultimately regulate the state in the control object N. The block diagram of the regulation system that implements this principle is presented in Figure 2, and the controlled movement of the control object itself will be described by the functional diagram presented in Figure 5 .

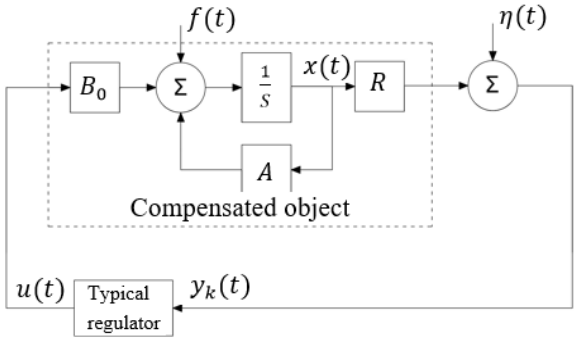

Fig. 5. Type of adjustable movement

According to, considered, method of dynamic compensation of delays, our object with delay, functioning according to (10) and (11) can be represented as follows [6]:

$$\vec{z}(t) = \overrightarrow{A_0}\,\vec{z}\,(t) + \overrightarrow{C_0}u(t) \quad (20)$$

$$z(t) = \overrightarrow{B_1^T}\,\vec{z}(t) \quad (21)$$

where, $\overrightarrow{B_1^T} = \overrightarrow{B_0^T} \exp(-\overrightarrow{A_0}\,\tau_L)$ – the fundamental matrix of the system with the value t = $-\tau_L$.

2.2. Differential equations of Langevin

Combining the RCP (educed continuous part) equation (12) and the modified Σ-FPM (8) – (9), we obtain the stochastic differential system in the Langevin form [14 - 16]:

$$\vec{z}(t) = \overrightarrow{A_0}\,\vec{z}(t) + \overrightarrow{C_0}u(t) + \vec{D}_0[\vec{z}]\vec{\mu}(t) \quad (22)$$

$$z(t) = \vec{L}_1^T\vec{z}(t), u(t) = \varphi\left[\frac{y_v(t)}{\Delta}\right] \quad (23)$$

$$y_v(t) = \alpha_\phi y_v(t) - k_\phi \vec{q}_0^T\tau_0\vec{z}(t) + N_0[y_v(t)]s(t) \quad (24)$$

where

$$\vec{z}(t) = [z_1 z_2]^T \quad \vec{\mu}(t) = [\mu_1 \mu_2]^T$$

$$\overrightarrow{D_0}[\vec{z}] = \begin{bmatrix} 0 & 0 \\ -z_1 & -z_2 \end{bmatrix}$$

$$N_0[y_v(t)] = -y_v$$

$$\vec{q}_0^T\tau_0 = \vec{q}_0^T\{\exp(-\overrightarrow{A_0}\vec{\tau}_0) - [\exp(-\overrightarrow{A_0}\vec{\tau}_m) - \vec{I}]\}$$

$\vec{I}$ – dimension unit matrix $(2 * 2)$.

3. Conclusion

An approach to the construction of mathematical stochastic sigma frequency – pulse systems of automatic control of objects with delay is proposed. For the mathematical model of the sigma frequency – pulse control system for objects with delay in the form of stochastic differential equations, a procedure for their construction, based on the equivalent and majorising systems, is proposed. We obtain stochastic differential equations in the Langevin form.

References

[1] Aitchanov B.H., Aitchanova Sh.K., Baimuratov O.A., Aldibekova A.N.: A Simplified Model of the Control System with PFM. XII International Conference on Information Technology and Engineerin. 17(5)/2015, 1465–1468.

[2] Aitchanov B.H., Aldibekova A.N.: Primenenie dinamicheskogo chastotnoimpulsnogo modulyatora v sistemah upravleniya s ispolzovaniem yadernogo magnitnogo rezonansa v ustroystvah omagnichivaniya zhidkostey. Vestnik KazNTU.

[3] Aitchanov B.H., Baimuratov O.A., Aldibekova A.N.: Pulse – Frequency control system of the fluids magnetization of the used nulear magnetic resonance. The 2nd International Virtual Conference on Advanced Scientific Results (SCIECONF – 2014), 473–477.

[4] Aitchanov B.H., Tergeusizova A.S.: Tehnologicheskij process vytjazhki opticheskih sterzhnej kak objekt avtomatizirovannogo upravlenija. Doklady Nacional'noj akademii nauk Respubliki Kazahstan 2/2017, 91–95.

[5] Aitchanov B.H.: Metody matematicheskogo opisanija chastotno-impulsnyh sistem upravlenija obektami s zapazdyvaniem. Vestnik KazNTU 2(30)/2002, 72–82.

[6] Aitchanov B.H.: Time-domain quantization in dynamic pulse-frequency systems with transport delay. Poisk, Natural and technical sciences series, 209–214.

[7] Aitzhanov B.Kh., Kurmanov B.K., Umarov T.F.: Dynamic Pulse Frequency Modulation in Objects Control with Delay. Asian Journal of Control 14(6)/2012, 1662–1668.

[8] Aitzhanov B.Kh., Nikulin V.V., Baimuratov O.A.: Mathematical Modeling of Digital Pulse-Frequency Modulation Control Systems Developed for Objects with Transport Delay. The Chinese Control and Decision Conference 2013, 1407–1411.

[9] Chostkovskij D.B.: Strukturnyj sintez sistemy upravlenija processom vytjazhki gradientnyh opticheskih volokon. Vestnik SamGTU. Serija Tehnicheskie nauki 4(27)/2010, 73–78.

[10] Friman R.: Volokonno-opticheskie sistemy svjazi. Tehnosfera, Moscow 2003.

[11] http://oplib.ru – Open Library – Open library of educational information (available 15.05.2019).

[12] Listvin A.V., Listvin V.N., Shvyrkov D.V.: Opticheskie volokna dla liniy sviazi. LESARart, Moscow 2003.

[13] Roy P., et al.: Active Optical Fibers: New design and alternative method of fabrication. Photonics, Dehli 2008.

[14] Sandoz F., et al.: A Novel process to manufacture high efficiency laser fibers. Photonics, Dehli 2008.

[15] Sarkar A., Orchanian B., Chan A.: A Novel VAD process. Proceedings of the International Wire & Cable Symposium, Providence 2008.

[16] Zhiro A.: Tehnologii proizvodstva opticheskih volokon. Obzor poslednih razrabotok. Nauka i tehnika 4/2009, 22–27.

M.Sc. Eng. Aliya Tergeussizova
e-mail: aliya55@mail.ru

Ph.D. student of the Faculty of Information Technology of the Al-Farabi Kazakh National University. Scientific research in the field of model development and research of the temperature control system for drawing optical fiber.

ORCID ID: 0000-0002-5084-8937

otrzymano/received: 15.05.2019 *przyjęto do druku/accepted: 15.06.2019*

DOI: 10.5604/01.3001.0013.2552

MODERN MANAGEMENT OF NATIONAL COMPETITIVENESS

Nataliia Savina[1], Olha Romanko[2], Sergii Pavlov[3], Volodymyr Lytvynenko[4]
[1]National University of Water and Environmental Engineering, [2]Ivano-Frankivsk National Technical University of Oil and Gas, [3]Vinnytsia National Technical University, [4]Kherson National Technical University

Abstract. *This article offers a modern approach to the policy of competitiveness of the national economy at the regional level. Based on the results and experience of domestic and foreign economists the author offers a system of indicators of regional activity and a method for determination of the integrated index of the competitiveness level in the region. This way of calculation makes it possible to carry out the analysis of the regional economic activity dynamics at the tactical (1 year) and strategic (5 years) levels. Three main policies to increase the competitiveness of the region have been proposed: refocus, dualistic, directive. The essence of major policies to increase the competitiveness of the region, its directions and objectives for the national economy have been characterized. The proposals concerning the application of the basic policies of the competitiveness of the region to the appropriate region of Ukraine on the relevant level of its competitiveness have been given.*

Keywords: territorial competitiveness, region, management, national economy, policy, decision making.

NOWOCZESNE ZARZĄDZANIE KONKURENCYJNOŚCIĄ KRAJU

Streszczenie. *Niniejszy artykuł przedstawia nowoczesne podejście do polityki konkurencyjności gospodarki narodowej na poziomie regionalnym. W oparciu o wyniki i doświadczenia ekonomistów krajowych i zagranicznych autorzy proponują system wskaźników aktywności regionalnej oraz metodę wyznaczania zintegrowanego wskaźnika poziomu konkurencyjności w regionie. Ten sposób obliczania umożliwia przeprowadzenie analizy dynamiki regionalnej aktywności gospodarczej na poziomie taktycznym (1 rok) i strategicznym (5 lat). Zaproponowano trzy główne polityki mające na celu zwiększenie konkurencyjności regionu: reorientacja, dualistyczna, dyrektywa. Scharakteryzowano istotę głównych polityk zwiększania konkurencyjności regionu, jego kierunki i cele dla gospodarki narodowej. Przedstawiono propozycje dotyczące zastosowania podstawowych polityk konkurencyjności regionu do odpowiedniego regionu Ukrainy na odpowiednim poziomie jego konkurencyjności.*

Słowa kluczowe: konkurencyjność terytorialna, region, zarządzanie, gospodarka narodowa, polityka, podejmowanie decyzji

Introduction

In order to achieve the efficiency of the competitiveness policy, there are more advantages in forming strategies at the regional rather than at the national level, as the region takes into account all the advantages and prospects for development, and the State carries it out superficially. The development of approaches to the strategy of efficient management of the region's competitiveness is faced with the greatest difficulty i.e. the choice of the policy implementation of a given regional sphere and filling it with mechanisms and technologies to achieve appropriate goals. The following choice of the appropriate policy for the region's competitiveness increase is recommended to be performed based on scientific developments and proposals that are scientifically and economically grounded.

For management decisions with increasing regional competitiveness, primarily, the qualitative assessment of the region's competitiveness is conducted. It is designed to not only provide a tangible result of the evaluation but also to provide an assessment of the main component elements of the region's competitiveness due to the well-selected scoring system.

1. Review of the literature

In order to achieve the efficiency of the competitiveness policy, there are more advantages in forming strategies at the regional rather than at the national level, as the region takes into account all the advantages and prospects for development, and the State carries it out superficially. The development of approaches to the strategy of efficient management of the region's competitiveness is faced with the greatest difficulty i.e. the choice of the policy implementation of a given regional sphere and filling it with mechanisms and technologies to achieve appropriate goals. The following choice of the appropriate policy for the region's competitiveness increase is recommended to be performed based on scientific developments and proposals that are scientifically and economically grounded.

For management decisions with increasing regional competitiveness, primarily, the qualitative assessment of the region's competitiveness is conducted. It is designed to not only provide a tangible result of the evaluation but also to provide an assessment of the main component elements of the region's competitiveness due to the well-selected scoring system.

Some authors prefer the formation system of various parameters that make up the integral index of the competitiveness of the region. The author of the research [20] believes that the most objective integrated indicator that combines the competitiveness of goods, producers, and industries is the indicator of regional competitiveness, which allows you to characterize the situation in the region in the national market, and in the country - in the world. In his research, he uses expert assessment, which is subjective. There is also a controversial issue to the grouping of indicators, such as the investment attractiveness of the region, which in our opinion should be attributed to the first group of parameters that characterize the presence and effectiveness of the use of resources.

Researchers in [13] argue that the competitiveness of the region is determined by the competitiveness of goods and organizations. As far as the region is the subsystem of the system of the higher level i.e. of the country, its competitiveness and efficiency of the operation will depend on the quality and intensity of impact on it by the system (i.e. the country). For the evaluation of the competitiveness of the region, the scientist offers the following formula.

In our opinion, the basic drawbacks in this approach are the attraction to identifying different levels of competitiveness (of the region or enterprise) and a significant exaggeration of their influence on each other.

There are quite a lot of approaches to the evaluation of the region's competitiveness and its specific indicators in the literary sources, but there is no consideration of indicators that fully characterize the region's business activity and its innovation and investment activity. Such activity is today one of the most necessary for regional development.

The purpose of the article is to develop proposals to enhance the region's competitiveness policy and their practical application by subjects of the hierarchy of regional management and to assess the level of regional competitiveness.

2. Methodological approaches to assessing the competitiveness of the region

According to the most common definition, offered by economist Boshma R. (2014), the regional competitiveness can be defined as the ability of a particular region to compete with one another both within and outside the territory of the State in the direction of the economic growth and prosperity. According to the

fact that some regions are more advanced than the others, many scientists have come to the conclusion that regional competitiveness is of a greater significance and is an underestimated economic process. There are enough global factors of influence towards the aggravation of the competitiveness between regions directly and indirectly. The difference in the competitiveness style depends on the achieved economic development [6].

Ukrainian scientists Y. Lazarieva and N. Yablonska (2011) [14] recommend to use a two-level system of indicators to determine the integrated indicator of the region's competitiveness, which includes 30 parameters that embrace the following regional spheres and activities as: the efficiency of investment in infrastructure; efficiency of financial activity; the effectiveness of socio-labor development; the level of political, economic, environmental and other risks. The authors in their research prefer financial indicators of activity in the region, without focusing attention on the industrial, technological and other indicators.

As Kovalska L. (2013) notes, the region's possibilities to compete should be compared with the index of the region's referentiality [12]. The regional competitiveness researcher Jonathan P. (2010) for the basis of the system of indicators uses a thing, that is accessible for all regions on the basis of the definition of the socio-economic level of regional development, as well as the ability of the region to attract foreign capital [17].

The data matrix takes into account the resources of Ukrainian statistics and modifies the existing research methods of regional competitiveness. The indices of regional competitiveness have been selected after singling out the incentives and disincentives. The matrix indicators consist of 23 indicators that are grouped in three blocks: the general economic condition of the region, the region's economic activity and innovation and investment activities in the region. These indicators thoroughly reflect regional business activity. The statistical data for the matrix of indices are taken over a period of 5 years (2014–2018) (Table 1).

*Table 1. Matrix of indicators of regional activity**

No	Block name	Indexes	Direction of influence
1	*Block 1 "General economic condition of the region"*	Gross regional product per person, (UAH)	stimulator
2		The economically active population (thousand people)	stimulator
3		The employed population (thousand people)	stimulator
4		The employed population (thousand people)	disintegrator
5		Number of EDRPOU entities (persons)	stimulator
6		Average monthly wages by region (per employee, UAH)	stimulator
7		Acceptance of the total living space per 1,000 permanent residents by region (m^2)	stimulator
8		Current expenditures on protection and rational use of natural resources (ths. UAH)	disintegrator
9	*Block 2 "Economic activity of the region"*	The volume of sold industrial products (goods, services) per capita (thousand UAH)	stimulator
10		Retail turnover (million UAH)	stimulator
11		Total export of goods (ths. US dollar)	stimulator
12		Total exports of services (ths. US dollar)	stimulator
13		Total volumes of import of services (ths. US dollar)	disintegrator
14		Total volume of import of goods (ths. US dollar)	disintegrator
15	*Block 3 «Innovative – investment activity of the region».*	Number of organizations performing scientific and scientific – technical works (units)	stimulator
16		Number of specialists performing scientific and scientific work (persons)	stimulator
17		Number of innovative enterprises in the industry (units)	stimulator
18		The volume of innovative products (ths. UAH)	stimulator
19		Implementation of innovative technological processes in the industry, (units of processes)	stimulator
20		Implementation of innovative types of products in industry (units of titles)	stimulator
21		Capital investment per capita (UAH)	stimulator
22		Foreign direct investment per capita by regions of Ukraine (USD)	stimulator
23		Distribution of total expenditures (ths. UAH)	disintegrator

* Developed by the author

Uses a grouping method for partial indices. According to the method, the partial indices are "reduced" to the aggregate index. In order to calculate the block aggregate index the formula for defining the geometric mean should be used: the N-th root of the product of the values of partial indices, where n is the number of indices included in the block.

For each region, three aggregate indices have been received for every year. They are to calculate the general aggregate index of the region. As the indices in blocks are heterogeneous, the arithmetic mean formula should be used:

$$I_j = (I_{1j} + I_{2j} + I_{3j})^{1/} \quad (1)$$

where I_{1j} – is the average value for the first block for each j-region; I_{2j} – is the average value for the second block for each j-region; I_{3j} – is the average value for the third block for each j-region.

The results of the calculation of the integral indicator of the competitiveness of the region for each year (tactical level) and for five (strategic level) years as a whole is presented in Table 2. The ranking of regions according to the level of competitiveness is built in the downward direction on the results of the regional competitiveness index at the strategic level.

*Table 2. Integrated Competitiveness Rating regions of Ukraine, 2014-2018**

No	Oblast/Region**	Aggregate competitiveness index I_j for each year					Regional Competitiveness index
		2014	2015	2016	2017	2018	
1	The city of Kyiv	1.2709	1.4001	1.4531	1.4301	1.5484	**1.42052**
2	Kharkiv	0.5293	0.5226	0.4584	0.5472	0.5881	**0.5291**
3	Lviv	0.3515	0.3761	0.3707	0.4598	0.497	**0.4110**
4	Kyiv	0.3499	0.3938	0.3763	0.4446	0.4609	**0.4051**
5	Odesa	0.3428	0.4016	0.3647	0.4446	0.4619	**0.4031**
6	Dnipropetrovsk	0.368	0.4262	0.3499	0.4012	0.4097	**0.3910**
7	Zaporizhzhia	0.3755	0.4065	0.3647	0.3924	0.4147	**0.3907**
8	Donetsk	0.3869	0.4389	0.289	0.2961	0.3411	**0.3504**
9	Ivano-Frankivsk	0.2933	0.2993	0.3081	0.3448	0.3646	**0.3220**
10	Sumy	0.2953	0.2945	0.2782	0.3251	0.3414	**0.3069**
11	Ternopil	0.2523	0.2883	0.2666	0.3444	0.3584	**0.3020**
12	Vinnytsia	0.2563	0.2778	0.2551	0.3411	0.3537	**0.2968**
13	Kherson	0.2729	0.3254	0.2984	0.2801	0.2953	**0.2944**
14	Mykolaiv	0.2707	0.3336	0.2469	0.2939	0.2892	**0.2868**
15	Cherkasy	0.262	0.297	0.2458	0.2944	0.2913	**0.2781**
16	Poltava	0.277	0.305	0.2552	0.2664	0.2716	**0.2750**
17	Zakarpatia	0.2156	0.291	0.2459	0.2978	0.3017	**0.2704**
18	Zhytomyr	0.2398	0.2695	0.2378	0.2996	0.3005	**0.2694**
19	Kirovohrad	0.2327	0.2504	0.291	0.2773	0.2692	**0.2641**
20	Chernivtsi	0.2244	0.2519	0.1994	0.2931	0.2806	**0.2498**
21	Khmelnytskyi	0.2276	0.2405	0.2265	0.2692	0.2816	**0.2490**
22	Volyn	0.2302	0.2468	0.2215	0.2691	0.2566	**0.2448**
23	Chernihiv	0.2085	0.2375	0.2114	0.2649	0.2813	**0.2407**
24	Rivne	0.2048	0.2429	0.2119	0.2601	0.2776	**0.2394**
25	Luhansk	0.3056	0.3141	0.1611	0.1593	0.1891	**0.2258**

*Calculated by the author on the basis of indicators of the State Statistics of Ukraine,
**The annexed Autonomous Republic of Crimea and parts of the occupied Donetsk and Luhansk regions are not taken into account in the study.

3. Principles of the policy of increasing the competitiveness of the region

The policy of the region's competitiveness cannot be common to all the regions of Ukraine. Mikhail K. notes (2017) that it is necessary to choose the most appropriate type of policy, taking into account the different state of the regional economy, directions of the development, economic conditions and competitive advantages [11]. Such compliance, according to Ervin S. (2018) will provide an opportunity to consider the region as a separate entity of the economic national system, and measures that are adaptive to its level of competitiveness will have an effective impact [18].

The basic principle of scientists' offers concerning the choice of policies to increase competitiveness in the region consists of the following: the higher the indicators of the competitiveness of the region, the less effective it is necessary to apply the tools of activation and stimulation and vice versa – the lower the indicators, the greater the impact is needed for the region's economic sphere from entities of regional management. Moreover, certain measures are carried out depending on the previous achievements of the region's competitiveness.

According to the levels of competitiveness, the grouping of the regions and the selection of the type of policy to increase the region's competitiveness is accomplished. The main types

of policy are directed towards increasing the region's competitiveness. Despite a universality of the proposed policy of increasing competitiveness towards a number of regions, we should agree with Allen J. (2007) that the strategy of the management of a specific region is always individual. In the process of adapting it to specific regions, all the factors regarding its functioning relationships should be taken into account, including the potential ones that provide new opportunities for the activities of the regional entities [1].

The basic types of policies to increase competitiveness in the region have been proposed: refocus, dualistic and directive. The refocus policy (originates from the Latin word "refocus" – change of direction) is relevant for regions with a high level of competitiveness at the strategic and tactical level.

The given policy can be grounded on the principles of the region's "smart development", which began to be developed in the 90's by Amnon F. and Idan P. (2017). It is relevant for regions that are faced with the challenges of resource scarcity, high levels of international and interregional competition, new technologies [10]. Its main purpose is the rational use of existing material and immaterial resources and the tandems of modern innovations.

The key is in the re-orientation of the region's economic achievements to other areas. Such a region is able to convert economic results into social, environmental and other benefits of increasing activity in the region. This is both the recommendation and a commitment of the regional managers to transform the economic growth because without it the socio-economic welfare of the people of the region can't be improved. The economic regionalism creates the foundation for the increase of the national competitiveness, and the refocus policy provides the increase of the regional prosperity of the population, which in turn is a source of generating competitive advantages of the region.

Some foreign countries with the proper high level of competitiveness of the regions direct the region's management policy towards the method of inclusive development. It is a complicated policy which is aimed at ensuring employment and high social standards based on the harmonious combination of high rates of economic growth along with the principles of sustainability [5]. For the first time, the concept of "inclusive development" was used in 2007 by the Asian Development Bank. This policy has arisen from the phenomenon of the rapid economic growth of some Asian countries and the emergence of a large number of people living in extreme poverty (on less than 1.25 dollars a day in the United States). Only in the Asia-Pacific region in 2011 their number reached 743 million people [3]. However, the growth rate of the national economy does not give grounds for the use of such experience to the full extent nowadays.

Dualistic policy (originates from the Latin word "dualis" meaning double) of increasing the region's competitiveness is based on two directions, which are aimed at keeping by the region its competitive benefits or at the improvement of the regional competitiveness.

To create sustainable competitive advantages on the tactical and strategic level, the dualistic policy of increasing the region's competitiveness should include an integrated transformation of all presented elements. Two approaches can be applied. The first approach is aimed at the simultaneous changes in all spheres and the incremental (evolutionary) transition to a higher level, and the second one provides an active change of individual segments which, ultimately, affect other areas. The first approach is simpler and does not require a complete change of management measures to improve regional competitiveness, as it is aimed at the gradual adaptation of management entities to control objects. This approach is aimed at keeping by the region its competitive approaches, but it requires a long time. The second approach is more difficult and risky, but it can provide more rapid changes in the development of the region through the development and implementation of innovative measures in the management of regional competitiveness.

The regional management entities recommend generating development skills of certain areas, particularly the regional infrastructure. The variety of types of infrastructure enables the region to show ambitions in projects both in the field of the region's purpose and in time intervals according to the research of Croatian academic Nevenky (2013). Almost all the infrastructure projects that have a high degree of importance for regional development are on the verge of altruism and are implemented through government intervention [8]. It is ineffective and quite slow in obtaining a competitive advantage. A high level of the region's competitiveness means that such a region can effectively use both its own and borrowed resources for its own regional objectives, and is able to cooperate and perform functions both at the State and regional level. That is, a region that counts on its own efforts in the development of its own infrastructure obtains competitive advantages in the long-term perspectives. A region which carries out the development of its own infrastructure for the future reduces its potential costs which can be redirected as an investment.

An important factor in the dualistic policy is the motivation to increase productivity, expand production and improve the competitiveness of goods and companies. According to economist Eredin A. (2011), the export increase of regional products evaluates the perspective and relevant priority guidelines of the region's development. The economic sector is expected to be modernized, improved, and the management institutional support will be changed towards the intensification of business activity in the region and the quality of management improvement [9].

Directive (originates from the Latin word. "dirigere" meaning to direct, to determine) policy to improve competitiveness is applied to regions that are in deep stagnant economic problems or to regions with enormous ambitious plans and minimal previous results with regional competitiveness. For these regions, the economic activity of the region, its intensification and stimulation become the main strategic goal, but not a means to achieve socio-economic benefits and improve the well-being of the population.

The gross part of measures to improve the regional competitiveness is aimed at activating, motivating and promoting the economic activity, and the region's limitedness in functional capabilities prefers support for small and medium entrepreneurship according to the point of view of Pelegrin G. (2007). The establishment of appropriate information and preproduction infrastructure for the economically active population of the region is the ability of each region, however, for this group of regions' competitiveness is a necessary element of the directive policy [16].

This policy provides for the increase in economic production rates (quantitative and qualitative). For the effectiveness of this policy at the strategic level, there is a need for applying the elements of innovation at the stages of the goods and services development to increase their competitiveness in the domestic market. The region is recommended to intensify its competitive fight for investment in regional development. Gilian B. (2006) stresses that the most effective is the practice of the Asian countries in attracting investments under the project, which will be realized by dozens of regional companies of this sphere [7]. This approach provides an opportunity for the regional management entities to support the priority areas of the economy or industry, and the approach of the fund's redistribution among entrepreneurs testifies the qualifying capacity of the region's managers.

Special attention deserves a regional approach for promoting dynamic and highly profitable types of economic activity, as the source of the increase of the region's business activity. These mostly include service industries including investment, credit, IT, informational and technological ones that do not require long-term costs for the resource provision, however, require a high level of workers' qualification [15].

According to the calculations in Table 2, one can group regions due to the value of the integrated index of competitiveness for the period of 2014-2018 (Table 3). For the range of size limits in the group, the average value of the integrated index of competitiveness with step 0.05 is used.

*Table 3. Grouping of regions of Ukraine in the main policy of increasing competitiveness**

	The refocus policy	RICI	The dualistic policy	RICI	The directive policy	RICI
Region/Oblast	The City of Kyiv	1.4	Lviv	0.410	Sumy	0.306
	Kharkiv	0.5	Kyiv	0.405	Ternopil	0.302
			Odesa	0.403	Vinnytsia	0.296
			Dnipropetrovsk	0.391	Kherson	0.294
			Zaporizhzhia	0.390	Mykolaiv	0.286
			Donetsk	0.350	Cherkasy	0.278
			Ivano-Frankivsk	0.322	Poltava	0.275
					Zakarpattia	0.270
					Zhytomyr	0.269
					Kirovohrad	0.264
					Chernivtsi	0.249
					Khmelnytskyi	0.249
					Volyn	0.244
					Chernihiv	0.240
					Rivne	0.239
					Luhansk	0.225

*Calculated according to the author's methodology based on the indicators of the State Statistics Committee of Ukraine

Seven regions belong to the group of application of the dualistic policy for improving the regional competitiveness. This group of regions is in the opposite position to the direction of the dynamics of the region's competitiveness. The policy effectiveness, in this case, is displayed in increasing the regional competitive positions with step-by-step development of innovation and investment activities of socio-economic development of the region.

Reflex policy in Ukraine can be used for two regions that have to become the most advanced regions of the State in building regional competitiveness at the strategic level of national significance. They are able to implement measures that are required by this policy and able to test and modernize them for national consumption.

4. Conclusions

Based on the conducted theoretical researches we believe that the policy of increasing the competitiveness of the region should be carried out, taking into account its innovation and investment activity. Under the condition of decentralization, the regions get the powers to carry out measures for such policies and are responsible for conducting the regional development in today's tandem of the world economic development. In this case, one can choose an efficient policy of increasing the region's competitiveness and would achieve the innovation and investment activity of Ukraine's regions.

References

[1] Allen J., Cochrane A.: Beyond the territorial fix: Regional assemblages, politics and power. Regional Studies, 41(9)/2007, 1161–1175 [DOI: 10.1080/00343400701543348].
[2] Artemenko V.: Indykatory stijkogho socialjno-ekonomichnogho rozvytku reghioniv. Reghionaljna ekonomika 2/2006, 90–97.
[3] Aziatsko -Tikhookeanskoy forum (2014) Summary of the outcome of the Asia-Pacific Forum on Sustainable Development for the Asian and Pacific Region, Bangkok, http://www.unescap.org/sites/default/ files/E70_33R.pdf (available 15.05.2019).
[4] Begg I.: Cities and competitiveness. Urban Studies 36/2010, 795–809.
[5] Biryukov A.V.: Inklyuzivnoe razvitie v kontekste globalnykh revolyutsiy. Ekonomicheskie strategii 12/2011, 81.
[6] Boschma R.A.: The Competitiveness of Regions from an Evolutionary Perspective. Regional Studies 38(9)/2014, 1001–1014.
[7] Bristow G.: Everyone's a 'winner': problematising the discourse of regional competitiveness, Journal of Economic Geography 5(3)/2006, 285–304.
[8] Chuchkovych N., Jurlin K., Vuchkovych V.: Measuring regional competitiveness: the case of Croatia. Southeast European and Black Sea Studies 13(4)/2013, 503–523.
[9] Eraydın A.: Regional policies at the crossroads: The new strategies in the long challenge for cohesion. Paper presented at the Regional Science/Regional Planning Conference, Ankara 2011.
[10] Frenkel A., Porat I.: An integrative spatial capital-based model for strategic local planning – An Israeli case. Planning Practice and Research 32(2)/2017, 171–196.
[11] Keating M.: Contesting European regions. Regional Studies 51(1)/2017, 9–18.
[12] Kovalska L. L.: Methodical approaches to analysis and estimation of region's competitiveness. Actual Problems of Economics, 141(3)/2013, 109–124.
[13] Kuzjmin O. Je., Ghorbalj N. I.: Upravlinnja mizhnarodnoju konkurentospromozhnistju pidpryjemstva. Kompakt-LV, Lviv 2005.
[14] Lazarjeva Je. V, Jablonsjka N. V.: Metodychnyj pidkhid do ocinky konkurentospromozhnosti reghionu. Reghionaljna ekonomika 1/2011, 23–31.
[15] Martin R.L.: A study on the factors of regional competitiveness. A draft final report for the European Commission Directorate-General Regional Policy. ECORYS-NEI, Rotterdam 2003.
[16] Pellegrin J.: Regional innovation strategies in the eu or a regionalized eu innovation strategy?. Innovation: The European Journal of Social Science Research 20(3)/2007, 203–221.
[17] Potter J.: Evaluating Regional Competitiveness Policies: Insights from the New Economic Geography. Regional Studies 43(9)/2010, 1225–1236.
[18] Sezgin E.: New regionalism in Turkey: questioning the 'new' and the 'regional'. European Planning Studies 26(4)/2017, 653–669.
[19] Shekhovceva L.S.: Ekonomycheskye problemy reghyonov y otraslevykh kompleksov. Problemy sovremennoj ekonomyky 3(23)/2007, 102–135.
[20] Zhurba I.Je.: Konkurentospromozhnistj reghionu: sutj, metody ocinky, suchasnyj stan. Ekonomika pidpryjemstva 3/2015, 45–49.

Prof. Nataliia Savina
e-mail: n.b.savina@nuwm.edu.ua

Conduct scientific, technical and innovative activities of the university, including the implementation of research results. Promotes the development of scientific relations with other universities, scientific institutions, centers and other enterprises, institutions and organizations. Organizes scientific relations with International centers, funds, programs, other foreign institutions.He has awards from the university, city and regional authorities, the Ministry of Education and Science of Ukraine, departmental awards.
Science interests: Opinion and Forecasting of Investment Efficiency in Logistics Projects, Logistic and Economic Systems, and Human Capital.

ORCID ID: 0000-0001-8339-1219

Ph.D. Olha Romanko
e-mail: olgaromanko11@gmail.com

Since 2006, he has been a member of the Department of Economics and Management. Manages the scientific projects of students. Organizes and develops the activities of the Student Club of Managers, as well as co-organizer of international scientific conferences of the Institute of Economics and Management. He is co-author of projects and strategies for the development of joint territorial communities in the context of decentralization management.
Science interests: Formulation, planning and implementation of competitiveness of competitiveness of the region and regional management

ORCID ID: 0000-0003-1587-1370

Prof. Sergii Pavlov
e-mail: psv@vntu.edu.ua

Vice-rector of for Scientific Work of Vinnytsia National Technical University, Doctor of Technical Sciences, Professor.
Science interests: Modeling socio-economic, medical systems, optoelectronics

ORCID ID: 0000-0002-0051-5560

Prof. Volodymyr Lytvynenko
e-mail: immun56@gmail.com

Doctor of Science, Head of the Department of Informatics and Computer Scienc, Professor, Kherson National Technical University.
Science interests: Modeling of complex systems in economics, biology, medicine, machine learning methods, neural networks, Bayesian networks, evolutionary algorithms.

ORCID ID: 0000-0002-1536-5542

otrzymano/received: 15.05.2019 *przyjęto do druku/accepted: 15.06.2019*

DOI: 10.5604/01.3001.0013.2553

APPLICATION OF HYDRAULIC AUTOMATION EQUIPMENT FOR THE EFFICIENCY ENHANCEMENT OF THE OPERATION ELEMENTS OF THE MOBILE MACHINERY

Leonid Polishchuk[1], Leonid Kozlov[1], Yuri Burennikov[1], Vasil Strutinskiy[2], Valerii Kravchuk[1]
[1]Vinnytsia National Technical University, [2]National Technical University of Ukraine "Igor Sikorsky Kyiv Polytechnic institute"

***Abstract**: The application of adaptive drives in working units of various technological and mobile machines is considered. The results of theoretical and experimental research have proved the effectiveness of their use for improving the dynamic characteristics of machines, reducing unproductive power losses during their operation.*

Keywords: hydroautomatics, tools, workstations, mobile machines

ZASTOSOWANIE WYPOSAŻENIA AUTOMATYZACJI HYDRAULICZNEJ W CELU POPRAWY EFEKTYWNOŚCI ELEMENTÓW OPERACYJNYCH MASZYN MOBILNYCH

***Streszczenie.** W pracy rozważane jest zastosowanie napędów adaptacyjnych w jednostkach roboczych różnych maszyn technologicznych i mobilnych. Skuteczność zastosowania tych algorytmów do poprawy charakterystyk dynamicznych maszyn, przy jednoczesnym zmniejszeniu nieproduktywnych strat mocy podczas pracy potwierdziły wyniki badań teoretycznych i eksperymentalnych.*

Słowakluczowe: hydraulika, narzędzia, stacje robocze, maszyny mobilne

Introduction

Greater parts of the mechanisms of various technological designation operate in variable loads mode. In particular, in civil engineering and industry mobile working mechanisms with the manipulators on the base of trucks and wheeled tractors, equipped with various movable working tools are widely used. The operation of the manipulators of the mechanisms with movableworking tools to provide optimal performing of the operation requires the proportion regulation of the working fluid consumption, supplied from the pump to the hydraulic motor which is not available in the mobile mechanisms, manufactured in our country andabroad.

Variable loads in the drive systems of the conveyors occur as a result of the irregularity of the load flows, arrived on the conveyor belts of the mobile mechanisms, for instance, clamp formers, beet harvesting machines, etc. This stipulates the onset of the mechanical oscillations, creating the conditions for the fatigue failure of the belt, parts and units of the mechanism. The solution of these problems requires the application of new drive constructions with the automatic adaptation of their parameters to variable operation modes. It enables to provide the decrease of the dynamic efforts in the elements of the drives construction and executive elements, decrease of the unproductive power losses in the process of their operation.

1. Analysis of the hydraulicautomatic equipment application for the technological machines with variable loading modes

The development of the hydraulic drives of the mobile and technological machines is accompanied by the wide application of the proportional hydraulic equipment andregulated pumps. Stable trend is the transition to the hydraulics drives, sensitive to loading [4, 5]. Application in such hydraulic drives of the equipment and pumps with the electrohydraulic control enables to improve the accuracy of the machines with hydraulic drive operation, decrease the unproductive power losses [21, 24].Usage of the hydraulic equipment with electric hydraulic control enables to apply in the hydraulic systems of the last generation freely programmable controllers and providesemiautomatic and automatic operation of modern machines [2, 8, 11]. The controllers, available in the adaptive hydraulic drives allow to realize the adaptive control of the machine, that enables of improve considerably static, dynamic and energy characteristics of the machines, adapt their operation modes to the constantly changing conditions in the process of the operation [12, 23].

Variable operation modes are also common for the mobile complexes, used in the process of the surface mining of the minerals resources or sugar beet clamping at the sugar mills.

Efficiency factor of the conveyors usage at mining enterprises is, on average, 50…70% by power and 60…70% by the operation duration [22]. Such inefficient usage of the conveyors is connected with the irregular load flows by the amplitude of the loading and interruptions in load supply, etc. These operation modes of the conveyor cause unjustified energy losses, belt and conveyor rollers wear, increase of the no-load run of the belt, down time of the equipment. That is why, greater part of the research [1, 13, 25, 26] is directed at the provision of the coordination of the belt conveyor drive operation modes with the parameters of the load flows by means of belt motion speed control and drum torque.

To provide the continuous operation of the belt conveyors drives, mobile complexes are equipped with and increase their production efficiency it is expedient to apply in the drive the additional hydraulic motor, installed in parallel with the main motor and enables to realize the active reservation of the torque at the drive drum. To switch on the drive it is necessary to install the hydroautomatic devices, sensitive to the load variations on the working organ. The solution of such problems is considered in [3, 6, 7, 16]. However, the suggested methods and control devices require both the technical improvement and theoretical substantiation of their parameters, which will provide the efficient operation of the device in non-stationary operation modes. This problem requires more detailed study and substantial analysis of the dynamic processes, occurring in the conveyors drives with devices or controlystems.

2. Hydraulic automatic devices for the operation elements of the mobile machines with variable loads

In the adaptive hydraulic drive of the manipulator for the trucks and working machines of different designation the regulated pump 1 with the regulator 6, proportional hydraulic distribution valve 2, freely programmable controller 3 and sensor 9, 10 (Fig. 1) are used.

Adaptive hydraulic drive provides the operation of the execution mechanism of the machine with trivialpower losses. Proportional control of the hydraulic cylinder provides the possibility to minimize the amount of the manipulator motions to the object, that increases the performance of the machine and quality of the executed work.

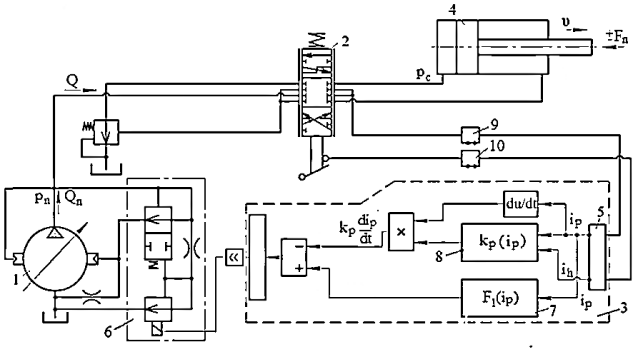

Fig. 1. Adaptive hydraulic drive of the manipulator

Freely programmable controller 3 performs the function of the adaptive regulator, changing the adjustment of the hydraulic drive when the external conditions of its operation change.

Adaptive regulator contains the switching unit 5, feedback unit 7, and correction unit 8. Feedback unit provides the transfer of the signals from the hydraulic cylinder to the regulator of the regulated pump. Unit of the feedback signal correction provides the suppression of the oscillations in the hydraulic drive in the transient processes. Feedback signal correction is realized by means of the addition to it the component $\Delta p_c = -k_p \frac{di_p}{dt}$. k_p is the coefficient of the correction component of the adaptive regulator signal, di_p/dt – is the derivative from the feedback signal. The value of the k_r coefficient greatly influences the quality of the transient processes in the adaptive hydraulic drive. The modeling of the hydraulic drive operation with the adaptive regulation is carried according to the mathematical model [10, 12].

In the adaptive hydraulic drive of the small-size mobile drilling installation (Fig. 2) regulated pump 1, hydraulic motor 2 of the main motion of the tool, hydraulic cylinder 3 of the tool supply, regulated throttle valves 4 and 5 with the electromagnetic control, controller 6, valve 7, hydraulic distribution valves 8, 9, and sensors 10, 11, 12, 13 are used.

Hydraulic drive operates in two modes. In the first mode both branches of the hydraulic drive operate independently. Pump 1 provides the motion of the hydraulic motor 2 and hydraulic cylinder 3 in the independent speed modes.

In the second mode the adaptive regulator 6 provides the coordinated operation of the hydraulic motor 2 and the hydraulic cylinder 3. When the load changes at the hydraulic motor M_1, the adaptive regulator changes the value of the supply $\upsilon_2$of the tool in accordance with the algorithm, which is determined by the program of the controller.

When the value of the pressure p_1, which is determined by the value of the moment M on the hydraulic motor increases, the speed υ_2 of the hydraulic cylinder 3 piston motion proportionally decreases. When the pressure value p_{c1} deceases, the speed value υ_2 increases.

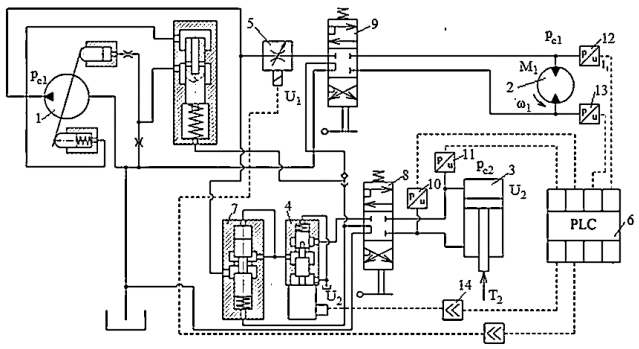

Fig. 2. Adaptive hydraulic drive for the small-size drilling installation

This process is provided by the controller 6 which realizes the cross-coupling in the hydraulic drive. Simulation of the adaptive hydraulic drive operation using the model presented in [9] was carried out. In case of the step-by-step change of the moment M_1 value from 200 Nm to 800 Nm (Fig. 3) the transient process in the branch, which feeds the hydraulic cylinder 3 passes more dynamically with the readjustments by the value of the pressure p_{c2}.

It is possible to decrease the negative impact of the cross-coupling on the dynamic characteristics of the adaptive hydraulic drive as a result of the introduction of the correction of the cross-coupling signal. Such correction is provided by the controller, which changes the cross coupling signal by the necessary law. It is suggested to form the cross-coupling signal as $U_2 = k_c(p_{c1} - k_p \frac{dp_{c1}}{dt})$. The following denotations are used: k_c is amplification factor of the amplifier 14, k_p is the coefficient of the correction component of the cross-couplingsignal. In the process of the simulation of the mechanotronic hydraulic drive operation the signal of the cross-coupling U_2 was supplied by the controller to the regulated throttle valve 6 with the delay ΔT_1.

For the belt conveyor of the mobile machine operating in the mode of variable load flows, the built-in hydraulic drive, sensitive to load changes is developed [15], its construction diagram is shown in Fig 3a.

Basic elements of the built-in hydraulic drive construction is the housing of the drum 1, where the drive consisting of two separate hydraulic motors – principal motor 2 and additional motor 3, is built-in, transmission mechanism, consisting of the pinion 4, intermediate 5 and crown 6 toothed wheels. The housing of the drum 1 is mounted on the compound axle, consisting of two half-axles 7 and 8, connected to the housing of thetransmission mechanism. The control device 9 in the form of the indirect action valve is installed in one of the radial channels of the half-axle 7 for the supply of the working fluid to the hydraulic motors 2 and 3. The control device (Fig. 3b) contains the valve of the first stage with the conical-cylindrical gate 10, which is pressed by the spring 11 to the seat 12, mounted in the housing 13 and regulating screw 14 for the adjustment for the preset pressure.

The valve of the second stage – tubular slide valve 15 is pressed by the spring 16 to the seat 17. The input of the additional hydraulic motor 3 in case of the switched off control device 9 is connected with the drain by the means of the relief valve 18.

The buil-in hydraulic drive operates in the following way. If the pressure at the input in the hydraulic system does not exceed the regulating pressure of the control device 9, then the torque at the drum housing 1 is transferred from the shaft of the main hydraulic motor 2 on across the drive gear 4, intermediate 5 and crown 6 totothed wheels.

In case of the sudden load increase the pressure at the input of the hydraulic system reaches the value p_2, that exceeds the nominal p_1,control device 9 is activated. Conical-cylindrical gate 10 is shifted relatively the seat 12 and the working fluid arrives to the drain across the hole 19. At the same time the pressure drop occurs at the throttle valve 20. As a result, the tubular slide valve 15 shifts in the housing 21 together with the rubber seal ring 22 relatively the seat 17 to the left. The working fluid aross the hole 23, hydraulic tube 24 arrives to the working chamber of the additional hydraulic motor 3, switching it on in parallel to the principal hydraulic motor 2. Throttle valve 25 is damping the tubular slide valve 15, increasing the dynamic stability of the control device. Besides it forms the valve pot (between the throttle valve 25 and the end face of the tubular slide valve 15), optimal value of its flexibility provides necessary transient characteristics of the valve. The throttle valve 25 does not influence the amplification factor by the losses of the first stage valve and does not worsen the static characteristics of the control valve. As a result of the interaction of the working fluid with the rotor elements of the hydraulic motors 2 and 3 the rotation of their output shafts takes place. The torque from these hydraulic motors across the driving gear 4 intermediate toothed wheels 5, crown wheel 6 is transferred to the drum housing 1. Having lost the energy, the working fluid across the output holes of the hydraulic

motors 2 and 3, pipelines 26 and 27, accordingly, radial 28 and axial 29 channels, located in the half shaft 8, arrives to the drain.

For the stable operation of the hydraulic drive, without vibrations, the characteristic of the control device must correspond to the graphic dependence shown in Fig. 4 (22). Such dependence of the valve opening on the pressure at its input is provided by the construction of the developed control device.

Theoretical studies of the dynamic processes in non-stationary operation modes of the hydraulic drive operation were carried out on the base of the developed mathematical model [14].

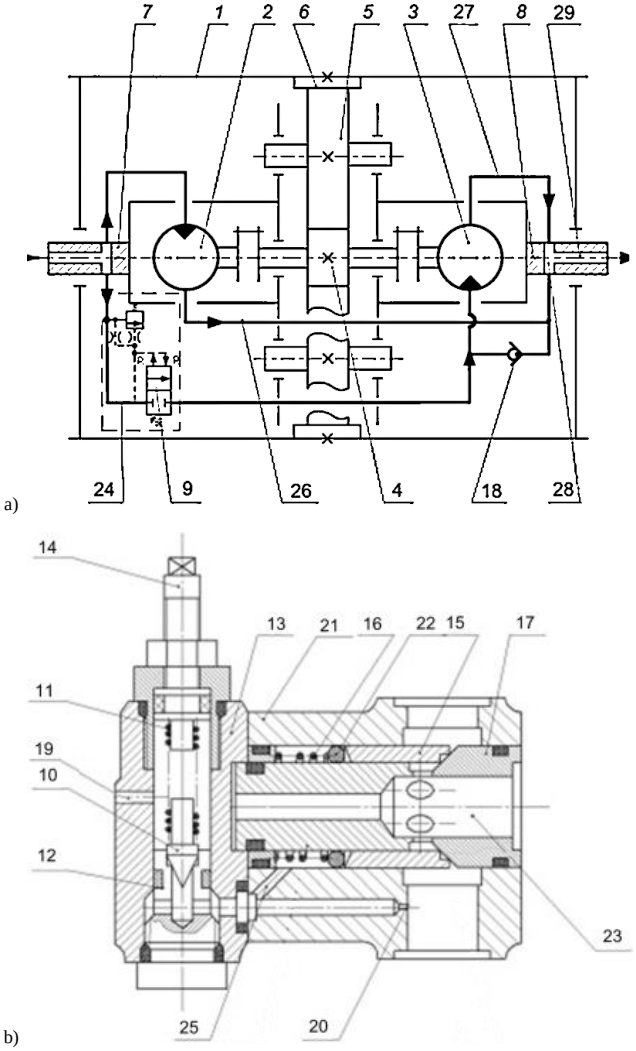

Fig. 3. Construction diagram of the built-in conveyor hydraulic drive, sensitive to the load change

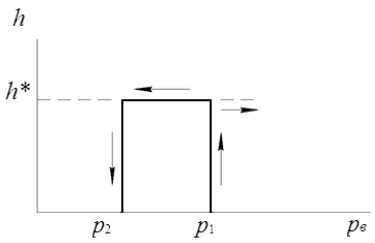

Fig. 4. Dependance of the value of the control drive opening on the pressure at the input of the hydraulic system

For the receiving conveyor of the clamp former K-65M253-K the construction [19] and technical documentation of the built-in hydraulic drive was developed, the construction diagram of the drive is shown in Fig. 5.

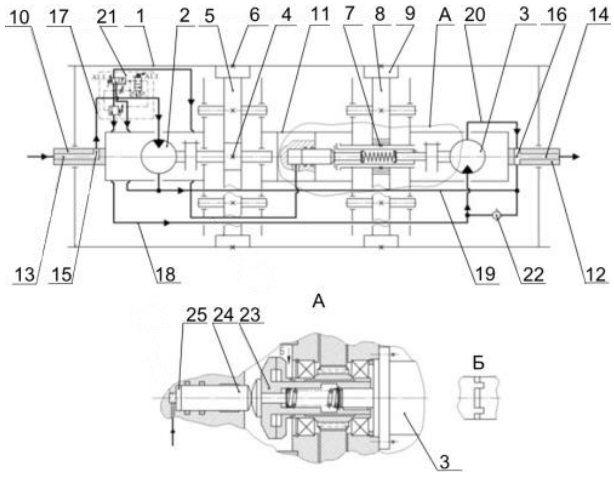

Fig. 5. Construction diagram of the buil-in hydraulic drive of the receiving conveyor of the clamp former K-65M253-K

The efficiency of the driveoperation is provided [17] applying in it the developed control system with the friction clutch for the switchingof the additional hydraulic motor. To reduce the resistance forces during the start of the addition hydraulic motor the control device of such system operates in such mode: first, with the small time delay the shaft displacement of the additional hydraulic motor occurs, then the friction clutch of the driving gear pinion is activated.

The controlled hydraulic electric cylinder motor contains the housing of the drum 1, where the drive is buil-in, the drive is realized in the form of two separate hydraulic motors – main 2and addition 3, and two transmission mechanisms. Each of them consists of the driving gears 4 and 7, intermediate 5, 8 and crown 6 and 9 gear wheels. The housing of the drum 1 is mounted on the axle, consisting of three parts 10, 11, 12. For the supply and drain of the working fluid to the hydraulic motors 2 and 3 in the middle of the left and right parts of the axle 10 and 12 the axial passages 13 and 14 are made. They are connected with the working channels of the hydraulic motors 2 and 3 by means of radial channels 15 and 16,as well as pressure pipes 17 and 18 and drainage pipeline 19 and 20. In the pressure pipeline 17 the control device 21 is installed. The input of the additional hydraulic motor 3, if the control unit 21 is switched off, is connected with the drain across the non-return valve 22.

The control unit 21 is realized in the form of the two-stage valve, provided with the functions of the hydraulic distribution valve.

In the second transmission mechanism the friction coupling 23 is installed betvean the shalt of the additional hydraulic motor 3 and driving gear 7, its left half coupling across the cone has the contact with the end spherical surface of the pressing plunger 24. It is mounted in the greater diameter of the central stepped hole, realized on the right side of the middle part 11 of the axel. Flat surface of the pressing plunger forms the cavity 25, connected with the cavity of the smaller diameter.

At nominal load on the working element of the conveyor the main hydraulic motor 2 operates, this motor by means of the transmission mechanisms puts in motion the body of the drum 1. At sudden increase of the load, the value of which corresponds to the values of “opening” pressure, control unit 21 starts operation.

First the switching on of the additional hydraulic motor 3 occurs, then friction coupling 23 starts its operation, and the torque from the shalf of the additionalhydraulic motor 3 is transferred across the transmission mechanism to the body of the drum 1.

After load reduction on the working element of the conveyor to the value that corresponds to “closing” pressure, control unit21 is actuated, it disconnects from the supply the additional hydraulic motor 3.

For studying the mutual impact of the parameters of the built-in hydraulic drive of the receiving conveyour with the control system and spring-inertial characteristics of its transporting part mathematical model, consisting of the equations, which describe the motion of the transport and drive parts of the conveyor and the switching control system of the additional hydraulic motor [24] is developed.

3. Results of the study of the hydraulic automation equipment of the mobile machines with variable loading working elements

The studies of the adaptive hydraulic drive of the manipulator determined that the oscillation of the hydraulic drive consistently decreases from 8-10 oscillations to 2-4 oscillations in the transient process, depending on its operation modes. The value of the readjustment decreases on the value of up to 40% and does not exceed 30%, at the operation of the manipulator of 7000 N carrying capacity.

Adaptive hydraulic drives provides high degree of the stabilization of motion speedυ of the actuating mechanism if the loadF_n changes. This enables to forecast better the motion of the actualingmechanism in the operation process, minimize the amount of the necessary motions when the manipulator is pointed on the object. The degree of the stabilization is evaluated by the dependence of the flow$Q$,that arrives to the hydraulic cylinder on the pressure value p_c at the input in the hydraulic cylinder (Fig. 6). If the pressure value p_c changes in the range of (0…16) MPa, the change of Q flow depends on the set value Q and changes in the range from 3% to 6% at the pressure drop value on the proportional hydraulic distribution valve 1.5 MPa.

The transition on the value of the pressure drop of 1.0 MPa increases the effort of the value Qchang from 5% to 10%.

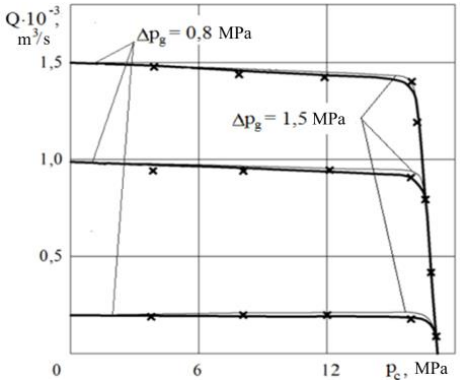

Fig. 6. Dependence of Q on the pressure $p_c$value at the input in the hydraulic cylinder

The important index of the manipulator operation quality is the pointing accuracy of the clamp on the object which determines the productivity of the nachineiperation stabilization of the manipulator modion speed allaws to increase the accuracy of the clamp pointing on the object [12]. Stady of the manipulator pointing accuracy, using the developed adaptive hydraulic drive is carried aut. The research is performed on the stand and using the technical,described in [12].

Fig. 7. shows the distribution of the results of the manipulator position measurements while directing it on the object. The results of the mensurements are in the range of $(37...43)\cdot10^{-2}$ m. The obtained distribution law is close to normal. Mean square error of the manipulator position deviation is $\sigma_1 = 1.02\cdot10^{-2}$ m and the distance between the middle of the field for the manipulator pointing and the arithmetic mean value of the manipulator position $\bar{x} = 40.3\cdot10^{-2}$ mis $\Delta x_1 = 0.42\cdot10^{-2}$ m.

The obtained results of measurements allow to assess the accuracy of the manipulator pointing on the object as such that allows to minimize the amount of motions in the operation cycle and increase the performance of the machine.

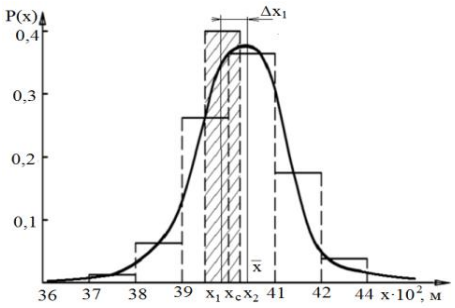

Fig. 7. Determination of the manipulatot pointing accuracy on the abject

At the stepped change of the momentM_1 value from 200 Nm to 800 Nm (Fig. 8) the transient process in the branch, which feeds the hydraulic cylinder, 3 occurs more dynamically with large readjustment by the pressure p_{c2} value.

The value of the delay changed in the process of the research in the range of $\Delta T_1 = (0.005…0.06)$ sec. The value of k_p coefficient of the correction component of the cross coupling signal varied in the range of $k_p' = (40…320)\cdot10^{-4}$ sec.

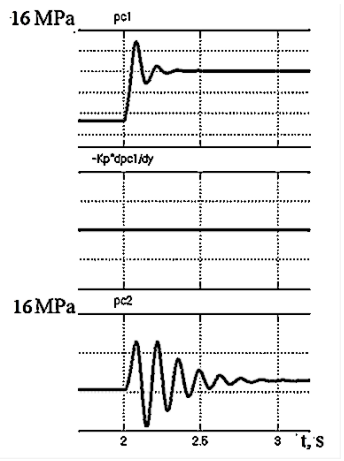

Fig. 8. Transient process in the adaptive hydraulic drive if the correction of the cross communication is missing

At the change of the delay value ΔT_1 of the transient coupling signal of more than 0.04 sec. and less than 0.02 sec. the readjustment in the adaptive hydraulic drive increases (Fig. 9)

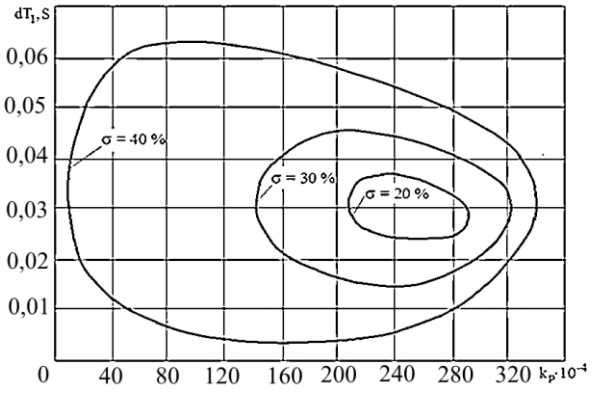

Fig. 9. Impact of the delay time ΔT_1 and the correction component coefficient k_p on the value of the readjustment in the adaptive hydraulic drive

At values of $\Delta T_1 = (0.025…0.04)$ sec. readjustment σ = 20% may be provided. For this purpose it is necessary to select the value k_p from the range $k_p = (200…280)\cdot10^{-4}$ sec. Change of the coefficient k_p value of less than $200\cdot10^{-4}$ sec. and the greater value $k_p = 280\cdot10^{-4}$ sec. leads of the increase of the readjustment value σ. The selection of the rational values of k_p and T_1 provides the deacrease of the regulation time t_p and readjustment value σ by the pressure p_{c2} at the input in the hydraulic cylinder 3.

Fig. 10 shows the transient process in the adaptive hydraulic drive, calculated by the mathematical model if the correction of the cross coupling signal is available.

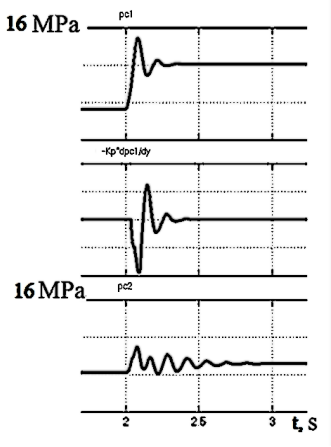

Fig. 10. Transient process in the adaptive hydraulic drive on case of the cross coupling correction

At the values of the correction component coefficient $k_p = 250 \cdot 10^{-4}$ sec. and correction component delay $\Delta T_1 = 0.02$ sec. the regulation time is $t_p = 0.9$ sec. and the readjustment value does not exceed 50%. For the simultaneous decrease of the regulation time t_p and readjustment value σ on the change of the coefficient k_p and delay value ΔT_1 the optimization nproblem must be solved.

The application of the adaptive regulator in the hydraulic drive of the small-size drilling installation enables to provide its operation in the semiautomatic mode.

The operation modes will vary depending on the type of the soil in which the drilling is performed.

The study of the dynamics of the hydraulic drive, sensitive to the load changes (Fig. 3) [18] was carried out on the base in the integration of the differential equctions of the developed mathematical model, applying the computer program, created on the base of Mathlab 13 package.

Analysis of the conditions of the hydraulically driven systems operation showed that the inertial loading, torsional shiffness, volume of the pressure pipe and the character of the load change influence the transient processes of the hydraulically driven installation [20].

Theoretical dependences regarding the character of the dynamic processes in the hydraulic drive, sensitive to load change have been obtained, one of these dependences is presented in Fig. 11: $p_1(t)$ – pressure in the main line of the main hydraulic motor; p_3 – pressure in the pipeline of the additional hydraulic motor after the activation of the control units; $Q_1(t)$, $Q_2(t)$ – working fluidconsumptionacross the main and additional hydraulic motor, correspondingly; $n(t)$ – drum rotationfrequency; $M(t)$ – moment on the drum from the acting load.

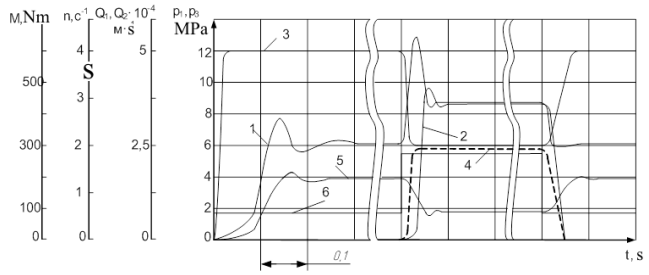

Fig. 11. Theoretical dependencies$p_1(t)$, $p_3(t)$, $Q_1(t)$, $Q_2(t)$, $n(t)$, $M(t)$ (curves 1, 2, 3, 4, 5, 6 correspondingly) at $p_{кв} = 12$ MPa, torsional stiffness$c_\varphi = 0.37 \cdot 10^{-3}$Nm/rad, ratio of the area of the conic-cylindrical gate $f_3/f_4 = 0.6$ and step-by-step load change

For the verification of the results of the theoretical studies and to specify the values of certain parameters, needed for carrying out the dynamic calculations experimental studies were performed.

Experimental and theoretical dependences of the impact on the time of the transient process of the start *t* and the activation of the control unit *to* during its opening and closing, torsional stiffness of the mechanical part c_φ (Fig. 12), inertia moment I_4 (Fig. 13), volume of the pressure cavity V_1 (Fig. 14) and the character of loads change $M(t)$ are constructed. It is determined that the 3 times increase of the torsional stiffness of the mechanical system of the conveyor causes the decrease of the duration of the transient processes of the start by 26% and control unit opening by 24%, as well as the increase of the readjustment pressures Δp_1 by 80% and control unit opening $\Delta p_{кв}$ by 44%; increase of the inertia load causes the increase of these parameters by 23%, 41%, 30% and 29%,correspondingy; the increase of the volume of the pressure cavity V_1increases the duration of the transient processes and reduces greatly the pressure readjustment. The comparison of the results of the theoretical and experimental research is carried out.

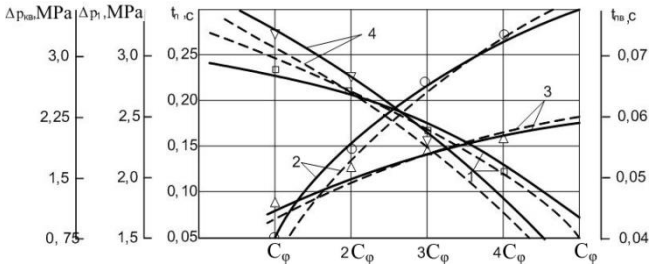

Fig. 12. Graph of the dependences $t_n(c_\varphi)$,$\Delta p_1(c_\varphi)$, $\Delta p_{кв}(c_\varphi)$, $t_{кв}(c_\varphi)$ (curves 1, 2, 3 and 4 correspondingly) at $p_{кв} = 12$ MPa, torsional stiffness $c_\varphi = 0.37 \cdot 10^3$ Nm/rad; $f_3/f_4 = 0.6$ and step-by-step change of the resistance moment M_o from 87 Nm to 280 Nm (--- theoretical, — experimental)

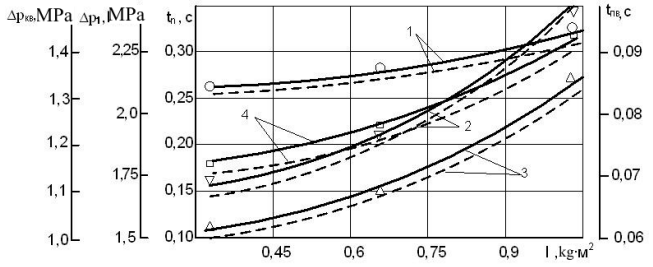

Fig. 13. Graph of the dependences $t_n(I)$,$\Delta p_1(I)$, $\Delta p_{кв}(I)$, $t_{кв}(I)$ (curves 1, 2, 3 and 4 correspondingly) at $p_{кв} = 12$ MPa, torsional stiffness $c_\varphi = 0.37 \cdot 10^{-3}$ Nm/rad; $f_3/f_4 = 0.6$ and step-by-step change of the resistance moment M_o from 87 Nm to 280 Nm (--- theoretical, — experimental)

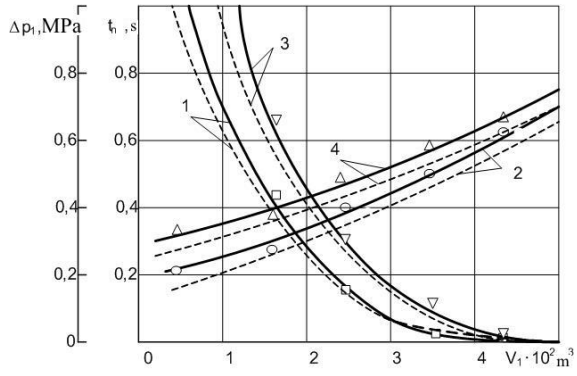

Fig. 14. Graph of the dependences $\Delta p_1(V_1)$, $t_n(V_1)$ (curves 1, 2 correspondingly) if the resistance moment is missing and $\Delta p_1(V_1)$, $t_n(V_1)$ (curves 3, 4 correspondingly) at $p_{кв} = 12$ MPa, torsional stiffness $c_\varphi = 0.37 \cdot 10^{-3}$ Nm/rad; $f_3/f_4 = 0.6$ and step-by-step change of the resistance moment M_o from 87 Nm to 280 Nm (curves 1, 2, 3 and 4 correspondingly) (--- theoretical, — experimental)

Theoretical investigations of the hydraulic drive of the clamp former receiving conveyor with the control system of the additional hydraulic motor switching were carried out. The solution of the system of the non- linear differential equations of the mathematical model was performed by means of the programming package Matlab Simulink. The study of the dynamic characteristics for the driving and transporting parts of the conveyor was performed on the base of the analysis of the

transient processes graphs $M(t)$, $p_n(t)$, $p_1(t)$, $p_2(t)$, $x(t)$,$y(t)$, $z(t)$ (Fig. 15). The moment on the drum changed from the nominal value of 5 kN·m to the overload value of 12 kN.m. Overload mode is characterized by three phases of the transient processes: the first – switching on of the additional hydraulic motor (0.11 sec $< t_{p1} < 0.15$ sec, $15\% < \Delta p_1 < 45\%$); the second – operation of the drive with two hydraulic motors (0.05 sec $< t_{p2} < 0.12$ sec, $4\% < \Delta p_2 < 12\%$); the third – load decrease and disconnection of the additional hydraulic motor (0.9 sec $< t_{p3} < 0.17$ sec, $20\% < \Delta p_3 < 55\%$).

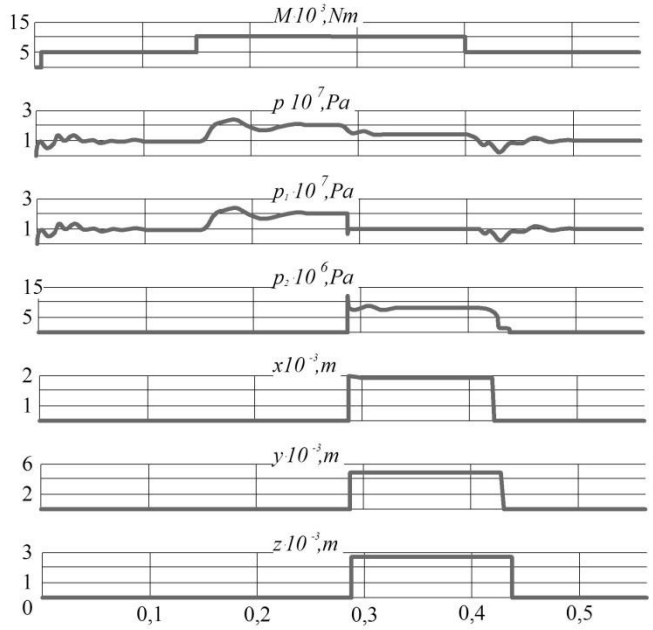

Fig. 15. Theoretical graphs of the transient processes of M(t), pn(t), p1(t), p2(t), x(t), y(t), z(t) change

For each of the above-mentioned phases of the transient process the impact of the pressure increase value Δp in the pressure pipe, torsional stiffness $c_f$and transmission mechanism damping, aggregate moment of the drum I b inertia, static E_s and dynamic h_s belt elasticity modulus, conveyor length L_s was analyzed (Fig. 16, Fig. 17)

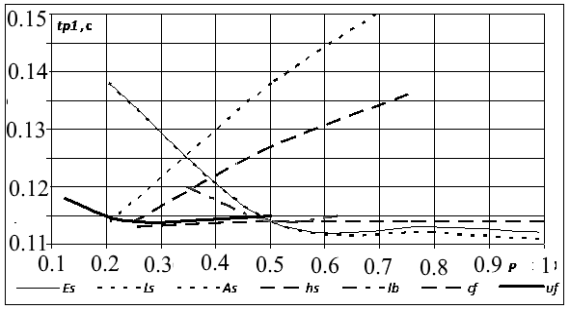

Fig. 16. Impact of the parameters of the driving and transporting parts of the conveyor on the transient process time for the first phase of the overloading

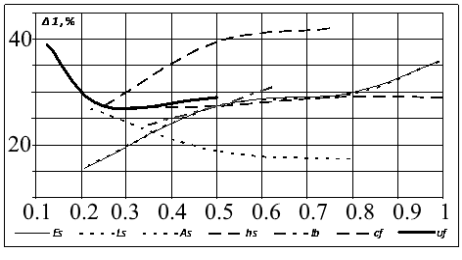

Fig. 17. Impact of the parameters of the driving and transporting parts of the conveyor on the pressure readjustment for the first phase of the overload

The obtained dependences will allow to optimize the duration of the transient processes $t_p$and the pressure increase Δp (and the dynamic component of the loading in the belt) at the expense of the selection of the above -mentioned parameters.

4. Conclusions

The research proves the efficiency of using the hydraulic automatic devices for the improvement of the technical-economic indices of the operation elements of the mobile machines.

The operation of the adaptive regulator at the optimal valve of the greatly decreases the readjustment value and regulation time at the expense of the intensive quench of the drive oscillations in the transient processes. It is determined that the value of coefficient depends on the operation modes of the hydraulic drive, namely, on the value of the working fluid supply Q_n to the hydraulic motor and pressure value p_c in the hydraulic drive.

The operation of the adaptive hydraulic drive in the small- size drilling installation provides the increase of the performance and decreases the readjustment by 30 – 60 %, depending on the operation modes that reduces the dynamic loading on the elements of the hydraulic drive.

The suggested hydraulic automation facilities provide trouble-free operation of the conveyor in the conditions of varying useful resistance forces and decrease of the dynamic impact in the transporting element.

Application of - the control system with the valve- type device, having the functions of the distributor and the friction clutch for the disconnection of the additional hydraulic motor of the built-in hydraulic drive enabled to improve its dynamic characteristics.

Compatibility of the considered adaptive drives of the technological and mobile machines [21] has been proved by the comparative economic calculations.

References

[1] Bing X., Ruqi D., Junhui Z., Min C., Tong S.: Pump valves coordinate control of the independent metering system for mobile machinery. Automation in Construction 2015, 98–11.

[2] Busquets E., Ivantysynova M.: Toward Supervisory-Level Control for the Energy Consumption and Performance Optimization of Displacement-Controlled Hydraulic Hybrid Machines. Mobile Hydraulics Paper 10(2)/2016, 163–174.

[3] Cheng G., Shuangxia P.: Adaptive sliding mode control of electro-hydraulic system with nonlinear unknown parameters. Control Engineering Practice 2008, 1275–1284.

[4] Du C.: Variable Supply Pressure Electrohydraulic System for Efficient Multi-axis Motion Control : A thesis submitted for the degree of Doctor of Philosophy University of Bath Department of Mechanical Engineering. University of Bath: November 2014.

[5] Finzel R.: New Electro-Hydraulic Control Systems for Mobile Machinery. Fluid Power and Motion Control 2008, United Kingdom 311– 321.

[6] Forental V., Forental M., Nazarov F.: Investigation of Dynamic Characteristics of the Hydraulic Drive with Proportional Control. Procedia Engineering. International Conference on Industrial Engineering (ICIE-2015) 129/2015, 695–701.

[7] Kotlobay A. Ya., Kotlobay A. A., Tamelo V. F.: Hydraulic assemblies of drive systems of the road equipment for road-building machines. Science and Technology 15(1)/2016, 69–77.

[8] Kozlov L.: Energy-saving mechatronic drive of the manipulator. Buletinulinstitutuluipolitehnic Din Iasi. Tomul LVII (LXI), Fasc. 3/2011, 231–239.

[9] Kozlov L.G., Burennikov Yu.A., Pylyavets V.G., Korinenko M.P. , Lizhov O.V.: Ensuring the stability of the mechanotronic hydraulic drive. Journal of Mechanical Engineering and Transport 1(9)/2019.

[10] Kozlov L.G., Polishchuk L.K., Piontkevych O.V., Korinenko M.P., Horbatiuk R.M., Komada P., Orazalieva S., Ussatova O.: Experimental research characteristics of counterbalance valve for hydraulic drive control system of mobile machine. PrzegladElektrotechniczny 95(4)/2019, 104–109.

[11] Kozlov L.G.: Mechatronhydrosystem of a mobile machine. Bulletin of the Volodymyr Dahl East-Ukrainian University 6/2012, 22–30.

[12] Kozlov L.G.: Scientific foundations for designing the systems of manipulator hydraulic drives with an adaptive neural network-based controllers for mobile working machines. Thesis for the scientific degree of Doctor of Science (Engineering). National Technical University of Ukraine Kyiv Polytechnic Institute, Kyiv 2015.

[13] Lauhoff H.: Speed Control on Belt Conveyors – Does it Really Save Energy? Bulk Solids Handling 22(6/)2005, 368–377.

[14] Polischuk L.K., Adler A.O., Sturma A.L.: Control device for hydraulic drive with variable load on the working body. Bulletin of the Volodymyr Dahl East Ukrainian National University 3(109)/2007, 195–200.
[15] Polischuk L.K., Adler A.O.: Embedded hydraulic drives of conveyors with a flexible pulling body, sensitive to load change. VNTU, Vinnitsa 2010.
[16] Polischuk L.K.: Dynamics of the built-in hydraulic drive of conveyors of mobile machines. VNTU, Vinnytsa 2018.
[17] Polishchuk L., Kharchenko Y., Piontkevych O., Koval O.: The research of the dynamic processes of control system of hydraulic drive of belt conveyors with variable cargo flows. Eastern-European Journal of Enterprise Technologies 2(8)/2010, 22–29.
[18] Polishchuk L.K., Adler O.O., Malyarchuk A.O.: Influence of the load change characteristics on the dynamics of the integrated hydraulic drive. Machine Science 11/2009, 31–35.
[19] Polishchuk L.K., Koval O.O.: Control system of a hydraulic drive of a belt conveyor with variable load. The Bulletin of the Vinnytsia Polytechnic Institute 2(191)/2015, 131–136.
[20] Polishchuk L.K., Kozlov L.G., Piontkevych O.V., Horbatiuk R.M., Pinaiev B., Wójcik W., Sagymbai A., Abdihanov A.: Study of the dynamic stability of the belt conveyor adaptive drive. Przeglad Elektrotechniczny 95(4)/2019, 98–103.
[21] Scherer M., Geimer M., Weis B.: Contribution on Control Strategies of Flow-On-Demand Hydraulic Circuits. The 13th Scandinavian International Conference on Fluid Power June 3-5 2013, Sweden, 531–540.
[22] Shakhmeister L.G., Dmitriev V.G.: Theory and calculation of belt conveyors. Engineering, Moscov 1978.
[23] Sidorenko V.S., Grishchenko V.I., Rakulenko S.V., Poleshkin M.S.: Adaptive hydraulic drive with volumetric regulation of the tool feed of a technological machine. Bulletin of Donetsk State Technical University 2/2017, 88–98.
[24] Stamm von Baumgarten T.: A novel system layout for extended functionality of mobile machines. Fluid Power and Motion Control 2008, United Kingdom, 13–25.
[25] Wheeler C.A.: Evolutionary Belt Conveyor Design – Optimizing Coasts. Bulk Material Handling by Conveyor Belt. 7, Littleton, Colorado 2008.
[26] Zaika V.T.: Influence of an adjustable drive on cargo flows and energy efficiency of the system of mine conveyor transport. Science bulletin of National Mining University 3/2015, 82–88.

Prof. Leonid Polishchuk
e-mail: leo.polishchuk@gmail.com

Works at the Faculty of Mechanical Engineering and Transport in Vinnytsia National Technical University. Head of the Department of Industrial Engineering.Conducts research on problem related to the dynamics and diagnostics of driving systems and metal support structures of heavy lifting and transportation machinery. The author of more than 200 scientific papers, including two monographs.

ORCID ID: 0000-0002-5916-2413

Prof. Leonid Kozlov
e-mail: osna2030@gmail.com

Head of the Department of Technology and Automation of Machine Building of Vinnytsia National Technical University (Ukraine). Specializes in hydraulic drives, hydroautomatics and mechatronics.The author of more than180scientific papers.Developments by Kozlov L.G. marked with 3 gold medals at international exhibitions in Yassi (Romania).

ORCID ID 0000 0001 9652 1270

Prof. Yuri Burennikov
e-mail: yu.burennikov@gmail.com

Dean of the Faculty of Mechanical Engineering and Transport of Vinnytsia National Technical University (Ukraine).Specializes in the field of hydraulic and hydroautomatics. The author of more than 140 scientific papers, including two monographs.Developments by BureniknikovaYu.A. marked with 3 gold medals at international exhibitions in Yassi (Romania). Honored Worker of Education of Ukraine.

ORCID ID 0000-0001-7341-6988

Prof. Vasil Strutinskiy
e-mail: kvm_mmi@ukr.net

Professor of the Department of Designing Machines and Machines of the National Technical University of Ukraine "Kyiv Polytechnic Institute named after Igor Sikorsky". Specializes in the development of the theory of designing machine tools, robotic systems and machines.The author of more than 500 scientific papers, including 12 monographs. Honored Worker of Science and Technology of Ukraine.Vice-President of the Association of Industrial Hydraulics and Pneumatics (Ukraine).

ORCID ID0000-0001-5533-9915

M.Sc. Valerii Kravchuk
e-mail: kravchuk.vntu@gmail.com

Postgraduate student at the Department of Industrial Engineering at Vinnytsia National Technical University. Specializes in the field of hydraulic drives and means of automation of technological and mobile machinery. The author of 10 scientific papers

ORCID ID: 0000-0003-4815-7384

otrzymano/received: 15.05.2019 *przyjęto do druku/accepted: 15.06.2019*